

AD-A055 262

MECHANICAL TECHNOLOGY INC LATHAM N Y  
TURBINE ENGINE ROTORDYNAMIC EVALUATION. VOLUME I.(U)

F/G 21/5

UNCLASSIFIED

JAN 78 R A RIO  
MTI-76TR41

AFAPL-TR-76-81-VOL-1

F33615-75-C-2035  
NL

1 OF 3

AD  
A055262



CL

FOR FURTHER TRAN

*Handwritten: 11-1-78*  
*Handwritten: 2*

AFAPL-TR-76-81  
Volume I

*AD 54533*

AD A 055262

## TURBINE ENGINE ROTORDYNAMIC EVALUATION

MECHANICAL TECHNOLOGY INCORPORATED  
968 ALBANY-SHAKER ROAD  
LATHAM, NEW YORK 12110

JANUARY 1978

TECHNICAL REPORT AFAPL-TR-76-81, Volume I  
Final Report for Period May 1975 - June 1976

DDC  
RECEIVED  
JUN 19 1978  
*Handwritten: A*

Approved for public release; distribution unlimited.

78 06 15 038

AIR FORCE AERO PROPULSION LABORATORY  
AIR FORCE WRIGHT AERONAUTICAL LABORATORIES  
AIR FORCE SYSTEMS COMMAND  
WRIGHT-PATTERSON AIR FORCE BASE, OHIO 45433

DDC FILE COPY



NOTICE

When Government drawings, specifications, or other data are used for any purpose other than in connection with a definitely related Government procurement operation, the United States Government thereby incurs no responsibility nor any obligation whatsoever; and the fact that the government may have formulated, furnished, or in any way supplied the said drawings, specifications, or other data, is not to be regarded by implication or otherwise as in any manner licensing the holder or any other person or corporation, or conveying any rights or permission to manufacture, use, or sell any patented invention that may in any way be related thereto.

This report has been reviewed by the Information Office (OI) and is releasable to the National Technical Information Service (NTIS). At NTIS, it will be available to the general public, including foreign nations.

This technical report has been reviewed and is approved for publication.

Robert Millard

William A. Tschala

FOR THE COMMANDER

H. I. Bush

H. I. BUSH  
Deputy Director  
Turbine Engine Division

ADDITIONAL BY	
NTIS	NTIS Section <input checked="" type="checkbox"/>
DTIC	DTIC Section <input type="checkbox"/>
JUSTIFICATION	
BY	
DISTRIBUTION/AVAILABILITY CODES	
BY	
AVAIL. AND M. SPECIAL	
A	

"If your address has changed, if you wish to be removed from our mailing list, or if the addressee is no longer employed by your organization please notify AFAPL/TBP, W-PAFB, OH 45433 to help us maintain a current mailing list".

Copies of this report should not be returned unless return is required by security considerations, contractual obligations, or notice on a specific document.

UNCLASSIFIED

SECURITY CLASSIFICATION OF THIS PAGE (When Data Entered)

REPORT DOCUMENTATION PAGE		READ INSTRUCTIONS BEFORE COMPLETING FORM
1. REPORT NUMBER AFAPL TR-76-81	2. GOVT ACCESSION NO.	3. RECIPIENT'S CATALOG NUMBER
4. TITLE (and Subtitle) TURBINE ENGINE ROTORDYNAMIC EVALUATION, Volume I	5. TYPE OF REPORT & PERIOD COVERED Final Report for Period 5/1/75 TO 6/1/76	6. PERFORMING ORG. REPORT NUMBER MTI-76TR41
7. AUTHOR(s) R. A. Rio	8. CONTRACT OR GRANT NUMBER(s) F33615-75-C-2035	
9. PERFORMING ORGANIZATION NAME AND ADDRESS Mechanical Technology Incorporated 968 Albany-Shaker Road Latham, New York 12110	10. PROGRAM ELEMENT, PROJECT, TASK AREA & WORK UNIT NUMBER 3066 1227	
11. CONTROLLING OFFICE NAME AND ADDRESS Air Force Aero Propulsion Laboratory Attn: AFAPL/TBP/William A. Troha Wright-Patterson Air Force Base, Ohio 45433	12. REPORT DATE February 1978	13. NUMBER OF PAGES 1278
14. MONITORING AGENCY NAME & ADDRESS (if different from Controlling Office) 12 278 P.	15. SECURITY CLASS. (of this report) UNCLASSIFIED	15a. DECLASSIFICATION/DOWNGRADING SCHEDULE
16. DISTRIBUTION STATEMENT (of this Report)  Approved for public release, distribution unlimited		
17. DISTRIBUTION STATEMENT (of the abstract entered in Block 20, if different from Report) 9 Final Rept. 1 May 75 - 1 Jun 76		
18. SUPPLEMENTARY NOTES  NONE		
19. KEY WORDS (Continue on reverse side if necessary and identify by block number)  Turbines                      Turboprop Jet Engines                  Turbofan Rotors Rotordynamic		
20. ABSTRACT (Continue on reverse side if necessary and identify by block number) Eight jet engine models within the Air Force inventory (the T56, J57, J79, J85, TF30, TF33, TF39 and TF41) have been analyzed to determine critical speeds, unbalance response, blade loss effects and maneuver deflections. The effects of dampers, thrust loads and balancing requirements, while not analyzed in depth, were noted where applicable in the description of the engine's dynamic behavior. Each rotor design was then classified into categories of dynamic sensitivity.  Five test elements were manufactured and vibrated to obtain experimental data		

DD FORM 1 JAN 73 1473

EDITION OF 1 NOV 65 IS OBSOLETE

Unclassified  
SECURITY CLASSIFICATION OF THIS PAGE (When Data Entered)


224 550

slf

UNCLASSIFIED

SECURITY CLASSIFICATION OF THIS PAGE(When Data Entered)

for correlation with analytical modeling predictions. The four cylindrical elements, each of which incorporated either a steep cone, shallow cone, flat plate or thin shell, were excited to obtain the first three lateral natural frequencies. Because of manufacturing problems with hardness and weld penetration, measured frequencies were below those predicted. The fifth test element was a machined flexible bearing support for use in parallel with a squeeze film damper. After static and dynamic testing of this representative flexible bearing support, the results were within 10% of the analytical prediction for this element.

The information from this analytical and experimental study has resulted in a technology plan whose goal is to improve the technological capabilities for the purpose of reducing costs associated with reliability and maintainability of U.S. Air Force engines. 

Unclassified

SECURITY CLASSIFICATION OF THIS PAGE(When Data Entered)



#### ACKNOWLEDGEMENT

The efforts reported in this document were performed by the Machinery Dynamics Center of Mechanical Technology Incorporated, under Contract F33615-75-2035 for the Air Force Aero Propulsion Laboratory, Wright-Patterson Air Force Base. Mr. William A. Troha was the AFAPL Project Manager and Dr. Robert H. Badgley was the MTI Project Manager.

This project was accomplished through the assistance of Mr. Mark Darlow and Mr. Walter Spodnewski in the analysis and testing of experimental hardware and Mrs. Freida Gillham who conducted the computer simulations of engine vibrations.

This program was initiated with FY75 Aero Propulsion Laboratory Director's Funds.

## TABLE OF CONTENTS

SECTION		PAGE
I	SUMMARY	1
II	INTRODUCTION	2
	A. Engine Modeling	2
	B. Critical Speeds and Mode Shapes	3
	C. Rotor Unbalance	3
	D. Blade Loss	4
	E. Maneuver Loads	4
	F. Engine Tests	5
III	ENGINE DYNAMIC BEHAVIOR	8
	A. T56-15 Engine	8
	B. J57 Engine	10
	C. J79 Engine	12
	D. J85-21 Engine	14
	E. TF30 Engine	15
	F. TF33 Engine	17
	G. TF39 Engine	19
	H. TF41 Engine	22
IV	DYNAMIC CLASSIFICATION	26
V	EXPERIMENTAL STUDIES	28
VI	TECHNOLOGY PLAN	34
	A. Current Needs	34
	B. Near-Term Needs	34
	C. Long-Term Needs	35
	D. Plan Element Discussion	35
VII	RECOMMENDATIONS	39

# LIST OF ILLUSTRATIONS

<u>Figure Number</u>	<u>Title</u>	<u>Page</u>
1	Critical Speed Map For T56-15 Rotor Bearing System. . . . .	40
2	Undamped Mode Shape at First Critical Speed For The T56-15 Rotor System (Turbine Mode) . . . . .	41
3	Undamped Mode Shape at Second Critical For The T56-15 Rotor System. . . . .	42
4	Calculated Unbalance Response For T56-15 Rotor System With Random Distributed Unbalance. . . . .	43
5	Compressor Rotor Amplitudes For a First Compressor Stage Blade Loss of The T56-15 Engine . . . . .	44
6	T56-15 Rotor No. 1 Bearing Radial Force For The First Com- pressor Stage Blade Loss. . . . .	45
7	Turbine Rotor Amplitudes For a Fourth Stage Turbine Blade Loss of The T56-15 Engine . . . . .	46
8	T56-15 No. 4 Bearing Radial Force For The Fourth Stage Turbine Blade Loss. . . . .	47
9	T56-15 Rotor Bow Analysis - Landing Condition . . . . .	48
10	T56-15 Rotor Bow Analysis - Flight Condition. . . . .	49
11	T56-15 Rotor Bow Analysis - Catapult Conditions . . . . .	50
12	Critical Speed Map For J57 Low Rotor Bearing System . . . . .	51
13	Undamped Mode Shape at First Critical Speed of J57 Low Rotor System (Low Turbine Mode) . . . . .	52
14	Undamped Mode Shape at Second Critical Speed of J57 Low Rotor System (Low Compressor Bounce Mode) . . . . .	53
15	Calculated Unbalance Response For J57 Low Rotor System With Random Distributed Unbalance. . . . .	54
16	Low Compressor Rotor Amplitudes For a First Fan Stage Blade Loss of The J57 Engine. . . . .	55
17	J57 Low Rotor No. 1 Bearing Radial Force For The First Fan Stage Blade Loss. . . . .	56
18	Low Turbine Rotor Amplitudes For a Third Stage Turbine Blade Loss of the J57 Engine. . . . .	57
19	J57 No. 4 Bearing Radial Force For The Third Stage Low Turbine Blade Loss. . . . .	58
20	J57 Low Rotor Bow Analysis - Landing Condition. . . . .	59
21	J57 Low Rotor Bow Analysis - Flight Condition . . . . .	60
22	J57 Low Rotor Bow Analysis - Catapult Condition . . . . .	61
23	Critical Speed Map For J57 High Rotor Bearing System. . . . .	62
24	Undamped Mode Shape at First Critical Speed For The J57 High Rotor System (Cantilevered Turbine Mode). . . . .	63
25	Undamped Mode Shape at Second Critical Speed For The J57 High Rotor System (Compressor Bounce Mode) . . . . .	64
26	Calculated Unbalance Response Vibration For The J57 High Rotor With Distributed Unbalance. . . . .	65
27	Compressor Amplitude For The High Rotor System of The J57 Engine For a First Compressor Stage Blade Loss. . . . .	66
28	No. 1 Bearing Radial Load For a First Stage Compressor Blade Loss of The J57 High Rotor System . . . . .	67



# LIST OF ILLUSTRATIONS (continued)

<u>Figure Number</u>	<u>Title</u>	<u>Page</u>
29	Turbine Amplitude For The High Rotor System of The J57 Engine For a High Turbine Blade Loss. . . . .	68
30	No. 3 Bearing Radial Force For a Turbine Blade Loss of The J57 High Rotor System . . . . .	69
31	J57 High Rotor Bow Analysis - Landing Condition . . . . .	70
32	J57 High Rotor Bow Analysis - Flight Condition. . . . .	71
33	J57 High Rotor Bow Analysis - Catapult Condition. . . . .	72
34	Critical Speed Map For J79 Rotor Bearing System . . . . .	73
35	Undamped Mode Shape at First Critical Speed For J79 Rotor System (Turbine Mode) . . . . .	74
36	Undamped Mode Shape at Second Critical Speed For The J79 Rotor System (Compressor Bounce Mode) . . . . .	75
37	Calculated Unbalance For J79 Rotor System With Random Distributed Unbalance . . . . .	76
38	Compressor Rotor Amplitudes For a First Compressor Stage Blade Loss of The J79 Engine. . . . .	77
39	J79 Rotor No. 1 Bearing Radial Force For The First Compressor Stage Blade Loss. . . . .	78
40	Rotor Amplitudes For The Third Compressor Stage Blade Loss of The J79 Engine . . . . .	79
41	J79 Rotor Bearing Radial Forces For The Third Compressor Stage Blade Loss. . . . .	80
42	Rotor Amplitudes For a Third Stage Turbine Blade Loss of The J79 Engine. . . . .	81
43	J79 Bearing Radial Forces For The Third Stage Turbine Blade Loss. . . . .	82
44	J79 Rotor Bow Analysis - Landing Condition. . . . .	83
45	J79 Rotor Bow Analysis - Flight Condition . . . . .	84
46	J79 Rotor Bow Analysis - Catapult Condition . . . . .	85
47	Critical Speed Map For J85-21 Engine Rotor Bearing System . . .	86
48	Undamped Mode Shape at First Critical Speed of J85-21 Engine Rotor System (Cantilevered Turbine Mode). . . . .	87
49	Undamped Mode Shape at Second Critical Speed of J85-21 Engine Rotor System (Compressor Bounce Mode) . . . . .	88
50	Calculated Unbalance Response For J85-21 Engine Rotor System With Random Distributed Unbalance . . . . .	89
51	Compressor Rotor Amplitudes For a First Fan Stage Blade Loss of The J85-21 Engine. . . . .	90
52	J85-21 Rotor No. 1 Bearing Radial Force For The First Fan Stage Blade Loss. . . . .	91
53	Turbine Rotor Amplitudes For a Third Stage Turbine Blade Loss of The J85-21 Engine . . . . .	92
54	J85-21 No. 3 Bearing Radial Force For The Third Stage Turbine Blade Loss. . . . .	93
55	J85-21 Rotor Bow Analysis - Landing Condition . . . . .	94
56	J85-21 Rotor Bow Analysis - Flight Condition. . . . .	95
57	J85-21 Rotor Bow Analysis - Catapult Condition. . . . .	96

# LIST OF ILLUSTRATIONS (continued)

<u>Figure Number</u>	<u>Title</u>	<u>Page</u>
58	Critical Speed Map For TF30 Low Rotor Bearing System. . . . .	97
59	Undamped Mode Shape at First Critical Speed For The TF30 Low Rotor System (Turbine Mode) . . . . .	98
60	Undamped Mode Shape at Second Critical Speed For The TF30 Low Rotor System (Compressor Bounce Mode) . . . . .	99
61	Calculated Unbalance Response For TF30 Low Rotor System With Random Distributed Unbalance. . . . .	100
62	Low Compressor Rotor Amplitudes For a First Fan Stage Blade Loss of The TF30 Engine . . . . .	101
63	TF30 Low Rotor No. 1 Bearing Radial Force For The First Fan Stage Blade Loss. . . . .	102
64	Low Turbine Rotor Amplitudes For a Third Stage Turbine Blade Loss of The TF30 Engine . . . . .	103
65	TF30 No. 4 Bearing Radial Force For The Third Stage Low Turbine Blade Loss. . . . .	104
66	TF30 Low Rotor Bow Analysis - Landing Condition . . . . .	105
67	TF30 Low Rotor Bow Analysis - Flight Condition. . . . .	106
68	TF30 Low Rotor Bow Analysis - Catapult Condition. . . . .	107
69	Critical Speed Map For TF30 High Rotor Bearing System . . . . .	108
70	Undamped Mode Shape at First Critical Speed For The TF30 High Rotor System (Cantilevered Turbine Mode). . . . .	109
71	Undamped Mode Shape at Second Critical Speed For The TF30 High Rotor System (Compressor Bounce Mode). . . . .	110
72	Calculated Unbalance Response For TF30 High Rotor System With Random Distributed Unbalance. . . . .	111
73	Compressor Amplitude For The High Rotor System of The TF30 Engine For a First Compressor Stage Blade Loss. . . . .	112
74	No. 1 Bearing Radial Load For a First Stage Compressor Blade Loss of The TF30 High Rotor System. . . . .	113
75	Turbine Amplitude For The High Rotor System of The TF30 Engine For a High Turbine Blade Loss. . . . .	114
76	No. 3 Bearing Radial Force For a Turbine Blade Loss of The TF30 High Rotor System. . . . .	115
77	TF30 High Rotor Bow Analysis - Landing Condition. . . . .	116
78	TF30 High Rotor Bow Analysis - Flight Condition . . . . .	117
79	TF30 High Rotor Bow Analysis - Catapult Condition . . . . .	118
80	Critical Speed Map For TF33 Low Rotor Bearing System. . . . .	119
81	Undamped Mode Shape at First Critical Speed of TF33 Low Rotor System (Low Turbine Bounce Mode). . . . .	120
82	Undamped Mode Shape at Second Critical Speed of TF33 Low Rotor System (Low Compressor Bounce Mode) . . . . .	121
83	Calculated Unbalance Response For TF33 Low Rotor System With Random Distributed Unbalance. . . . .	122
84	Unbalance Response Mode Shape at Operating Speed of 4500 RPM For The TF33 Low Rotor System . . . . .	123
85	Low Compressor Rotor Amplitudes For a First Fan Stage Blade Loss of The TF33 Engine . . . . .	124

# LIST OF ILLUSTRATIONS (continued)

<u>Figure Number</u>	<u>Title</u>	<u>Page</u>
86	TF33 Low Rotor No. 1 Bearing Radial Force For The First Fan Stage Blade Loss. . . . .	125
87	Low Compressor Rotor Amplitudes For a Second Fan Stage Blade Loss of The TF33 Engine . . . . .	126
88	Low Turbine Rotor Amplitudes For a Third Stage Turbine Blade Loss of The TF33 Engine . . . . .	127
89	TF33 No. 4 Bearing Radial Force For The Thrid Stage Low Turbine Blade Loss. . . . .	128
90	TF33 Low Rotor Bow Analysis - Landing Condition . . . . .	129
91	TF33 Low Rotor Bow Analysis - Flight Condition. . . . .	130
92	TF33 Low Rotor Bow Analysis - Catapult Condition. . . . .	131
93	Critical Speed Map For TF33 High Rotor Bearing System . . . . .	132
94	Undamped Mode Shape at First Critical Speed For The TF33 High Rotor System (Cantilevered Turbine Mode). . . . .	133
95	Undamped Mode Shape at Second Critical Speed For The TF33 High Rotor System (Compressor Bounce Mode). . . . .	134
96	Calculated Unbalance Response Vibration For The TF33 High Rotor With Distributed Unbalance. . . . .	135
97	Compressor Amplitude For The High Rotor System of The TF33 Engine For a First Compressor Stage Blade Loss. . . . .	136
98	No. 1 Bearing Radial Load For a First Stage Compressor Blade Loss of The TF33 High Rotor System. . . . .	137
99	Turbine Amplitude For The High Rotor System of The TF33 Engine For a High Turbine Blade Loss. . . . .	138
100	No. 3 Bearing Radial Force For a Turbine Blade Loss of The TF33 High Rotor System. . . . .	139
101	TF33 High Rotor Bow Analysis - Landing Condition. . . . .	140
102	TF33 High Rotor Bow Analysis - Flight Condition . . . . .	141
103	TF33 High Rotor Bow Analysis - Catapult Condition . . . . .	142
104	Critical Speed Map For Fan-Shaft Rotor System - TF39. . . . .	143
105	Undamped Mode Shape at First Critical Speed of TF39 Fan Spool . . . . .	144
106	Undamped Mode Shape at Second Critical Speed of TF39 Fan Spool . . . . .	145
107	Calculated Peak Unbalance Response Vibration For TF39 Fan Spool . . . . .	146
108	Shaft Amplitudes For Low-Rotor System For First Fan Stage Blade Loss. . . . .	147
109	Shaft Amplitude For Low-Rotor System For Second Fan Blade Loss. . . . .	148
110	Bearing Forces For No. 1 Bearing With Fan Blade Loss. . . . .	149
111	Shaft Amplitude For TF39 Low-Rotor System For Sixth Low Turbine Stage Blade Loss. . . . .	150
112	Bearing Forces For TF39 No. 3 and No. 4 Bearings For Low Turbine Blade Loss. . . . .	151
113	TF39 Low Rotor Bow Analysis - Landing Condition . . . . .	152



# LIST OF ILLUSTRATIONS (continued)

<u>Figure Number</u>	<u>Title</u>	<u>Page</u>
114	TF39 Low Rotor Bow Analysis - Flight Condition. . . . .	153
115	TF39 Low Rotor Bow Analysis - Catapult Condition. . . . .	154
116	Critical Speed Map For TF39 Gas Generator Rotor . . . . .	155
117	Undamped Mode Shape at First Critical Speed of TF39 Gas Generator Spool . . . . .	156
118	Undamped Mode Shape at Second Critical Speed of TF39 Gas Generator Spool . . . . .	157
119	Calculated Peak Damped Unbalance Response Vibration For TF39 Gas Generator Spool. . . . .	158
120	Rotor Amplitudes For a First Compressor Stage Blade Loss For The TF39 Gas Generator Spool. . . . .	159
121	No. 1 Bearing Force For First Compressor Stage Blade Loss For TF39 Gas Generator Spool. . . . .	160
122	Rotor Amplitudes For a Second Turbine Stage Blade Loss For The TF39 Gas Generator Spool. . . . .	161
123	No. 4 Bearing Force For Second Turbine Stage Blade Loss For TF39 Gas Generator Spool. . . . .	162
124	TF39 Gas Generator Spool Static Deflection - Landing Condition . . . . .	163
125	TF39 Gas Generator Spool Static Deflection - Flight Condition . . . . .	164
126	TF39 Gas Generator Spool Static Deflection - Catapult Condition . . . . .	165
127	Critical Speed Map For TF41 LP Rotor Bearing System . . . . .	166
128	Undamped Mode Shape at First Critical Speed of TF41 LP Rotor Bearing System. . . . .	167
129	Undamped Mode Shape at Second Critical Speed of TF41 LP Rotor Bearing System. . . . .	168
130	Calculated Peak Unbalance Response Vibration For TF41 LP Rotor Bearing System (Undamped) . . . . .	169
131	Low Compressor Rotor Amplitude For a First Fan Stage Blade Loss of The TF41 Engine . . . . .	170
132	TF41 Low Rotor System No. 1 Bearing Force For The First Fan Stage Blade Loss. . . . .	171
133	Low Turbine Rotor Amplitudes For a Second Turbine Blade Loss of The TF41 Engine . . . . .	172
134	TF41 Low Rotor System No. 4 Bearing Force For The Second Turbine Blade Loss. . . . .	173
135	TF41 Low Rotor Bow Analysis - Landing Condition . . . . .	174
136	TF41 Low Rotor Bow Analysis - Flight Condition. . . . .	175
137	TF41 Low Rotor Bow Analysis - Catapult Condition. . . . .	176
138	Critical Speed Map For TF41 HP Rotor Bearing System . . . . .	177
139	Undamped Mode Shape at First Critical Speed of TF41 HP Rotor Bearing System. . . . .	178
140	Calculated Peak Unbalance Response Vibration For TF41 HP Rotor Bearing System (Undamped) . . . . .	179

# LIST OF ILLUSTRATIONS (concluded)

<u>Figure Number</u>	<u>Title</u>	<u>Page</u>
141	Unbalance Response Mode Shape at 7,000 RPM For TF41 HP Rotor Bearing System (Undamped) . . . . .	180
142	TF41 High Compressor Rotor Amplitude For a First Stage Compressor Blade Loss . . . . .	181
143	TF41 High Rotor No. 1 Bearing Radial Load For a First Stage Compressor Blade Loss . . . . .	182
144	TF41 High Turbine Rotor Amplitude For a Second Stage High Turbine Blade Loss. . . . .	183
145	TF41 High Rotor No. 3 Bearing Radial Load For a Second Stage High Turbine Blade Loss . . . . .	184
146	TF41 High Rotor Bow Analysis - Landing Condition. . . . .	185
147	TF41 High Rotor Bow Analysis - Flight Condition . . . . .	186
148	TF41 High Rotor Bow Analysis - Catapult Condition . . . . .	187
149	Rotor Configurations and Classifications. . . . .	188
150	Rotor Configurations and Classifications. . . . .	189
151	Rotor Configurations and Classifications. . . . .	190
152	Rotor Configurations and Classifications. . . . .	191
153	Cylindrical Test Specimens. . . . .	192
154	Flexural Support Test Element . . . . .	193
155	Schematic of The Test Setup with a List of Equipment. . . . .	194
156	Pictorial View of Test Setup to Obtain Cylindrical Specimen Natural Frequency . . . . .	195
157	Hardness Measurements For The Flat Plate Test Element . . . . .	196
158	Hardness Measurements For The Shallow Cone Test Element . . . . .	197
159	Hardness Measurements For The Steep Cone Test Element . . . . .	198
160	Shell Modes Observed on The Thin Cylindrical Element During Vibration Excitation Tests. . . . .	199
161	Flexible Support Response at The Overhung Mass Section. . . . .	200
162	Flexible Support Response at The Overhung Mass with a 5.5 lb Mass Added. . . . .	201
163	Squirrel Cage Flexure Static Load Test. . . . .	202
164	Flexural Support Spokes . . . . .	203
165	Trapezoidal Representation of Spoke Cross-Section . . . . .	203
166	Calculated Unbalance Response at Turbine for TF33 Low Rotor System with Random Distributed Unbalance. . . . .	204
167	Calculated Unbalance Response at Turbine for J85-21 Engine Rotor System with Random Distributed Unbalance . . . . .	205
168	Calculated Unbalance Response at Compressor for J85-21 Engine Rotor System with Random Distributed Unbalance . . . . .	206
169	Calculated Unbalance Response at Turbine for J79 Rotor Systems with Random Distributed Unbalance . . . . .	207

## SECTION I

### SUMMARY

1. The dynamic characteristics of the major inventory of large Air Force jet engines have been determined, classified and compared using state-of-the-art analytical capabilities. Several simplifying assumptions were made for this analysis such as, the engine system was modeled as uncoupled single rotor units, and the stiffness of the bearing support was assumed to be equal to the engine mount stiffness to ground. These simplifying assumptions should be recognized in reviewing the analytical calculations. The calculations have not been verified using actual engine test data.
2. All of the jet engines studied had to either pass through critical speeds on their acceleration to the operating range or had critical speeds within the operating range. With dual spool engines (independent low pressure and high pressure rotors) the trend is towards more modes, higher sensitivity to unbalance and greater need to improve the rotor dynamic technology.
3. Test models which duplicate engine components are very sensitive to the fabrication technique. The stiffness of cones, hubs and flat plates should be experimentally determined from actual engine hardware. A parametric test sequence should be performed to provide a design tool for advanced technology engines.



## SECTION II

### INTRODUCTION

In recent years, the technology of rotordynamics for turbine engines has expanded to encompass the dynamic interaction of the rotor, its bearings, the bearing support structure, and in many cases the engine casing itself. It is fully recognized that rotordynamics considerations must be heeded as significant constraints upon the mechanical design of the engine.

Rotordynamic vibration considerations are important because the symptoms of vibration, if uncontrolled, can compromise the operational integrity and safety of the engine. The symptoms of large vibrations are:

- Large amplitudes of motion
- Lack of clearance control at critical locations
- Large dynamic stresses
- Large forces transmitted to the bearings
- Noise
- Catastrophic failures

Excessive vibration is not just an undesirable by-product which accompanies gas turbine engine problems. It is, rather, one of the most important sources of engine casualties, which evidence themselves as bearing and seal failure, cracking of entry guide vanes, cracking of diffusers, sumps, casing, exhaust annuli, bolt failures, rubbing of blade tips, and failure of auxiliary drives and control components, to name only a few problem areas.

Excessive vibration arises because the rate at which vibration energy is produced is not adequately counterbalanced by the rate at which it is dissipated in the engine. The science which permits this energy balance to be understood and controlled in a complex structure such as a gas turbine, is rotordynamics. The first step in understanding the problems of engine vibration is to obtain detailed, accurate information relative to current engine designs. Following discussion and review of various Air Force engines during the initial part of the investigations, the following engines were selected for evaluation:

<u>Engine</u>	<u>AF Management Center</u>	<u>Engine Manufacturer</u>
J57	OCAMA	P&WA
J79	OCAMA	GE
TF30	OCAMA	P&WA
TF33	OCAMA	P&WA
TF41	OCAMA	DDA
T56	SAAMA	DDA
J85	SAAMA	GE
TF39	SAAMA	GE

#### A. Engine Modeling

Design data had been gathered for these engines including rotor and bearing assemblies, subassemblies and detailed drawings. Using this data, the rotor assembly was analytically modeled to depict its mass and elastic characteristics. As shown in Figure I, small sections of the assembly were analyzed independently to obtain the weight, bending stiffness, shear stiffness, and inertial properties and then combined to make up the entire rotor analytical model.

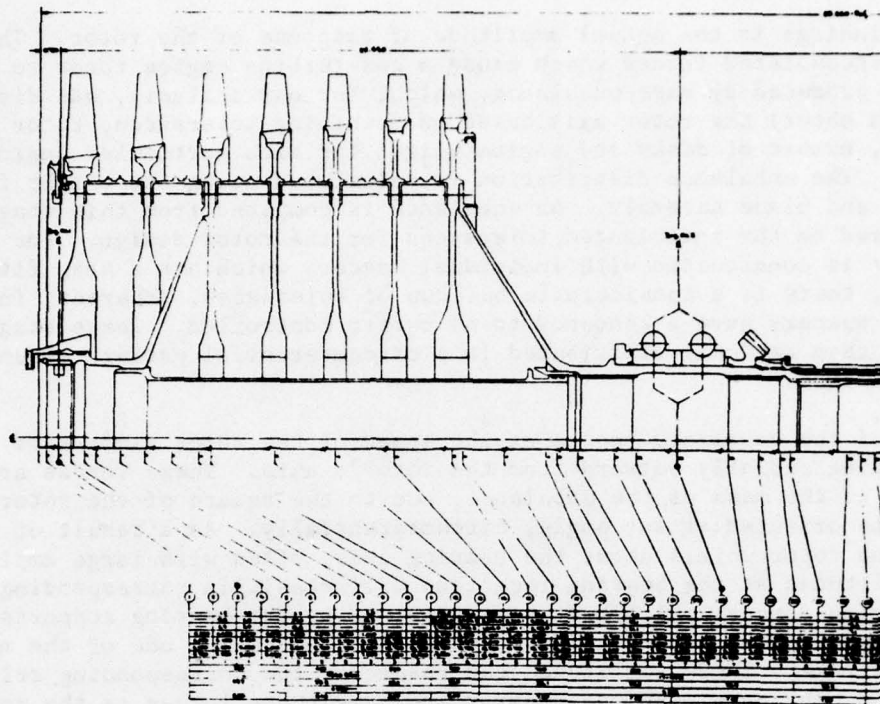


Figure I

#### B. Critical Speeds and Mode Shapes

The analytical effort for each engine model included the identification of the lateral critical speeds, unbalance response, blade loss effects and maneuver loads. A rotor lateral critical speed is, quite simply, the condition in which the rotor speed matches the undamped natural frequency of the rotor-bearing system. At such a frequency, the system's mass and elastic properties combine to form a resonant condition, in which relatively large amplitudes are possible at low input energy levels. Since the rotor is formed from shapes which have distributed mass, the system has infinitely many critical speeds. In practice, however, particularly in the case of turbine engine rotors in which mass tends to be somewhat concentrated in the form of disks, only the lowest several critical speeds are of interest.

When rotor operational speed is near one of its critical speeds, the rotor will vibrate with high amplitudes in a particular "mode" of vibration. The shape of the elastic axis of the rotor at the critical speeds were calculated in terms of relative amplitudes to examine the rotor displacement. Such a presentation shows the amount of rotor bending, which is an indication of rotor flexibility. The analytical study included the mode shapes for each engine study.

#### C. Rotor Unbalance

While the information obtained from the undamped critical speed map is very useful for evaluating the dynamic behavior of these rotor-bearing systems, it must be stressed that the mode shapes and critical speed maps are only intermediate results in the vibration analysis. An important analysis after these

initial findings is the actual amplitude of response of the rotor. The most commonly encountered forces which cause a gas-turbine engine rotor to respond are those produced by mass unbalance, which, for our analysis, was distributed along (and about) the rotor axis based on machining tolerances, rotor construction, number of disks and engine weight for each particular engine analyzed. The unbalance distribution is calculated using the weight from each disk and blade assembly. An unbalance is computed from this stage weight and is based on the anticipated tolerances for the rotor design. For example, if a rotor is constructed with individual spacers which are a snap fit to each disk, there is a considerable buildup of tolerances. Whereas, integral disks and spacers have a tendency to be better controlled. These stage unbalances are then randomly distributed in a circumferential pattern around the rotational axis.

Rotation of the unbalance masses at the speed of the rotor gives rise to forces acting radially outward from the rotor's axis. These forces are proportional to the mass of the unbalance, and to the square of the rotor speed. They may be oriented at any angle, circumferentially. As a result of these forces, the rotor whirls about the bearing axis, often with large amplitudes. Large amplitudes at the bearing locations will result in correspondingly large bearing forces, which must be restrained by the bearing supports. When the unbalance forces are distributed such that they match one of the mode shapes, extremely large amplitudes can result at the corresponding critical speed. The unbalance response program analyzes these forces as the rotor increases in speed and calculates the rotor deflections as the critical speeds are traversed.

#### D. Blade Loss

The blade loss analysis is an extension of the unbalance response calculations. The loss of an airfoil caused by high frequency fatigue, foreign object damage, or stress rupture, etc., can cause a very large unbalance on the rotor at a discrete axial and circumferential location. An unbalance, which simulates the airfoil weight at the radius of the airfoil cg, was applied to each rotor at the design speed. The response of the rotor and the resultant bearing loads were calculated as the rotor was decelerated through its critical speeds.

#### E. Maneuver Loads

The maneuver load conditions were derived from the accelerations to be expected during landing, flight or catapult conditions. The g forces resulting from these maneuvers are a combination of down loads and side load factors. These have been combined vectorially and are shown in Table I. These loads have been applied to each mass along the rotor to determine the rotor bow deflections for each engine model.

TABLE I

<u>Condition</u>	<u>Down Loads</u>	<u>Side Load</u>	<u>Total Load</u>
Flight ( $\pm 2$ rad/sec)	6.0 g	4.0 g	7.2 g
Flight	10.0 g	1.5 g	10.1 g
Landing	10.0 g	2.0 g	10.2 g
Catapult	5.5 g	2.0 g	5.85 g



#### F. Engine Tests

The analytical results discussed in this report are only useful when they duplicate experimental hardware. There is a need to collect data on the vibration response of each engine model. This will not only assist in the verification of the analysis but will also show the variations in critical speed location which must be taken into account from engine to engine. If there are critical speeds just outside the operating range, the tolerance on components such as bearing supports, external cases and support vanes play an important part in determining if the resonance will be a potential problem for a percentage of the engines built.

As a general rule, the support stiffness between the rotor and the external engine case is about the same magnitude as the engine support stiffness to ground. For lower modes, the case will respond at one half the value of the rotor journal. Since the vibration sensors are mounted on the case, the observed amplitudes are much lower than the rotor midspan. The trend is toward more flexible rotors which will eventually require bearing mounted seismic sensors and shaft proximeters to monitor engine vibration.

There are certain techniques for taking this data which are important if the information is to be useful at some future date. During slow accelerations and decelerations of the engine, vibration data from the bill-of-material engine vibration sensors should be recorded using a tracking filter to obtain the rotor participation. Part of the Engine Dynamic Behavior section gives critical speeds in the form of mode shapes. This should provide information for the most sensitive location of sensors to obtain the rotor dynamic characteristics of the particular engine model. But, this only provides a very general guideline for the jet engines described in this text. The importance of this area indicates the need for the Air Force to take a positive role in specifying allowable vibration levels, instrumentation, monitoring, test techniques, and technical approval of new engines and existing engines for new applications.

In the area of instrumentation and monitoring equipment, the classification of jet engines into types is an excellent method of accurately measuring vibration. The vibration sensor locations can be specified for three separate classes of rotating machinery. These locations can be incorporated during the development and certification test of the engine model. During the production acceptance test of each engine, or if the engine model has been used in service for a representative period of time, the engine manufacturer may want to specify a reduced number of vibration sensors if the dynamic characteristics of the engine are easily detectable. A class 1 engine are those which are lightweight, such as auxiliary power units or small aircraft engines. Class 1 engines use antifriction type bearings and the rotor weight is generally 1/3 or more of the total engine weight. Class 2 gas turbines use fluid film bearings or squeeze film dampers in series with antifriction type bearings and the rotor weight is generally less than 1/3 of the total engine weight. There is some question as to where oil film

dampers would fit. But, when you consider the transmissibility of vibrations through an oil film, the characteristics would be more toward that of a journal bearing than an antifriction bearing and support structure. Also, as rotors become more flexible, it will become necessary to directly measure shaft motion to obtain any degree of sensitivity for monitoring rotor vibration. These flexible rotors will require squeeze film dampers to dissipate energy and seem to fit most favorably in Class 2.

The Class 3 rotating machinery is designated for shaft and spool pieces which are used to interconnect the engine drive train such as a helicopter tail rotor shafts. The type of vibration sensor is to be capable of accurately recording displacement, velocity, or acceleration within the frequency of the specific gas turbine model.

Class 1 - Vibration Sensors are to be located on one of the engine case flanges at each interface with a main rotor support. In addition, sensors for measuring both horizontal and vertical motions are required at each mounting plane. If an engine mount plane coincides with a rotor support interface, one vibration sensor to record horizontal motion and one to record vertical motion are acceptable.

Class 2 - At least one vibration sensor for each major subassembly, such as the low pressure compressor or drive turbine, should be located at the bearing housing. These sensors must be capable of indicating vibration in two planes. For bearing supports with oil film dampers or journal bearings, each vibration sensor must consist of a probe to measure shaft motion and a sensor to measure bearing housing motion.

Class 3 - Vibration Sensors are to be mounted on all shaft supports including those which interface with major drive train components. These sensors are required to measure vibration in only one plane. The probes should measure shaft motion if the support bearings are fluid or squeeze films. For shafts mounted in antifriction bearings, the sensors can be used to measure bearing housing vibration.

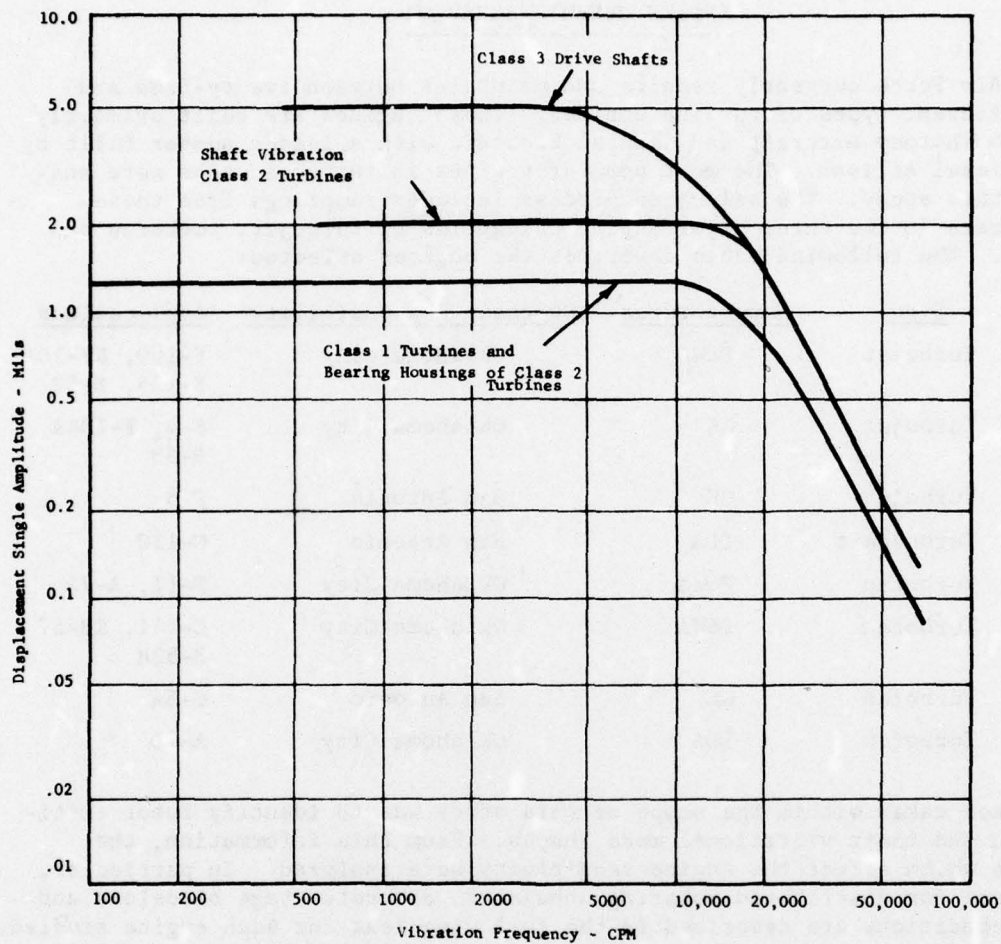
Once the sensory location has been determined, the engine must be tested in a manner which provides as much information as possible and then this vibration information has to be evaluated for acceptability.

A plot of the continuous transient and steady state vibrating response versus rotor speed for each vibration sensor should be made. The continuous transient response data consists of the overall vibration signal versus rotor speed. If at any point the overall vibration signal exceeds defined limits (example limits are shown in Figure II), a spectral analysis of the signal should be made to show that each individual component of the overall signal does not exceed these limits. This should be verified at any speed up to and including maximum overspeed, under steady state and transients operating conditions.

The Drive Train system vibration acceptance test to be performed by the aircraft manufacturer with the engine installed in its final drive system configuration will consist of two accelerations and decelerations from idle to 102% normal rated speed. Vibration levels induced in the installed engine, drive train and airframe by components of the specific driven system, including, but not limited to, propeller blade, shafting, controls, clutches, couplings, external auxiliaries, and gearing, shall not exceed the vibration limits described above at any speed up to and including maximum overspeed, under any operating conditions including steady state and transients.



Figure II - Sample Allowable Vibration Limits



The engine test technique and instrumentation described above should be used to provide the technical data required to make evaluations of the jet engine rotordynamics. The eight engines selected in this study have been modeled and analyzed for critical speeds, unbalance response, blade loss effects, and maneuver deflections. These types of analyses have been described above. The next section presents the detailed rotordynamics results for each engine.



SECTION III  
ENGINE DYNAMIC BEHAVIOR

The U.S. Air Force currently repairs and maintains between twenty-five and thirty different types of turbine engines. These engines are built primarily by Pratt & Whitney Aircraft and General Electric with a lesser number built by Detroit Diesel Allison. The most popular engines in terms of usage were analyzed in this study. The selection process included samplings from these manufacturers in the three major engine categories of turbojet, turbofan and turboprop. The following table describes the engines selected:

<u>Engine</u>	<u>Type</u>	<u>Manufacturer</u>	<u>Overhaul Responsibility</u>	<u>Applications</u>
J57	Turbojet	P&WA	Oklahoma City	F-100, RF-101 F-105, B-52
J79	Turbojet	GE	Oklahoma City	F-4, F-104A B-58
J85	Turbojet	GE	San Antonio	F-5
T56	Turboshaft	DDA	San Antonio	C-130
TF30	Turbofan	P&WA	Oklahoma City	F-11, A-7A
TF33	Turbofan	P&WA	Oklahoma City	C-141, RB-57 B-52H
TF39	Turbofan	GE	San Antonio	C-5A
TF41	Turbofan	DDA	Oklahoma City	A-7D

The approach taken within the scope of this study was to identify rotor critical speeds and their vibrational mode shapes. From this information, the parameters which affect the engine sensitivity were analyzed. In particular, the response for distributed rotating unbalance, discrete stage bladefloss and maneuver conditions are described in the following text for each engine studied. In some cases, the reasons for excessive rotor sensitivity have been identified. The trends in rotor system flexibility and the resultant response can be obtained from this study.

A. T56-15 Engine

The T56 turboprop engine consists of a fourteen stage compressor and four stage turbine supported on four main rotor bearings. The critical speed map for this engine is shown in Figure 1. Figures 2 and 3 indicate that there is a turbine vibration mode below idle and a compressor vibration mode within the operating range for a nominal design stiffness. The compressor and turbine stages are straddle-mounted, which would indicate there is support damping from both bearings. A closer look at the mode shape for the compressor critical speed of 11,345 rpm shows the No. 2 bearing to be almost nodal because of the very flexible rear hub of the compressor. The rotor response to distributed unbalance is given in Figure 4 and bears out the higher sensitivity due to compressor unbalance at the 11,300 rpm resonance. The rotor is fairly insensitive to turbine unbalance (0.7 oz-in.) with a maximum rotor deflection of 1.2 mils. The compressor rotor response is 8.0 mils for a randomly distributed unbalance of 6 oz-in. This is an unacceptably high level of vibration caused by the flexibility of the integral 14th stage compressor disk and No. 2 bearing

hub. These calculations would indicate that the compressor would require precision balancing during assembly and field trim balancing operations will probably be frequent.

The blade loss response for the first stage compressor is shown in Figures 5 and 6. Even though the compressor critical speed is very sensitive, the lightweight airfoils help to keep the response down. The maximum rotor deflection of 60 mils occurs at the 11,300 rpm resonance which will have to be traversed during the deceleration. Combined with a No. 1 bearing load of 20,000 lbs, the rotor will probably rub on the case and seals with minor damage to the bearing.

The turbine foils are somewhat larger and, even though the turbine resonance is less sensitive than the compressor mode, the increased unbalance from a blade loss in the turbine negates the lower sensitivity. Because the turbine has tighter seal clearances than in the compressor, the rub damage could be extensive. The turbine rotor deflection and bearing load for a fourth stage turbine blade loss are shown in Figures 7 and 8. The 90 mil deflection and 17,500 lb bearing load would cause the blades to extensively rub the case and seals. The bearing will also be permanently deformed under this cyclic loading. Although the turbine bearing support should accept this transient loading without being overstressed, the total engine damage could be moderate to heavy.

The maneuver deflections for the T56 engine rotor during landing, flight and catapult conditions are shown in Figures 9 through 11. Because of the very flexible rear compressor hub, the rotor bow analysis shows a severe change in slope in the compressor, which causes the number two bearing journal to be deflected upward during the maneuver loads. The hinge joint at the compressor shaft is obvious and shows that the compressor and turbine modules act almost independently. The compressor bow is only 2.7 mils and the turbine deflection is 5.7 mils. Both modules are very tolerant to the g load conditions and no seal rubbing or performance loss would be anticipated.



## B. J57 Engine

### 1. J57 Low Rotor Dynamic Behavior

The J57 is a dual-spool turbojet engine. The low rotor consists of a nine-stage compressor and two-stage turbine mounted on three main bearings with an additional intershaft roller bearing between the high and low shafts. The critical speed map for the J57 low rotor is shown in Figure 12. For the nominal design springrates, the low turbine critical speed is within the operating range of 4000 rpm to 6800 rpm. The compressor mode at 10,736 rpm is well above maximum speed. The compressor mode shape does show participation of the No. 2 ball bearing. Since this is a thrust bearing, the radial springrate will vary somewhat due to the thrust load. But, since this resonance is so far above the operating speed, the variations in No. 2 bearing springrate due to axial loads are not expected to affect the system dynamics within the operating speed range of the J57 low rotor. The undamped mode shapes for these two resonance are shown in Figures 13 and 14. The turbine mode is typical of most jet engines. Because the turbine exhaust case bearing support structure is normally soft to accept thermal transients, the turbine critical speed is low with most of the motion at the No. 4 bearing support. The compressor, on the other hand, is supported on hard bearings and case structure. The compressor rotor spacers are at a larger diameter which compensates for the increased bearing-to-bearing distance. The net result is to have compressor modes either near maximum speed or above the operating range of the machine.

Figure 15 shows the response of the J57 low rotor for random distributed unbalance. The compressor mode is so far above the speed range that the rotor does not respond to the 2.3 oz-in. in that mode, but the turbine unbalance of 1.5 oz-in. is a prime factor in the observed vibration levels. The peak rotor response is 2.7 mils at the turbine critical speed of 5625 rpm.

The rotor response and bearing loads for blade losses in the compressor and turbine are shown in Figures 16 through 19. Even though the compressor mode is well above maximum speed, the unbalance created by a compressor blade loss is not something to be neglected. At 6800 rpm, the amplification factor to this mode is small but the unbalance is very large. The compressor rotor only deflects 11 mils but the bearing load is 7500 lbs. This is the effect of a stiff rotor with large unbalances. Multiple airfoil losses would surely guarantee bearing failure.

The turbine blade loss dynamics are also very severe. Since the turbine mode is in the engine operating speed range, heavy engine damage cannot be avoided. The free rotor deflection of 250 mils would definitely cause blade, seal and case damage. Bearing load of over 40,000 lbs. would probably cause failure of the turbine case bearing support rods. The low shaft would probably rub on the high turbine disk, failing the shaft and releasing the entire turbine section. Only the energy absorption created by blade-to-stator meshing is available, and is not considered sufficient to reduce the extensive damage expected for a low turbine blade loss.

The rotor bow analysis is shown in Figures 20 through 22. The maximum deflection of 12.5 mils occurs at the turbine because the relatively soft No. 4 bearing support is the controlling element for maneuver load deflections. This deflection is not severe enough to cause extensive seal rub and will probably not be detrimental to the overall engine performance.



## 2. J57 High Rotor Dynamic Behavior

The J57 high rotor consists of a straddle-mounted, seven-stage high compressor with a cantilevered, single-stage turbine on three bearing supports. The critical speed map for the J57 high rotor is shown in Figure 23. At the nominal bearing support stiffness, there are two modes of concern. The first is the cantilevered turbine mode shown in Figure 24. This mode is below the operating range at 4077 rpm. The second mode, Figure 25, is the compressor critical speed (predominantly cylindrical rotor motor) which is calculated at 11,090 rpm and is just above the operating range of 6000 rpm to 10,000 rpm. Both critical speeds are very sensitive to unbalance as is shown in the unbalance response plot of Figure 26. But, since the operating range is between these modes, the maximum rotor deflection is only 0.9 mil for 1.8 oz-in. of rotor unbalance. In addition, the acceleration and deceleration rates are fast enough to avoid excessive amplitude buildup at the turbine critical speed.

Vibration test data on several engines would be a good indication of the production tolerances on the rotor support stiffnesses. For bearing supports without oil dampers, these stiffnesses are primarily controlled by the compression springrate of the vanes and the shell type bending stiffness of the case as the load from these vanes is distributed to the outer case. With these thin members, the tolerances could cause a  $\pm 10\%$  variation in springrate.

For the J57 high rotor, these springrates have to be very close to the calculated values or else there will be more response at the top end of the operating range, due to a drop in the compressor mode, or response at the low end due to an increase in the turbine critical speed. The blade loss loads are also affected by these tolerances.

Figures 27 and 28 show the dynamic response and bearing loads for the first-stage high compressor blade loss. The maximum rotor deflection is 4.0 mils and the No. 1 bearing radial load is 3700 lbs. Both values occur at the maximum operating speed of 10,000 rpm and show a sharp increase in response for increasing speed, which enforces the need for strict control of the compressor bearing support springrates. The turbine blade loss response and bearing loads are shown in Figures 29 and 30. Even though the turbine mode is not in the operating range, the engine must pass through this resonance during the deceleration. The question becomes how fast can the rotor decelerate to prevent a high response? The maximum displacement is 200 mils with a bearing load of 10,000 lbs. These values would indicate severe damage potential but the sharpness of the peak holds out some hope for a rapid transient to avoid such high amplitudes. With this type of response and a reasonable excursion rate, blade rubbing and curling should be expected with the associated damage to the case and seal structure. Bearing damage will probably be avoided and little or no damage to the bearing support structure would be expected. So, the total engine damage would be classified in the moderate range.

The J57 rotor deflected shapes from the bow analysis are shown in Figures 31 through 33. The cantilevered turbine is sensitive to maneuver loads, deflecting over 24 mils which would indicate potential seal rub and performance degradation.

### C. J79 Engine

The J79 engine rotor system consists of a seventeen-stage compressor and three-stage turbine mounted on three bearings and supports. The compressor section is mounted on a roller bearing at the number one location and a single row ball bearing at the number two position. This ball bearing serves a dual purpose by being the rear support of the compressor and the front support of the turbine. The turbine section is also supported in the rear by a roller bearing. The critical speed map for this rotor-bearing system is shown in Figure 34. The first mode at 5516 rpm, shown in Figure 35, is the turbine critical and is dependent upon the stiffness and damping of the No. 3 roller bearing. The second mode at 6869 rpm, shown in Figure 36, is the compressor bounce critical speed with both the first and second bearing supports participating in the deflected shape. These mode shapes show that the compressor and turbine modes are not isolated. There is some compressor deflection at the turbine mode and visa versa. What this means is that unbalance in the compressor will excite the turbine mode causing vibration at the No. 3 bearing even if the turbine is well balanced. Also, for the opposite condition of a well balanced compressor with the unbalance in the turbine, the compressor rotor will vibrate at the 6869 rpm critical speed.

A distributed unbalance must be applied to this rotor system to obtain the response and effective sensitivity. The unbalance distribution is calculated using the weight from each stage's disk and blade assembly and computing an unbalance based on the machining tolerances for the type of rotor construction (separate spacers, integral disk and spacers, curvic couplings, doweled bolts, etc.). These stage unbalances are then randomly distributed in a circumferential pattern around the rotational axis.

The rotor response to 3.3 oz-in. of distributed unbalance is shown in Figure 37 and bears out the mode shape predictions. Notice that the compressor rotor is responding at the turbine critical speed and the turbine rotor is vibrating at the compressor resonance. Additionally, the turbine mode is fairly sensitive and the narrow peak indicates very little damping from the No. 3 bearing support. The dynamic condition of this rotor-bearing system presents a maintenance nightmare. If an engine is vibrating over acceptable limits at the 5516 rpm critical speed, the response could be caused by unbalance in either module; therefore, some trial and error procedure has to be used to determine the location of the unbalance. It is also possible to unbalance one module to compensate for the other with the result being a low response at 5516 rpm, but, when the rotor is accelerated to 6819 rpm, the vibration will get worse, causing the operator to repeat the entire balancing procedure at the higher speed. This procedure does not guarantee that the new correction weights have not caused an unbalanced condition at the first resonance.

Because of the interaction of compressor and turbine response, the blade loss analysis includes turbine deflection for compressor blade loss and vice versa. In addition, two compressor blade loss stations were analyzed because of the turbine mode shape. The first stage of the compressor is almost nodal at the turbine critical speed; therefore, the turbine would not respond during this condition. But, for blade loss stages further back in the compressor, the turbine critical speed will respond causing turbine rotor deflections.



The first-stage compressor blade loss response is shown in Figures 38 and 39. The rotor deflection is 47 mils and would not be considered severe but the No. 1 bearing load of 30,000 lbs would probably cause permanent damage and further deflection of the rotor resulting in some blade curling and seal rub. The engine damage would be classified in the moderate range. A blade loss analysis was also done for the third-stage compressor to determine the effect on the turbine mode at 5516 rpm. Figures 40 and 41 show the rotor deflection and bearing loads for this event. If a blade is lost near maximum speed, the compressor module will deflect 32 mils at the upper mode and 16 mils at the lower mode. The turbine module will respond to the excitation created by this large compressor unbalance. The turbine will deflect 60 mils at the 5516 rpm critical speed during the deceleration. The peak is sharp which would indicate a potential reduction in vibration for a rapid deceleration. The bearing loads are at marginal levels. Minor bearing damage such as scoring of the inner and outer races is possible. A multiple blade loss or downstream damage from a single blade loss would cause extensive damage to both the compressor and turbine modules.

The rotor response to a third-stage turbine blade loss is shown in Figures 42 and 43. The deflection and bearing loads are not severe for the 6819 rpm critical speed. But, both the compressor and turbine modules have excessive response as the heavily unbalanced turbine is decelerated through the lower mode. It would be anticipated that both the No. 2 and No. 3 bearings would fail and the rotor vibration would cause extensive damage to the blades, seals and case structure of both the compressor and turbine modules.

The J79 engine rotor maneuver deflections for landing, flight, and catapult conditions are shown in Figures 44 through 46. The maximum bow of 13.1 mils at the last turbine stage is caused by the deflection of the relatively soft number three bearing support. The turbine tip seal clearance would probably accept this transient turbine motion without rubbing. No performance degradation would be anticipated except for the most severe g load conditions.



#### D. J85-21 Engine

The J85-21 is a single-spool turbojet engine with a nine-stage compressor and two-stage, cantilevered turbine mounted on three bearing supports. The critical speed map for this system is shown in Figure 47. There are two modes within the operating range. For the nominal bearing support stiffness, the turbine mode is at 9697 rpm and the compressor resonance occurs at 13,192 rpm. The undamped mode shapes, shown in Figures 48 and 49, are typical for cantilevered turbines and straddle-mounted compressors. There is some compressor displacement for the turbine mode and turbine response at the compressor critical speed. This creates some interaction as is shown in the engine response for random distributed unbalance, Figure 50. Partly due to the high operating speed, both modes are sensitive to unbalance. The compressor and turbine modules must be precision balanced before assembly to prevent vibration rejections. The rotor deflections are 7.0 mils for .25 oz-in. in the compressor and 3.9 mils for .15 oz-in. in the turbine. As a general rule, the stiffness between the bearing and the case is about the same as the stiffness between the case and ground. Therefore, the case will respond at one half the value of the rotor. Since the vibration sensors are mounted on the case, the observed amplitudes are lower than the rotor response. The assembly has to be closely balanced to result in a very small residual unbalance and lower rotor response.

Figures 51 through 54 show the rotor response and bearing loads for a blade loss in either the first compressor or last turbine stages. As stated before, these modes are sensitive to unbalance and the blade loss cases only point this problem out more directly. For the compressor blade loss, the deflections and loads would indicate severe blade, case and seal damage. The bearing would probably be permanently deformed depending upon secondary load paths through the shrouded blades during rubbing. It should be noted that the deflected shape of the rotor would be similar to the undamped critical speed shape of Figure 49. This would indicate that blade-to-case contact would be observed for the entire compressor. For the turbine blade loss condition, the resultant rotor damage would also be severe. Blade, case, seal and bearing damage would be anticipated. The turbine bearing support structure is not a telescoping rod type construction (ref. J57 turbine support) and may be capable of withstanding the transient loads without failure. But, for either blade loss case, the engine damage would be classified in the heavy range.

The J85-21 rotor is lightweight and relatively stiff. The resonances are high but so is the operating range which makes the response and blade loss dynamics a problem. The maneuver deflections, on the other hand, are very low because of this high stiffness-to-mass ratio. The results of the rotor bow analysis are shown in Figures 55 through 57. The cantilevered turbine shows the typical deflected shape but the maximum deflection is only 5.0 mils. The J85 engine should be insensitive to maneuver deflections.

## E. TF30 Engine

### 1. TF30 Engine Low Rotor Dynamic Behavior

The TF30 low rotor has a three-stage fan and six-stage compressor section straddle-mounted on an oil damped No. 1 bearing and a single-row, axial thrust bearing at the No. 2 location. The shaft and three-stage turbine are supported by an intershaft bearing approximately midspan of the low shaft and an oil-damped roller bearing at the turbine exhaust case. The intershaft bearing is located between the high and low rotors. Because the high rotor has a larger diameter and has ground supports near the intershaft connection, the low rotor is successfully supported by this interconnection. The surface speed of the rollers is relatively low because the bearing actually observes only the difference in rotational speed of each rotor.

The critical speed map, Figure 58, shows two natural frequencies within the operating speed range. The undamped mode shapes are shown in Figures 59 and 60. The first critical speed is the turbine mode and is dependent upon the springrate and damping characteristics of the No. 4 bearing oil damper. The second mode is the compressor critical speed and is influenced by the damper at the No. 1 bearing location. These oil damper springrates are sensitive to oil temperature, machinery tolerances and unbalance load. It should, therefore, be expected that both critical speeds will vary from engine to engine because of these effects. Even though there are two critical speeds within the operating range, the response of the rotor to random distributed unbalance, Figure 61, does seem to be fairly well suppressed by these dampers. The turbine rotor response for 2.3 oz-in. of unbalance is less than 0.5 mil and the compressor rotor response for 3.0 oz-in. of unbalance at its critical speed is 2.0 mils. It should be noted that case vibration sensors will record approximately one half the value because the stiffness between the rotor and the case is approximately the same as that between the case and ground.

The blade loss response is shown in Figures 62 through 65. With both critical speeds in the operating range, they would have to be traversed during the deceleration. Because of the heavy unbalance created by a fan stage blade loss, the compressor deflection would cause interference with the case. With the shrouded fan blades, alternate load paths may be created which will save the bearing but severe compressor blade, case and seal damage would be anticipated. The turbine blade loss condition is not any better. Even though the unbalance created by the airfoil loss would be less, the No. 4 bearing support is somewhat softer resulting in deflections which would cause blade-to-case rubbing and seal damage.

The results of the three rotor bow analyses (landing, flight and catapult conditions) are shown in Figures 66 through 68. The landing condition is the most severe and could cause 8.6 mils of rotor deflection in the compressor and 17.0 mils of rotor deflection in the turbine. The turbine rotor will probably "kiss" the case resulting in a small increase in seal clearance.

### 2. TF30 High Rotor Dynamic Behavior

The TF30P-100 high rotor consists of a seven-stage compressor mounted on a front roller bearing and a single-row ball bearing at the compressor exit. The single-stage turbine is cantilevered from the No. 3 roller bearing.

The critical speed map for this system is shown in Figure 69. At the nominal design bearing stiffness, there are no critical speeds within the operating range.



The cantilevered turbine mode at 5362 rpm, Figure 70, is below idle and the compressor critical speed, Figure 71, at 17,107 rpm is above redline speed. The turbine natural frequency is dependent upon the springrate and damping of the No. 3 bearing and support. The compressor mode shape shows almost equal participation from both the No. 1 and No. 2 bearings. Since the No. 2 bearing is a ball bearing, the radial springrate is dependent upon the axial thrust load. Within this study, it was not possible to obtain compressor critical speeds as a function of thrust load, but instead, a maximum value of springrate was used. Therefore, this resonant speed will probably vary as a function of thrust load and may occur at the top of the operating speed range.

The response for 4.5 oz-in. of distributed unbalance is shown in Figure 72. The rotor is operating in the valley between critical speeds so the amplitude is less than a mil for the entire speed range. But, at the maximum speed, the rotor is approaching the steep part of the response curve and, with variations in thrust load on the No. 2 bearing, may respond to the compressor critical speed. The rotor is relatively insensitive to the airfoil loss unless the compressor mode drops down into the speed range. As is shown in Figures 73 and 74, the rotor deflection is only 1.5 mils with an associated bearing radial load of 1250 lbs. The turbine blade loss is not as mild. The high turbine resonance must be traversed during the deceleration. The response is shown in Figures 75 and 76. A maximum displacement of 50 mils with a bearing load of 7000 lbs could be expected. The peaks are fairly broad which precludes a rapid deceleration to avoid high response. Some blade, case and seal damage is expected, but without permanent deformation of the bearing or support housing. The damage would probably be classified in the moderate range.

The rotor bow results are shown in Figures 77 through 79. The high turbine deflects over 16 mils during the landing condition. This is mainly caused by the cantilevered construction. The rear bearing support only deflects 7.5 mils and the remainder is caused by the slope of the overhung stage. Seal rub and performance degradation are possible after this maneuver condition.



## F. TF33 Engine

### 1. TF33 Low Rotor Dynamic Behavior

The TF33 low rotor is supported on four bearings. The two fan stages and seven compressor stages are straddle mounted on a roller bearing in the front and a double-row ball bearing at the rear of the compressor. Two roller bearings support the turbine and shaft, one of which is an intershaft bearing between the two rotor systems. Figure 80 shows the undamped critical speed map for the TF33 low rotor system. For the nominal design bearing support springrates, only the low turbine mode, shown in Figure 81, is within the operating ranges of 3300 rpm to 6900 rpm. The second critical speed, which is a low compressor mode shown in Figure 82, is above the operating speed at 8576 rpm. It should be noted that the third critical speed is the low shaft mode. The mode is well above the operating range because of the stiff support created by the intershaft bearing. That bearing is extremely important to the structural integrity of the low rotor system. Without it, or if it were relatively soft, the shaft bending mode would cause severe engine damage in the form of shaft rub and eventual failure.

The response analysis is shown in Figure 83. This analysis applies a random distributed unbalance to the rotor based upon machining tolerances and mass distribution. The results show the low turbine mode, which is in the operating range, is very sensitive to 1.2 oz-in. of turbine unbalance. Without an oil damped bearing, the soft low turbine bearing support allows the rotor to vibrate with relatively small amounts of unbalance. Figure 84 shows the peak amplitudes along the rotor axis at the low turbine bounce mode. As much as 7 mils of rotor displacement could be expected with this unbalance. The turbine module must be well balanced to avoid vibration induced failures.

Because the low compressor mode is above the operating range, the response to 1.6 oz-in. of unbalance is relatively small. Both front bearing supports respond in this mode thereby adding damping to the system and reducing the sensitivity to unbalance. But, if the calculated springrates for the compressor bearing supports are too stiff, this mode could be responding at the upper end of the speed range since the engine running range is in the steep part of the response curve. Figures 85 through 87 show the rotor response and No. 1 bearing loads for the loss of a blade at either the first or second fan stage. The rotor response for the first and second stage fan blade loss were almost identical. The difference in unbalance between the stages is offset by their relative radial deflections. Even though the compressor mode is above the operating range, the rotor is starting to be influenced by this critical speed. Coupled with the large unbalances created by a fan stage blade loss, the rotor response is approximately 50 mils at maximum speed and will reduce with decreasing speed. The No. 1 bearing radial load is 28,000 lbs at 6900 rpm. The rotor will thus deflect into the case causing seal, blade and static structure damage. The first fan blade has a mid-span shroud, which may prevent bearing failure by creating alternate load paths, relieving the bearing loads and prevent failure.

The turbine rotor response is shown in Figure 88. Since the turbine mode is very sensitive to unbalance, the blade loss response is extreme. The calculated free rotor deflection is 780 mils and the bearing force, shown in Figure 89, is over 100,000 lbs. This would definitely indicate blade, seal and static structure damage as well as bearing failure and possibly a failure of the bearing supports.

The rotor deflections from maneuver and landing conditions are shown in Figures 90 through 92. The softness of the low turbine bearing support ( $1.5 \times 10^5$  lb/in.) dominates the deflected shapes, causing the maximum motion of 20 mils to occur right at the bearing. The compressor section is only slightly affected with a center span deflection of 5.5 mils. This turbine deflection is fairly severe with blade/tip seal contact and scuffing expected.

## 2. TF33 High Rotor Dynamic Behavior

The TF33 high rotor consists of a straddle-mounted, seven-stage, high compressor with a cantilevered, single-stage turbine on three bearing supports.

The critical speed map for the TF33 high rotor is shown in Figure 93. At the nominal bearing support design stiffness, there are two modes of concern. The first is the cantilevered turbine mode shown in Figure 94. This mode is below the operating range at 4077 rpm. The second mode, Figure 95, is the compressor critical speed which is calculated at 11,090 rpm and is just above the operating range of 6000 rpm to 10,000 rpm. It is very possible that the rotor bearing system was designed with this dynamic characteristic in mind (i.e., to have normal operating in the "response valley" between two critical speeds). Both critical speeds are very sensitive to unbalance as is shown in the unbalance response plot of Figure 96. But, since the operating range is between these modes, the maximum rotor deflection is only 0.9 mil for an .8 oz-in. unbalanced rotor. In addition, the acceleration and deceleration rates are fast enough to avoid excessive amplitude buildup at the turbine critical speed. This is an ideal situation but the test results could be somewhat different. Vibration test data on several engines would be a good indication of the production tolerances on the rotor supported stiffnesses. These springrates have to be very close to the calculated values or else there will be more response at the top end of the operating range, due to a drop in the compressor mode, or response at the low end due to an increase in the turbine critical speed.

Production tolerances in support springrates play an important role in predicting the blade loss response because the ends of the operating range are at the steep parts of the response curve. Figures 97 and 98 show the dynamic response and bearing loads for the first-stage high compressor blade loss. The maximum rotor deflection is 4.0 mils and the No. 1 bearing radial load is 3700 lbs. Both values occur at the maximum operating speed of 10,000 rpm and show a sharp increase in response for increasing speed, which reinforces the need for strict control of the compressor bearing support springrates. The turbine blade loss response and bearing loads are shown in Figures 99 and 100. Even though the turbine mode is not in the operating range, the engine must pass through this resonance during the deceleration. The question becomes how fast can the rotor decelerate to prevent a high response? The maximum displacement is 200 mils with a bearing load of 10,000 lbs. These values would indicate severe damage potential, but the sharpness of the peak holds out some hope for a rapid transient to avoid such high amplitudes. With this type of response and a reasonable excursion rate, blade rubbing and curling should be expected with the associated damage to the case and seal structure. Bearing damage will probably be avoided and little or no damage to the bearing support structure would be expected. So, the total engine damage would be classified in the moderate range.

The TF33 high rotor maneuver deflections are shown in Figures 101 through 103. The cantilevered turbine construction is dominant in the rotor's bowed shape. The maximum deflection of 24 mils is a result of both rotor and support deflections. Some seal rub could be anticipated during the more severe conditions.



## G. TF39 Engine

### 1. TF39 Rotor Dynamic Behavior

The TF39 fan rotor consists of two fan stages cantilevered from the first two bearings. The No. 1 bearing is a roller type while the No. 2 single-row bearing takes the axial thrust and is also the front support for the long shaft. The six-stage turbine is straddle mounted on two roller bearings in the aft end of the machine. Figure 104 presents the undamped critical speed map for the TF39 fan spool. Note that the first critical speed of the fan rotor-bearing system is very close to the maximum rotor speed of 3600 rpm.

The undamped vibratory mode shapes for the first two critical speeds are shown in Figures 105 and 106. The cantilevered fan mode at 3800 rpm is only 5.5% above the operating speed range. The low turbine mode is well outside the operating range.

The response analysis for 3.8 oz-in. of distributed unbalance is shown in Figure 107. Because the turbine mode is far outside the operating range, there is very little turbine rotor deflection. But, the cantilevered fan mode is very close to maximum speed, with the effects of the mode being observed within the operating range. At maximum speed, the rotor deflects only 1 mil but the rotor is operating on the steep part of the response curve. Depending on tolerances from engine to engine, the rotor support stiffness may vary enough to have this mode drop into the operating range. There is a possibility that a small percentage of engines will have severe vibration problems.

The loss of a single airfoil in the fan or turbine creates a significant unbalance, especially in a high bypass engine where the fan blades are very large.

For the TF39 fan rotor system, three separate blade loss analyses were performed. The engine response for the loss of one foil at either the first-stage fan, the second-stage fan or the last turbine disk has been calculated and is shown in Figures 108 through 110. The first critical speed, which is a cantilevered fan mode at 3800 rpm, is in close proximity to the operating speed of 3600 rpm. Even though the rotor does not have to pass through this critical speed during the deceleration, the mode is close enough to cause response at the operating speed. For the loss of a first-stage fan blade (Figure 108), the rotor deflection at the blade loss is 70 mils and 42 mils at the second fan stage. The deflected rotor shape would be similar to the first critical speed mode shape (Figure 105) which shows a bearing deflection of two-fifths the rotor or in this case, 28 mils. The maximum deflection occurs at 3600 rpm and will decrease during the deceleration.

The second-stage fan blade loss (Figure 109) is somewhat more severe because the reduction in moment arm from the blade loss stage to the bearing is not sufficient to compensate for the much larger unbalance. The maximum free rotor deflection of 100 mils still occurs at the first fan stage with the blade loss stage experiencing a 70 mil deflection. Again, these deflections occur at 3600 rpm and decrease during the deceleration. Figure 110 shows the No. 1 bearing load for both a first and second-stage fan blade loss. The bearing load could be as high as 15,000 lbs at the operating speed and gradually decrease with speed reduction. Bearing failures under severe load



conditions such as these are very much dependent upon the rate of deceleration. But, given the inertia and response lags of a turbofan engine, bearing damage would be inevitable. With the large fan stage deflections discussed above, fan blade-to-case rubbing, blade curling and seal damage would also be anticipated. The total engine damage would be classified in the medium to heavy range.

Figure 111 shows the rotor response for a blade loss at the sixth low turbine stage. Since the low turbine critical speed is well above the operating speed, the TF39 is very insensitive to a low turbine blade loss. The deflections at the fan stages due to a turbine blade loss were insignificant. The third and fourth rotor bearing loads were also calculated for a sixth stage low turbine blade loss (Figure 112). Again, as was the case for rotor deflection, the low turbine mode is so far removed from the running range that no bearing damage would be anticipated.

In summary, the TF39 fan stages are very sensitive to a blade loss occurrence. The rotor deflections alone are severe enough to cause extensive damage. The resultant No. 1 bearing load will also cause permanent deformation of the bearing. Even though the entire rotor support will not be lost, this failure will cause rotor deflections which will make contact with the fan case. Extensive blade rubbing will cause damage to the case and seals. The fan blade tips will be curled.

The TF39 low rotor maneuver deflections are shown in Figures 113 through 115. The maximum deflection is 57 mils at the tip of the first fan stage. Because of the cantilevered construction and relatively soft low compressor rotor lateral stiffness, the slope of the fan/compressor section causes a relative deflection from the No. 1 bearing to the first fan stage of 39.5 mils. Some blade tip rubbing could be expected during this condition. The remaining 17.5 mils deflection is caused by the load on the No. 1 bearing.

## 2. TF39 Gas Generator Rotor Dynamic Behavior

The TF39 gas generator rotor consists of a sixteen-stage compressor connected by the high shaft to a two-stage turbine. The compressor and turbine are both straddle mounted. Two roller bearings support the compressor while a single-row ball bearing in the front and a roller bearing support the turbine section. Figure 116 presents the undamped critical speed map for the TF39 gas generator spool. Note, for the design bearing stiffness, that the second critical speed at 7090 rpm is within the operating range of 6200 rpm to 9800 rpm. One mode at 4200 rpm is below idle and the third mode at 11,540 rpm is 17% above maximum speed.

The undamped vibratory mode shapes for these three critical speeds are shown in Figures 117 through 118. All of the modes have coupled responses between the turbine and compressor modules. This type of response is typical of three bearing straddle mounted designs (Ref. J79 dynamic behavior). The result is that unbalance in either the turbine or the compressor will excite all the modes. The unbalance response for the TF39 gas generator is shown in Figure 119. The response to the first mode is below idle and should, therefore, not be too much of a concern. The second mode in the low end of the operating range has both compressor and turbine amplitude with the latter being more severe. When this mode is observed in the engine condition, it is not possible to determine if the unbalance is located in the compressor or

turbine. This coupled phenomenon causes the maintenance and trim balancing operations to be more difficult. At the top end of the operating speed range, the rotor is starting to respond to the third mode which has predominantly more compressor than turbine motion.

Figures 120 through 123 show the rotor deflection and bearing loads for a first-stage high compressor blade and a last-stage high turbine blade failure. When compared to the fan rotor, the high compressor is relatively insensitive to a single blade loss. This is because the stiffer high rotor with a straddle-mounted arrangement is a design which has more system damping. In addition, the blade airfoils are much smaller than the fan stages. The maximum rotor deflection is .65 mils at 9800 rpm (Figure 120) and the loss of several adjacent airfoils would be required to cause blade-to-case rubbing. The high rotor No. 1 bearing load is shown in Figure 121 and has the same characteristics as the deflection curve. The maximum load of 780 lbs for a single airfoil loss would not seem sufficient to cause bearing deformation.

The high turbine is somewhat more sensitive to a blade loss condition because of the softer rear bearing support. Since the high turbine blades are hollow, the unbalance created by a single blade loss is relatively small. Therefore, several adjacent turbine airfoils would have to be lost before case rubs would be anticipated. The maximum rotor deflection which occurs at the operating speed of 7050 rpm is 1.3 mils as shown in Figure 122. The radial load at the fourth high rotor bearing is shown in Figure 123. The maximum load of 550 lbs occurring at the high rotor speed of 7050 rpm.

In summary, the TF39 high rotor system is not sensitive to a blade loss from either the high compressor or the high turbine. Multiple blade losses from either stage would be required to cause blade-to-case rubs or bearing failures.

The TF39 high rotor has both a straddle-mounted compressor and turbine section. As is shown in Figures 124 through 126, the total deflected shapes are not as severe on the low rotor. The maximum deflection is 3.4 mils with 36 percent of this due to bearing support motion.



## H. TF41 Engine

### 1. TF41 Rotor Dynamic Behavior

The TF41 low rotor is supported on four bearings. The first fan stage is cantilevered from the No. 1 roller bearing. The remaining two fan and two compressor sections are supported at the rear by the second roller bearing. The long low shaft and front of the turbine are mounted on a single row ball bearing which takes the axial thrust. The remaining roller bearing is the aft support for the two turbine stages.

Figure 127 presents the critical speed map of the TF41 LP rotor bearing system. Note that the first two critical speeds lie within the rotor's design speed range, and that the third critical occurs at about 10,200 rpm.

Figures 128 and 129 show the undamped vibratory mode shapes for the first two criticals for the nominal bearing stiffnesses expected to exist in the engine. Both modes are of the rigid body type with all support motion and very little rotor bending. The lower mode at 3670 rpm is a turbine excited resonance showing the predominant motion there. The upper mode at 9340 rpm shows the cantilevered fan as the major contributor. Since the major components respond separately, one sensor in the front of the compressor to record fan unbalanced excited vibration near maximum speed, and one sensor at the low turbine case to record turbine unbalance excited vibration at the low power settings would be required.

The engine must traverse two natural frequencies before reaching maximum speed with the fan resonance not far removed from the maximum operating point. The third mode, which is a bending type of the low shaft, is only 500 rpm above red-line speed.

Figure 130 presents the rotor response for distributed unbalance. The low turbine rotor responds to the low speed resonance but is reasonably controlled by the damping in the rear bearing support which is at the maximum deflection point. Also, the unbalance was assumed to be only 0.75 oz-in. because of the face spline construction which should allow for precision assembly and balance control. If increased part tolerances or wear become a factor, then response to this mode could be anticipated.

The fan/low compressor vibration with 5.4 oz-in. of unbalance is much more severe. The first stage fan deflects 7 mils and the No. 1 bearing journal has 5.6 mils of vibration. As shown in the mode shape of Figure 128, the No. 1 bearing is the only source of damping and, because of the cantilevered construction, is not at the maximum deflection location. The vibration level is high and the fan/low compressor must be well balanced to prevent excessive amplitudes. The engine will also be sensitive to unbalance in the fan created by FOD or blade rub.

The general dynamic characteristics of the TF41 low rotor system has shown that there are two critical speeds in the operating range. When blade loss conditions are considered, this means that two modes have to be traversed with a heavily unbalanced rotor. Figures 131 through 134 show the rotor response and resultant bearing loads for either a first stage fan or second stage turbine blade loss.



The first fan stage will result in a free deflection of almost 2 inches. Obviously there will be severe damage from case to blade rubbing. The associated bearing load of  $1 \times 10^6$  lbs would obviously cause permanent deformation of the bearing and support. These loads and deflections will never be obtained because of the extensive damage created by this blade loss condition.

The turbine blade loss is not nearly as severe. The second stage turbine blade loss results in much less unbalance than the first stage fan blade loss. The straddle-mounted construction of the turbine as opposed to the cantilevered fan construction, helps to desensitize the turbine assembly. Only 60 mils of deflection and a No. 4 bearing load of 2500 lbs are anticipated as the rotor is decelerated through this critical speed. With a fairly rapid deceleration, the blades may only show slight rubbing on the case and the damage would be considered light.

The TF41 low rotor maneuver deflections are shown in Figures 135 through 137. There is an interesting comparison between the TF41 and TF39 engines. The cantilevered fan construction is similar but, because of the increased length between No. 1 and No. 2 bearings (which provide moment restraint for the TF41), the shorter overhand and higher stiffness/mass ratio of the compressor, the TF41 fan deflection is only 8.0 mils, compared to 57 mils for the TF39 fan. The TF41 low turbine actually deflects more than the fan because of the softer bearing supports and more flexible turbine rotor. The rotor deflection of almost 30 mils does indicate potential rub condition during the flight and landing conditions.

## 2. TF41 HP Rotor Dynamic Behavior

The TF41 high rotor is mounted on three main bearings. It consists of an eleven stage compressor section mounted on a roller bearing in the front and, in the rear, a single row ball bearing for taking axial thrust. The two stage turbine is cantilevered from a roller bearing which also supports the high shaft.

Figure 138 presents the critical speed map for the TF41 HP rotor bearing system. Note that the first critical speed lies below the rotor design speed range. The design speed range lies between the first and second critical speed, which indicates good design practice.

Figure 139 shows the undamped vibratory mode shape for the HP rotor for the nominal bearing stiffnesses expected to exist in the engine. Note that the first critical is essentially a bending critical, with the majority of the deflection occurring in the coupling just aft of the No. 2 bearing.

Figure 140 shows the calculated unbalance response of the rotor for 0.5 oz-in. of unbalance. This data was also calculated with no bearing support damping in order to illustrate critical speed location. The first critical speed peak is generally high and broad in nature, and thus, measurable vibrations will probably appear in most engines unless both good balance and damping are provided.

Note also that the first critical speed peak lies within the operating speed range of the LP rotor. Thus, vibration transmitted from the LP rotor to the HP rotor across the intershaft bearing may cause the HP rotor to vibrate sub-synchronously, which is one type of non-integral order vibration. This is because the HP running speed lies in the range of 10,160-12,842 rpm, while the vibration induced by the LP rotor will occur in the speed range of 3,280-9,700 rpm.

Figure 141 shows predicted vibration amplitudes along the rotor axis at 7000 rpm, just below the first critical speed. Note that the largest vibration levels occur at the turbine, and that the coupling apparently also has relatively low shear stiffness.

The TF41 high rotor does not have any critical speeds within the operating range from idle to redline, but a high compressor mode is just above the maximum speed and a high turbine mode will have to be traversed during the deceleration. Because there are no modes in the speed range, the normal engine response should be acceptable but the blade loss values could present a completely different story.

The high compressor blade loss response and bearing load is shown in Figures 142 and 143. The rotor deflection is only 9 mils, which in itself would not be a problem, but with a No. 1 bearing force of 11,000 lbs, some permanent deformation of the bearing is possible. The combination of the bearing deflection and that of the rotor could cause some rubbing of the blade tips with the case flowpath. The engine damage would probably be classified as being light. This is a typical blade loss response for high compressors of dual-spool jet engines. The straddle-mounted rotor and relatively small blades make the high compressor somewhat more tolerant to a blade loss condition.

Figures 144 and 145 show the high turbine blade loss response and rear bearing radial load. Cantilever rotor constructions are, in general, very sensitive to unbalance and the TF41 high turbine is no exception. The high turbine mode is at 7000 rpm and the peak deflections and loads occur at this speed. The free rotor deflection is over 200 mils with a radial load of 17,000 lbs. Severe blade, case and seal rubs would be anticipated along with probable bearing failure. The engine damage would be in the moderate to heavy range, depending on the deceleration rate.

The TF41 high rotor construction consists of a straddle-mounted compressor and cantilevered turbine. Figures 146 through 148 show the deflected shape for the three maneuver conditions. The compressor rotor is relatively rigid with the turbine disk deflection almost 12 mils. From this analysis, the TF41 engine is relatively insensitive to maneuver loading with possible local scuffing of the high and low turbine tip seals as the only minor potential damage.

#### SECTION IV

##### DYNAMIC CLASSIFICATION

Based on the critical speed maps and mode shapes described in the previous section, Figures 149 through 152 show the classification of the dynamic characteristics based on the rotor configurations. The compressor generally has fairly hard supports and their modes are generally above redline or near the top speed. The stiffer supports and straddle mounted construction provide damping and lower sensitivity to unbalance. Overhung fan stages have a tendency to reduce the resonance frequency and increase sensitivity to unbalance. The large gyroscopic stiffening effects from these fan stages help to keep the natural frequencies up, thus desensitizing the rotor to unbalance.

Turbine rotors are generally designed with relatively soft bearing supports to accept thermal excursions requirements. The result of this design practice is to have turbine-excited modes below idle or in the low end of the operating speed range. These vibration modes are generally more sensitive to unbalance because of the lower support stiffness. The degree of sensitivity increases for overhung turbines versus straddle mounted arrangements.

The results of maneuver loads on the deflections of the rotors has been discussed in the previous section. A summary of these deflections and their potential effects on the respective engines is given in Table II.



TABLE II

## SUMMARY OF MANEUVER DEFLECTIONS

Maximum deflection (Mils)

<u>Engine</u>	<u>Landing</u>	<u>Flight</u>	<u>Catapult</u>	<u>Comments</u>
<u>TF39</u>				
Fan/Low Compressor	57.0	56.4	32.7	TF39 will probably experience some fan blade to case rubs.
Low Turbine	12.0	11.6	6.9	
High Compressor	3.4	3.36	1.95	
<u>TF41</u>				
Fan/Low Compressor	8.0	7.5	4.0	TF41 engine is sensitive to maneuver loads. Could cause rub and blade tip/shroud wear.
Low Turbine	29.5	29.0	17.0	
High Compressor	1.8	1.8	1.0	
High Turbine	11.6	11.4	6.7	
<u>TF33</u>				
Fan/Low Compressor	5.4	5.35	3.1	TF33 high and low turbines are sensitive. Could rub and cause blade tip/shroud wear.
Low Turbine	20.2	20.0	10.9	
High Compressor	2.8	2.7	1.5	
High Turbine	24.8	24.5	14.0	
<u>TF30</u>				
Fan/Low Compressor	8.7	8.6	5.0	TF30 high and low turbines will probably rub seals during loading.
Low Turbine	17.0	16.8	9.8	
High Compressor	1.2	1.2	0.8	
High Turbine	15.2	15.1	9.5	
<u>J57</u>				
Fan/Low Compressor	3.1	3.0	1.8	J57 high turbine could rub severely during maneuver and cause blade tip/shroud wear.
Low Turbine	12.7	12.5	7.3	
High Compressor	2.4	2.7	1.5	
High Turbine	24.8	24.5	14.0	
<u>J58</u>				
Compressor	1.8	1.7	1.2	J58 is insensitive to maneuver loads.
Turbine	5.0	4.9	2.8	
<u>J79</u>				
Compressor	9.3	9.2	5.3	Under the worst loading, the J79 will probably experience turbine seal rubs.
Turbine	13.2	13.1	7.4	
<u>T56</u>				
Compressor	2.7	2.6	1.6	T56 engine is lightweight on stiff supports, therefore, insensitive to maneuver loads.
Shaft/Couplings	3.6	3.5	2.0	
Turbine	5.7	5.6	3.3	

## SECTION V

### EXPERIMENTAL STUDIES

During this experimental studies task, MTI conducted a baseline natural frequency calculation and experimental verification of state-of-the art analytical treatments of those elements which significantly influence the dynamic behavior of an engine rotor. In particular, those elements which separate modern engine rotors from those which can be described via the conventional "elastic beam" concept, were identified.

An important input to the task's performance was the engine rotor-bearing system review and classification efforts described in previous sections. The data obtained in those tasks were used to identify, as a function of engine classification, the presence, location, critical dimensions and influence on dynamic behavior of mechanical joints and flexible members.

Commonly among these elements, the quantity subject to most uncertainty is flexibility. The usual critical speed analysis incorporates lumped masses connected by massless flexible beams. In the complicated jet engine structures, it is much easier to calculate the weight of the disk and blades than to determine the bending and shear stiffnesses of the connecting pieces. In some cases, the problem is the complexity of calculations (e.g., with tapered conical sections), and in other cases, the problem is the difficulty of establishing a precise analytical model (e.g., with bearing support flexures). For example, the T56-15 second critical speed mode shape (Figure 3) shows a severe change in slope (kink) at the No. 2 bearing location. The cause of this effect is the rear hub of the compressor which is a flat plate connected to a spline joint aft of the bearing. When an engine is modeled and the critical speeds are determined, it is important to establish a procedure for identifying potentially flexible joints which will cause errors in the analysis and vibration problems in production. A simplified procedure is outlined below.

- Carefully model the rotor, making sure all changes in the direction of the primary load pattern are accounted for.
- Perform an initial critical speed analysis. To identify potentially flexible joints, stiff bearing support springrates are recommended.
- Plot the deflected shape of the critical speed. Identify severe slope changes, kinks, or shear discontinuities. Obviously, a rotor with uniform curvature is desirable.
- The flexibility of critical joints which will influence the rotor dynamics should be verified by more complicated shell or finite element analyses. An alternative approach is to construct a test specimen which duplicates the design function and verify the flexibility experimentally.

The approach taken for this task was to isolate the element of interest and to investigate its static and dynamic flexibilities. A representative geometry was selected for each element to be investigated. A detailed analytical model designed to yield the required flexibility information was prepared. State-of-the-art axisymmetric, thin shell analysis methods were used, where appropriate, for the purpose of analytical prediction.

For the purpose of establishing a streamlined experimental program, five elements were selected for test. The basis for this selection included:

- The uncertainty associated with flexibility predictions for the element.
- Frequency of application of the elements in current and advanced engines.
- Influence of the element on the typical dynamic behavior of engine rotor-bearing system.

Test rotor specimens (essentially scaled down portions of rotors) were fabricated — one for each element of interest. The flexibility and mass properties of each specimen were such that the element of interest, in each case, had a dominant effect upon the dynamic behavior of the test rotor specimen. The specimens selected were:

1. Shallow cone (9.4° cone angle from shaft axis)
2. Steep cone (60° cone angle from shaft axis)
3. Flat plate element
4. Thin shell cylinder
5. Bearing Support flexural element

These specimens are shown in Figures 153 and 154. The test setup, shown in Figures 155 and 156, was used to obtain the first three free-free natural frequencies of the four cylindrical test elements. These natural frequencies have been experimentally determined for the step-change, shallow-cone steep-cone test components. The critical speed analysis for each element was run to obtain predictions for these resonances. Table III below lists the experimental and analytical modes and the percent error.

TABLE III  
NATURAL FREQUENCIES (Hz)

<u>Specimen</u>		<u>Experimental</u>	<u>Analytical Prediction</u>	<u>Percent Error</u>
Step Change	1st mode	200	291	+ 45.5
	2nd mode	1228	1305	+ 6.3
	3rd mode	2602	2835	+ 9.0
Shallow Cone	1st mode	772	817	+ 5.8
	2nd mode	2090	2207	+ 5.6
	3rd mode	3592	4079	+ 13.6
Steep Cone	1st mode	910	1482	+ 62.9
	2nd mode	3804	4309	+ 13.3
	3rd mode	5552	7265	+ 30.8



The analytical predictions were all high compared to the experimental results. Additionally, the error was largest in modes which showed bending in the weld joint. Investigations were started to determine if there were any deficiencies in the material properties of these specimens which could have caused this. Each of the three welded specimens, the shallow-cone, steep-cone and step-change elements, were tested for material hardness and the results are shown in Figures 157 through 159. Not only was there a drastic reduction in material hardness for the weld joint, but the base material was also affected. The weld process created a "heat-affected zone" as much as two inches away from the weld. With the short test elements in the steep-cone and flat plate specimens, this means that the entire section of interest had a lower stiffness than the unaffected base metal at the ends of the cylinders. Additional information was obtained from the shallow-cone specimen. The tubular sections at the ends have approximately the same hardness with a large reduction in hardness at the weld joint as was observed in the other specimens. But, additionally, the shallow-cone midsections, which should not have been affected by the weld, also had a somewhat reduced hardness. The conical section is machined from aluminum stock instead of tubes which could have been the reason for material property differences. The specimens were X-rayed for weld characteristics. The results showed that both cone specimens had poor penetrations, weld flaws and voids. So, not only did the specimens have drastic reductions in material hardness, but they also had a lack of joint integrity. The hardness check and X-ray data showed that, because the analysis assumed a uniform material property and load transfer between sections of each specimen, the experimental results were much lower than the analytical predictions.

The thin shell element has also been tested for resonances. During the tests, some interactions were noted between shell and beam modes. The first two shell modes, shown in Figure 160, correlate well with the analytical predictions. Table IV shows these results.

TABLE IV

THIN SHELL ELEMENT NATURAL FREQUENCIES (CPS)

	<u>Experimental</u>	<u>Analytical</u>	<u>Percent Error</u>
2 Nodal Diameters	240	238.7	- 0.5
3 Nodal Diameters	710	675.2	- 5.0

The beam modes were not easily determined. The analytical prediction of the first free-free mode is at 1480 Hz. But, as the driving frequency was increased, the shell modes became more complex to the point where beam bending could not be measured. Stiffeners were added to each end of the cylinder to obtain at least two hard points for measuring beam deflection. Three modes were observed at 820 Hz, 1036 Hz and 1260 Hz. With the instrumentation available, it was not possible to determine the amount of shell participation in each mode and how it affected the observed natural frequencies.

The tubular test specimens had three different cross sections. The conical test elements had cylinders with a thickness to radius ratio ( $t/r$ ) of 0.073 and 0.146. The thin shell element had a  $t/r$  ratio of 0.02. From this testing, there seems to be a dynamic limit to the allowable thickness to radius ratio. Sensitive shell modes, especially in rotating shafts, will cause high vibratory stress

and potential fatigue failure. On engine cases which can be excited by blade passing pressure pulses, the requirement for lighter weight will cause the need for stiffening rings to eliminate potentially excited nodal diameter patterns from the operating range.

The flexible support test specimen was mounted on the Ling shaker (Model No. B335, PP-35/70VC power amplifier). The displacement and frequency were varied until the first mode of the flexible support member had been determined. In addition, a known weight was added to the free end of the flexures and resonated to increase the accuracy for determining the lateral springrate of this test element. Figures 161 and 162 show the experimental results of this test. The analysis was run to account for all the machining tolerances in the experimental hardware. Table V shows the comparison of the analytical prediction and the experimental results.

TABLE V  
FLEXIBLE SUPPORT NATURAL FREQUENCIES (CPS)

	<u>Experimental</u>	<u>Analytical</u>	<u>Percent Error</u>
Flexible support	327	429	23.8%
Flexible support with 5.5 lb mass added	221	296	25.3%

The observed natural frequency of 327 Hz was surprisingly low compared to the calculations. Hand-held probes showed that the mounting structure between the test element and the shaker was also vibrating. A lack of stiffness in the mounting would have caused the resonant frequency to drop. To check the results, the flexible element was mounted on a bedplate and a static load test was performed. Figure 163 shows the results of this test. The deflection of the squirrel cage was isolated from that of the mounts. The flexible element springrate is approximately 80,000 lbs/in. and the mount springrate is 400,000 lbs/in. While the flexible test element was still in this configuration, a portable shaker was used to excite the overhung mass. This time the resonant frequency was 394 Hz. This value was somewhat higher than the original resonant test because the bedplate mount was stiffer than the original shaker supports.

The required combined flexure and mount springrate to obtain a 394 Hz natural frequency is 74,000 lbs/in. The combined springrate from the static load test results was only 67,000 lbs/in. which would indicate a potential ten percent discrepancy in the measurements. The flexible test element springrate, based on this test data, could be between 80,000 lbs/in. and 90,000 lbs/in. The analysis of the flexible element, which is shown next, predicted a springrate of 88,200 lbs/in.

The flexure spokes were formed by machining parallel slots in a hollow sleeve. The sides of the slots were parallel. The resulting cross-sectional shape of the spokes is shown (exaggerated) in Figure 164. For the purpose of our calculations, the cross section was analytically represented to be the trapezoid shown in Figure 165, where  $A_1$  and  $A_2$  represent the inside and outside arc lengths, respectively, of each spoke and  $(r_2 - r_1)$  represents the thickness. The area moment of inertia of the trapezoidal representation of this spoke is given in Equations (1) and (2).

$$I_x = (r_2 - r_1)^3 \left[ \frac{A_2^2 + 4A_2A_1 + A_1^2}{36(A_2 + A_1)} \right] \quad (1)$$

$$I_y = \frac{(r_2 - r_1)(A_2 + A_1)(A_2^2 + A_1^2)}{48} \quad (2)$$

Where:  $I_x$  is the area moment of inertia about the X-axis  
 $I_y$  is the area moment of inertia about the Y-axis  
 $r_1$  is the inside radius of the flexure  
 $r_2$  is the outside radius of the flexure  
 $A_1$  is the ID arc length of one spoke  
 $A_2$  is the OD arc length of one spoke

For the flexural support tested:

$$A_1 = 0.1255 \text{ in.}$$

$$A_2 = 0.1901 \text{ in.}$$

$$(r_2 - r_1) = 0.1605 \text{ in.}$$

Substituting into equations (1) and (2) yields;

$$I_x = 5.77 \times 10^{-5} \text{ in.}^4$$

$$I_y = 5.61 \times 10^{-5} \text{ in.}^4$$

The transverse spring rate of a flexible support is:

$$K = \frac{NAE}{L} \left[ \frac{6I_x}{AL^2 + 12K_o \lambda I_x} + \frac{6I_y}{AL^2 + 12K_o \lambda I_y} \right] \quad (3)$$

where  $N$  = the number of spokes (16)

$L$  = the length of each spoke (1.495")

$E$  = the modulus of elasticity ( $28 \times 10^6$ )

$A$  = the cross-sectional area of each spoke ( $.0253 \text{ in}^2$ )

$K_o$  = shape factor (1.2)

$\lambda$  = 2.58 (for steel)



Substituting:

$$K = 88,200 \text{ lbs/in.}$$

In the experiments described above, simulated rotor components which are most sensitive to modeling discrepancies were analyzed and tested to obtain a better understanding of their characteristic flexibilities. The results are summarized below:

1. The radial stiffness of the flexible support or squirrel cage can be accurately defined by Equation 3 above. There are applications of flexible bearing supports to accept thermal deflections and to act as a centering device and rotor support for fluid film dampers. This analysis should be used to effectively model this component when performing critical speed analyses.
2. There is a limiting thickness to radius ratio when designing components for beam stiffening. Between .02 and .073 t/r, the modes excited change from those of a beam to shell natural frequencies. These shell natural frequencies then must be accounted for in the design and analysis of advanced technology jet engines.
3. Simulated rotor components such as hubs, diaphragm couplings, and thin sections are very sensitive to fabrication techniques. Additional testing should be done but only with actual engine hardware. There is no published data which provides information on the stiffness of a cone as it progresses from a cylinder to a flat plate. By using several engine components, a family of curves could be provided which would act as a design tool for critical speed analyses of these conical elements. The face spline coupling should not be overlooked in future test work. Again, there is no published data and there is a reasonably frequent use of face splines or curvic couplings in rotor construction.

SECTION VI  
TECHNOLOGY PLAN

Utilizing the information in the previous sections, a detailed plan has been prepared which defines the steps to be taken to resolve current shortcomings in the technology of rotordynamics, as it applied to Air Force gas turbine engines. The main inputs to this task have been the elements of the program as described previously. These tasks have identified major classifications of current Air Force engines from a dynamic standpoint, and have identified limitations in existing capabilities for modeling current Air Force engine configurations.

The plan defines the required analytical developments, the required tests to verify the predictions of the analysis, the required developments in methods to suppress and control vibration, and the required developments in methods of vibration measurement, vibration data analysis, and data interpretation.

The Technology Plan has been broken down into three areas. The first area addresses current needs which require immediate attention to solve engine problems caused by rotor vibration. The second area treats near-term needs (3 to 5 years). These needs can be met via currently available technology which can be used to improve engine maintainability and reduce operating costs. The third area treats long-term rotordynamics needs (more than 5 years). These activities involve improvements to engine design and manufacturing methods, with parallel efforts to improve the analytical techniques for predicting dynamic behavior. Within this framework, requirements for technological improvements have been identified from the analytical efforts completed under this contract.

The programs in the near-term and long-term needs areas should be started now. The goal of each program is reached only after the completion of a logical progression of technical tasks over the indicated length of time.

A. Current Needs

1. Jet Engine Demonstration Balancing. Evaluate advanced trim and on-board balancing procedures to provide data for establishing balancing criteria.
2. Evaluation of Implement Component/Modular Balancing Procedures. Make recommendations relative to the present assembly and balancing procedures to reduce the subassembly residual unbalance, vibration rejection rates, and balance time/complexity.

B. Near-Term Needs

1. Experimental Evaluation of Modeling Techniques. Test engine hardware to provide experimental results of rotor component stiffnesses. GOAL: Application of improved modeling techniques for accurate rotordynamics predictions.
2. Dynamic Analysis of Advanced Lightweight Designs. Identify the potentially troublesome modes of vibration. GOAL: Development and application of balancing criteria to an advanced flexible engine.

3. Engine Vibration Test Data Correlation. Based upon experimental data, identify each engine's most sensitive and predominant modes of vibration, and compare the results to the analytical predictions.

#### C. Long-Term Needs

1. Evaluation of Squeeze Film Dampers for Jet Engines. Analytically identify engines and their modes of vibration which would be suppressed by the addition of squeeze film dampers. GOAL: Engine application and demonstrations of vibration reduction with a squeeze film damper.
2. Experimental Evaluation of Squeeze Film Dampers. Determine the dynamic characteristics for a suitable damper for use in a current jet engine. GOAL: Along with 1. above, obtain engine sensitivity to unbalance with and without the damper.
3. Improvements of Design Methods for Squeeze Film Dampers. Based on the above mentioned data, identify and implement refinements in existing predictive methods for damper response. GOAL: Advance the state-of-the-art in damper design tools.
4. Special Problems. Technical information sessions should be conducted to determine the degree of severity and the attention required for special problems such as:
  - Tower shaft failures
  - Instabilities (nonsynchronous whirl)
  - Bowed rotor (hot restart) vibration
  - Surge deflections

The above discussion described the general programs which require attention and provided some general priorities. Next, a technology plan requires a schedule which can be used in a building block fashion to develop the technology in an orderly manner to meet the time frame required. The following page is a phasing diagram for rotordynamic technology tasks. As shown, the specific items are outlined over a five year period and the technology areas are subdivided into general categories of technology needs.

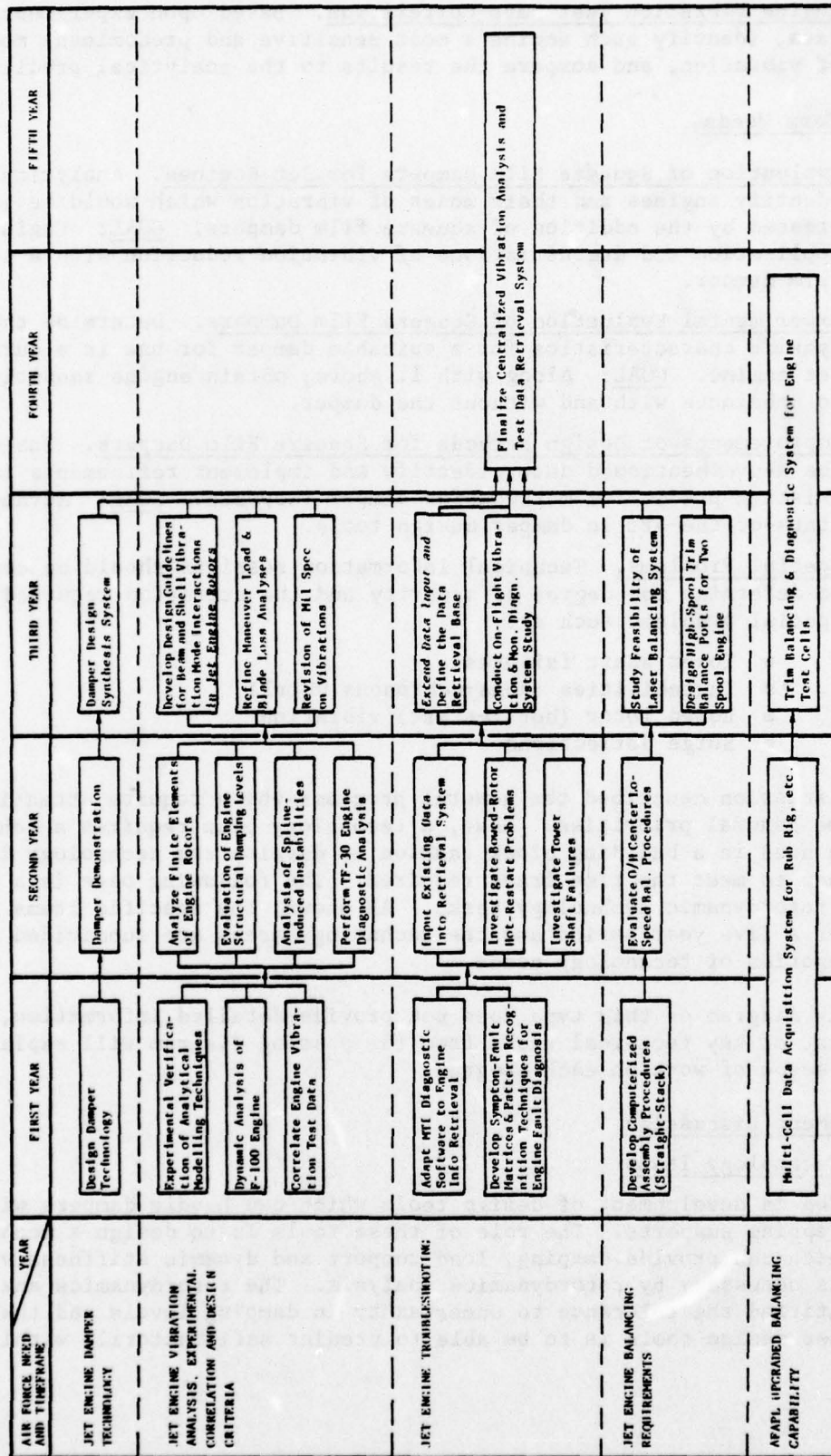
Since a block diagram of this type does not provide detailed information, the following list of key technical tasks from the phasing diagram will explain the general scope of work on each program.

#### D. Plan Element Discussion

##### 1. Damper Technology Items

What is needed is development of design tools which can handle dampers with and without spring supports. The role of these tools is to design a mechanical component which can provide damping, load support and dynamic stiffness values identified as necessary by rotordynamics analysis. The rotordynamics analysis further identified the tolerance to uncertainty in damping levels and the goal for the damper design tools is to be able to predict satisfactorily within these levels.





PHASING DIAGRAM FOR ROTORDYNAMICS TECHNOLOGY TASK AREAS BY NEED CATEGORY

## 2. Experimental Verification of Analytical Modeling Techniques

Potentially the most flexible elements within a rotor system are the hubs which connect the rotor drum to the bearing journals. These elements often are presently modeled using a series of short cylindrical sections, which could be one of the reasons for the generally poor correlation between analysis and test data. One of this report's recommendations is to develop an analytical procedure for determining hub flexibilities, using finite element or body-of-revolution computer programs. The modeling guidelines and analytical tools would then be verified using production engine hardware.

## 3. Dynamic Analysis of the F100 Engine

Since this is a key advanced technology engine, there is a need to develop a dynamic model along the lines of those models previously developed for other Air Force engines.

## 4. Correlate Engine Vibration Test Data

Under the present AFAPL/MTI program to evaluate the rotordynamics characteristics of turbine engines, the rotor models were single rotordynamic level systems with equivalent springs to ground. These models were intended to describe the fundamental engine rotor vibration modes, and were highly successful. One of the recommendations of the report of this work was to perform a multilevel critical speed analysis, combining the rotor models already generated with models of the case and mount structures.

## 5. Develop Computerized Assembly Procedure

It is possible to develop a computerized straight stack procedure which would eliminate elaborate fixture setups and substantially reduce the manpower required for the engine assembly. The part tolerances would be premeasured and then, with that information fed into the computer program, an optimum orientation of each part relative to its mating partners could be established to obtain the best stacking arrangement. This computerized assembly tool could also be used to identify out-of-tolerance components which would not allow the rotor to be assembled within some predetermined maximum allowable runout.

## 6. Finite Element Analysis of Engine Rotors

Certain aspects of engine rotors and engine structures would be handled by finite element rather than traditional transfer matrix (Mykelstad-Prohl) methods; in particular, hubs, bearing supports, and joints.

## 7. Evaluation of Engine Structural Damping Levels

This is a program to get more solidly based information on damping to be expected in engine structures and bearing supports.

## 8. Analysis of Spline-Induced Instabilities

The Air Force program should direct itself at getting more comprehensive design data, identifying undesirable design trends in those splines typical of Air Force engines and expanding the basic analytical methods where necessary.

## 9. Perform TF30 Engine Diagnostic Analysis

The ALC should have an extremely detailed matrix of faults which are unidentifiable using the appropriate instrumentation and recording equipment. This detailed matrix will assist in reducing maintenance costs by permitting pin-point fault diagnosis.

#### 10. Refine Maneuver Loads and Blade Loss Analyses

As engine rotors become more flexible, maneuver deflections will increase causing rubs, high bearing loads, and potential vibration instabilities. To evaluate these effects, it will be necessary to take more care in analyzing these events during design using the available rotor models. This task identifies the need for a transient analysis using only the essential rotor design data to calculate the actual maneuver loads.

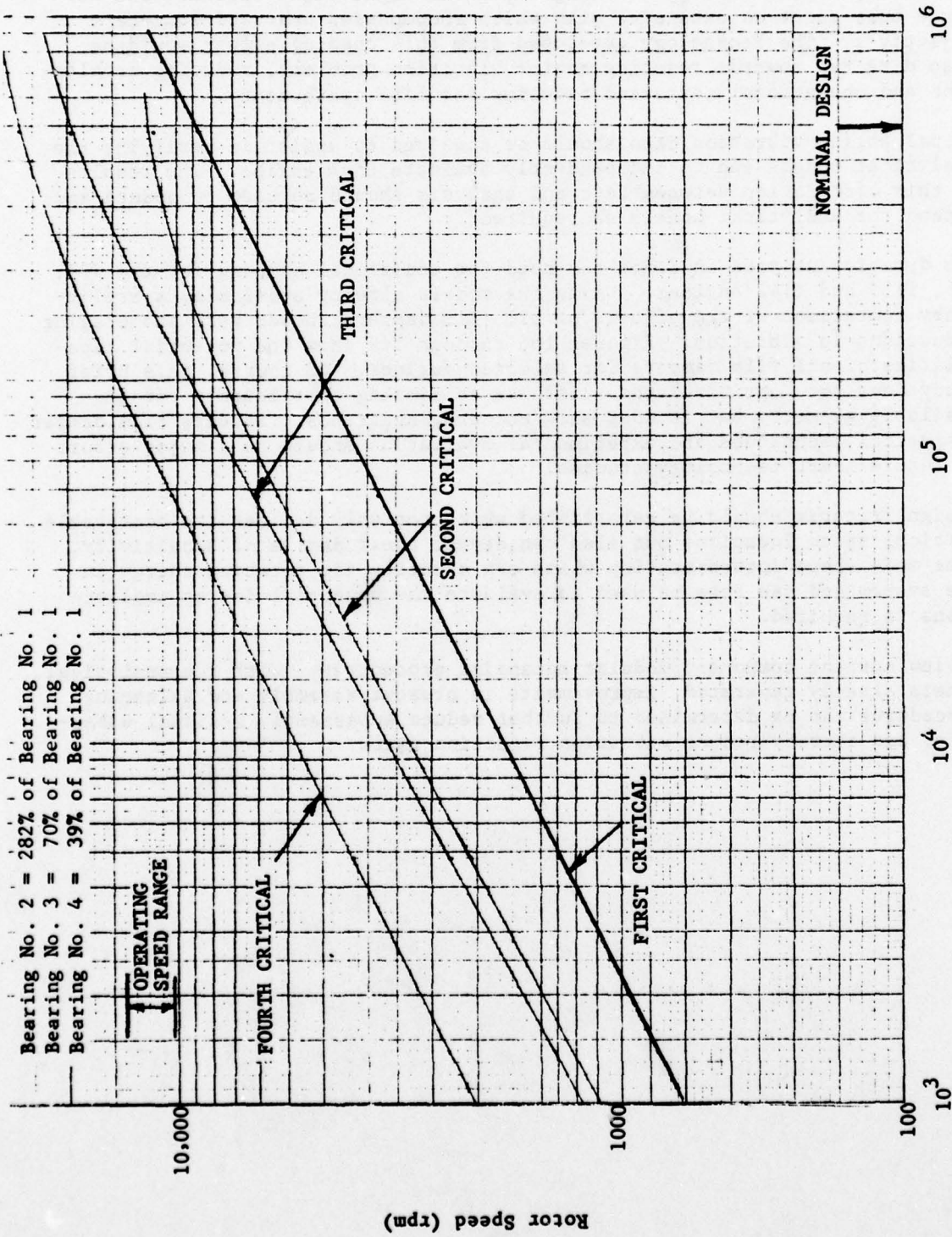
#### 11. Centralized Vibration Analysis and Test Data Retrieval System

There is a need to consolidate technology developed in the analytical and experimental areas, together with test data and validated engine models, in a system which can be used to store and retrieve all pertinent information.



SECTION VII  
RECOMMENDATIONS

1. To develop the technology to design advanced lightweight engines, the Air Force must adopt an extensive plan which encompasses near and long-term objectives. The technology developed from this ongoing effort would be also directed towards reducing engine vibration problems, reducing development and operational costs and reducing the life cycle cost.
2. Actual engine vibration data should be acquired to assist in verifying the analytical models and to independently evaluate each engine. The results of this correlation between test and analysis should be used to update and expand the analytical models as required.
3. The dynamic analyses indicate the need for additional damping for the J79, J85, TF33 and TF41 engines. Using the models already available, a preliminary comparison of the effects of oil film dampers showed very encouraging reductions in vibration. Figures 166 through 169 show the potential capabilities of oil film dampers for selected engines. Of course, this brief study does not "optimize" the stiffness or damping coefficients for the available geometry but it does show encouraging trends. Squeeze film damper analytical techniques and experimental evaluation should be a major effort in future AFAPL technology studies.
4. Design criteria should be established which not only defines the acceptable critical speed locations but also can depict their degree of sensitivity. Some mode shape interpretation which can quantify the rotating energy in the system and can then be used to evaluate the potential design implications is required.
5. Review current component/modular balancing procedures. With the analytical models already generated, improvements in present assembly and balancing procedures can be determined to further reduce subassembly residual unbalance, and thereby reduce vibration rejection rates.



Bearing Stiffness (No. 1 = 100%) (lb/in.)

Fig. 1 Critical Speed Map for T56-15 Rotor Bearing System

THIS PAGE IS BEST QUALITY PRACTICABLE  
FROM COPY FURNISHED TO DDG

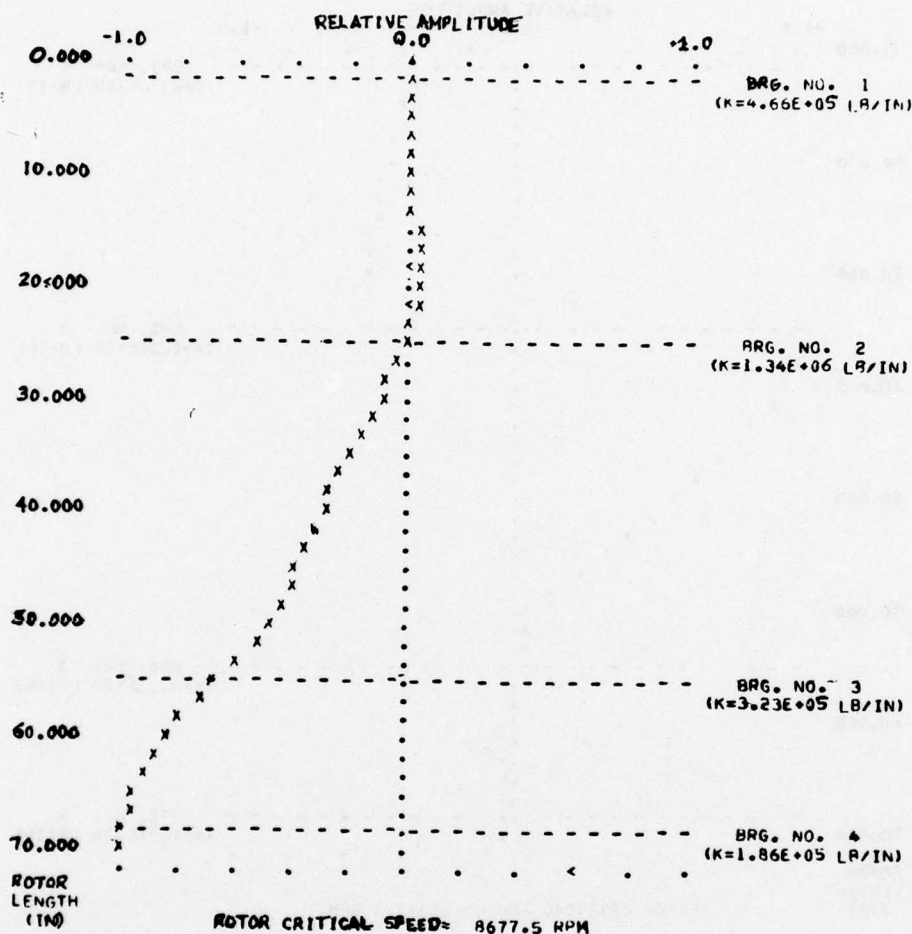


Fig. 2 Undamped Mode Shape at First Critical Speed for the  
T56-15 Rotor System (Turbine Mode)



THIS PAGE IS BEST QUALITY PRACTICABLE  
FROM COPY FURNISHED TO DDG

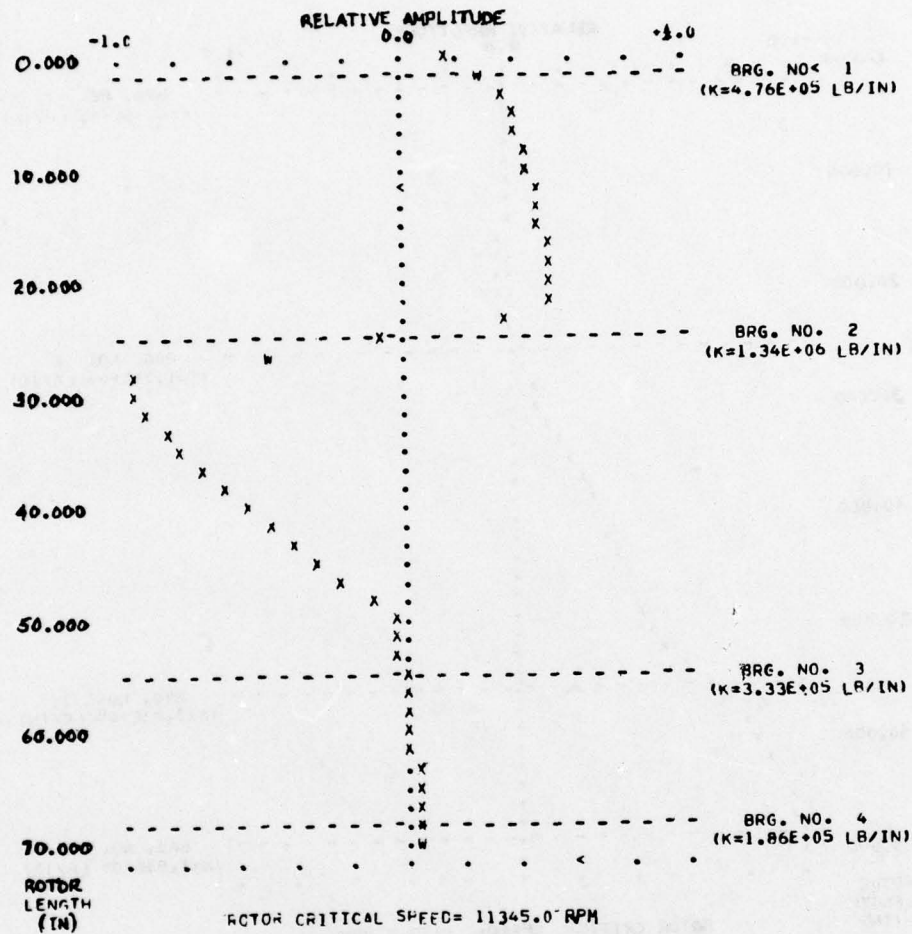


Fig. 3 Undamped Mode Shape at Second Critical  
for the T56-15 Rotor System

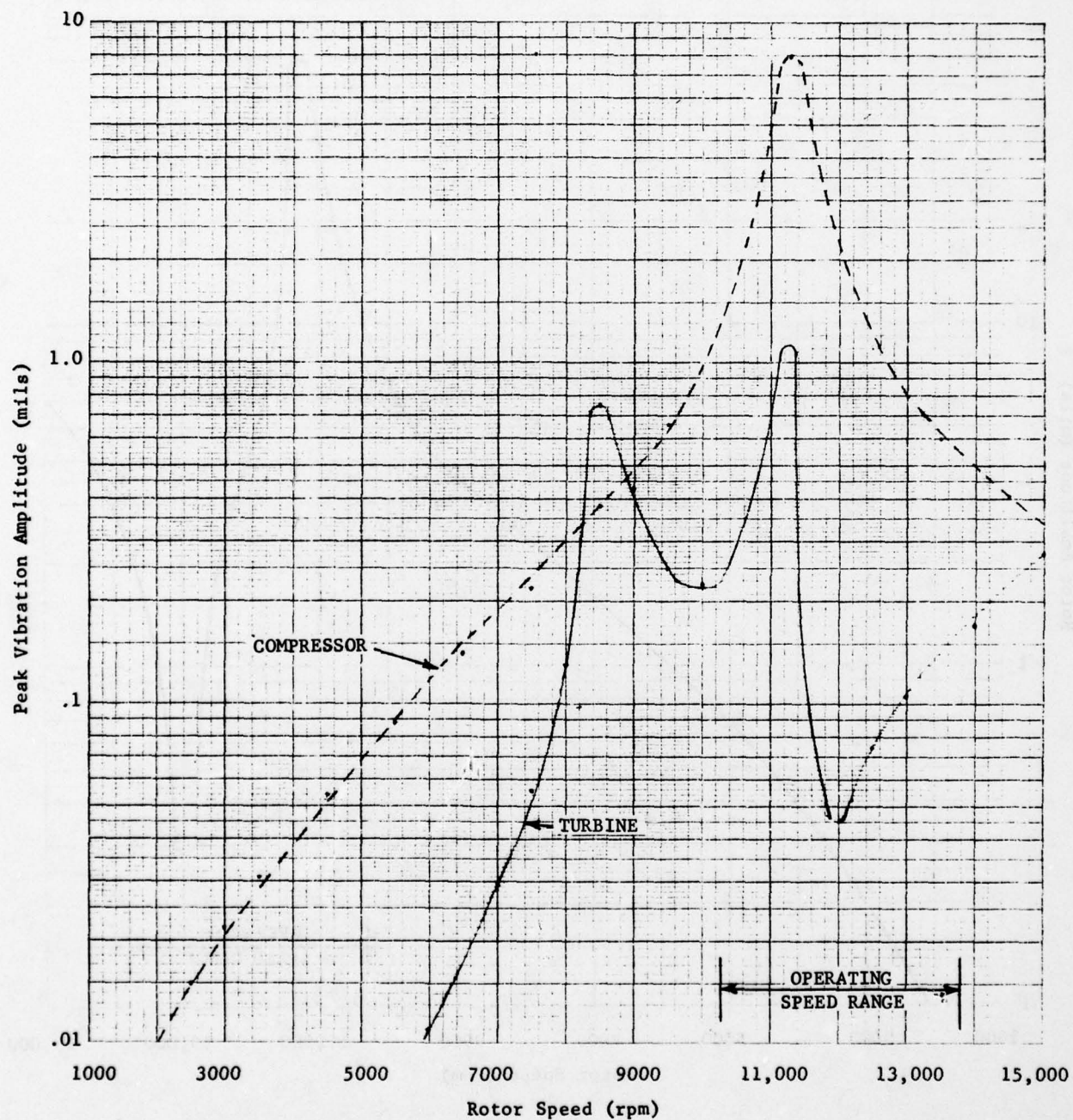


Fig. 4 Calculated Unbalance Response for T56-15 Rotor System With Random Distributed Unbalance

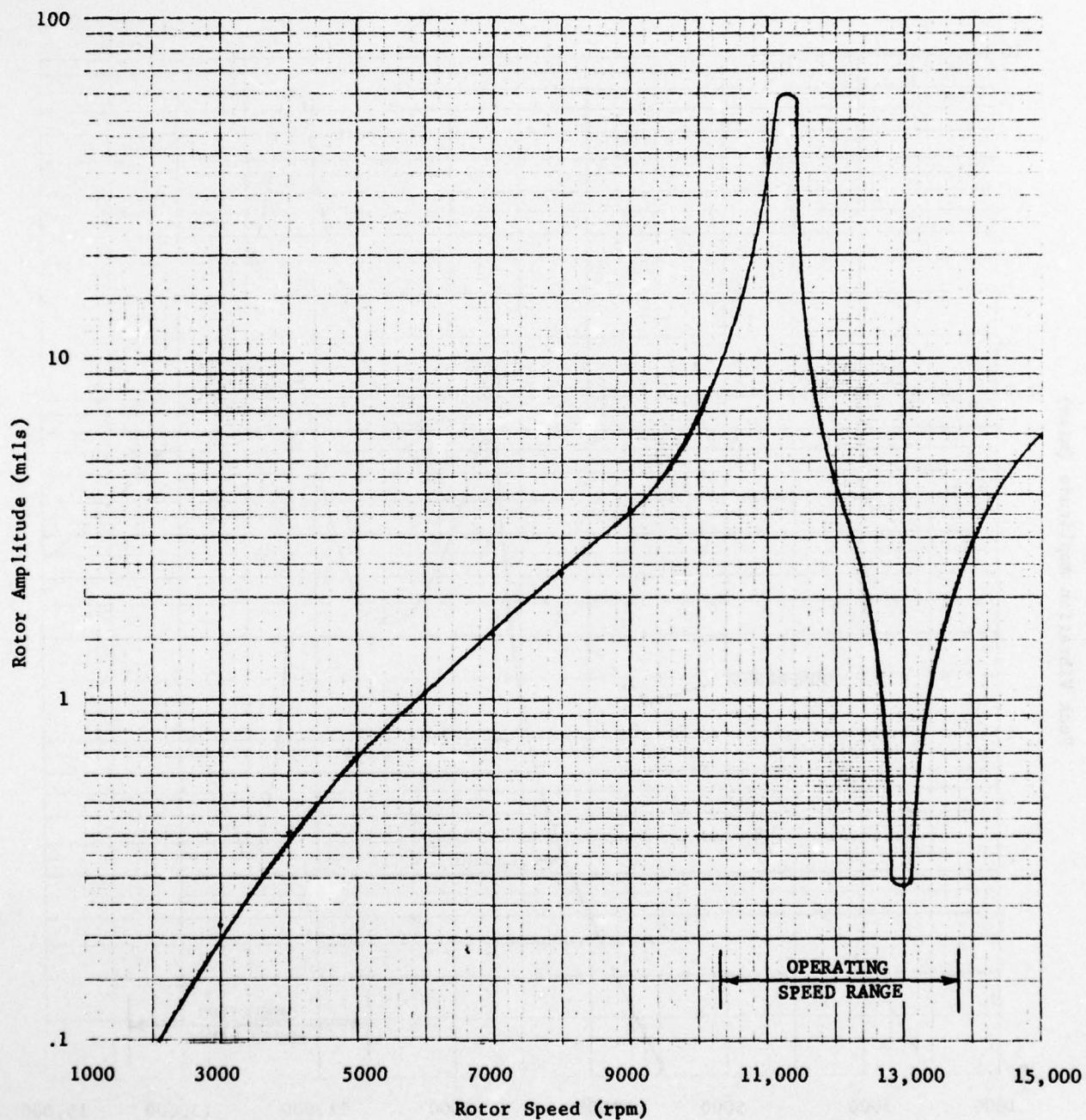


Fig. 5 Compressor Rotor Amplitudes for a First Compressor Stage Blade Loss of the T56-15 Engine



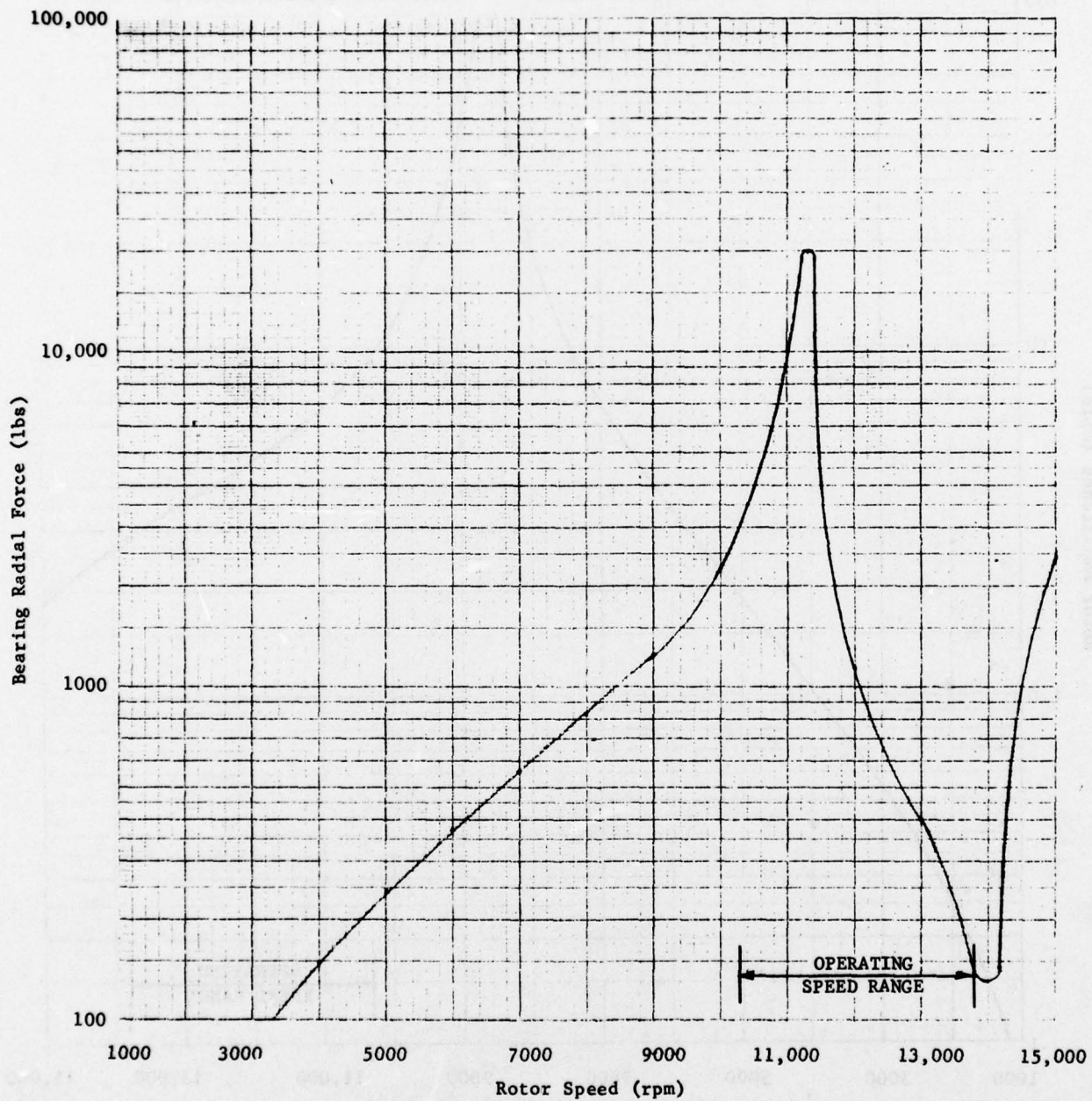


Fig. 6 T56-15 Rotor No. 1 Bearing Radial Force for the First Compressor Stage Blade Loss

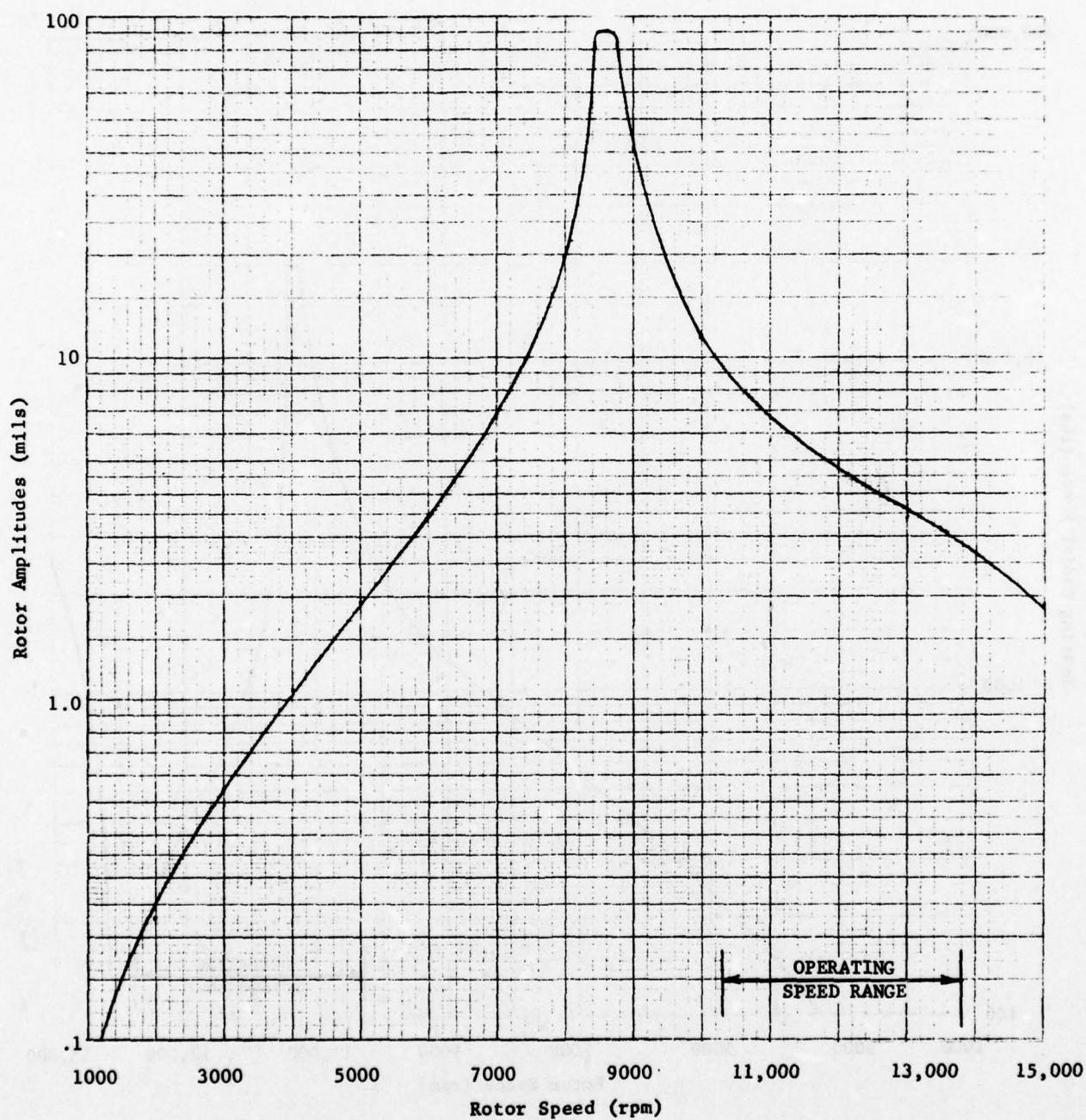


Fig. 7 Turbine Rotor Amplitudes for a Fourth Stage Turbine Blade Loss of the T56-15 Engine

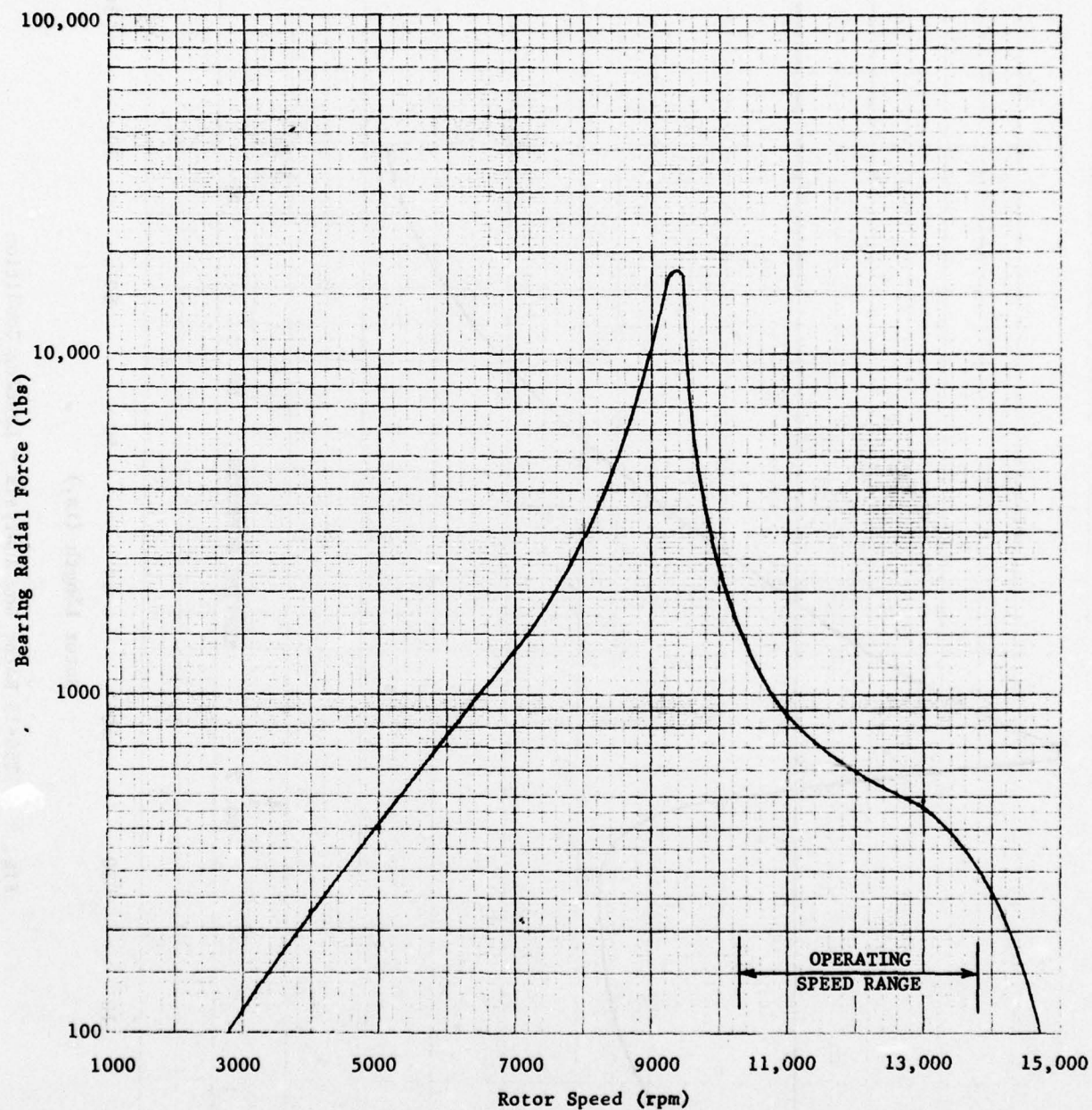


Fig. 8 T56-15 No. 4 Bearing Radial Force for the Fourth Stage Turbine Blade Loss



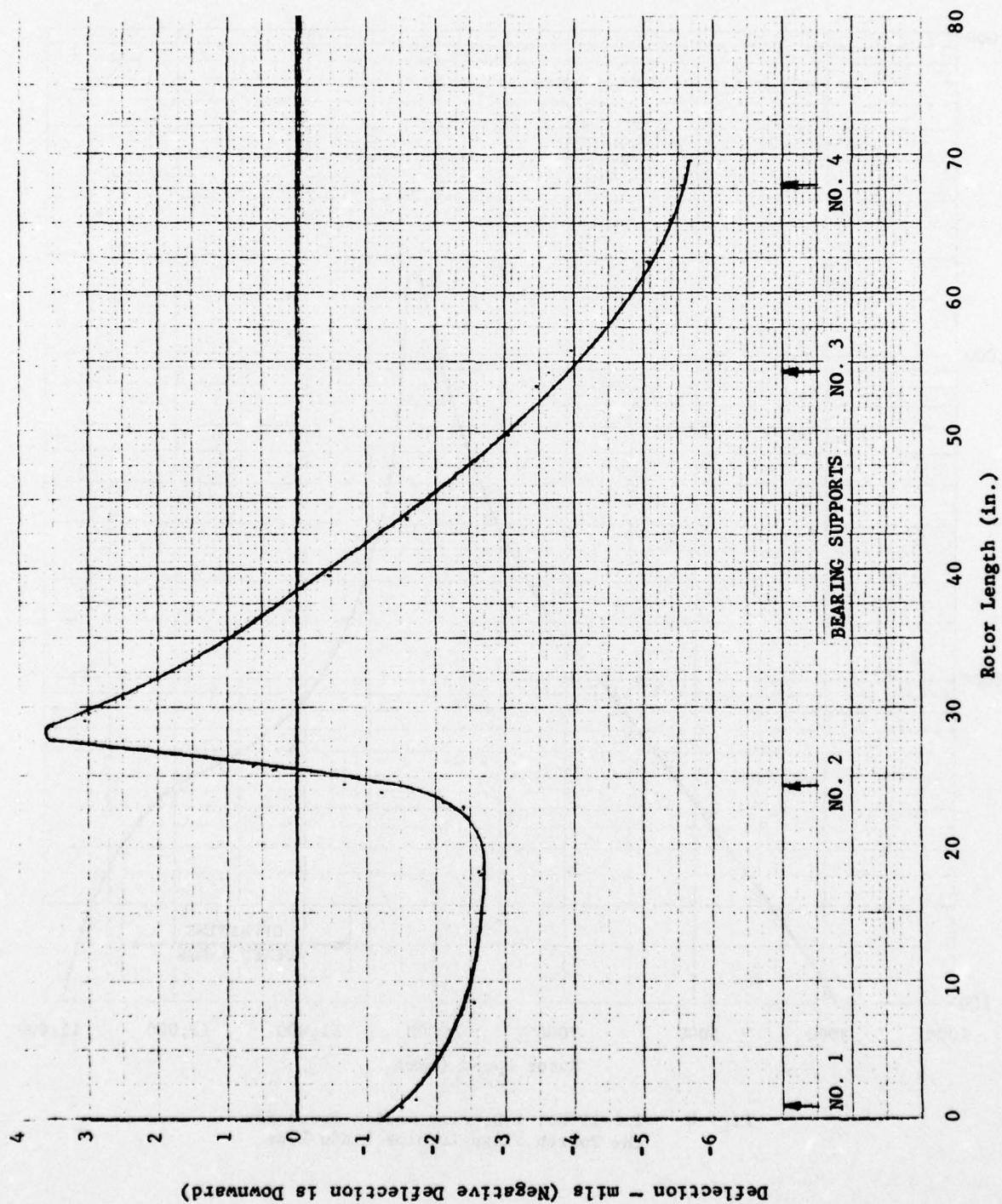


Fig. 9 T56-15 Rotor Bow Analysis - Landing Condition

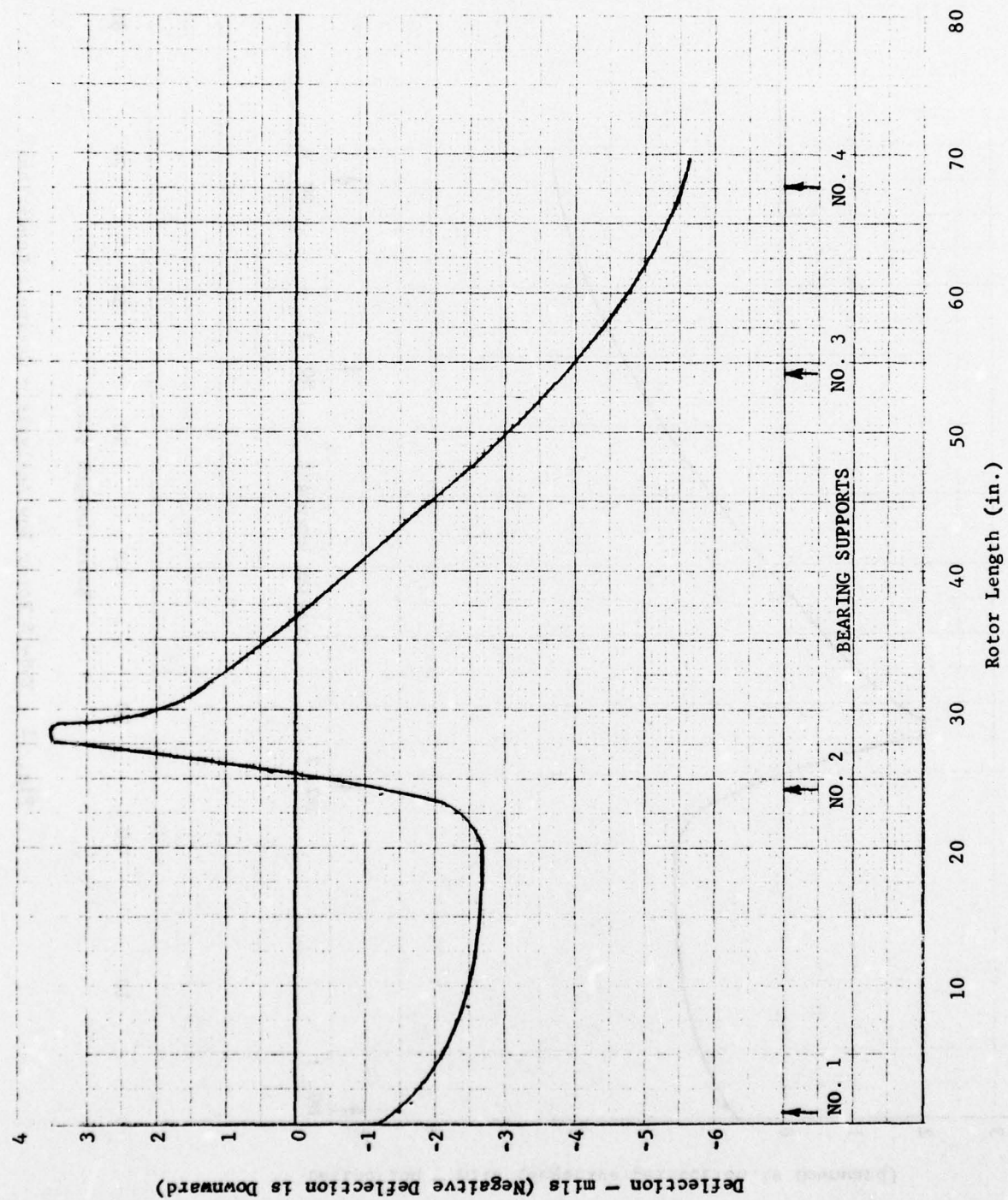


Fig. 10 T56-15 Rotor Bow Analysis - Flight Condition

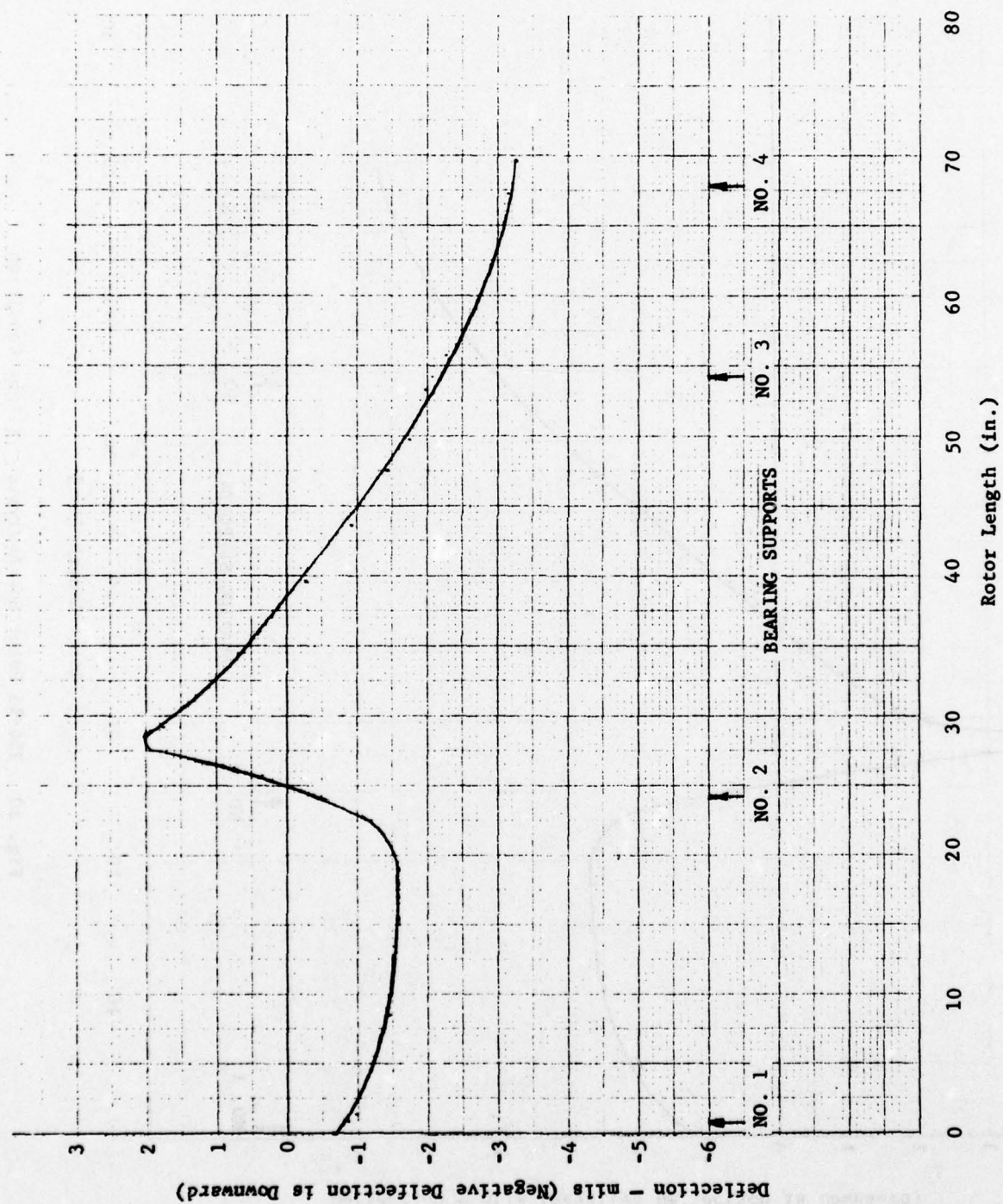


Fig. 11 T56-15 Rotor Bow Analysis - Catapult Conditions



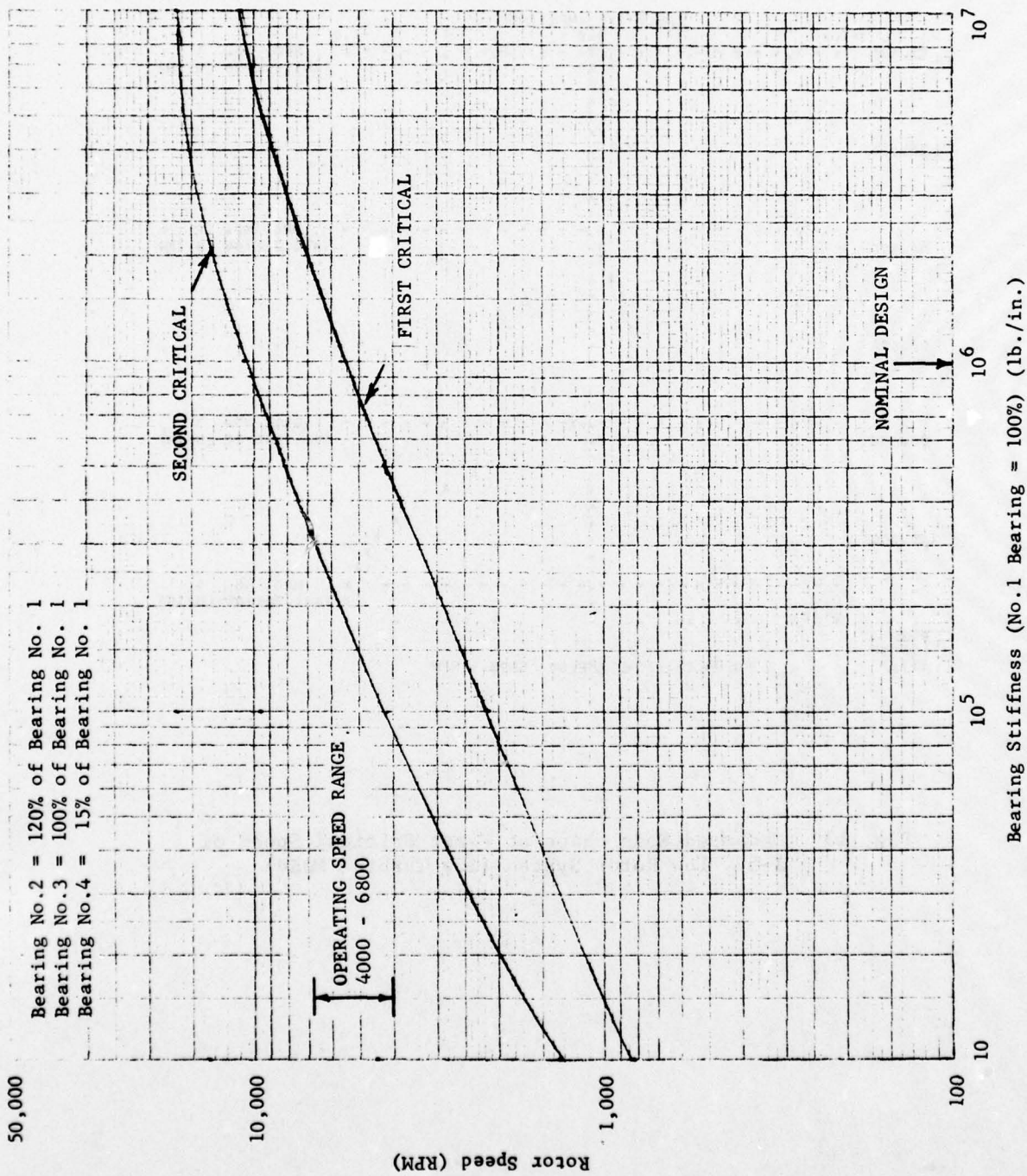


Fig. 12 Critical Speed Map for J 57 Low Rotor Bearing System

THIS PAGE IS BEST QUALITY PRACTICABLE  
FROM COPY FURNISHED TO DDG

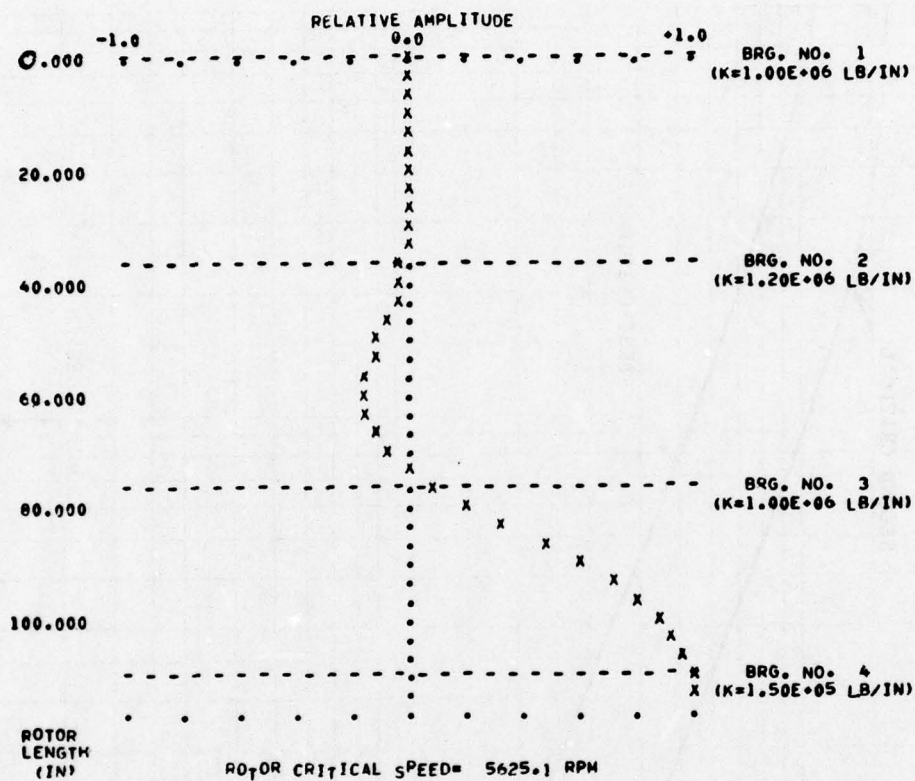


Fig. 13 Undamped Mode Shape at First Critical Speed of  
J-57 Low Rotor System (Low Turbine Mode)

THIS PAGE IS BEST QUALITY PRACTICABLE  
FROM COPY FURNISHED TO DDG

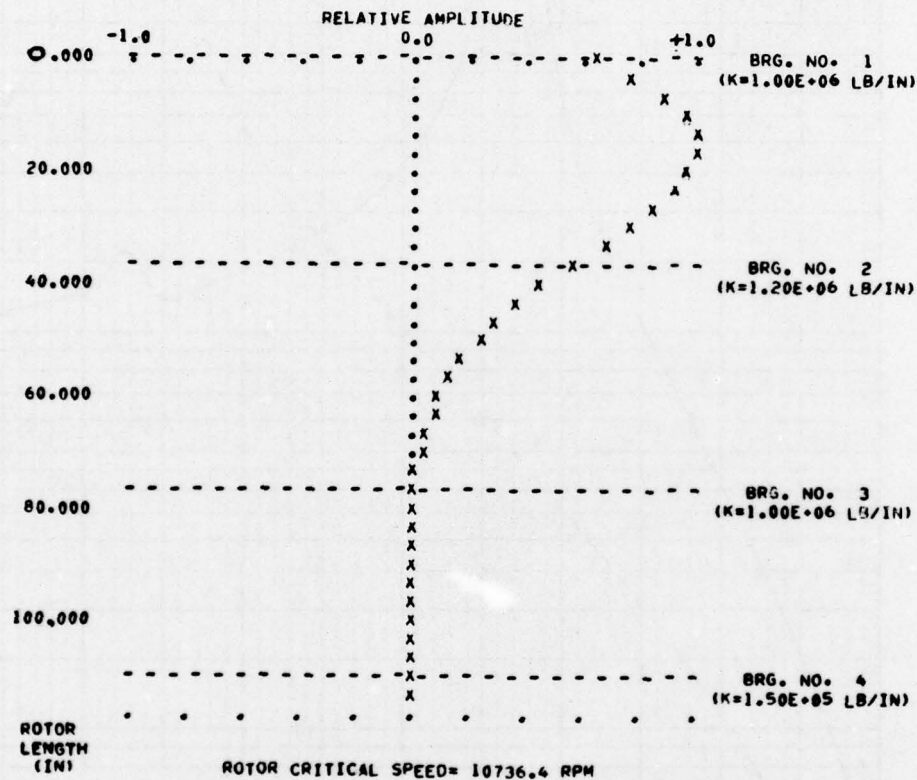


Fig. 14 Undamped Mode Shape at Second Critical Speed  
of J 57 Low Rotor System (Low Compressor  
Bounce Mode)



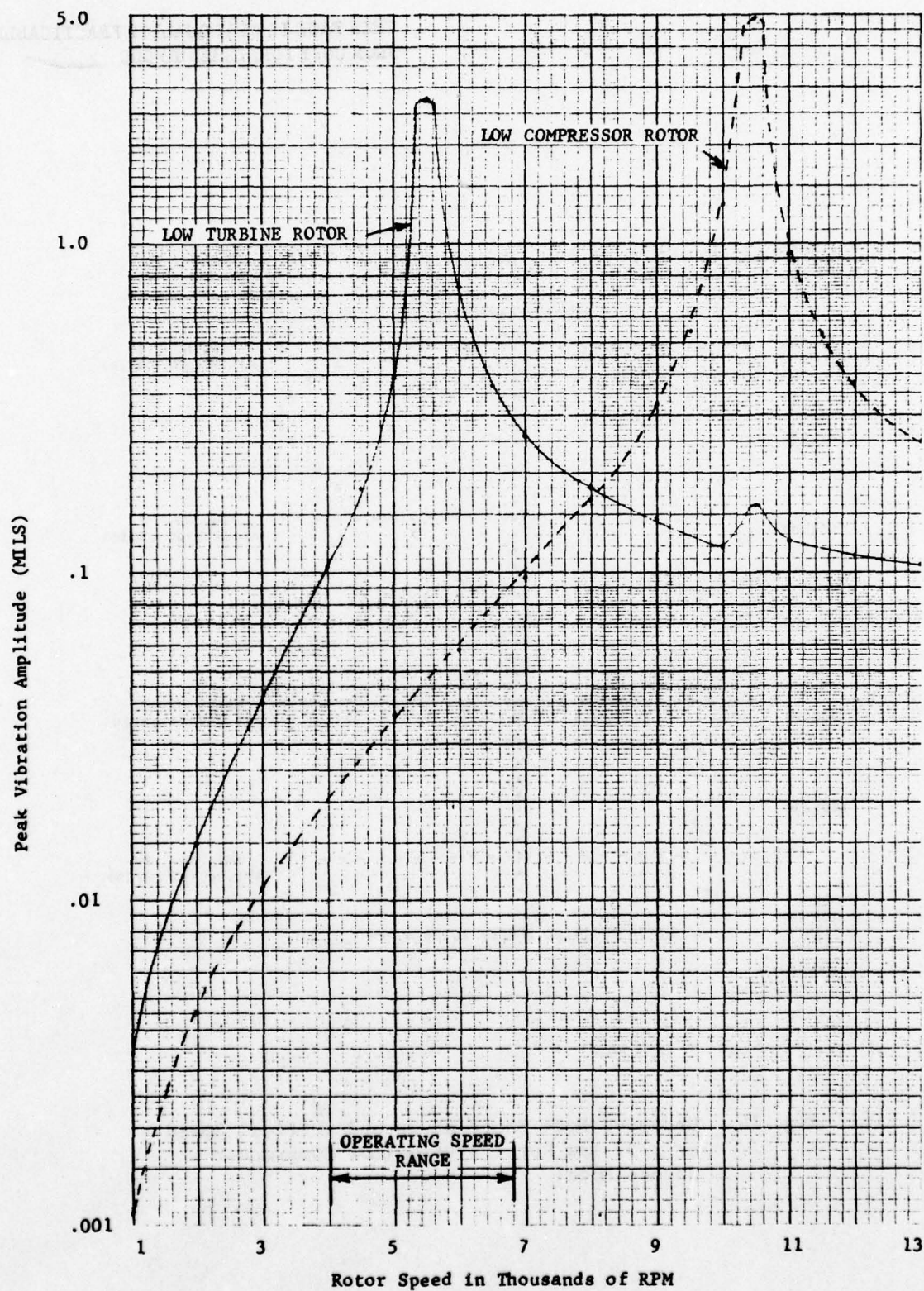


Fig. 15 Calculated Unbalance Response for J 57 Low Rotor System with Random Distributed Unbalance

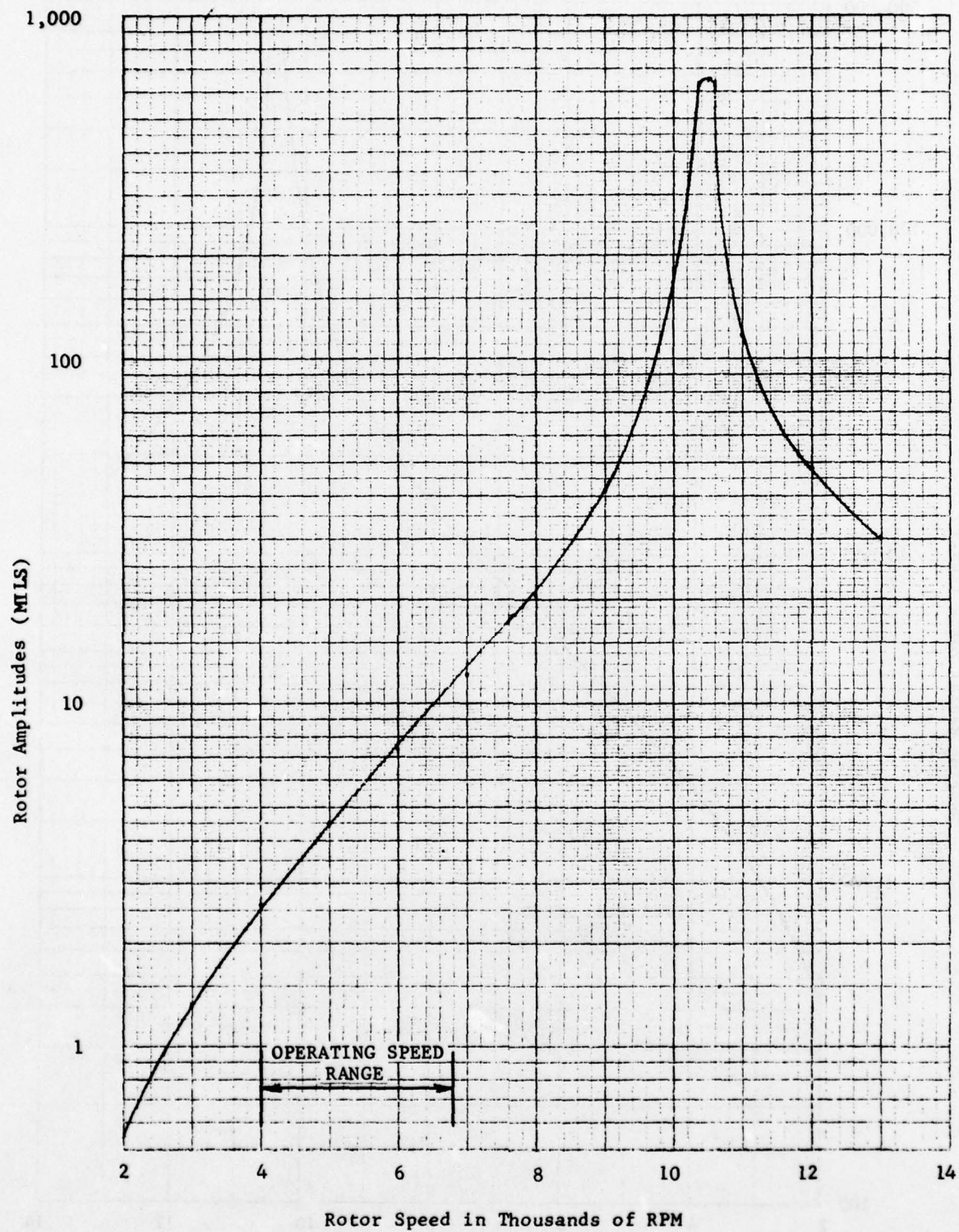


Fig. 16 Low Compressor Rotor Amplitudes for a First Fan Stage Blade Loss of the J-57 Engine



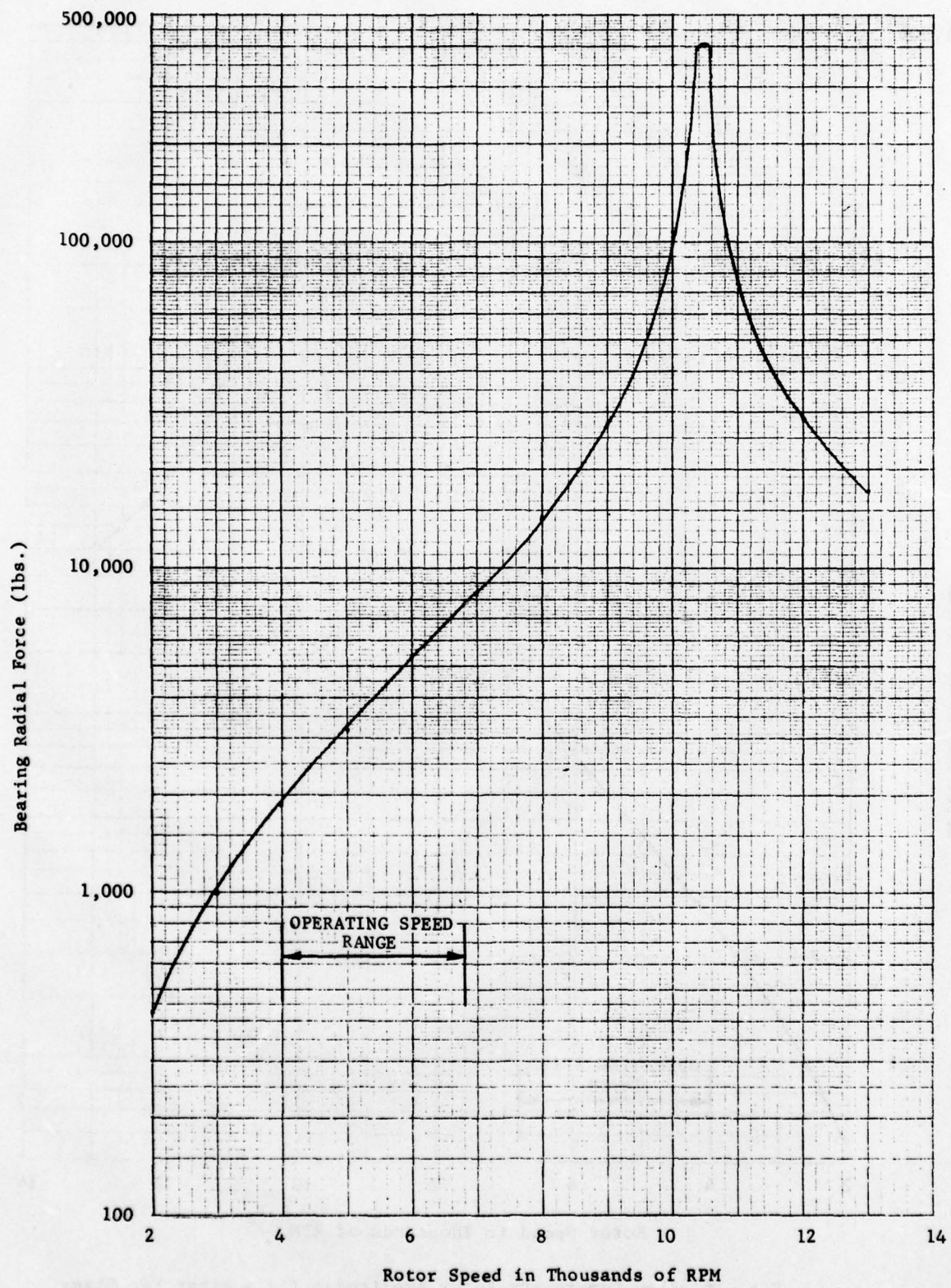


Fig. 17 J 57 Low Rotor No.1 Bearing Radial Force for the First Fan Stage Blade Loss



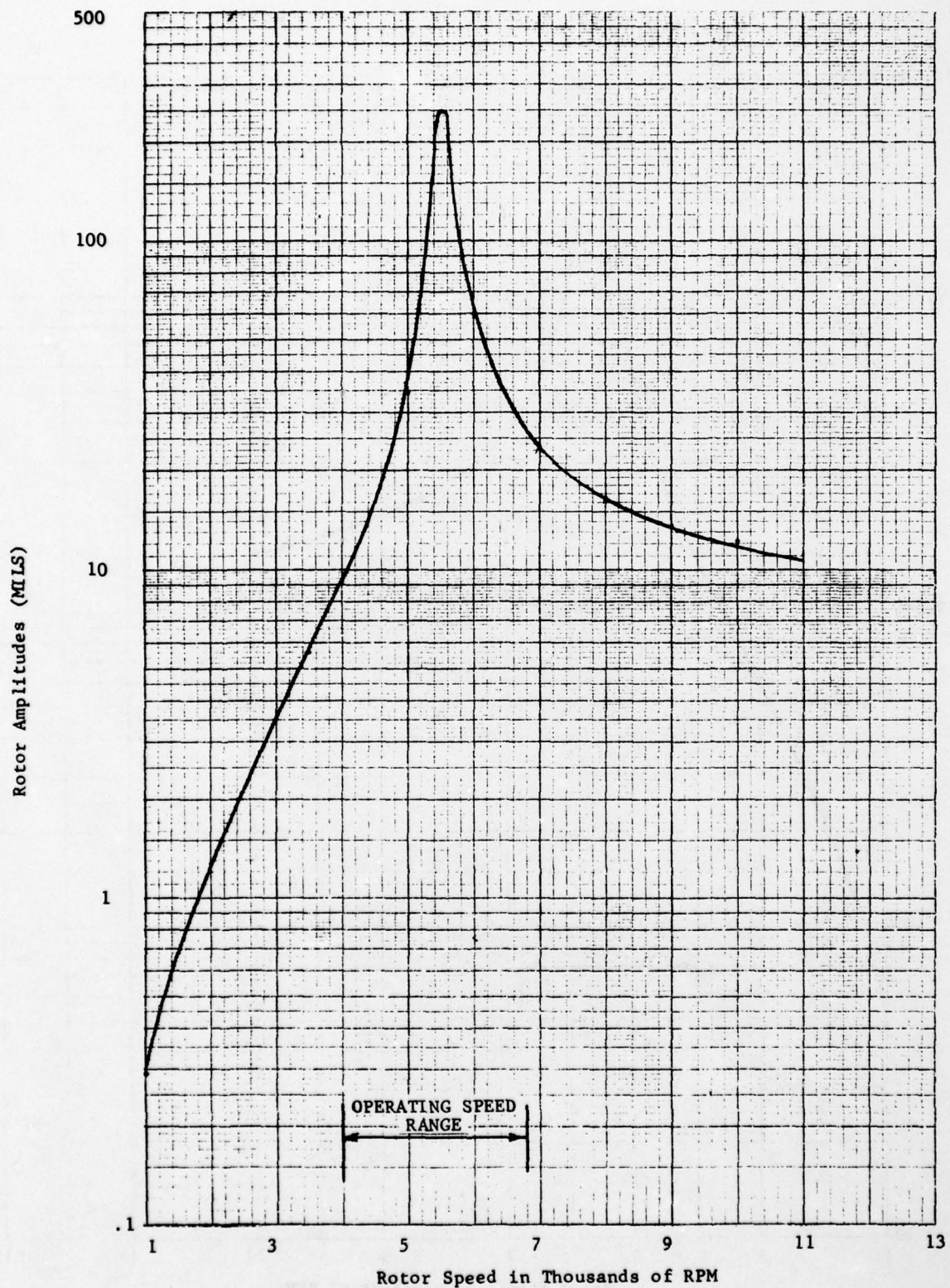


Fig. 18 Low Turbine Rotor Amplitudes for a Third Stage Turbine Blade Loss of the J-57 Engine

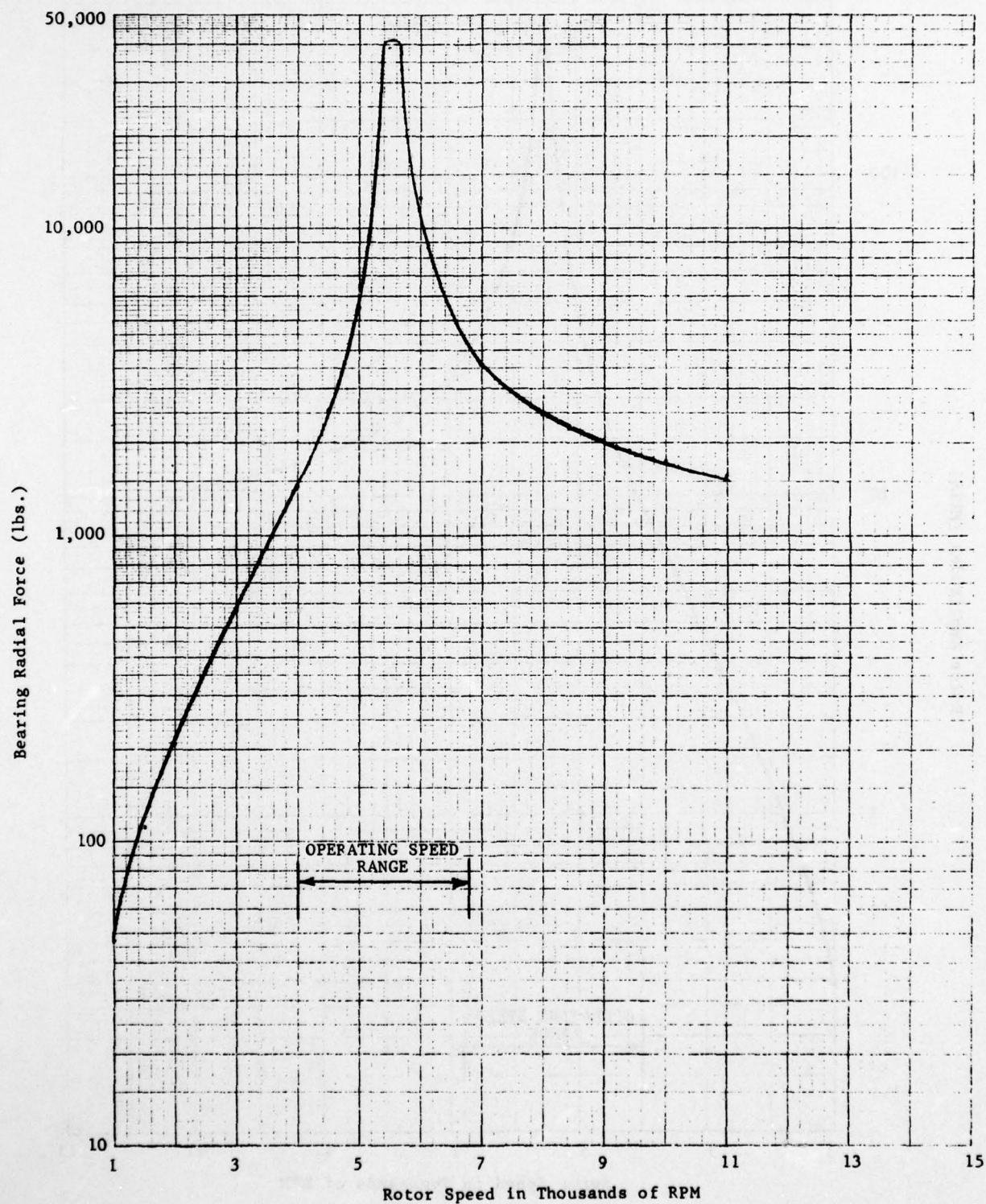


Fig. 19 J 57 No.4 Bearing Radial Force for the 3rd Stage Low Turbine Blade Loss



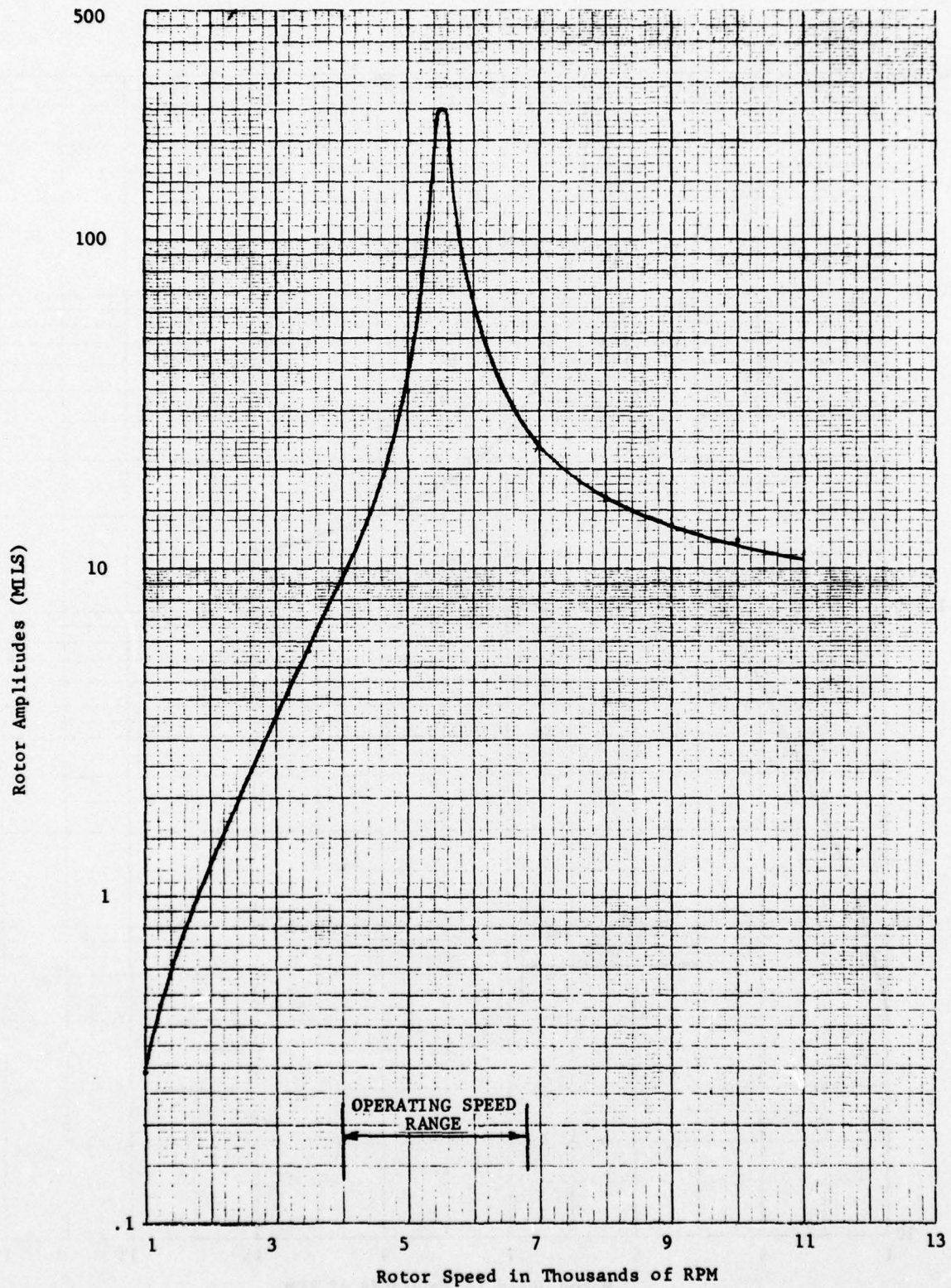


Fig. 18 Low Turbine Rotor Amplitudes for a Third Stage Turbine Blade Loss of the J-57 Engine



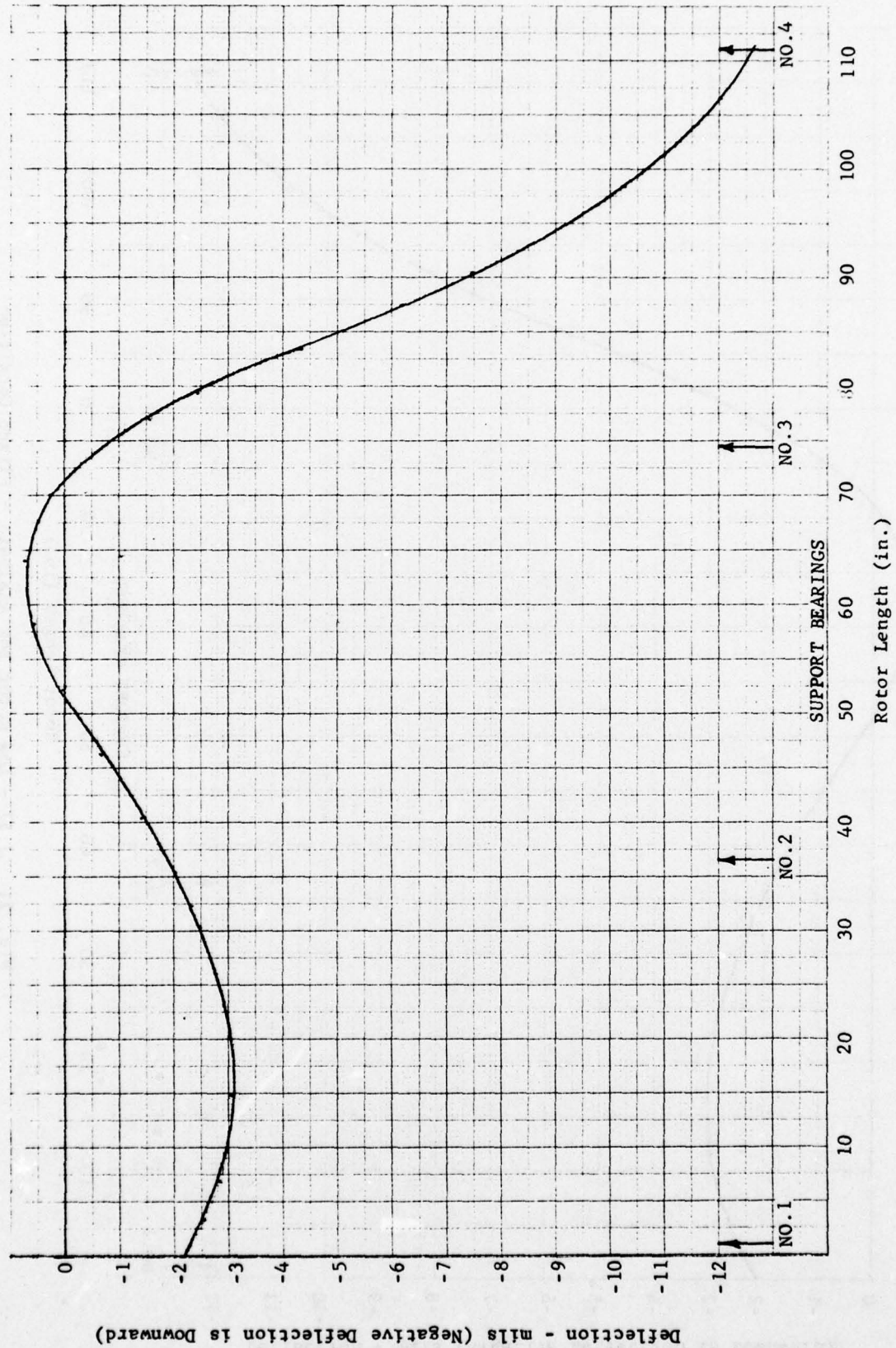


Fig. 20 J 57 - Low Rotor Bow Analysis - Landing Condition

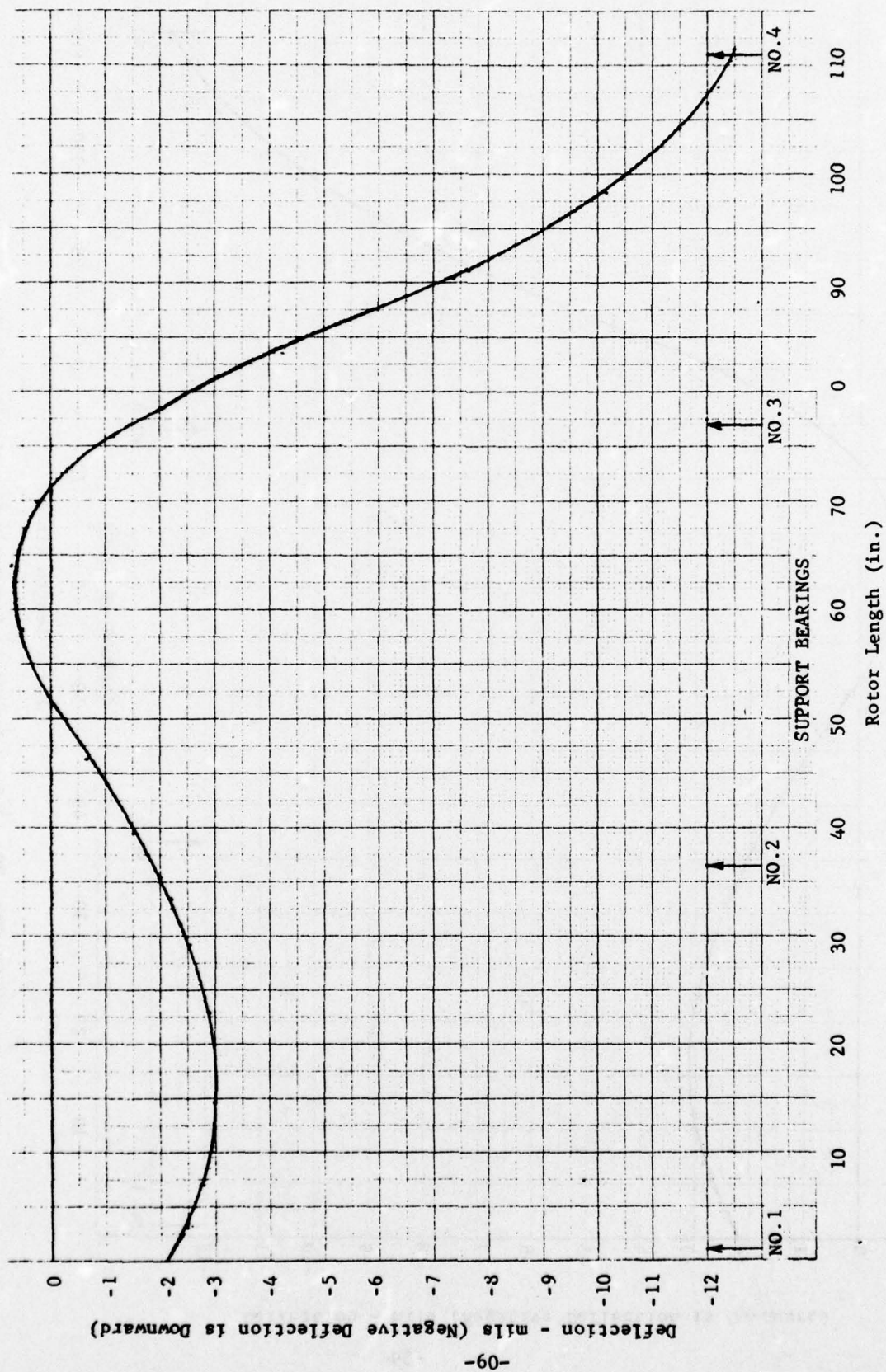


Fig. 21 J 57 - Low Rotor Bow Analysis - Flight Condition

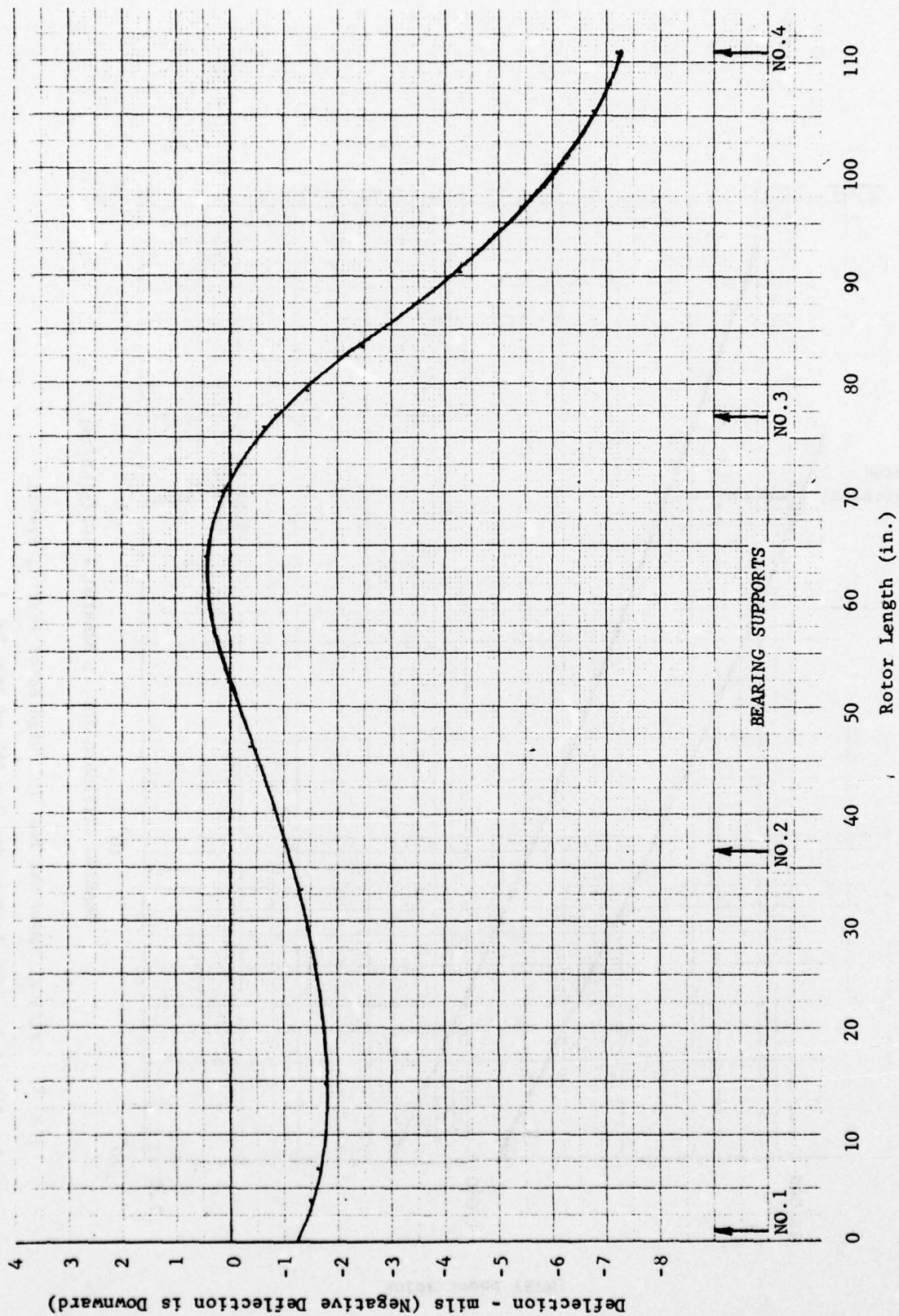


Fig. 22 J 57 Low Rotor Bow Analysis - Catapult Condition



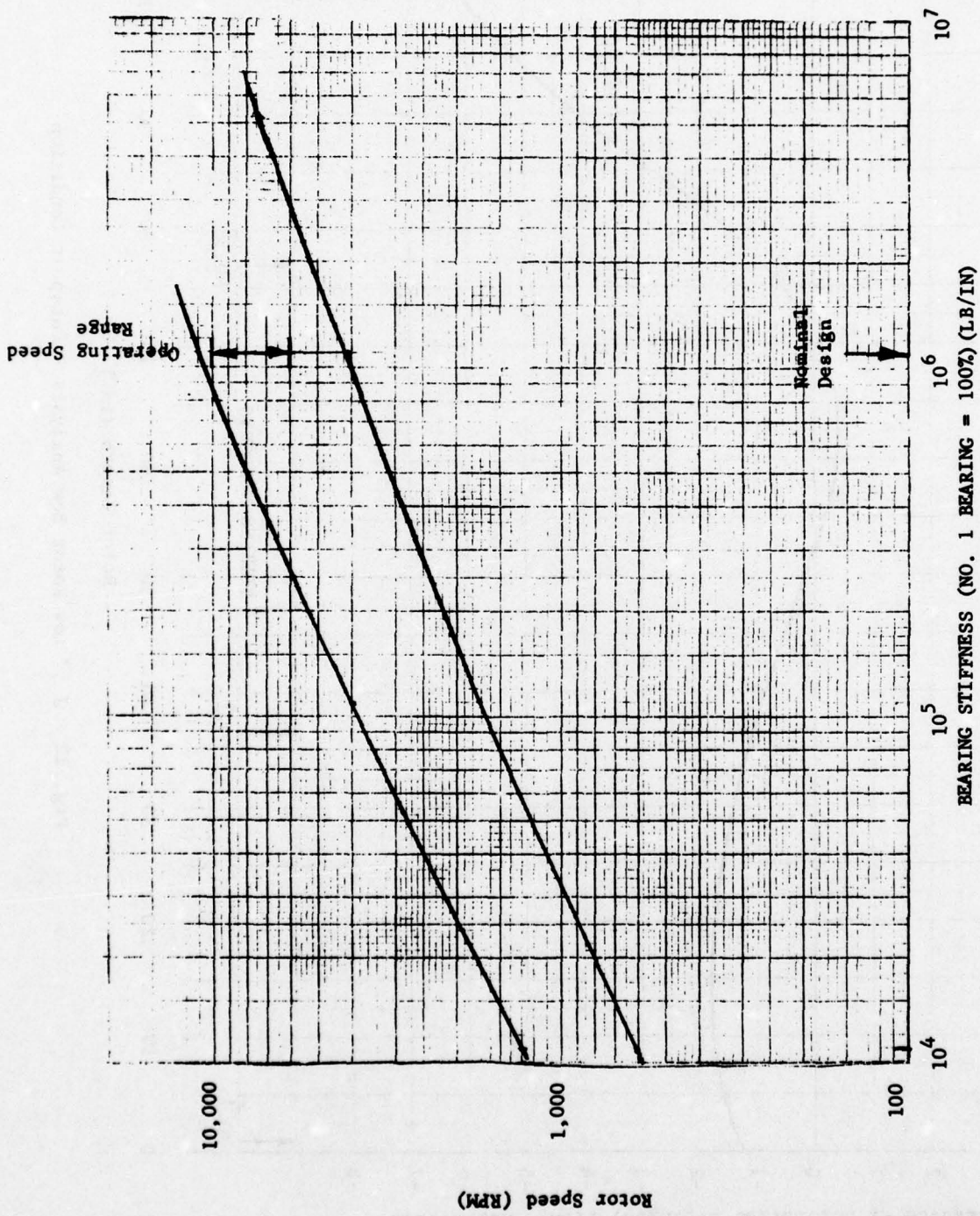


Fig. 23. Critical Speed Map for J57 High Rotor Bearing System.

Brg. No. 2 = 91% of Brg. No. 1; Brg. No. 3 = 16% of Brg. No. 1

THIS PAGE IS BEST QUALITY PRACTICABLE  
FROM COPY FURNISHED TO DDG

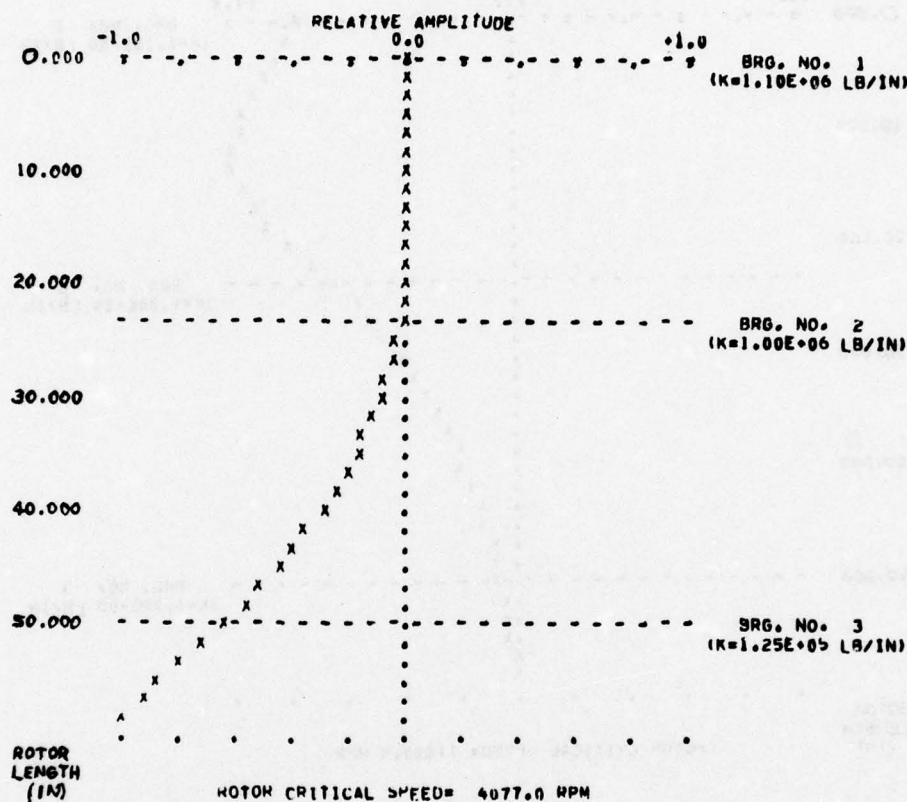


Fig.24. Undamped Mode Shape at First Critical Speed for the  
J57 High Rotor System (Cantilevered Turbine Mode).

THIS PAGE IS BEST QUALITY PRACTICABLE  
FROM COPY FURNISHED TO DDC

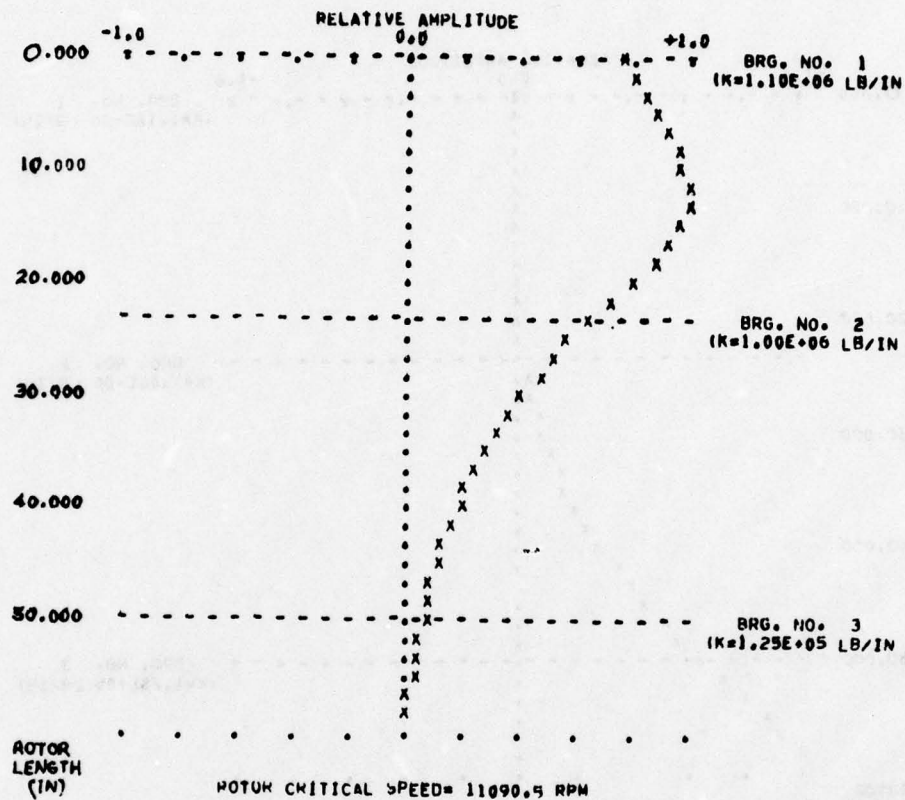


Fig. 25. Undamped Mode Shape at Second Critical Speed for  
the J57 High Rotor System (Compressor Bounce Mode).



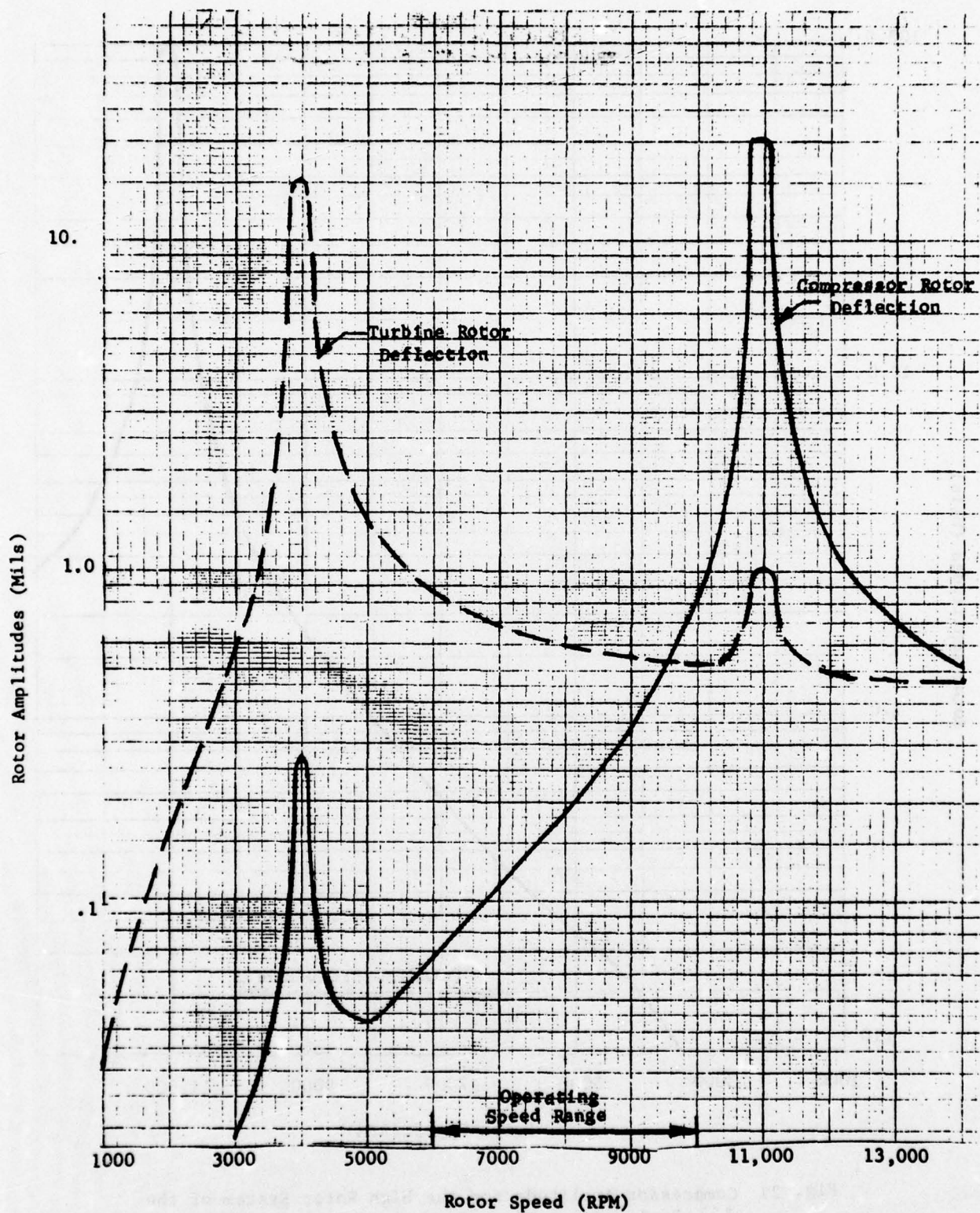


Fig. 26. Calculated Unbalance Response Vibration for the J57 High Rotor with Distributed Unbalance.

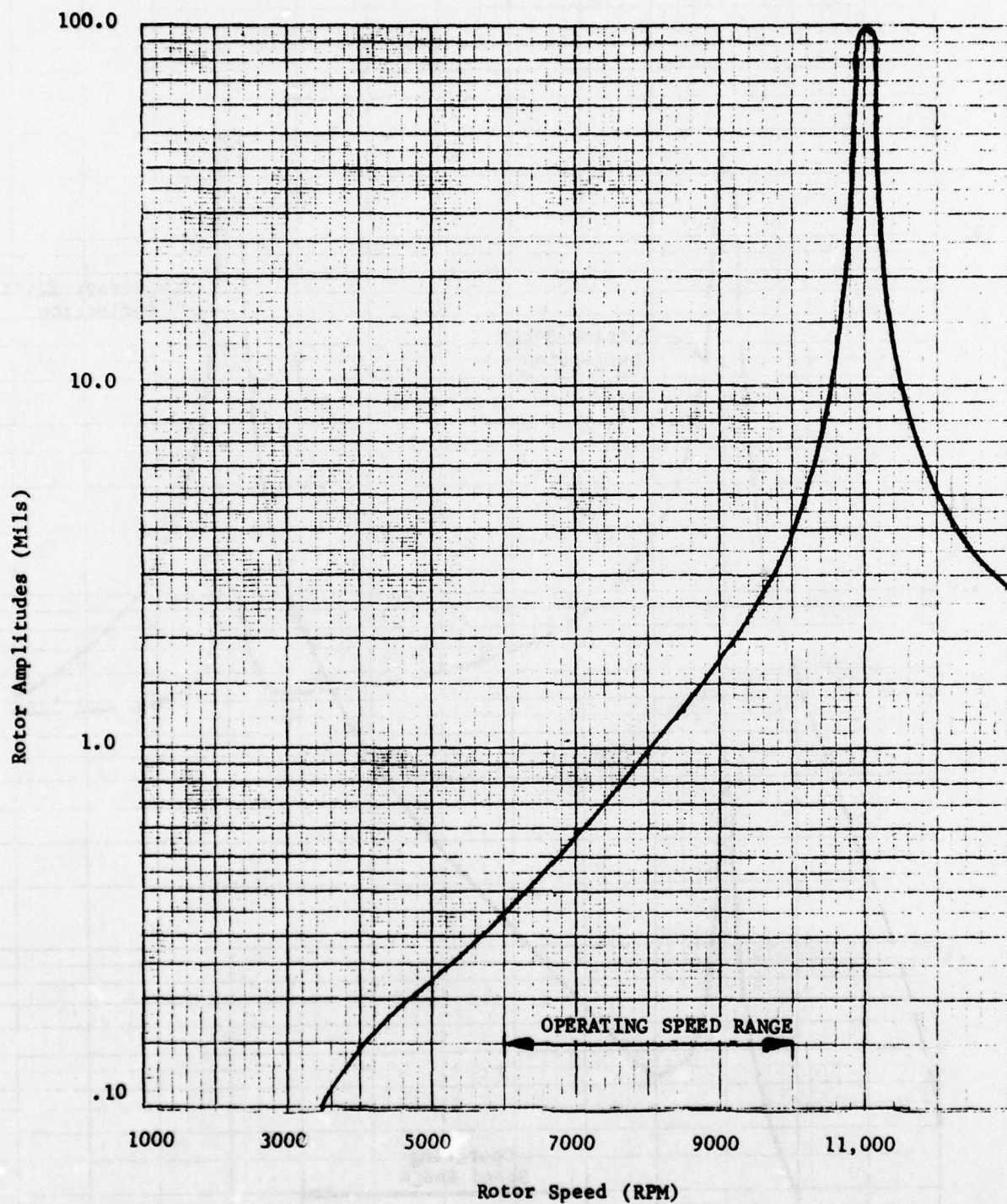


Fig. 27 Compressor Amplitude for the High Rotor System of the J57 Engine for a First Compressor Stage Blade Loss.



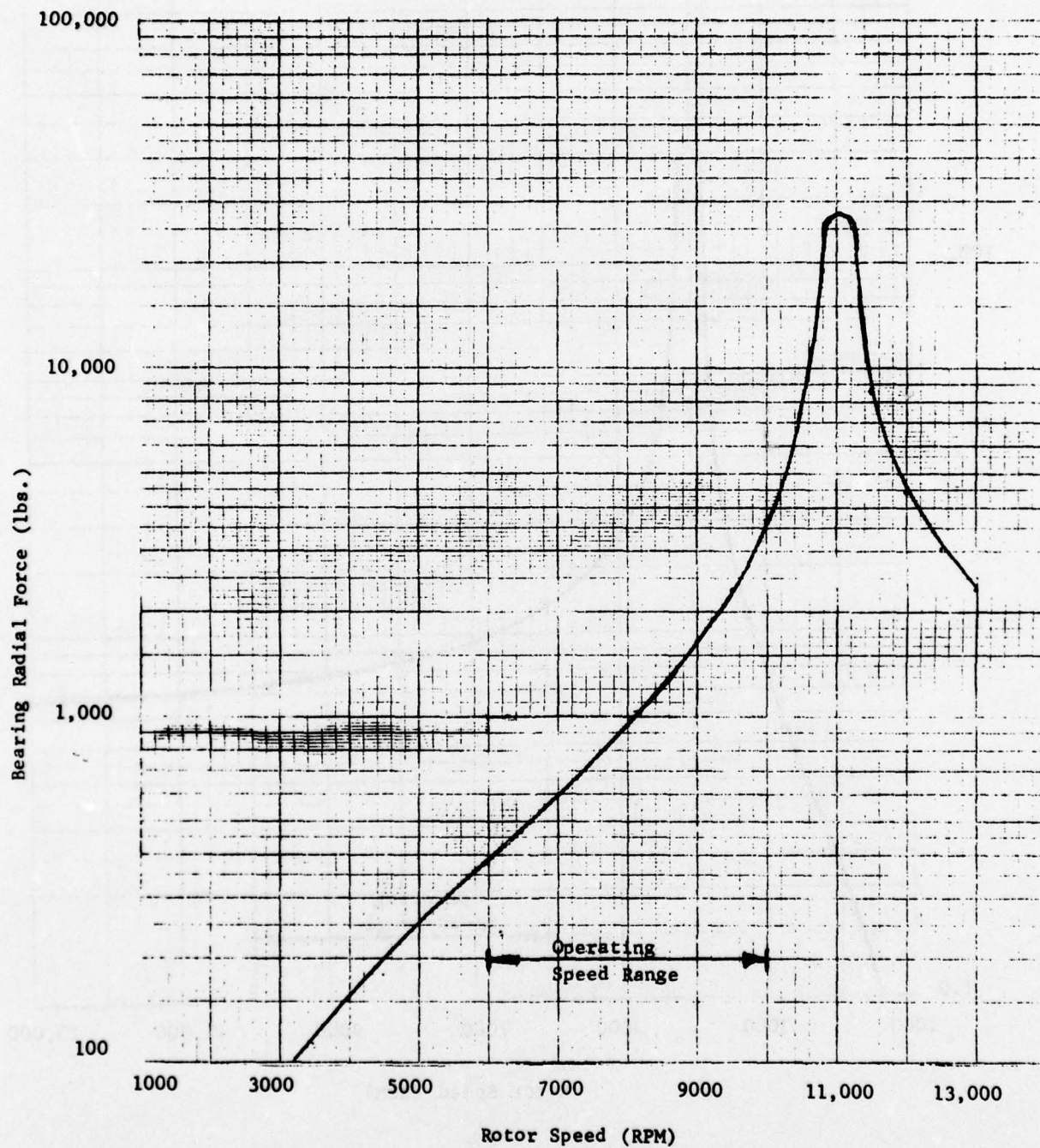


Fig. 28. No. 1 Bearing Radial Load for a First Stage Compressor Blade Loss of the J 57 High Rotor System.



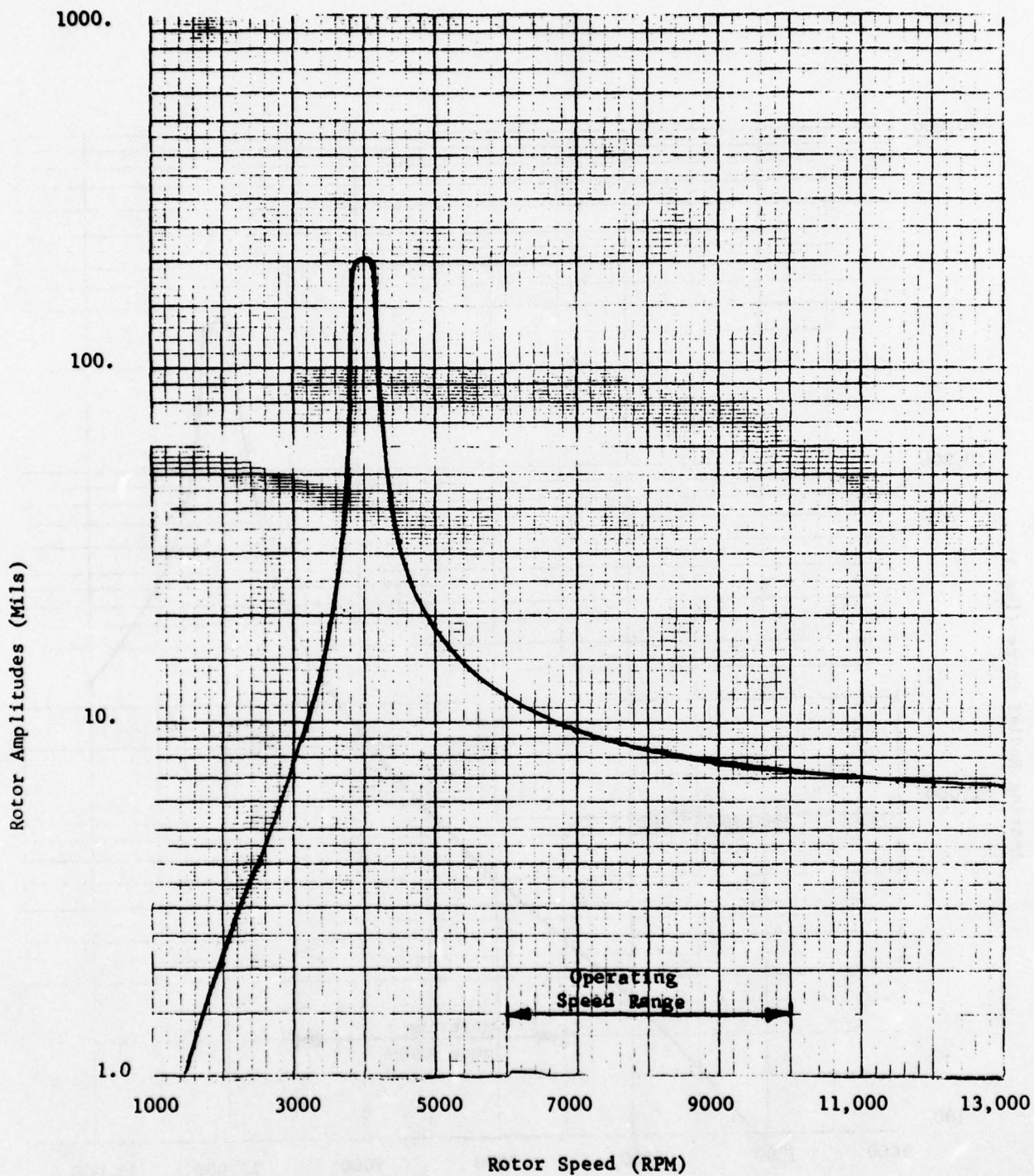


Fig. 29. Turbine Amplitude for the High Rotor System of the J57 Engine for a High Turbine Blade Loss.

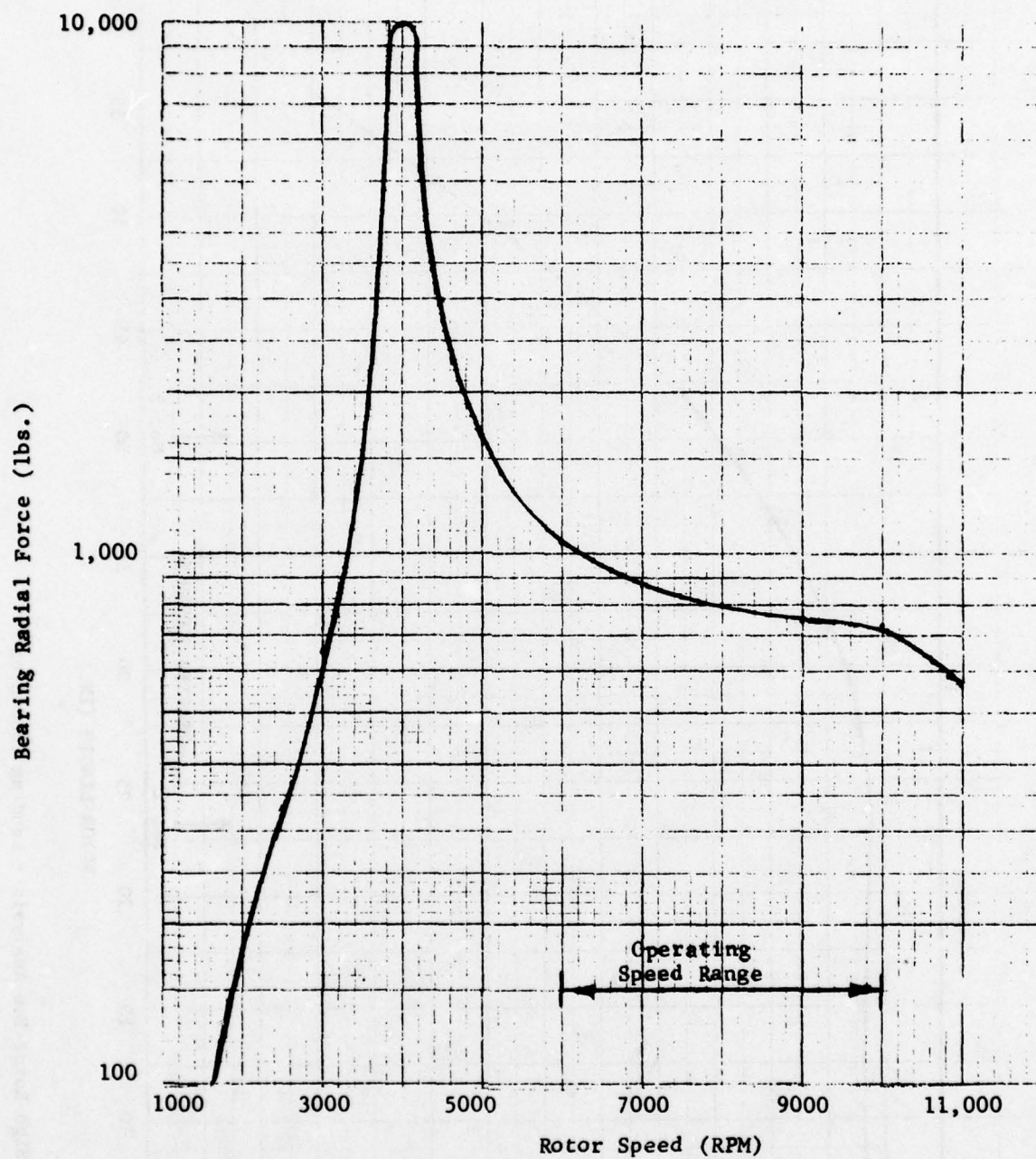


Fig. 30. No. 3 Bearing Radial Force for a Turbine Blade Loss of the J 57 High Rotor System.

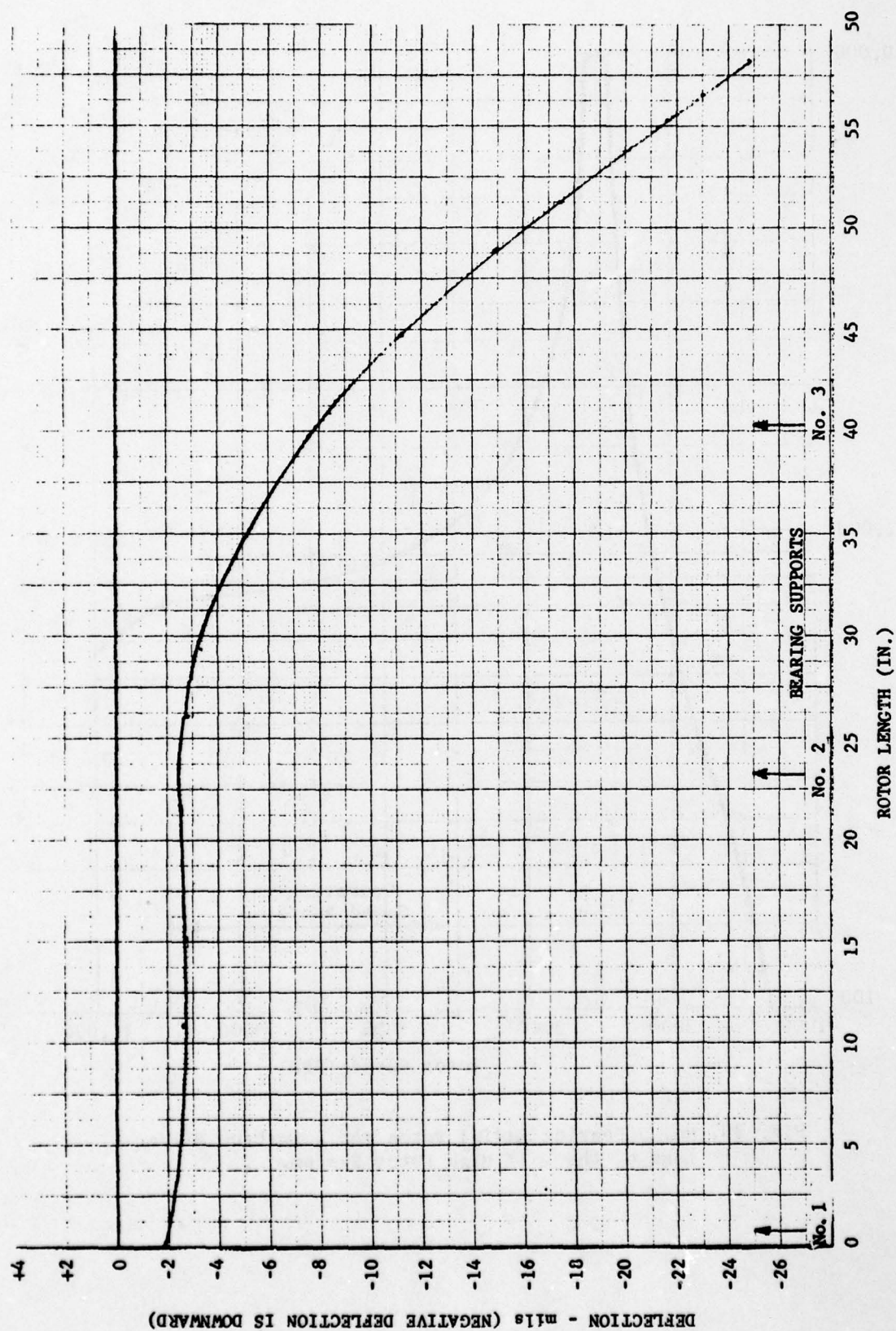


Fig. 31 J57 High Rotor Bow Analysis - Landing Condition



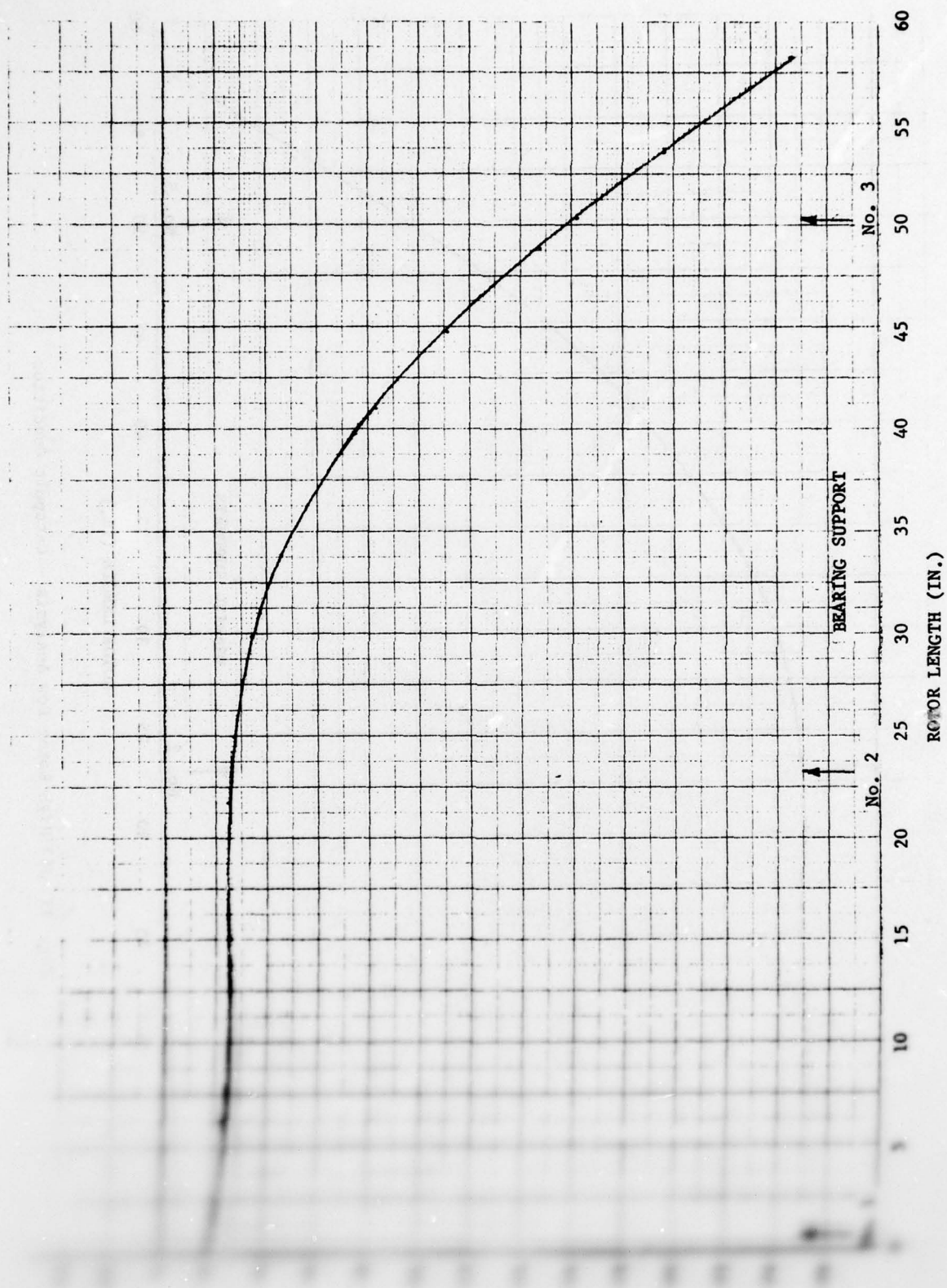


FIG. 12. J57 High Rotor Bow Analysis - Flight Condition

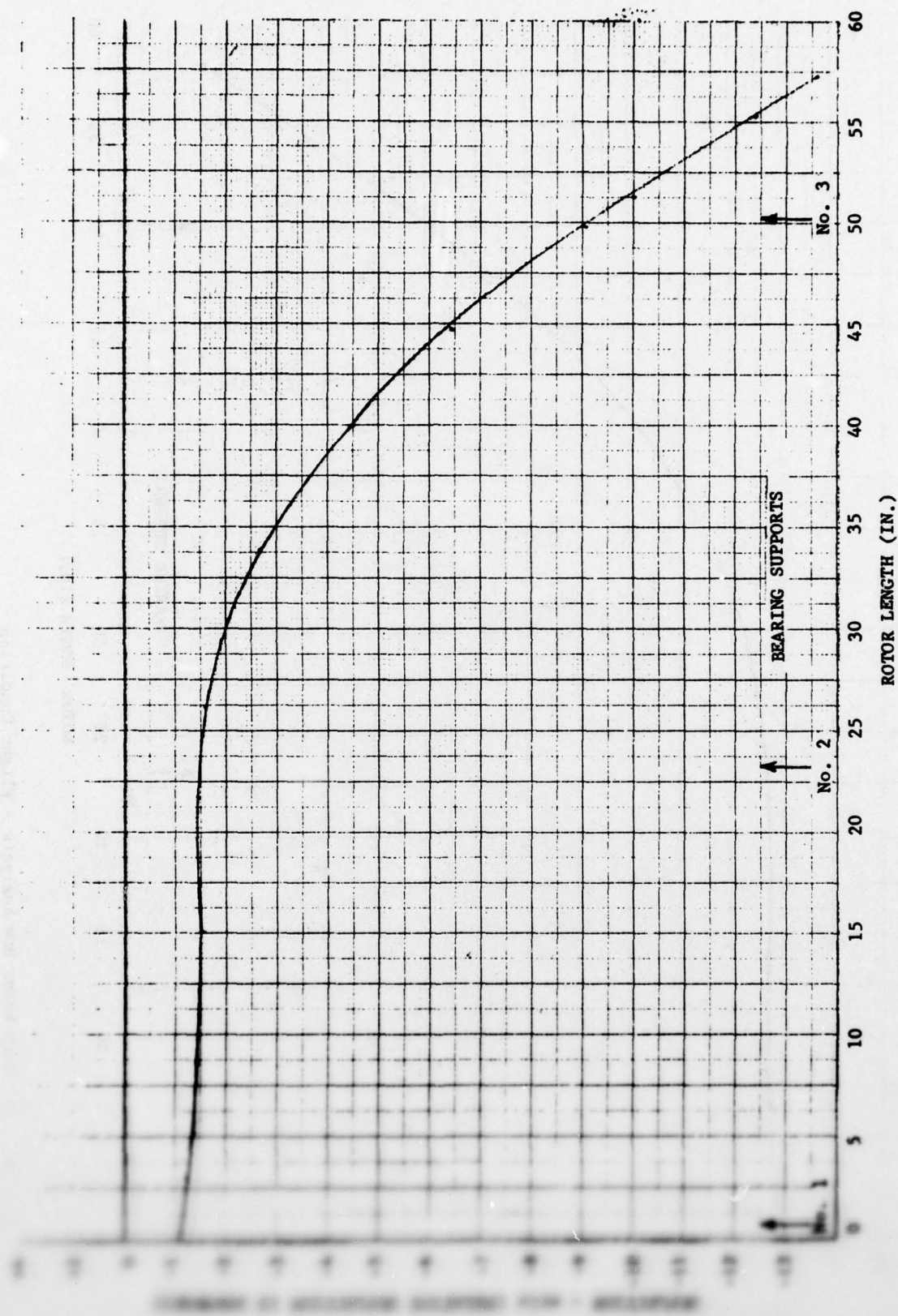


Fig. 33 J57 High Rotor Bow Analysis - Catapult Condition

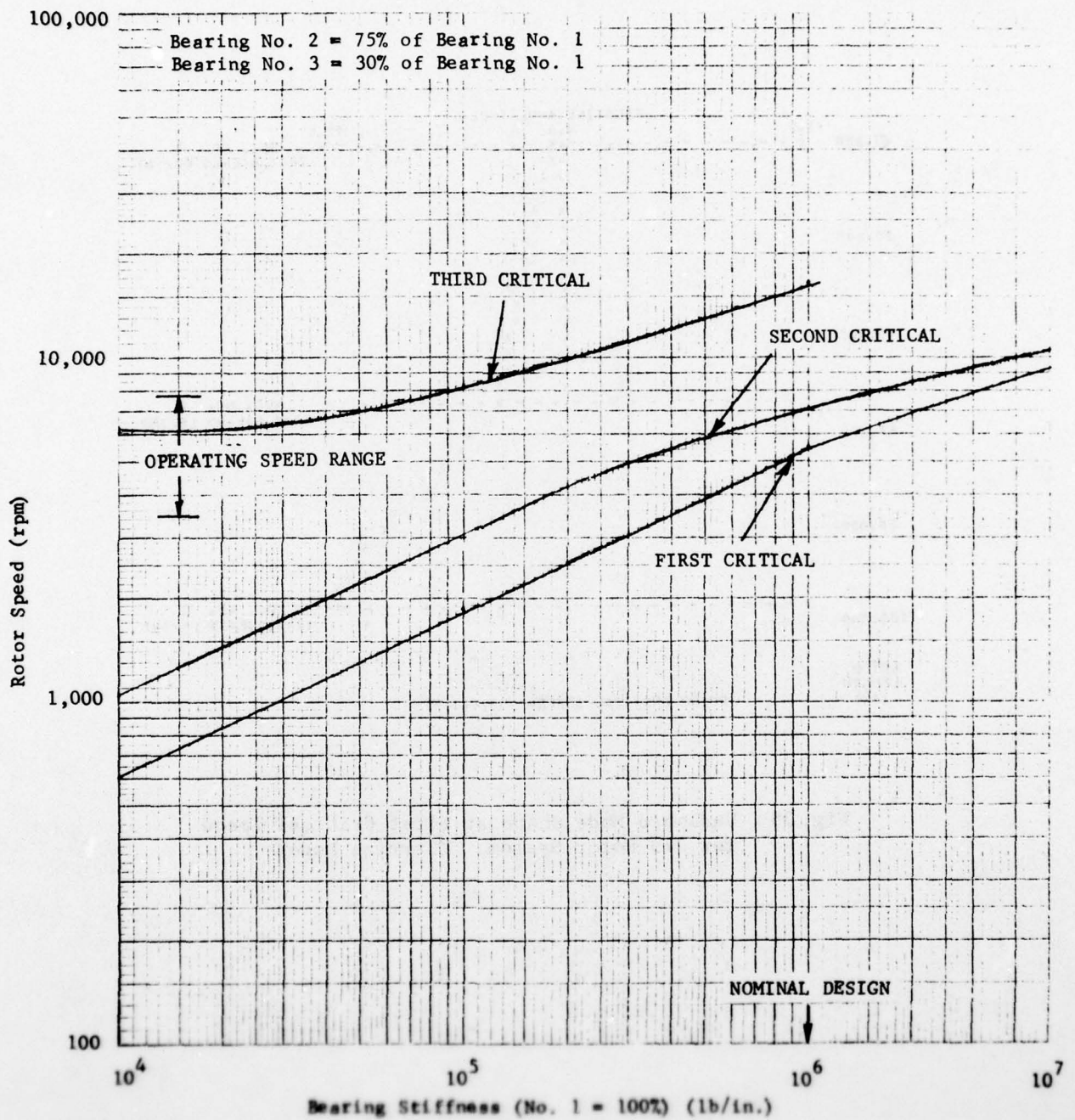


Fig. 34 Critical Speed Map for 379  
Rotor Bearing System



THIS PAGE IS BEST QUALITY PRACTICABLE  
FROM COPY FURNISHED TO DDG

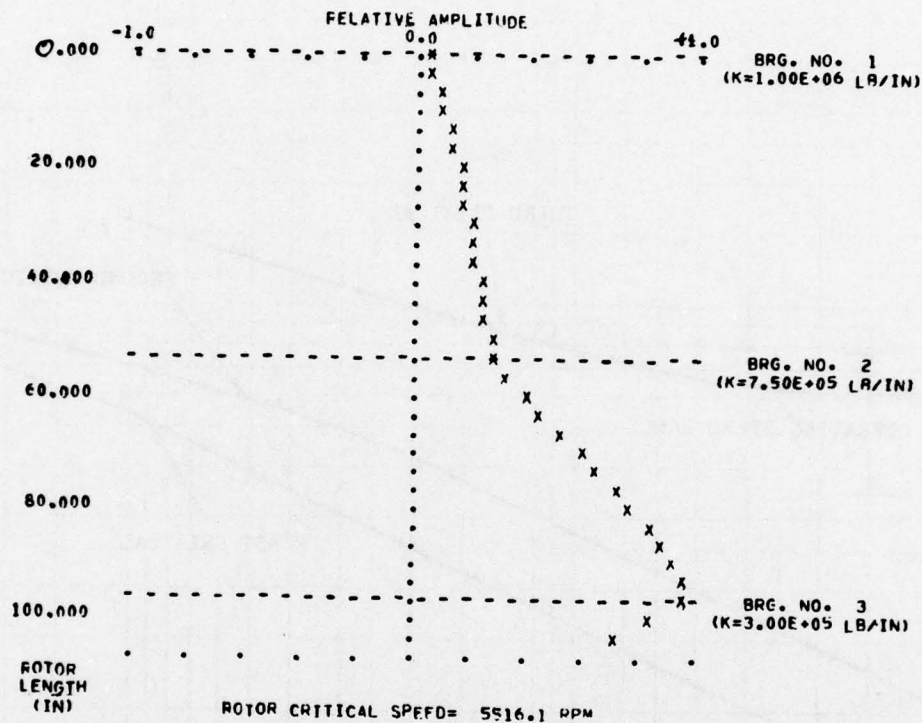


Fig. 35 Undamped Mode Shape at First Critical Speed  
for J79 Rotor System. (Turbine Mode)

THIS PAGE IS BEST QUALITY PRACTICABLE  
FROM COPY FURNISHED TO DDG

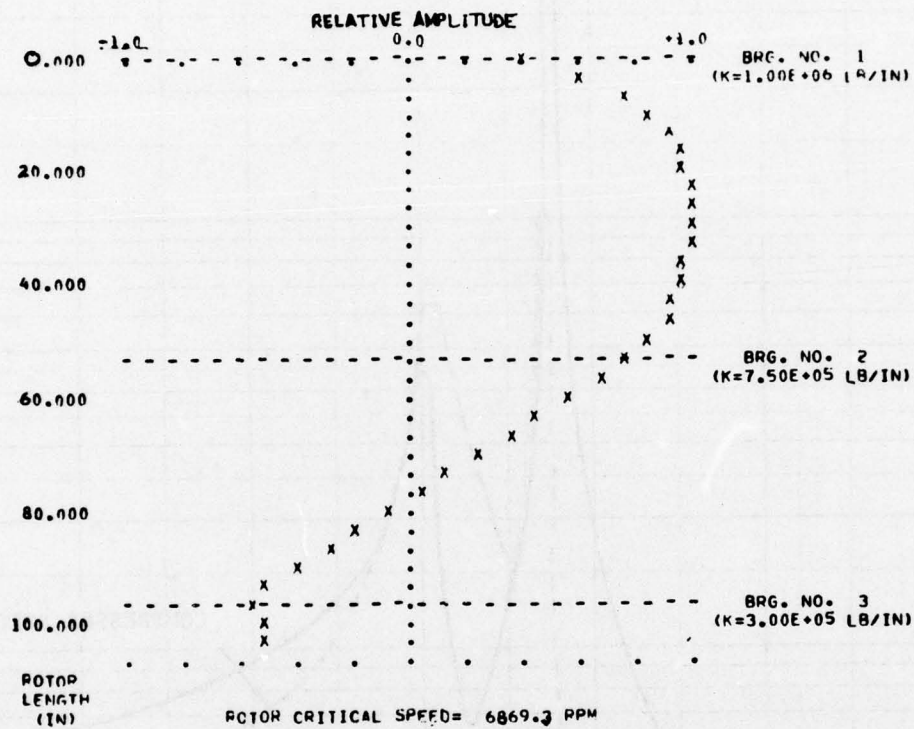


Fig. 36 Undamped Mode Shape at Second Critical Speed  
for the J79 Rotor System. (Compressor  
Bounce Mode)

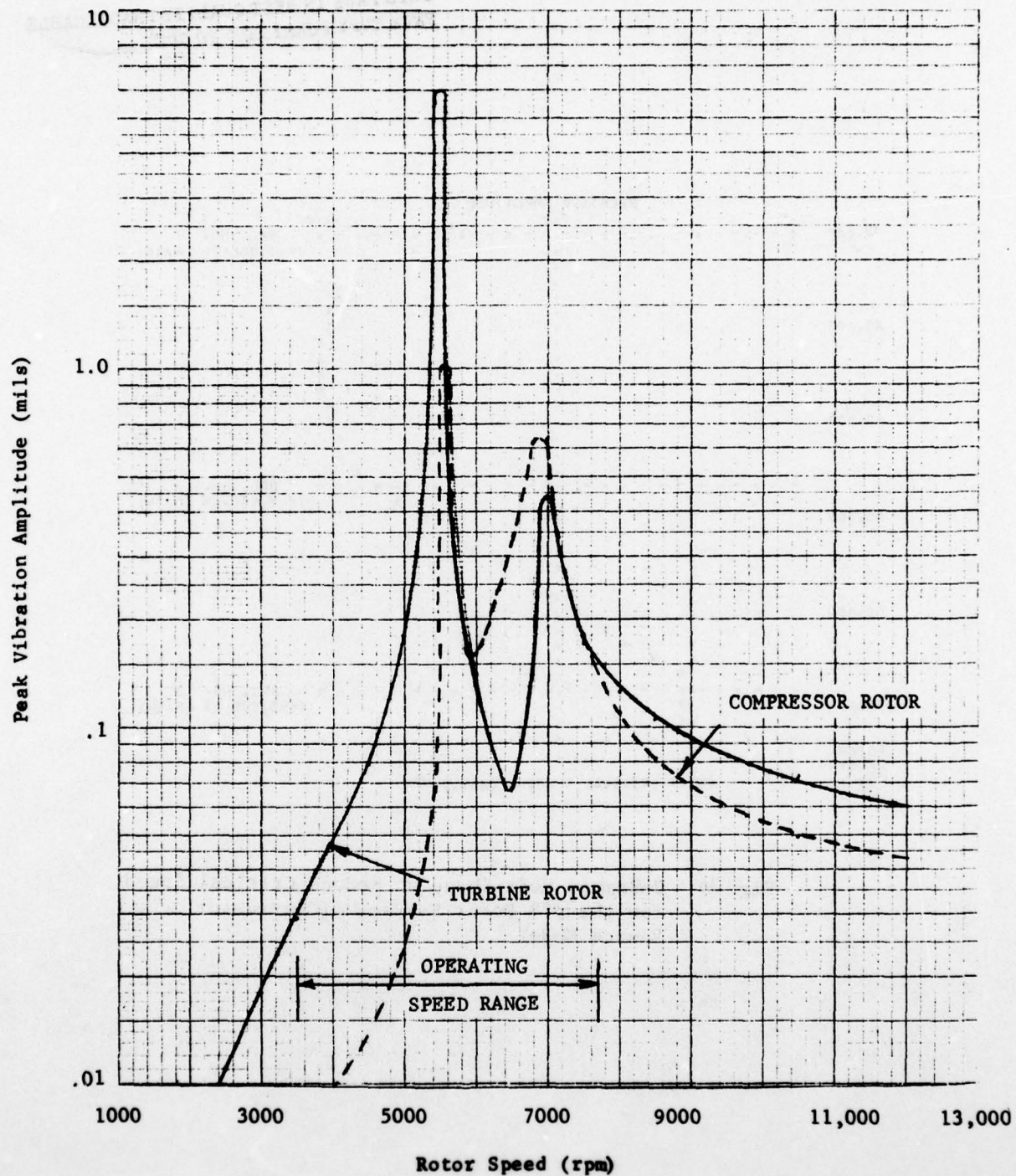


Fig. 37 Calculated Unbalance for J79 Rotor System With Random Distributed Unbalance



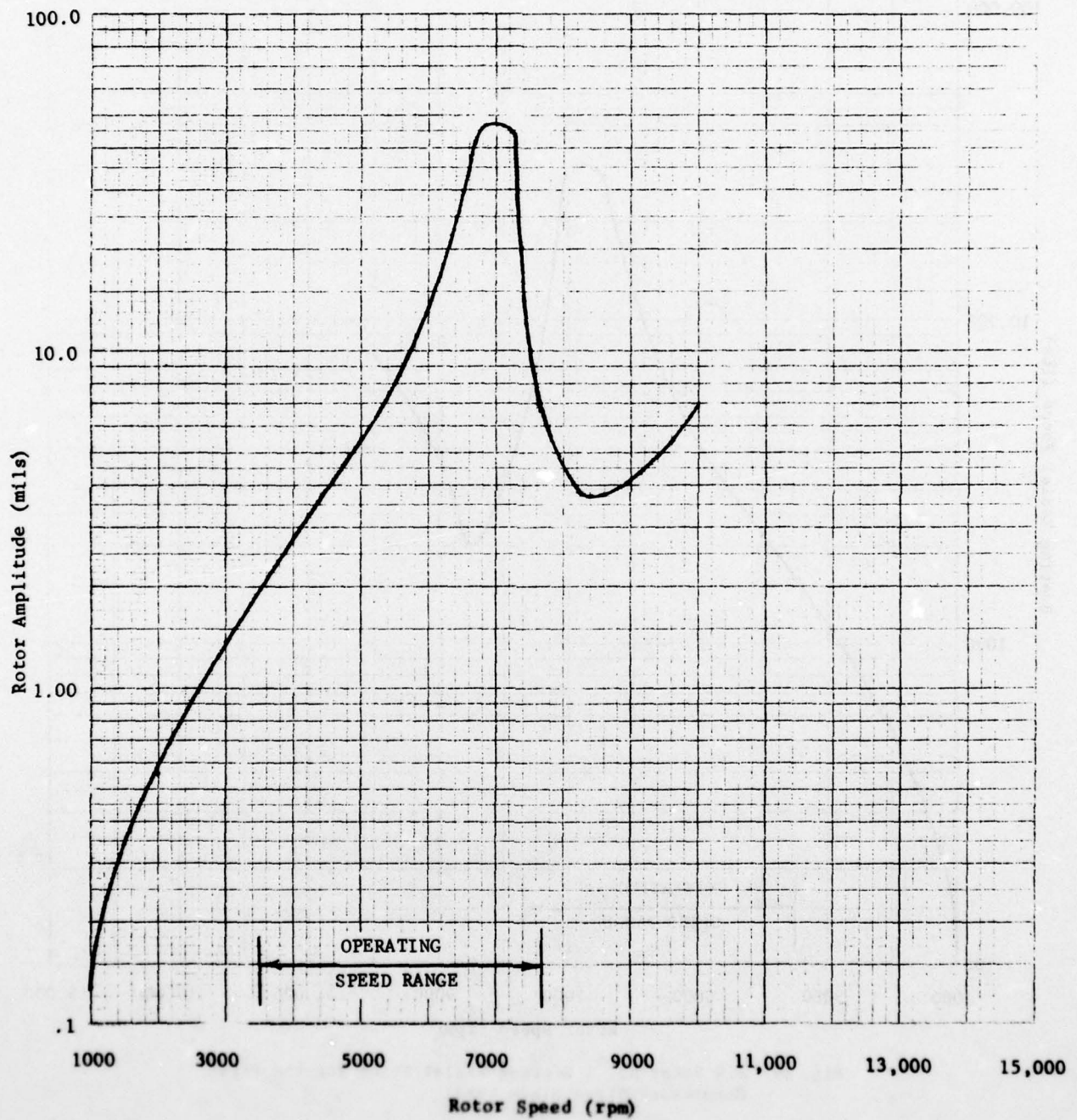


Fig. 38 Compressor Rotor Amplitudes for a First Compressor Stage Blade Loss of the J79 Engine

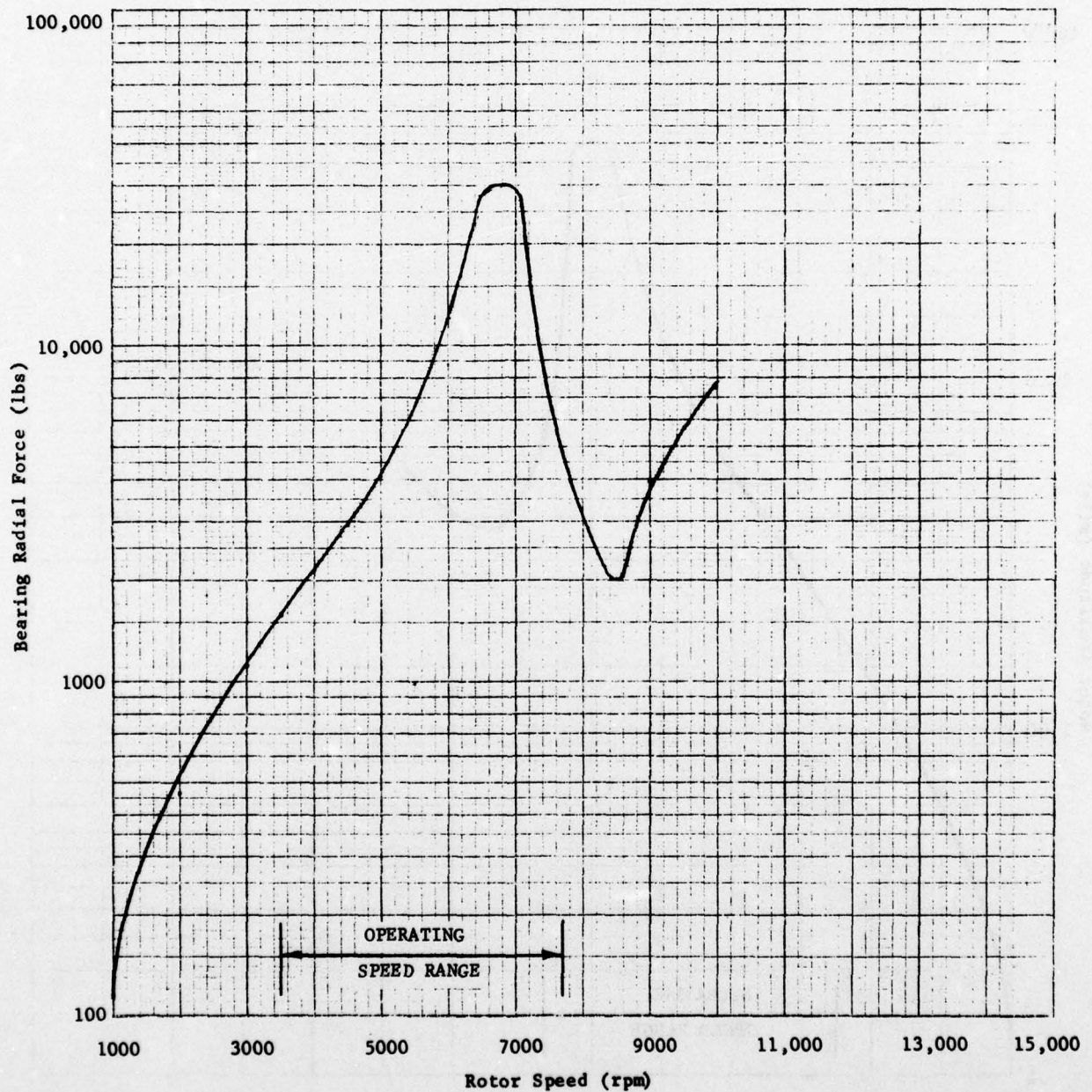


Fig. 39 J79 Rotor No. 1 Bearing Radial Force for the First Compressor Stage Blade Loss

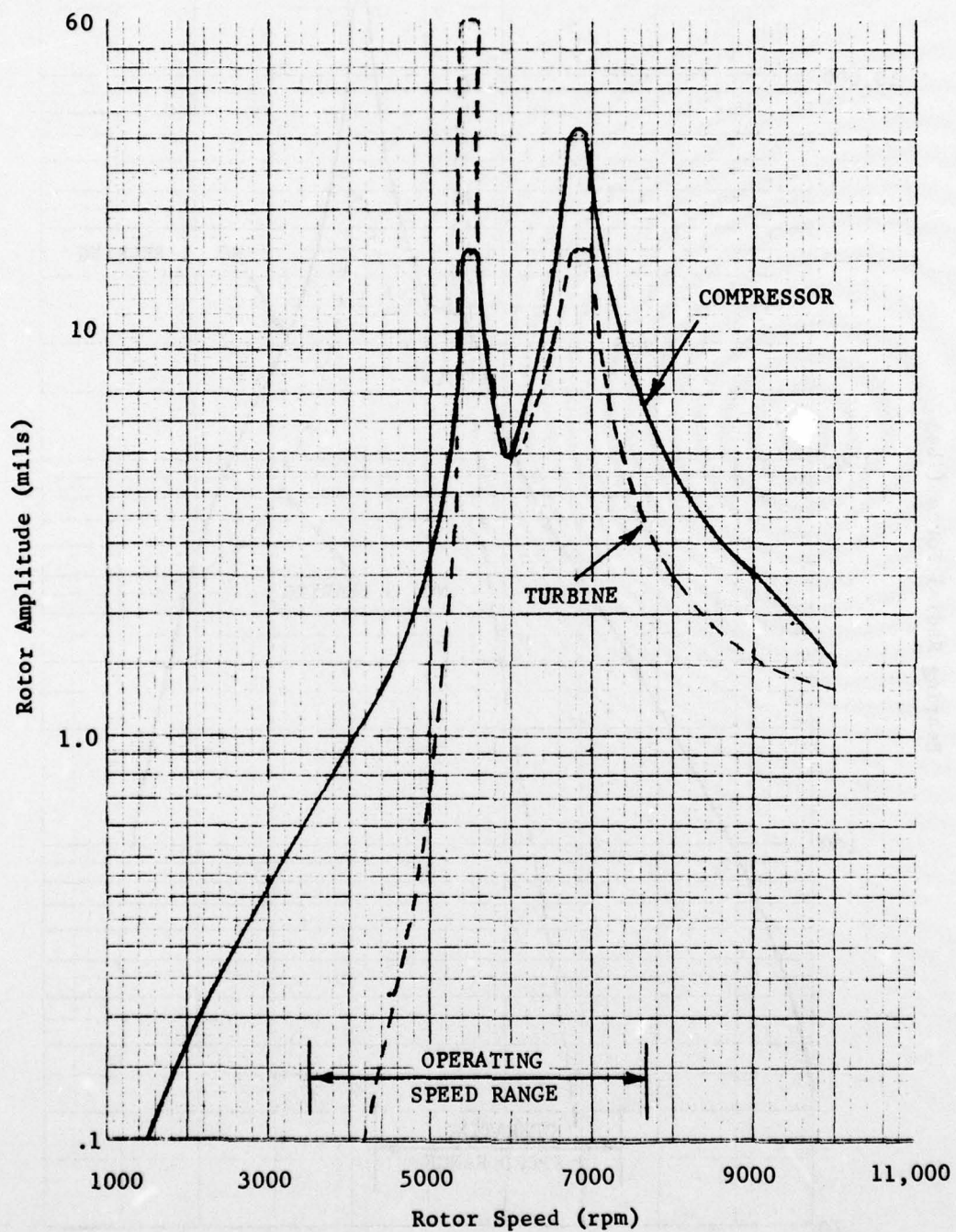


Fig. 40 Rotor Amplitudes for the Third Compressor Stage Blade Loss of the J79 Engine



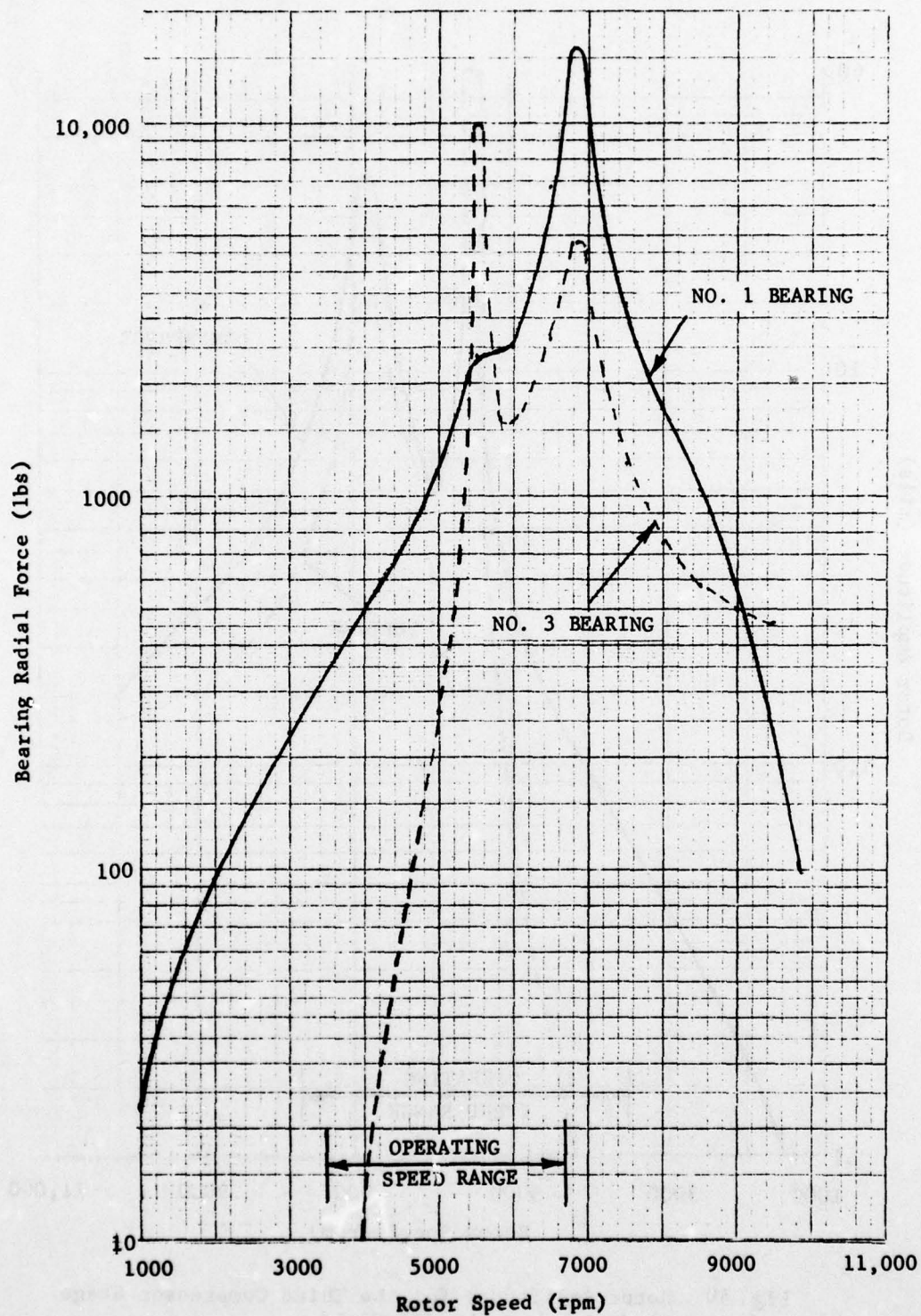


Fig. 41 J79 Rotor Bearing Radial Forces for the Third Compressor Stage Blade Loss

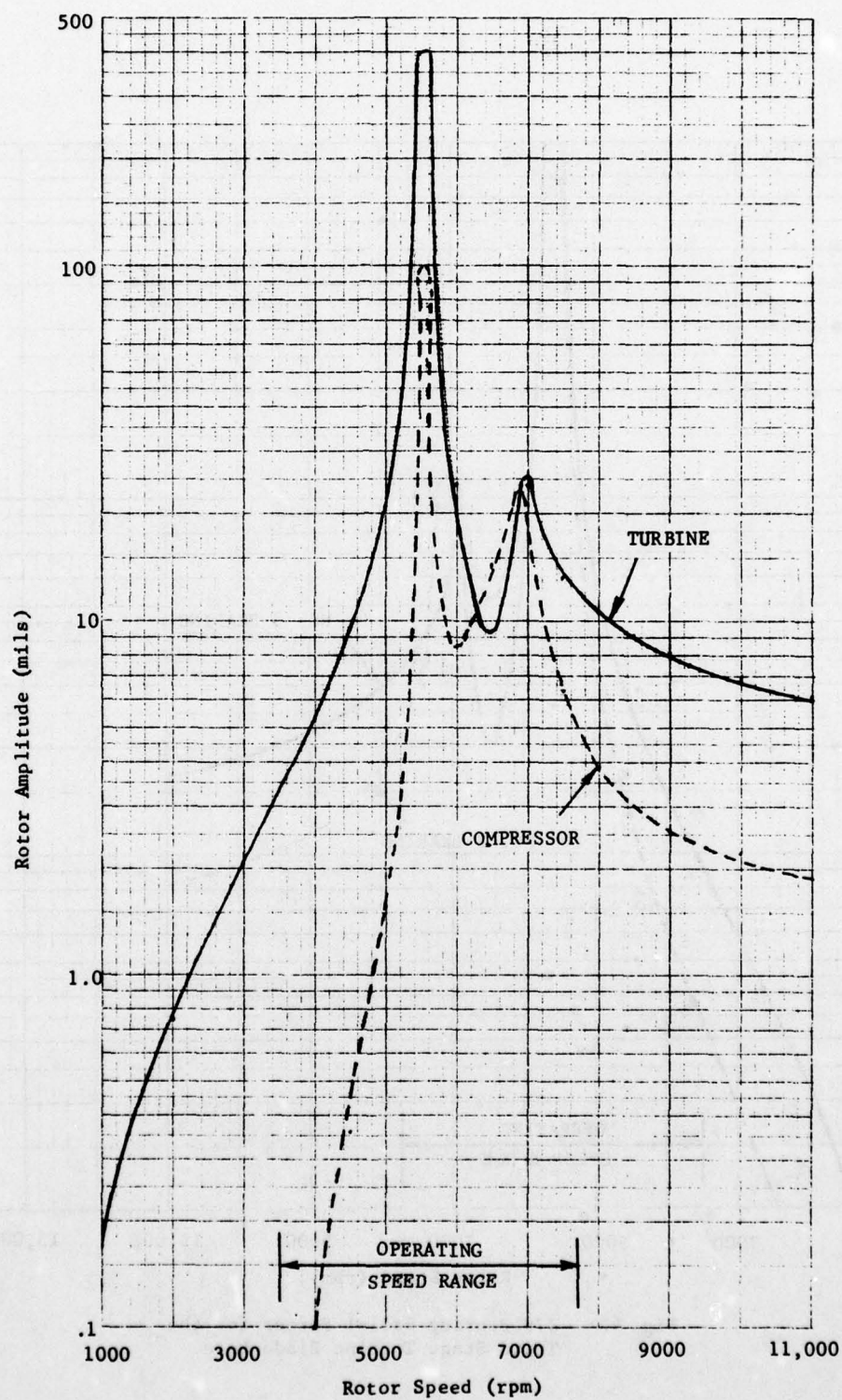


Fig. 42 Rotor Amplitudes for a Third Stage Turbine Blade Loss of the J79 Engine

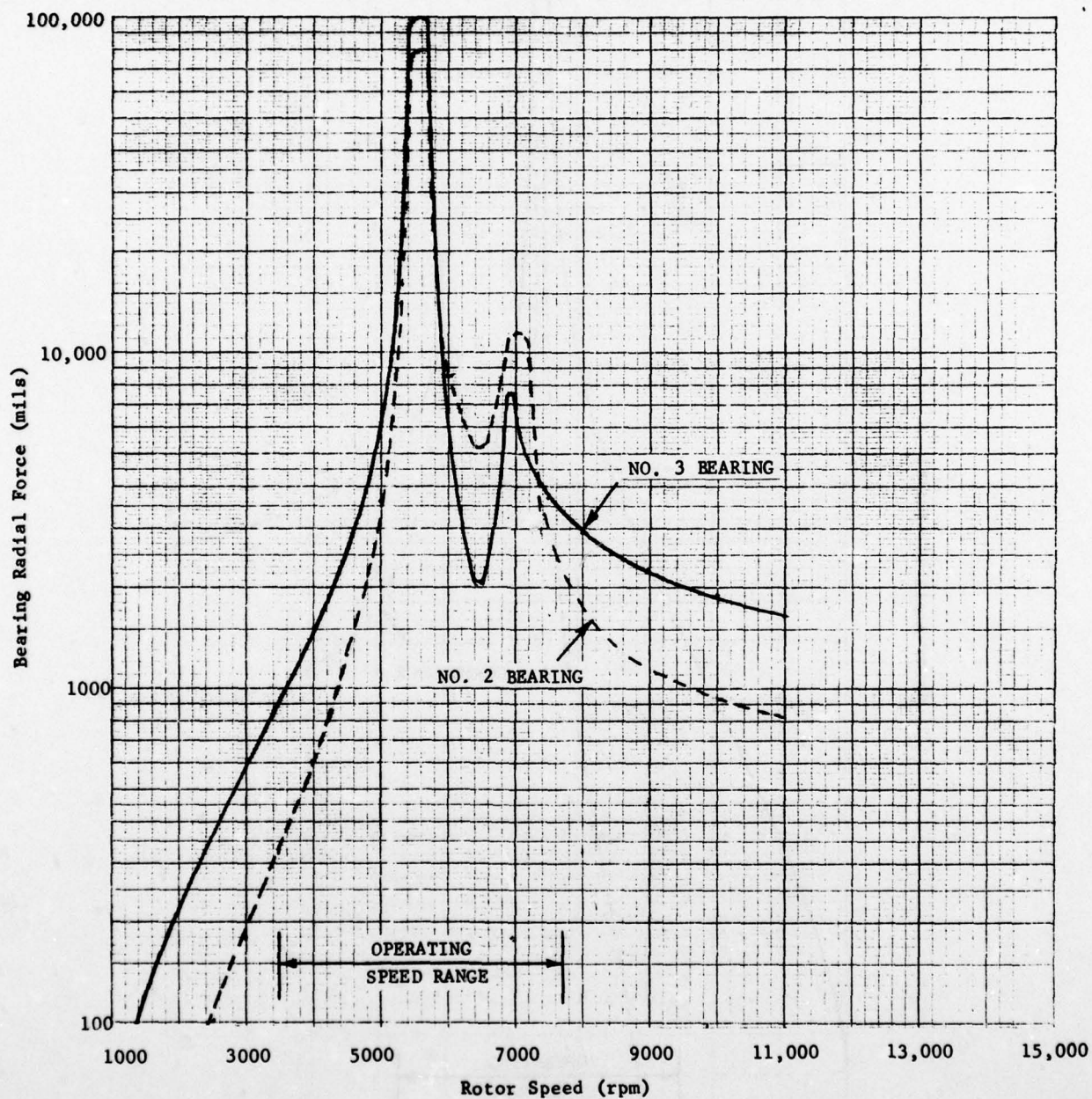


Fig. 43 J79 Bearing Radial Forces for the Third Stage Turbine Blade Loss



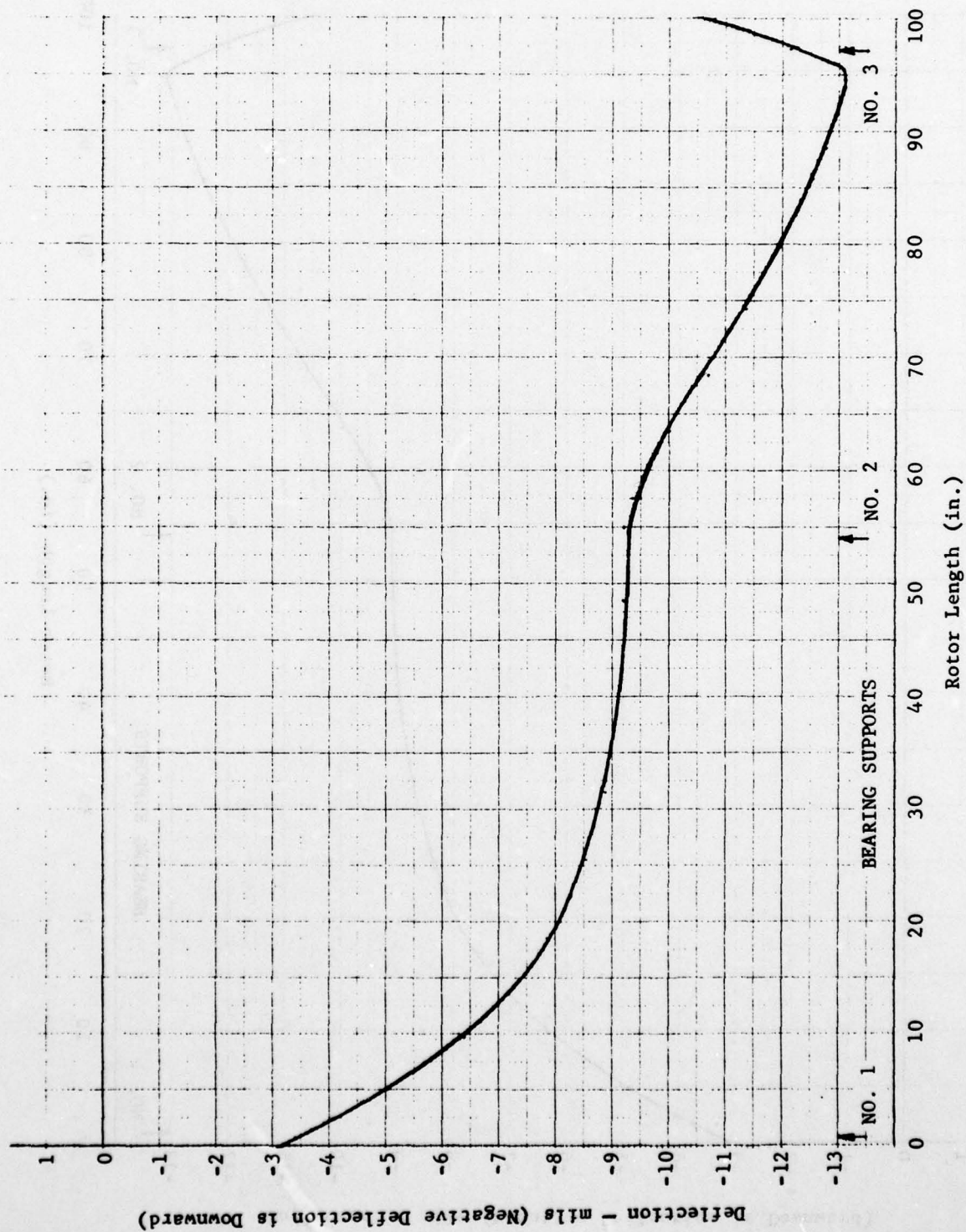


Fig. 44 J79 Rotor Bow Analysis - Landing Condition

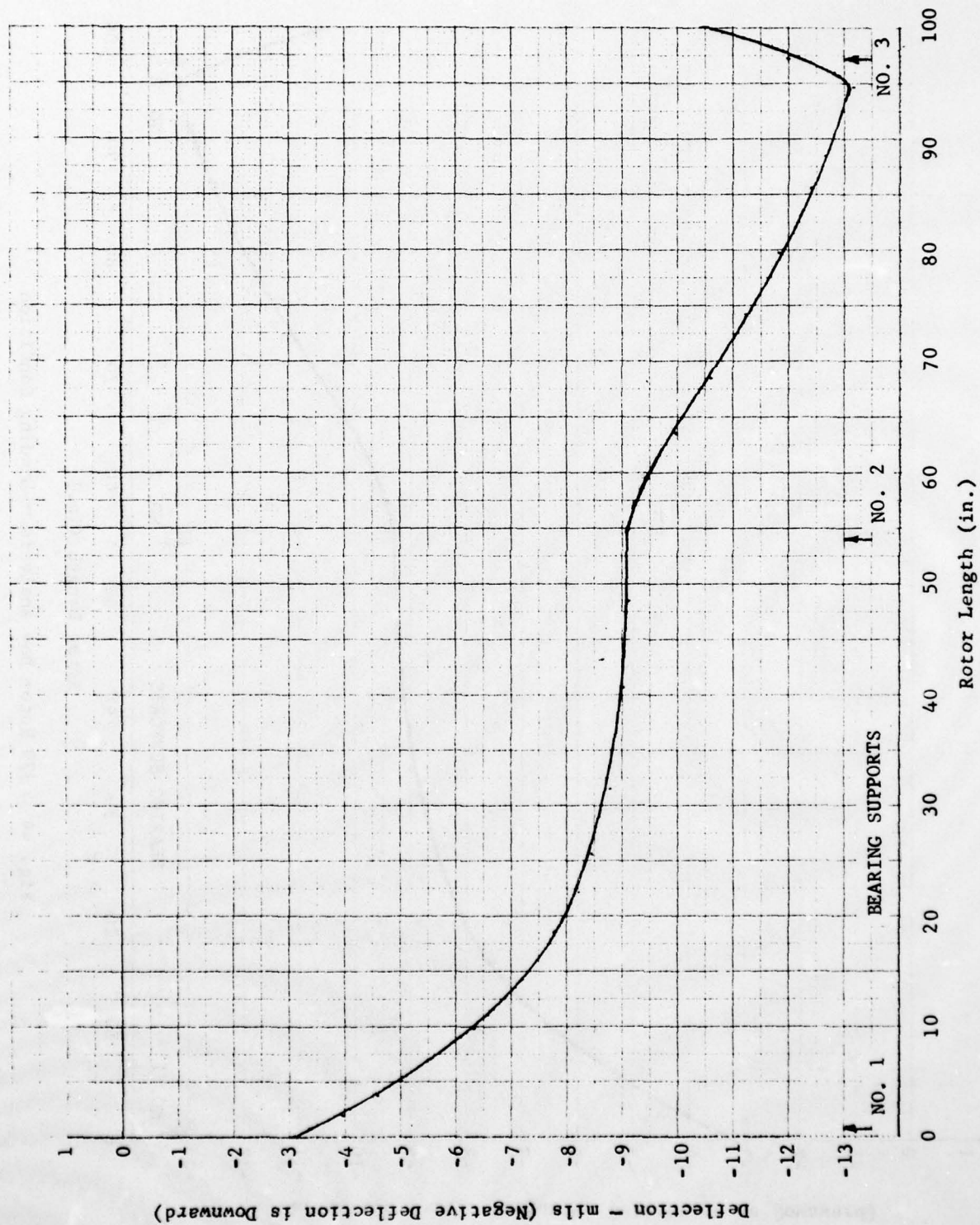


Fig. 45 J79 Rotor Bow Analysis - Flight Condition

D-A055 262

MECHANICAL TECHNOLOGY INC LATHAM N Y  
TURBINE ENGINE ROTORDYNAMIC EVALUATION. VOLUME I.(U)  
JAN 78 R A RIO  
MTI-76TR41

F/G 21/5

UNCLASSIFIED

F33615-75-C-2035  
NL

AFAPL-TR-76-81-VOL-1

2 OF 3

AD  
A055262





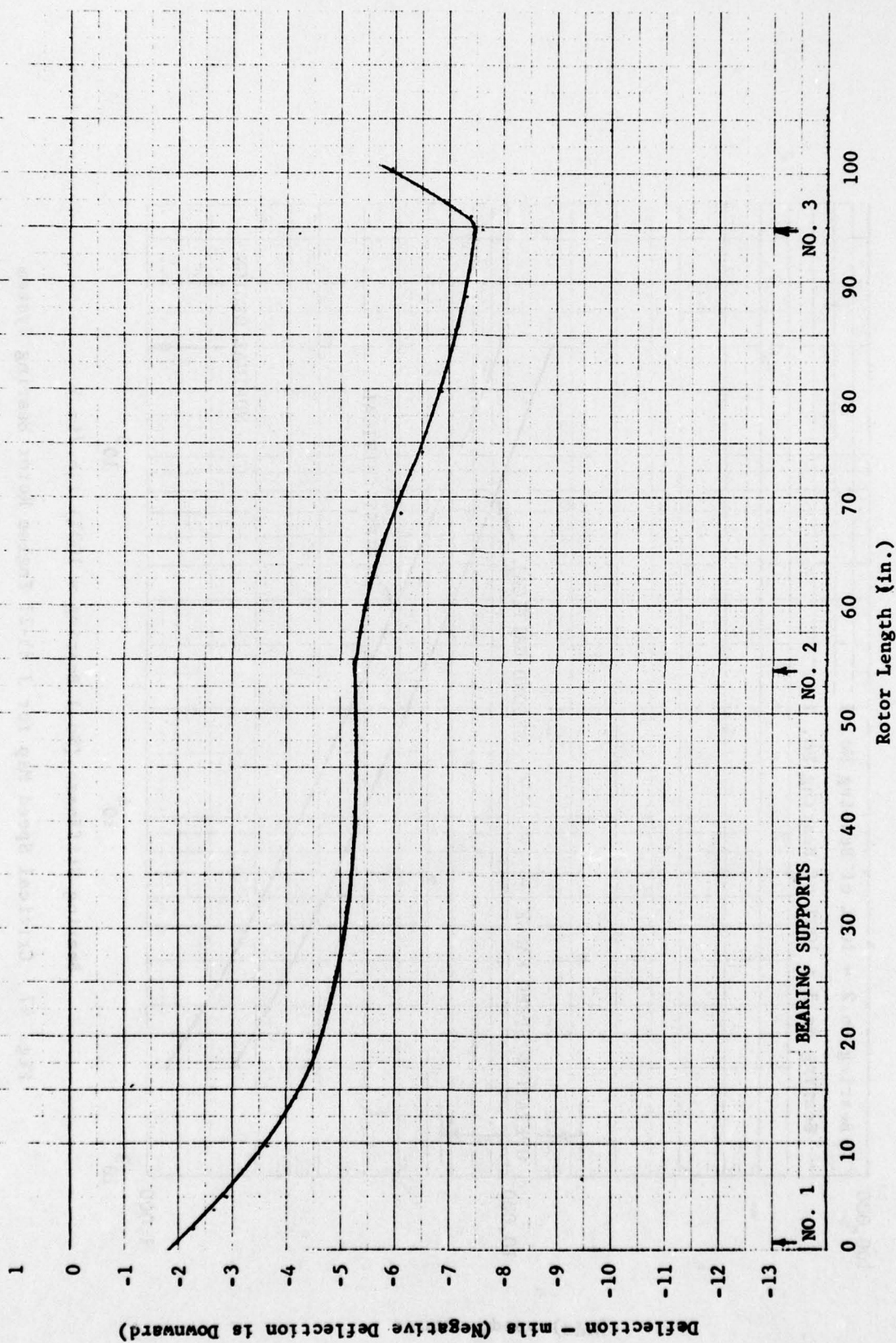
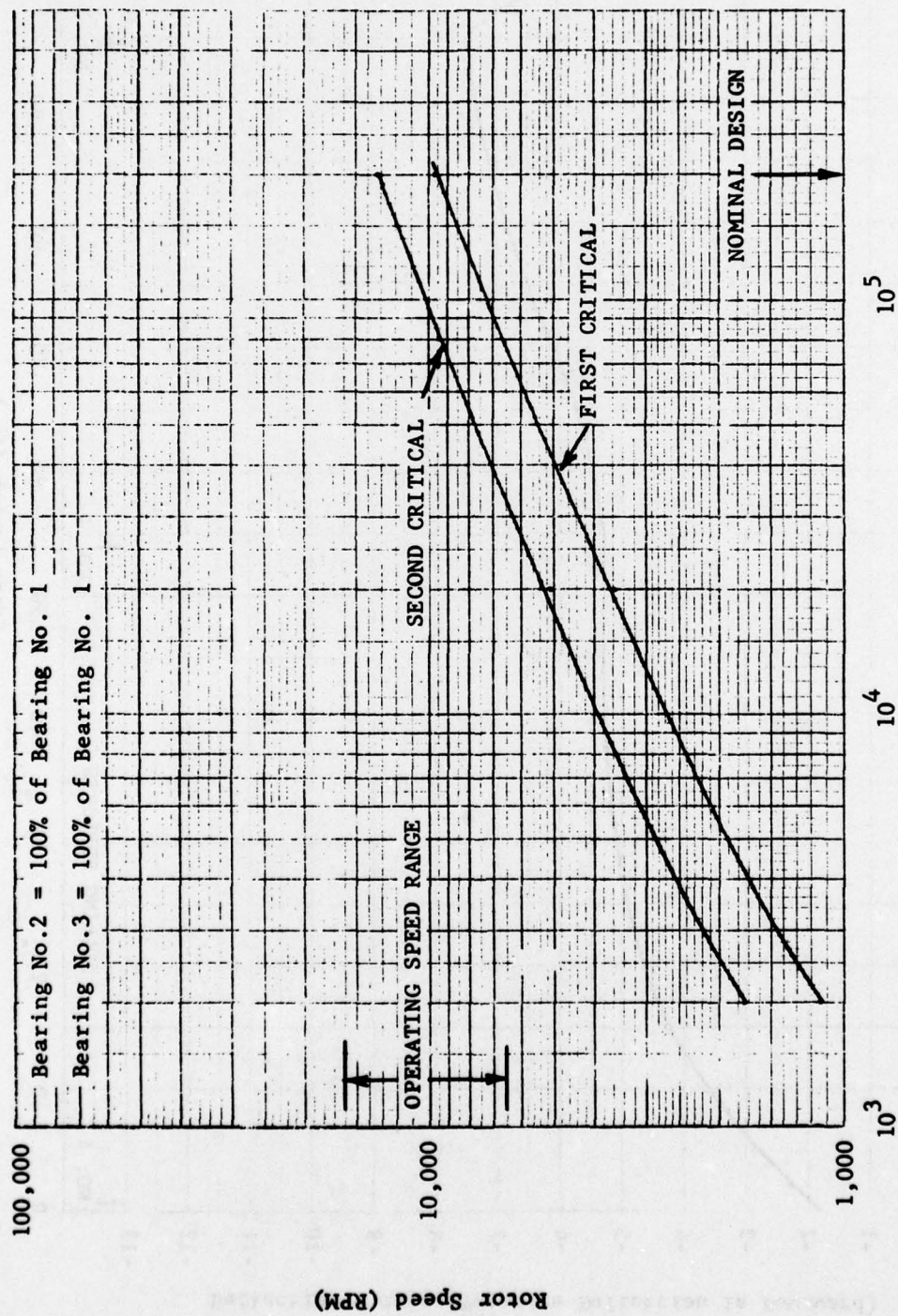


Fig. 46 J79 Rotor Bow Analysis - Catapult Condition



Bearing Stiffness (No. 1 Bearing = 100%) (lb./in.)

Fig. 47 Critical Speed Map for J 85-21 Engine Rotor Bearing System

THIS PAGE IS BEST QUALITY PRACTICABLE  
FROM COPY FURNISHED TO DDG

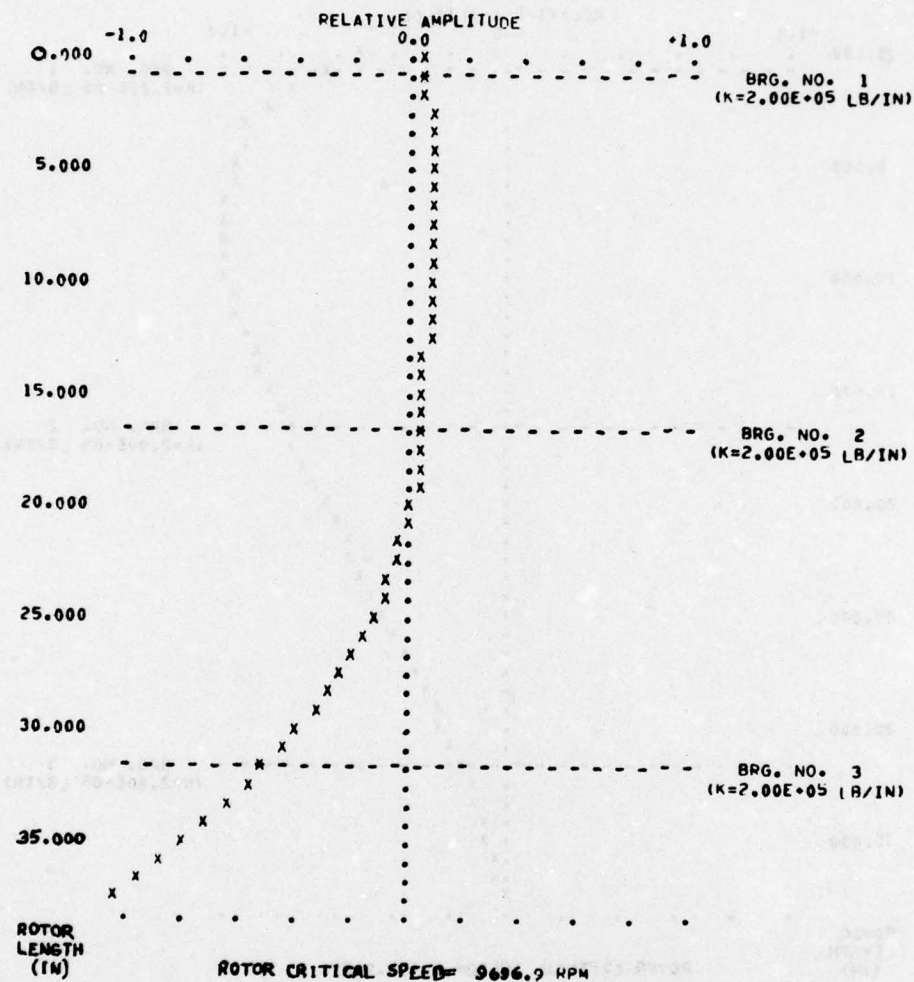


Fig. 48 Undamped Mode Shape at First Critical Speed  
of J 85-21 Engine Rotor System (Cantilevered  
Turbine Mode)



THIS PAGE IS BEST QUALITY PRACTICABLE  
FROM COPY FURNISHED TO DDG

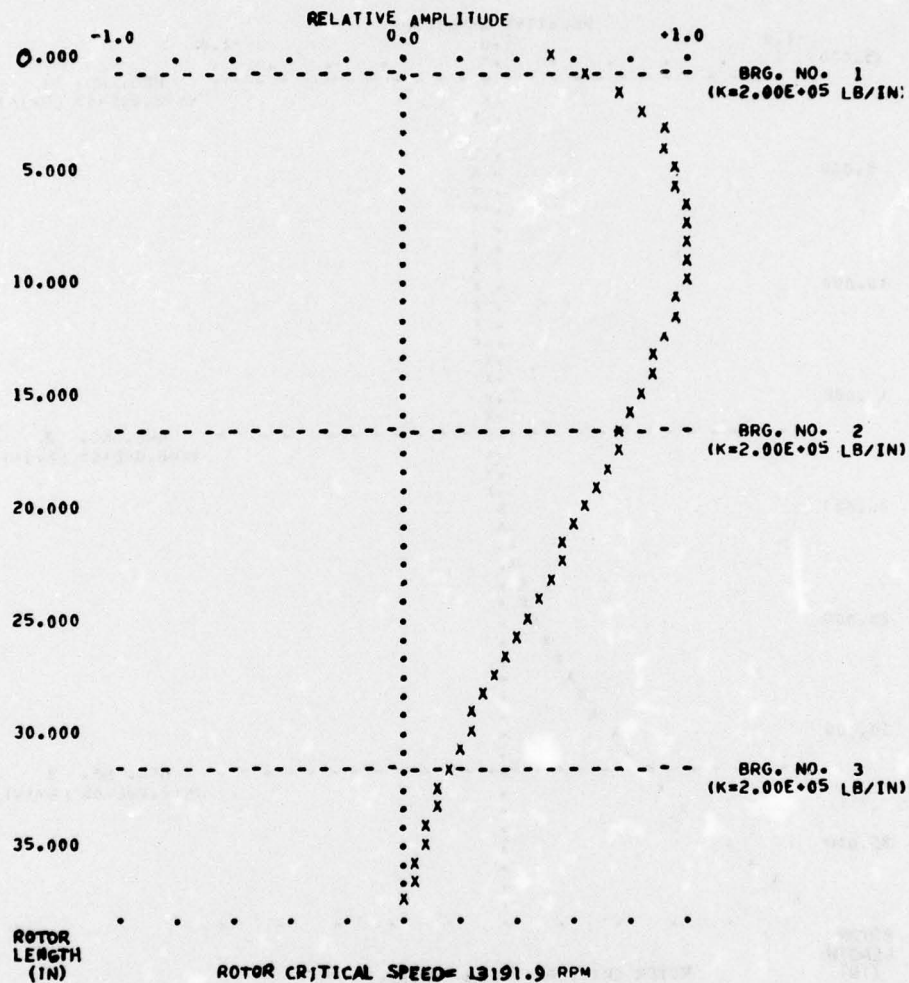


Fig. 49 Undamped Mode Shape at Second Critical  
Speed of J 85-21 Engine Rotor System  
(Compressor Bounce Mode)

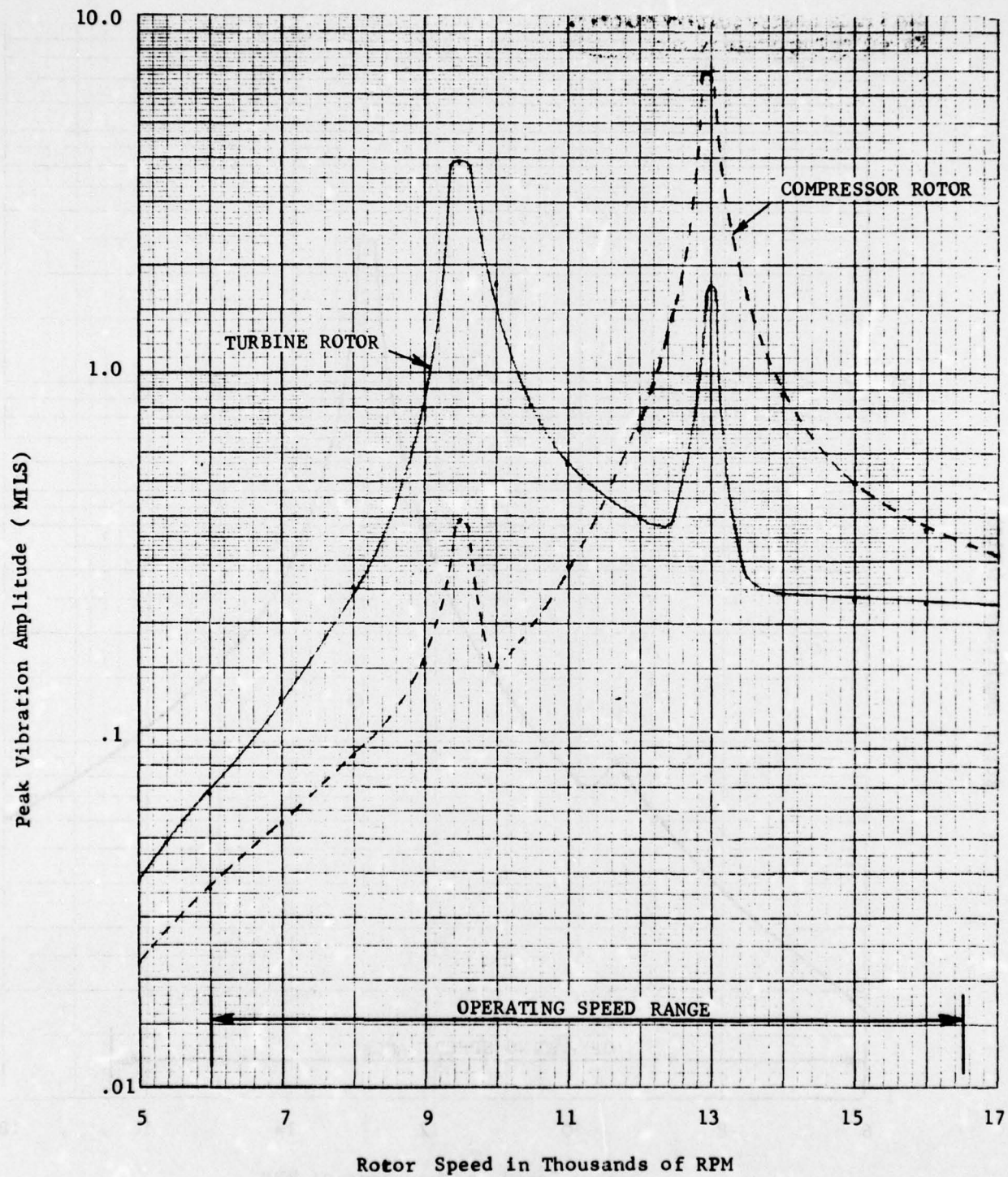


Fig. 50 Calculated Unbalance Response for J 85-21 Engine Rotor System with Random Distributed Unbalance

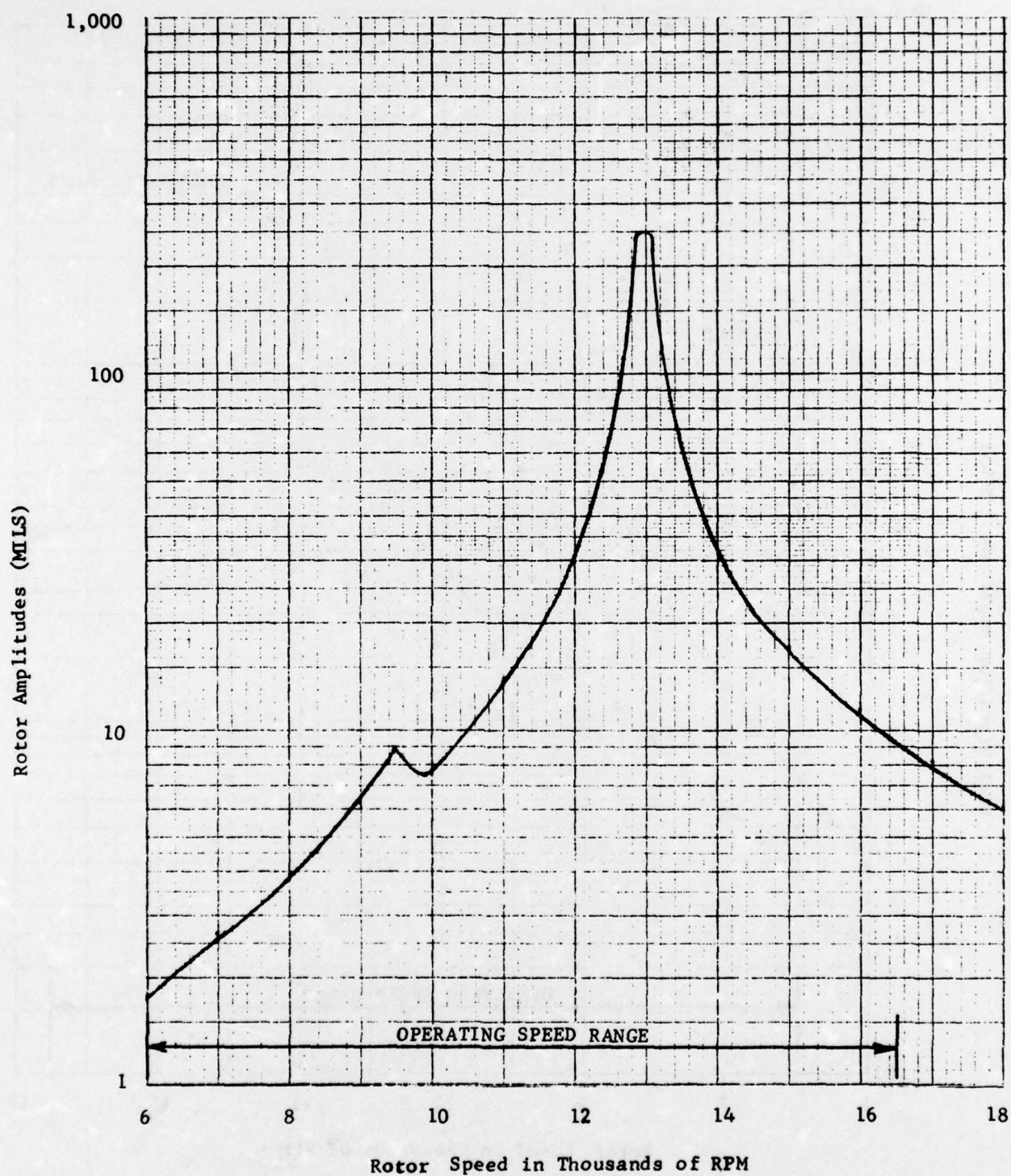


Fig. 51 Compressor Rotor Amplitudes for a First Fan Stage Blade Loss of the J 85-21 Engine



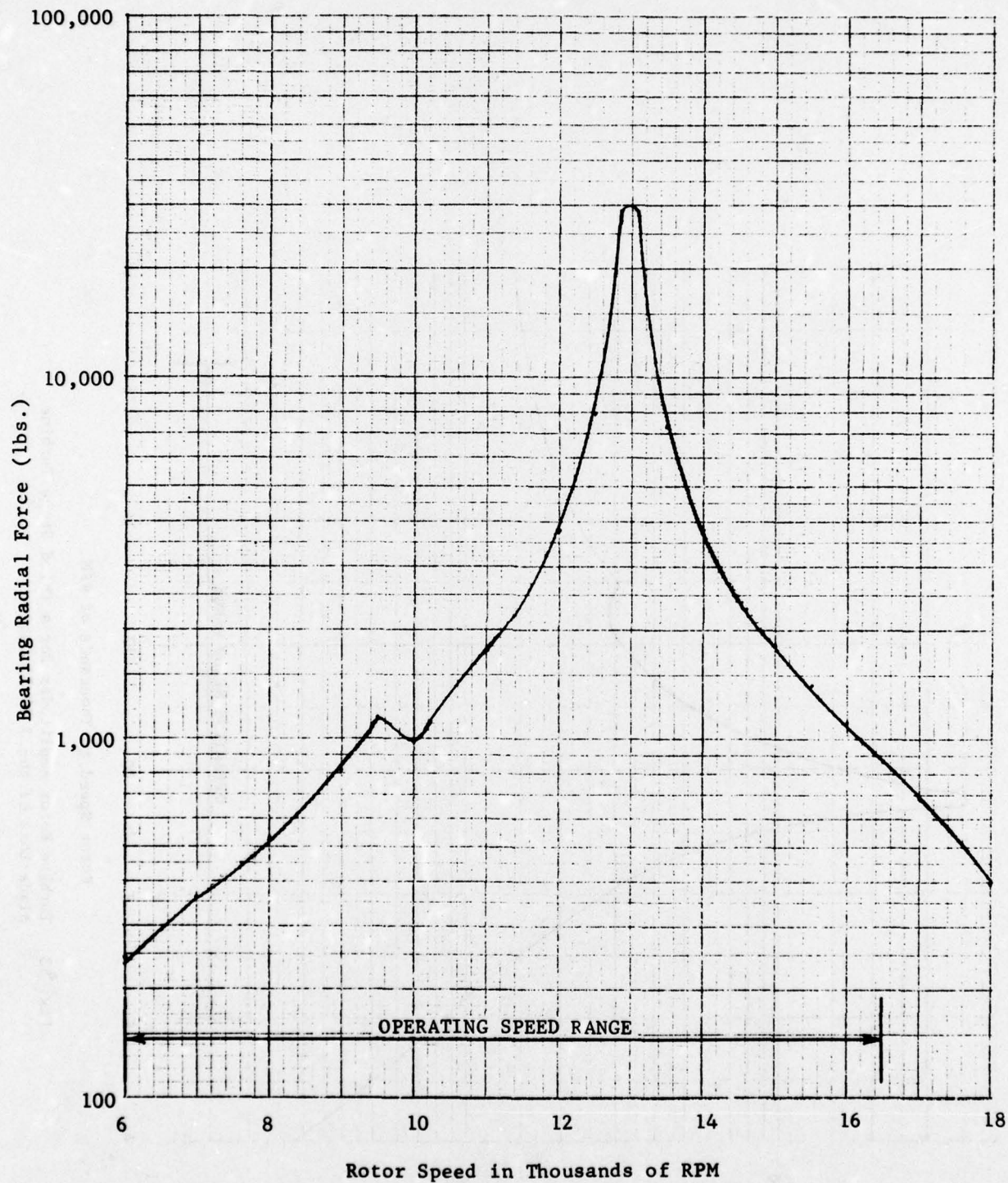


Fig. 52 J 85-21 Rotor No. 1 Bearing Radial Force for the First Fan Stage Blade Loss

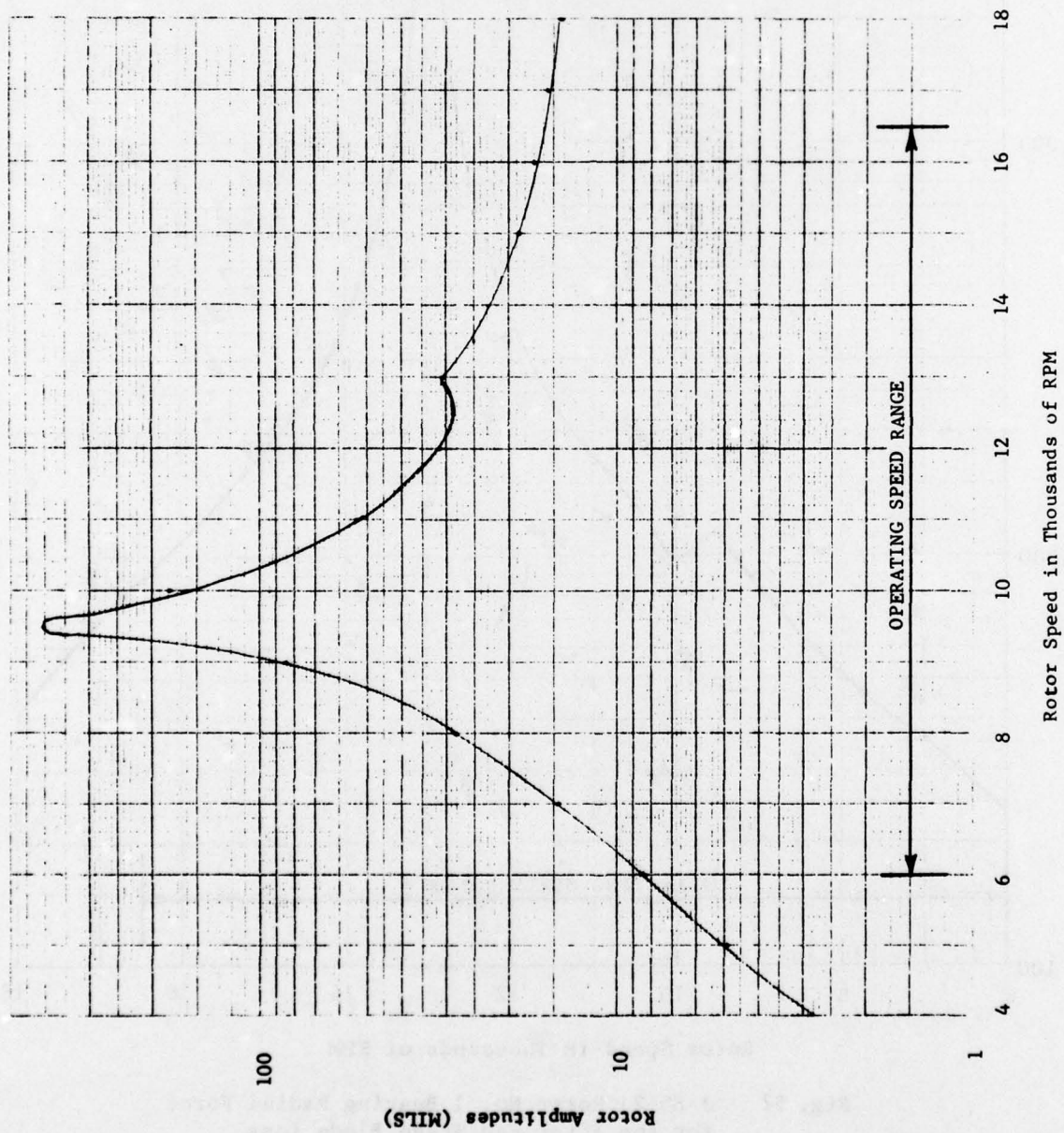


Fig. 53 Turbine Rotor Amplitudes for a Third Stage Turbine Blade Loss of the J 85-21 Engine

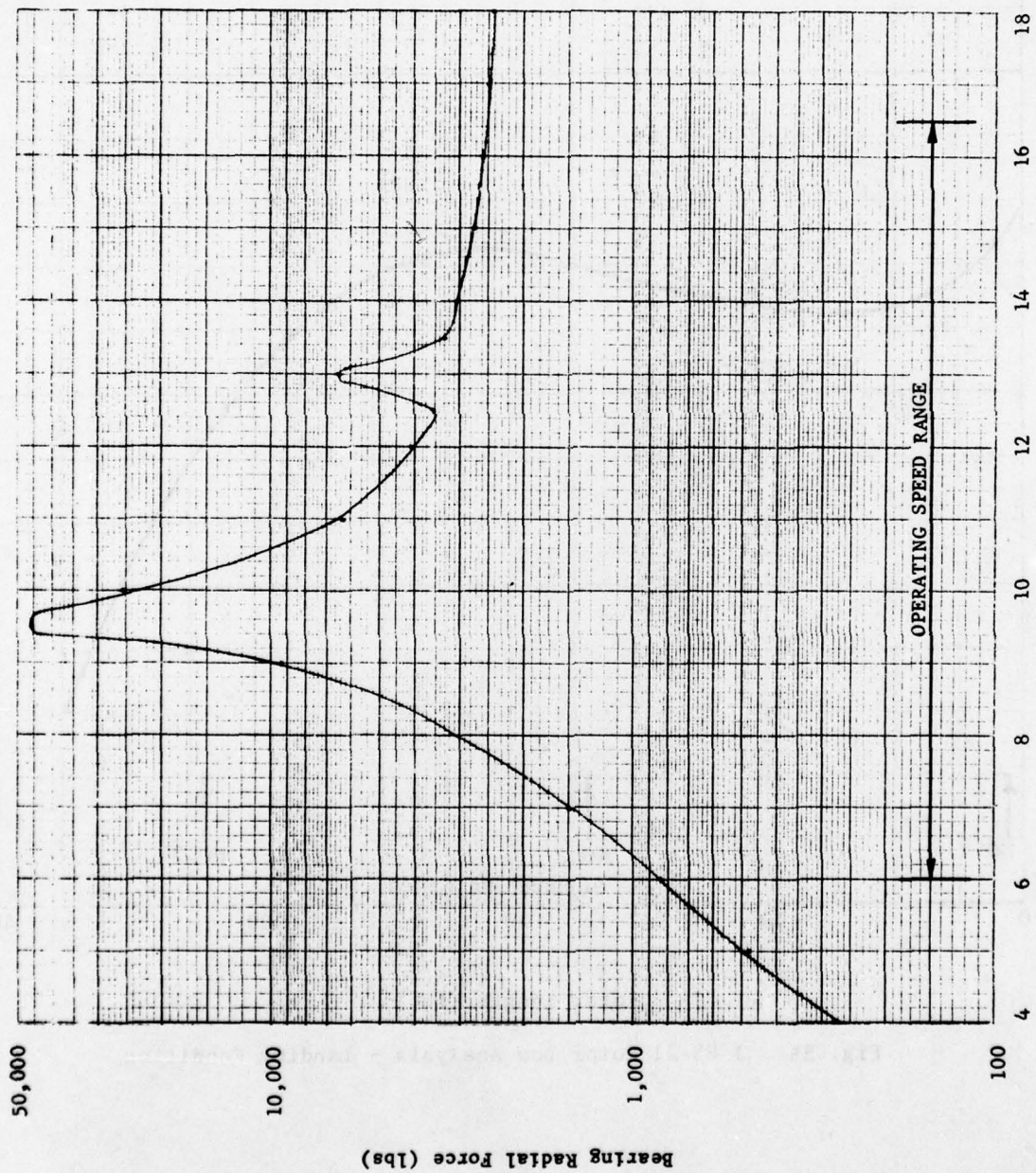


Fig. 54 J 85-21 No. 3 Bearing Radial Force for  
the Third Stage Turbine Blade Loss



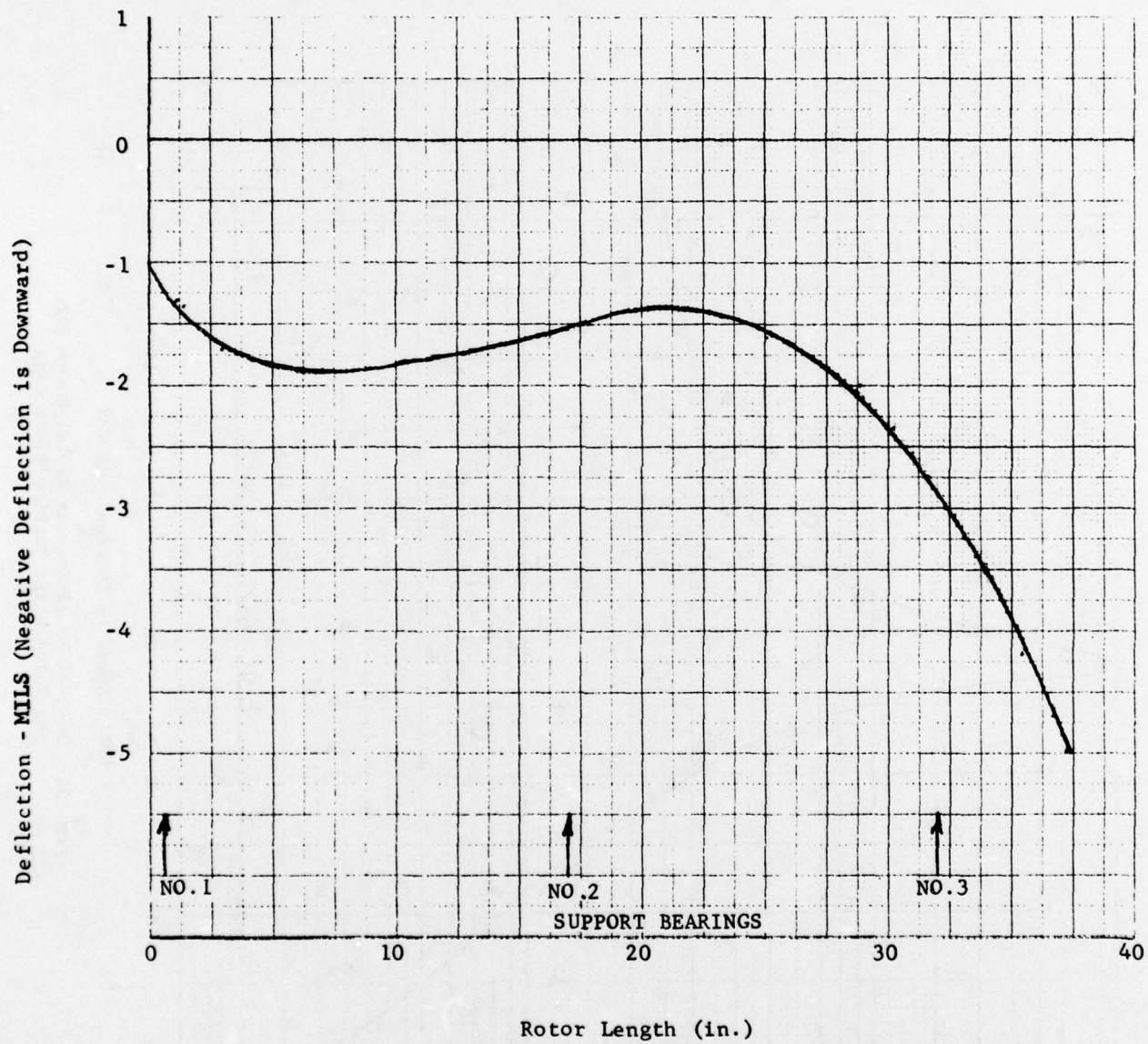


Fig. 55 J 85-21 Rotor Bow Analysis - Landing Condition

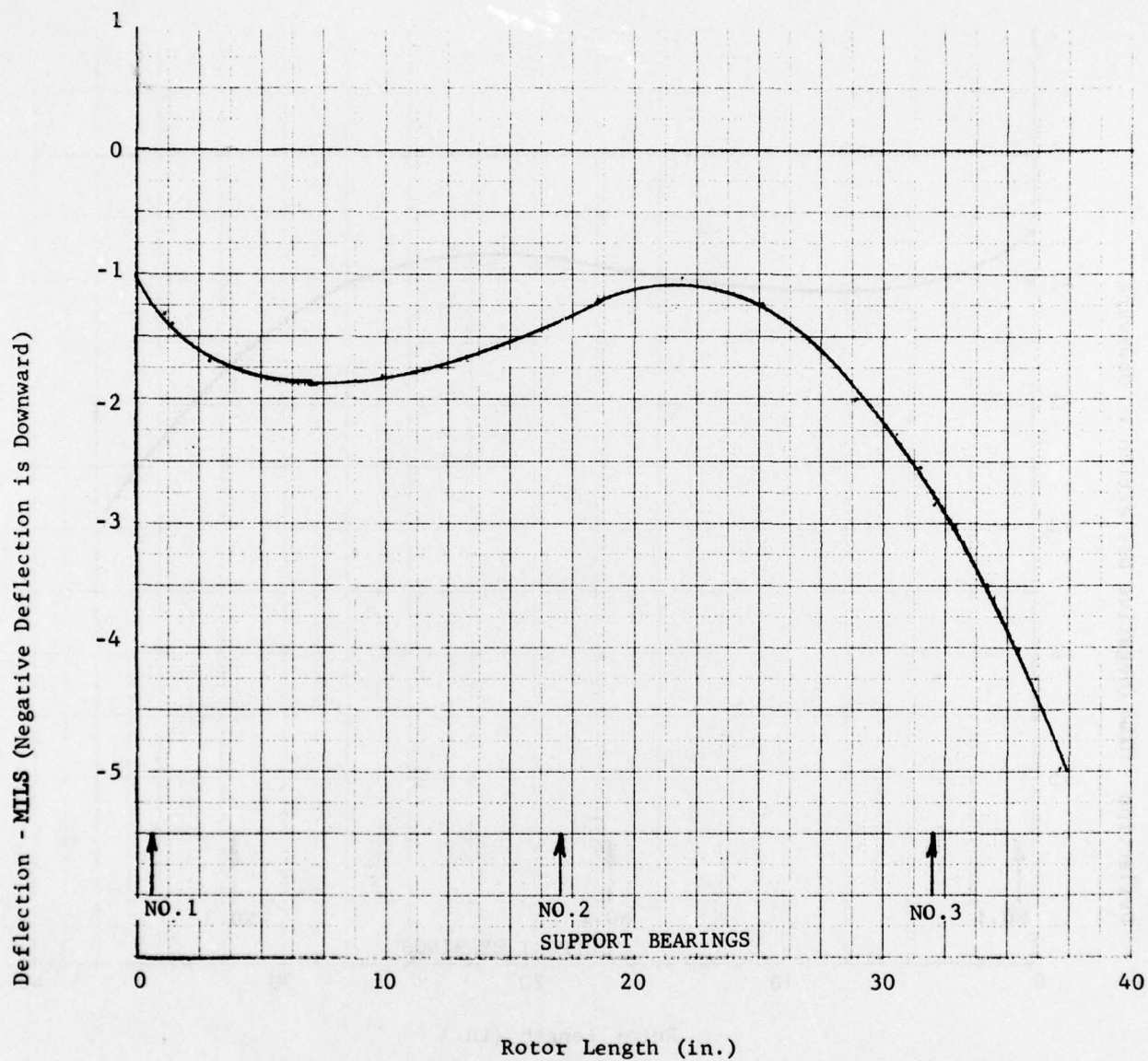


Fig. 56 J 85-21 Rotor Bow Analysis - Flight Condition

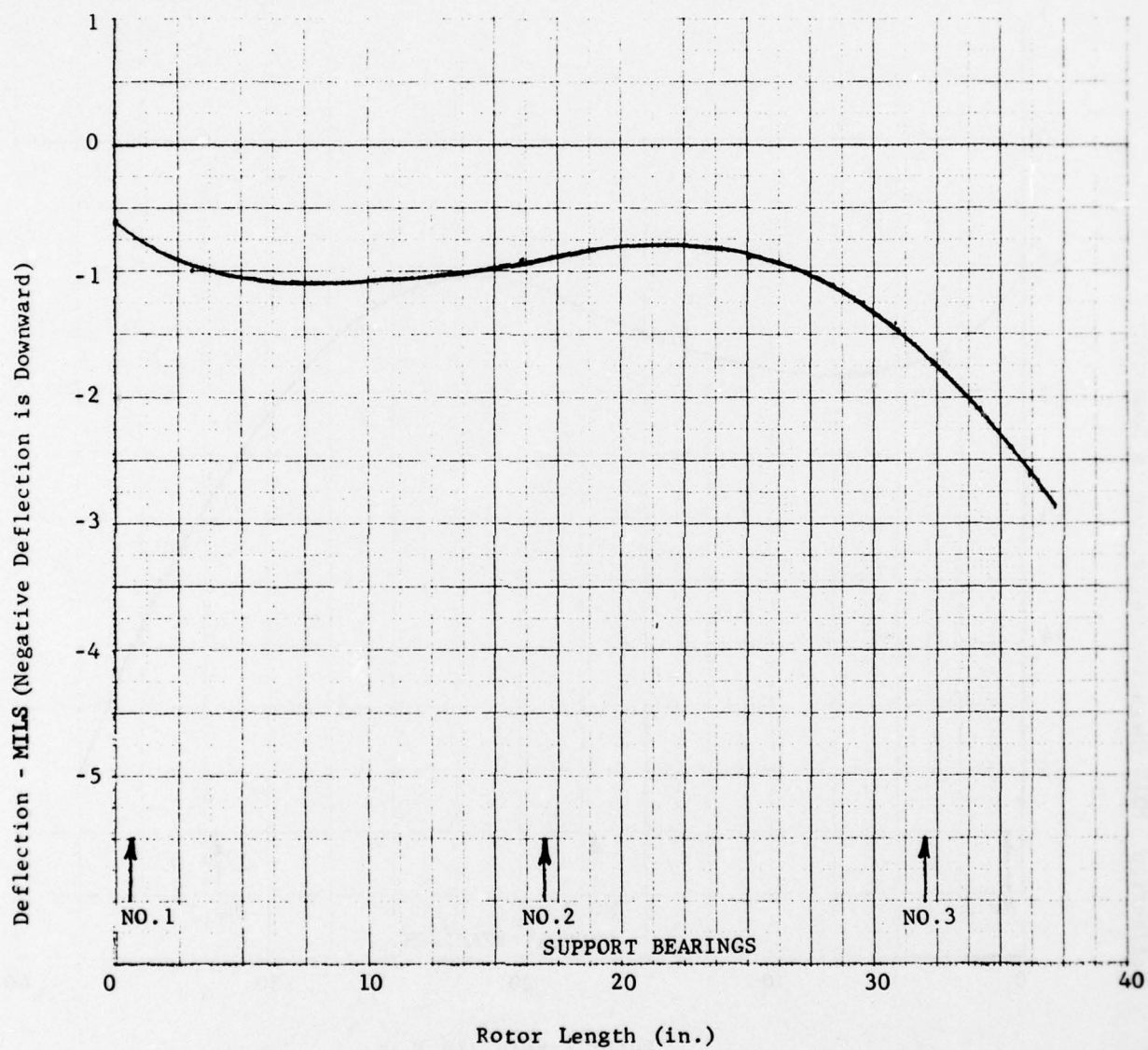


Fig. 57 J 85-21 Rotor Bow Analysis - Catapult Condition



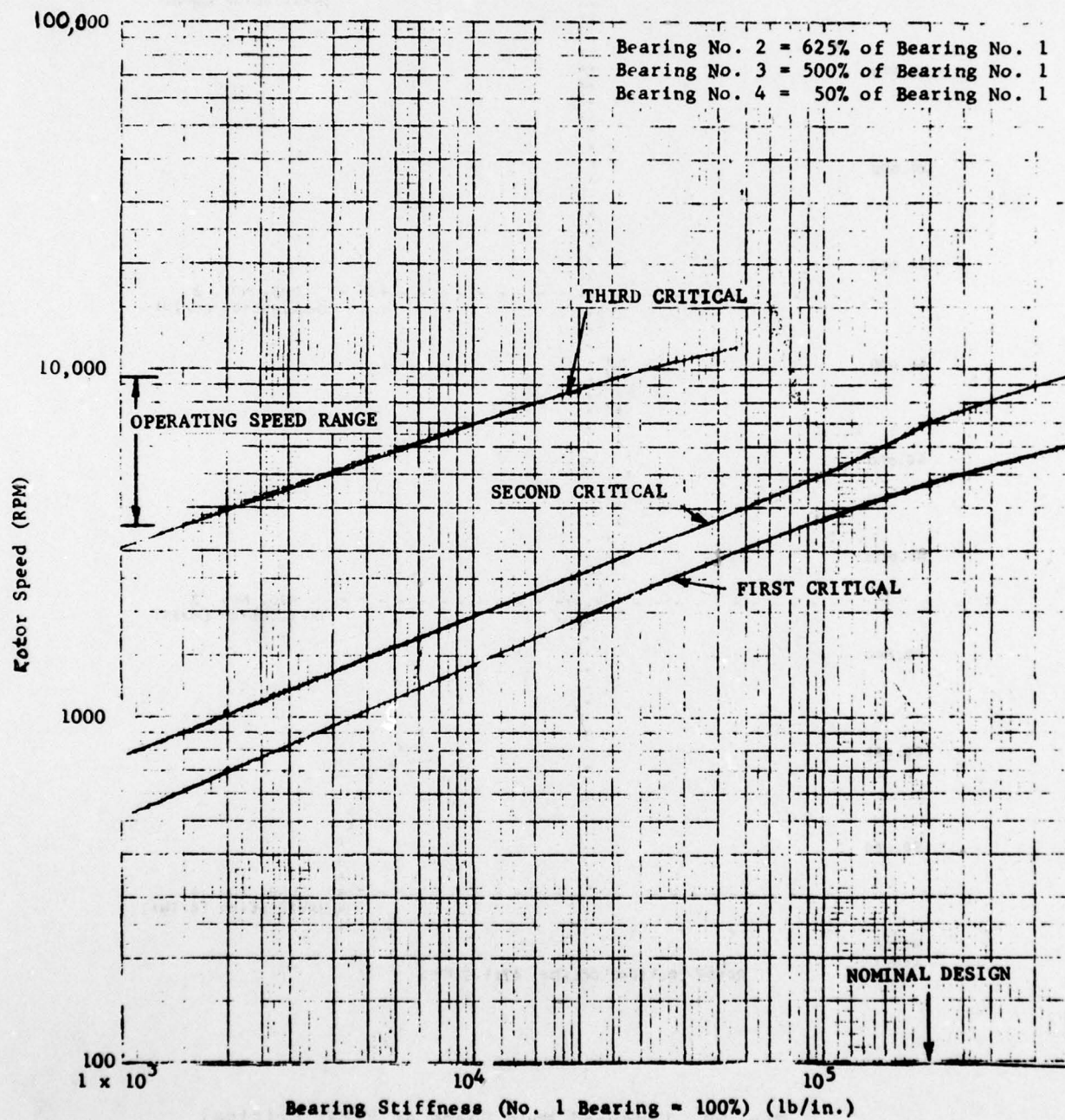


Fig. 58 Critical Speed Map for TF30 Low Rotor Bearing System

THIS PAGE IS BEST QUALITY PRACTICABLE  
FROM COPY FURNISHED TO DDG

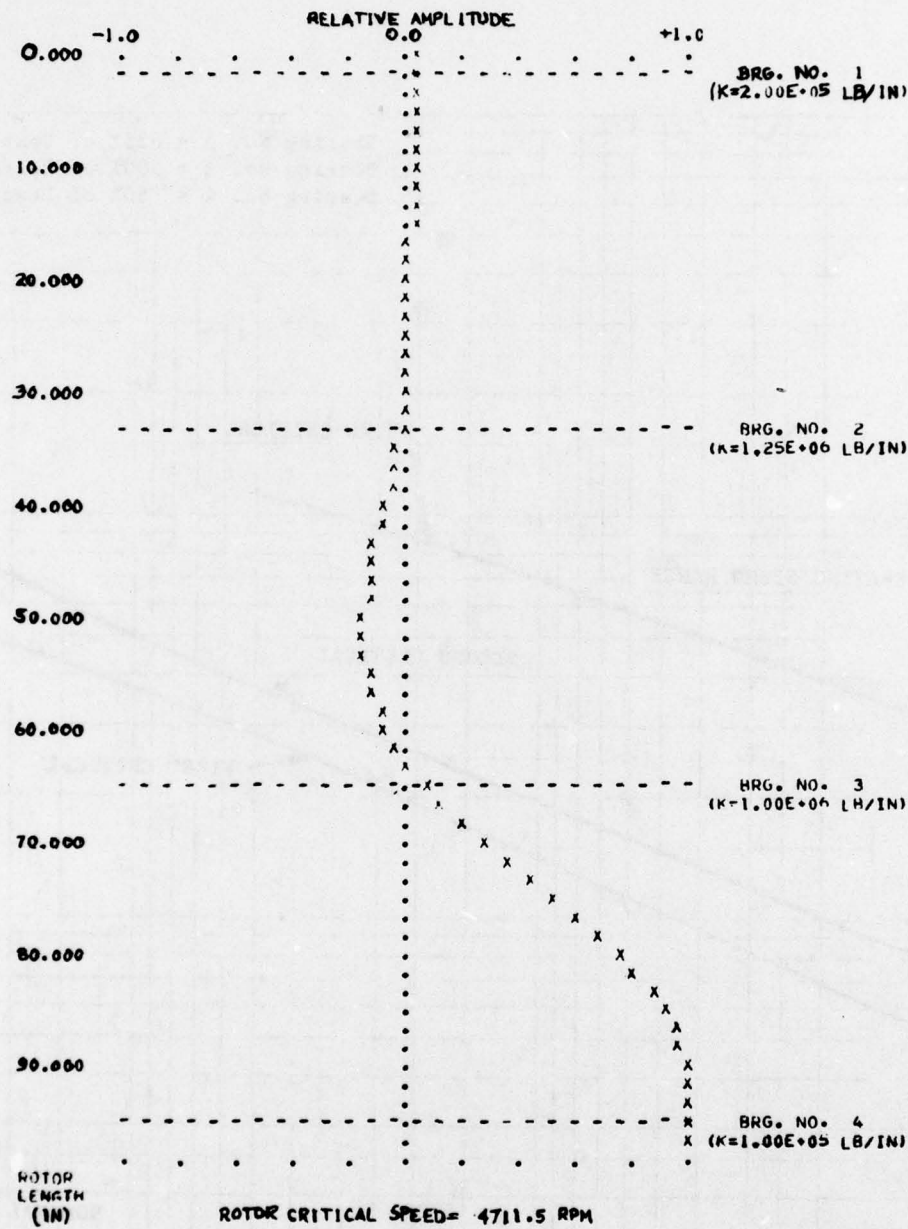


Fig. 59 Undamped Mode Shape at First Critical Speed for the TF30 Low Rotor System (Turbine Mode)

THIS PAGE IS BEST QUALITY PRACTICABLE  
FROM COPY FURNISHED TO DDG

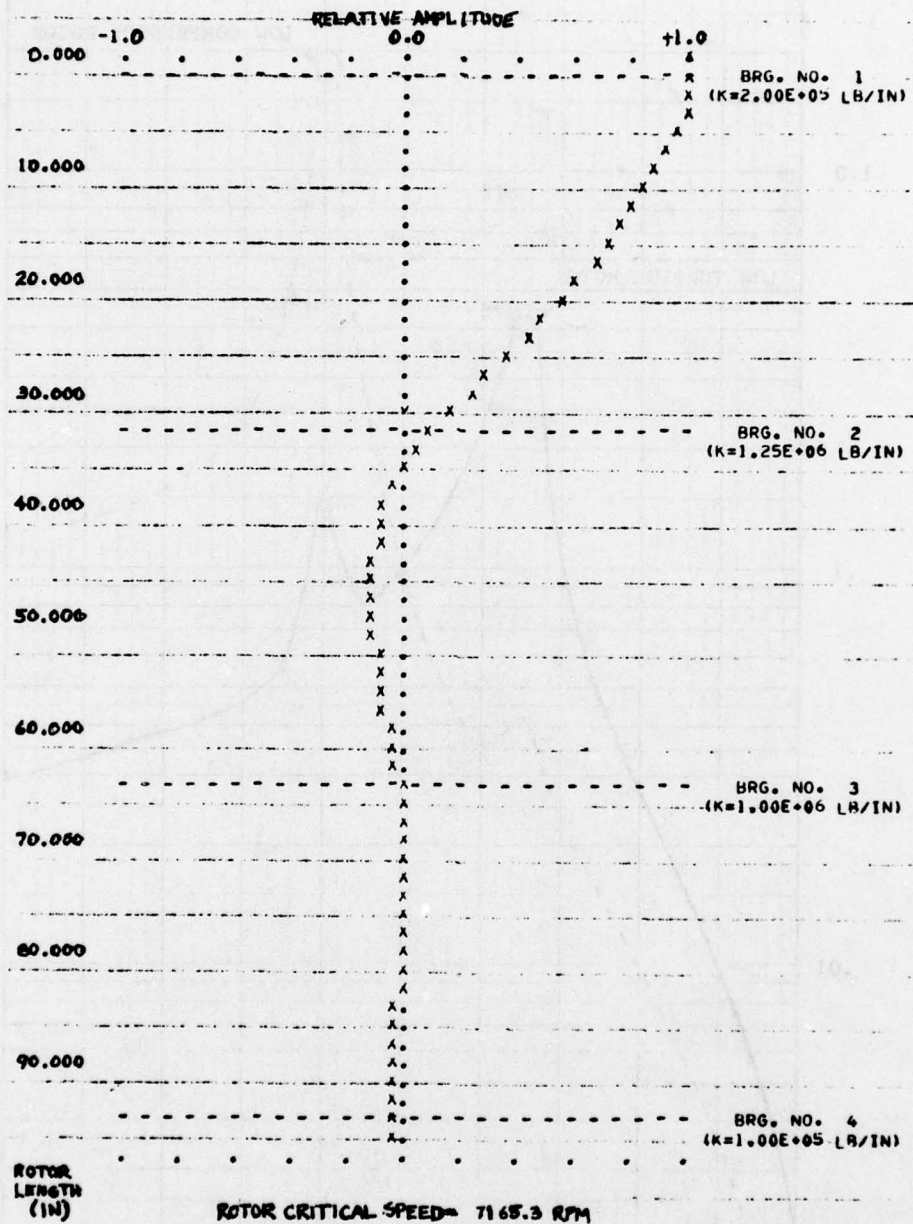


Fig. 60 Undamped Mode Shape at Second Critical  
Speed for the TF30 Low Rotor System  
(Compressor Bounce Mode)



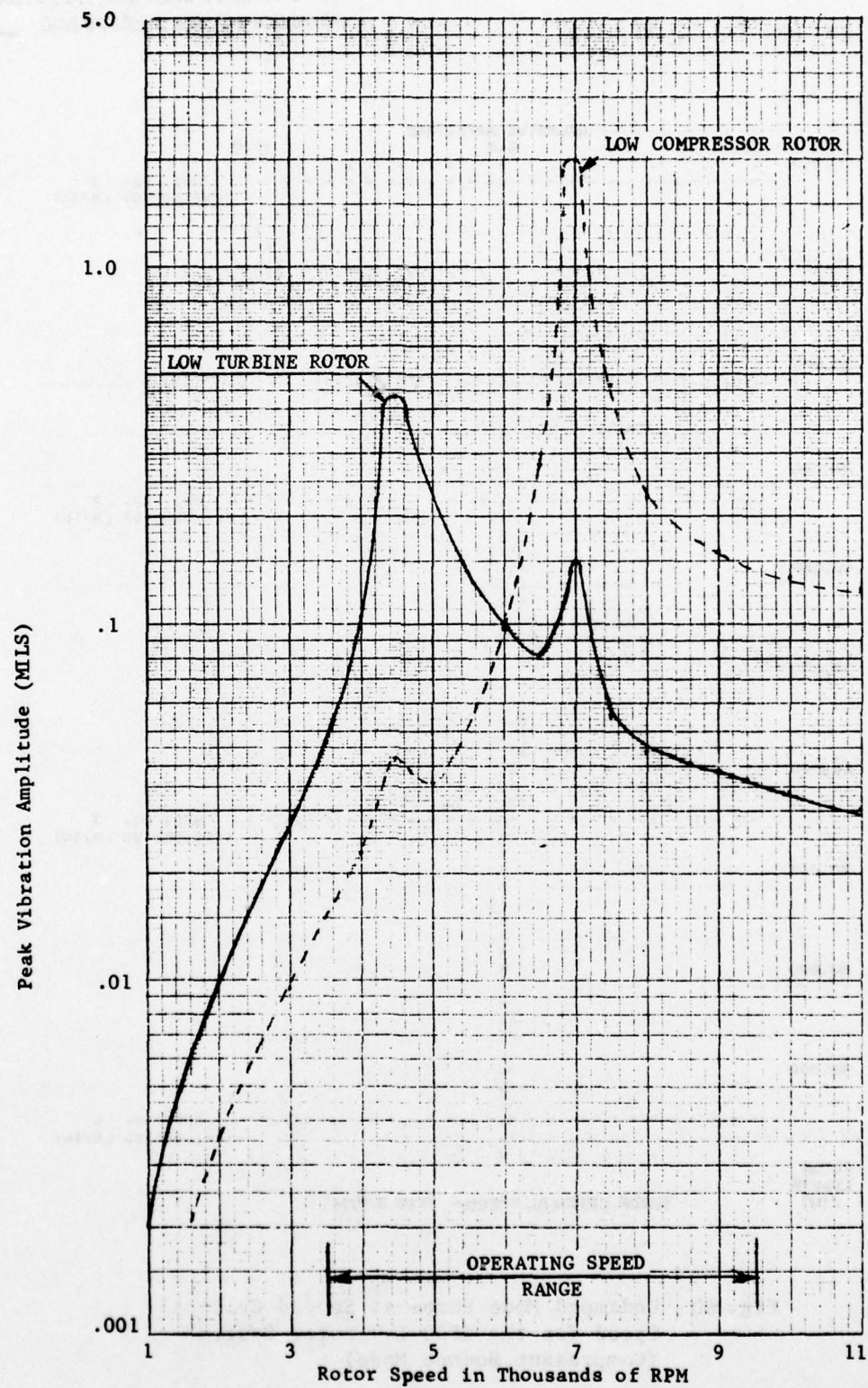


Fig. 61 Calculated Unbalance Response for TF30 Low Rotor System with Random Distributed Unbalance

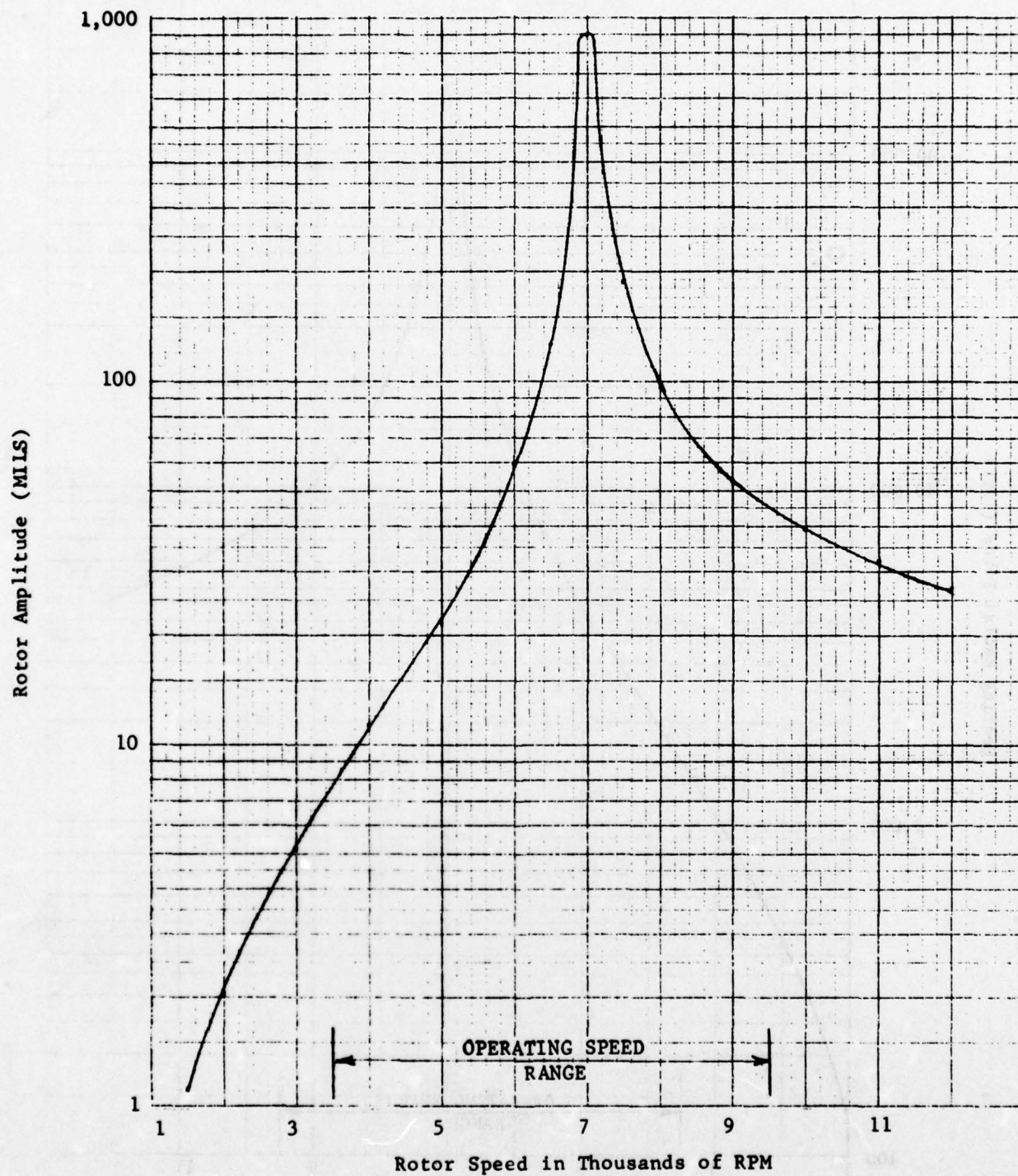


Fig. 62 Low Compressor Rotor Amplitudes for a First Fan Stage Blade Loss of the TF30 Engine

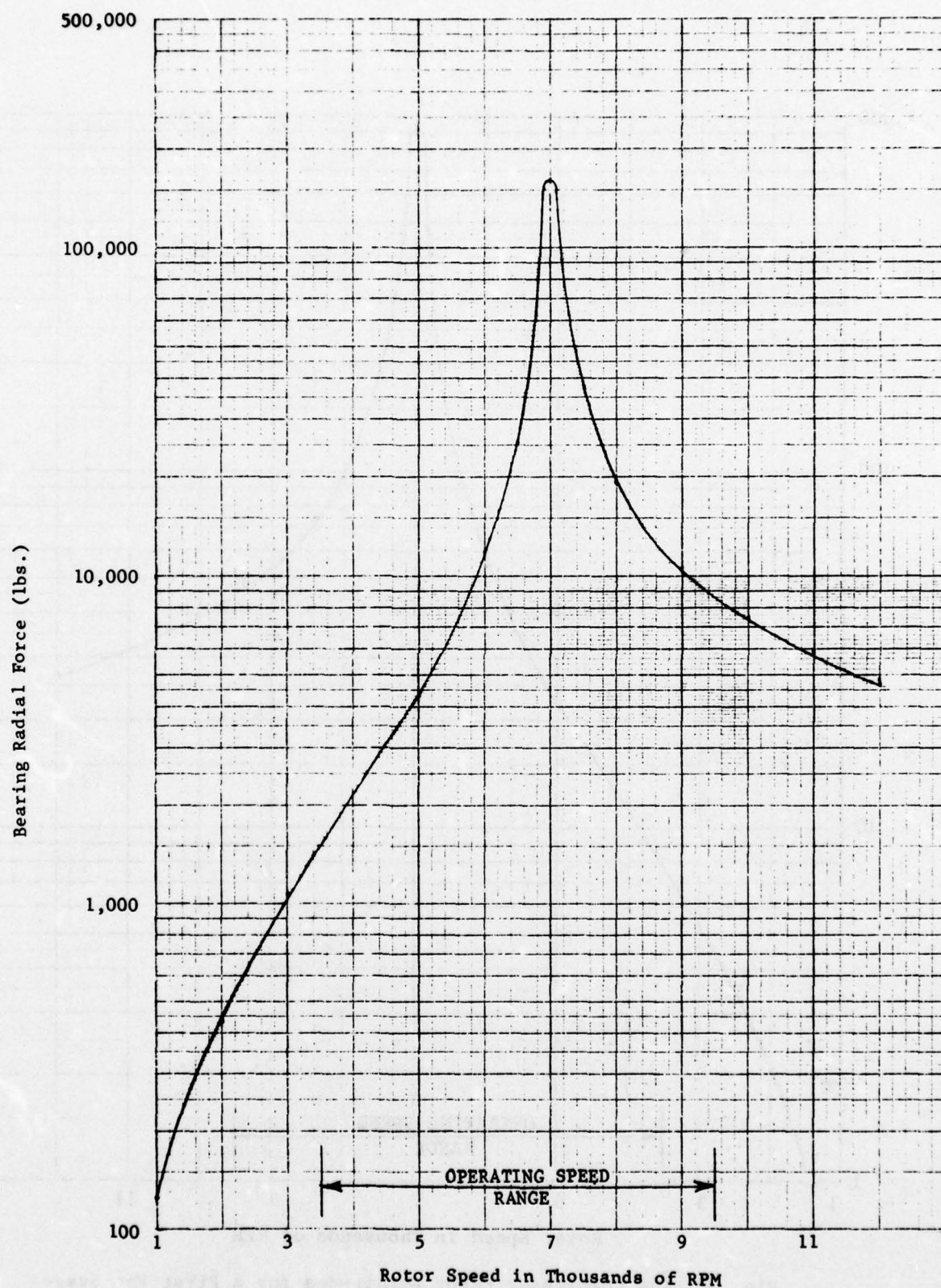


Fig. 63 TF30 Low Rotor No.1 Bearing Radial Force for the First Fan Stage Blade Loss



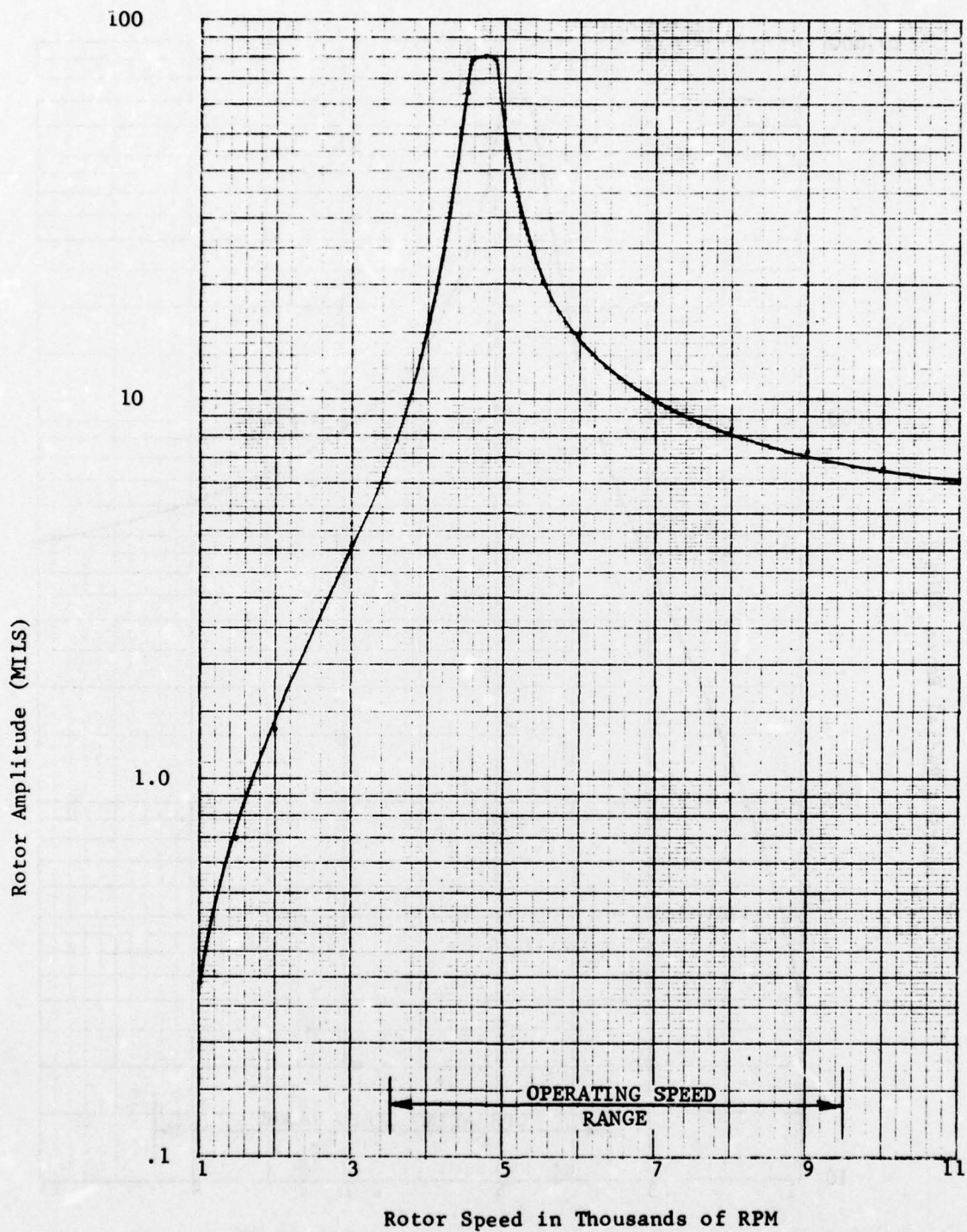


Fig. 64 Low Turbine Rotor Amplitudes for a Third Stage Turbine Blade Loss of the TF30 Engine

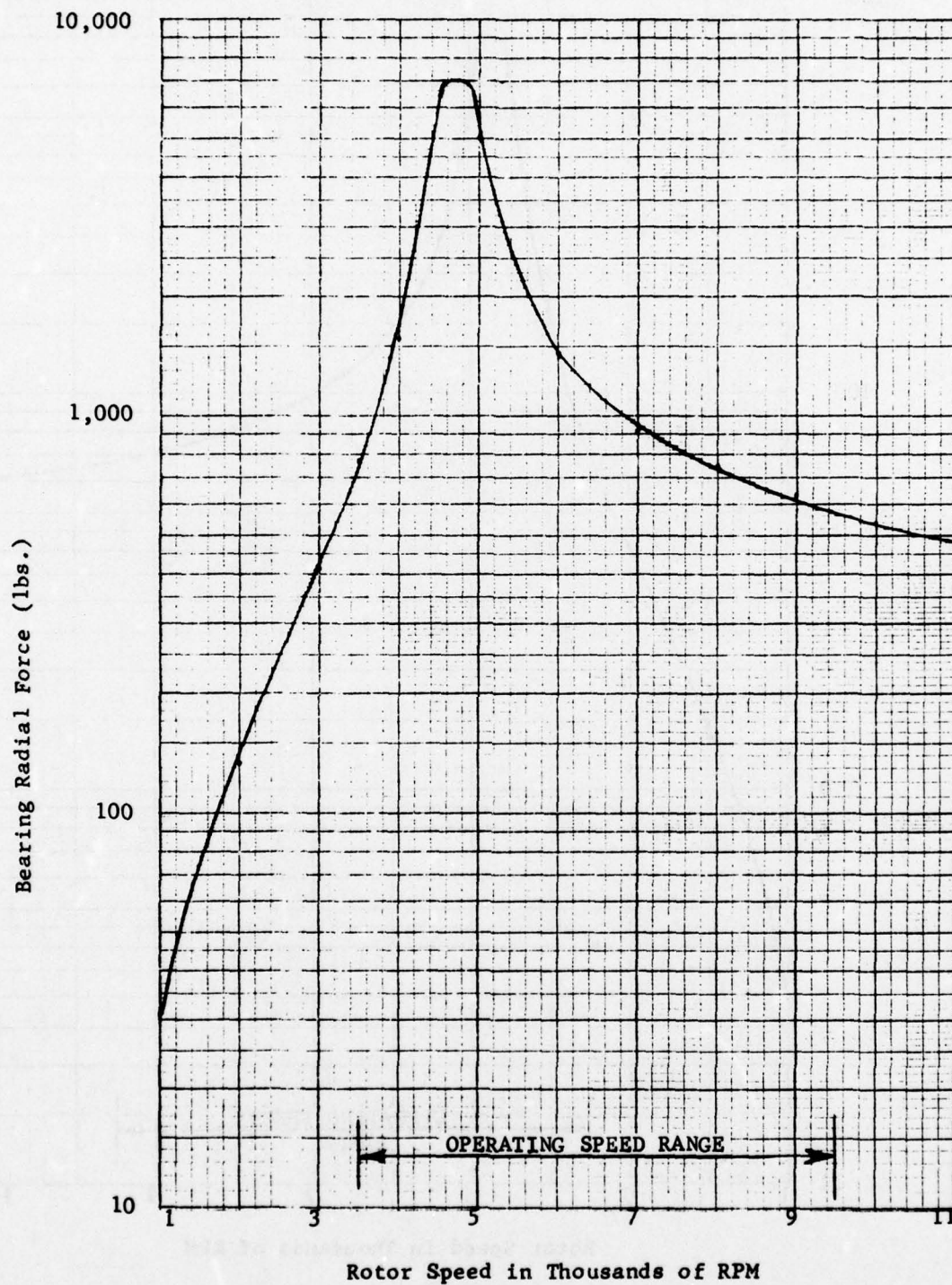


Fig. 65 TF30 No. 4 Bearing Radial Force for the 3rd Stage Low Turbine Blade Loss

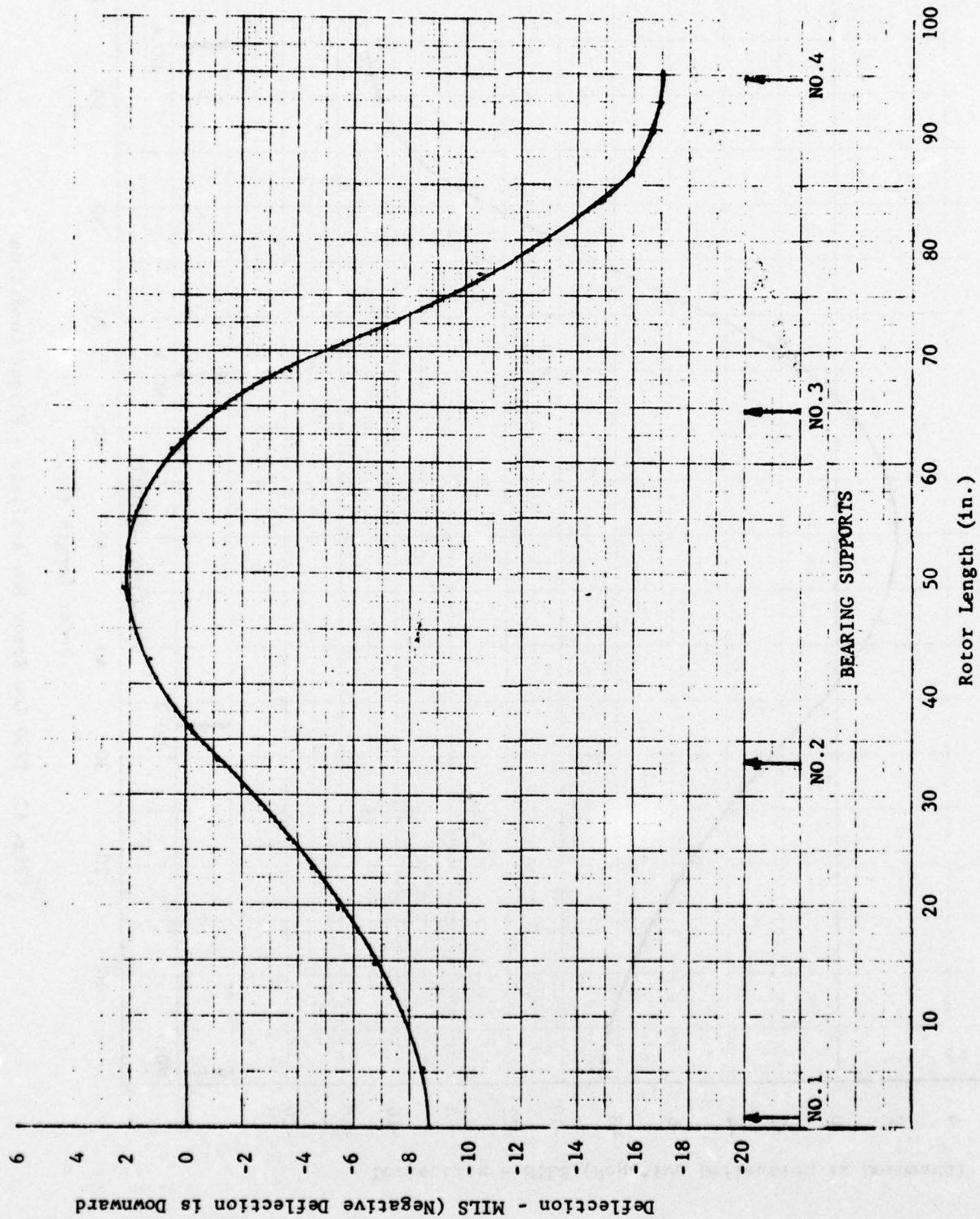


Fig. 66 TF30 Low Rotor Bow Analysis - Landing Condition



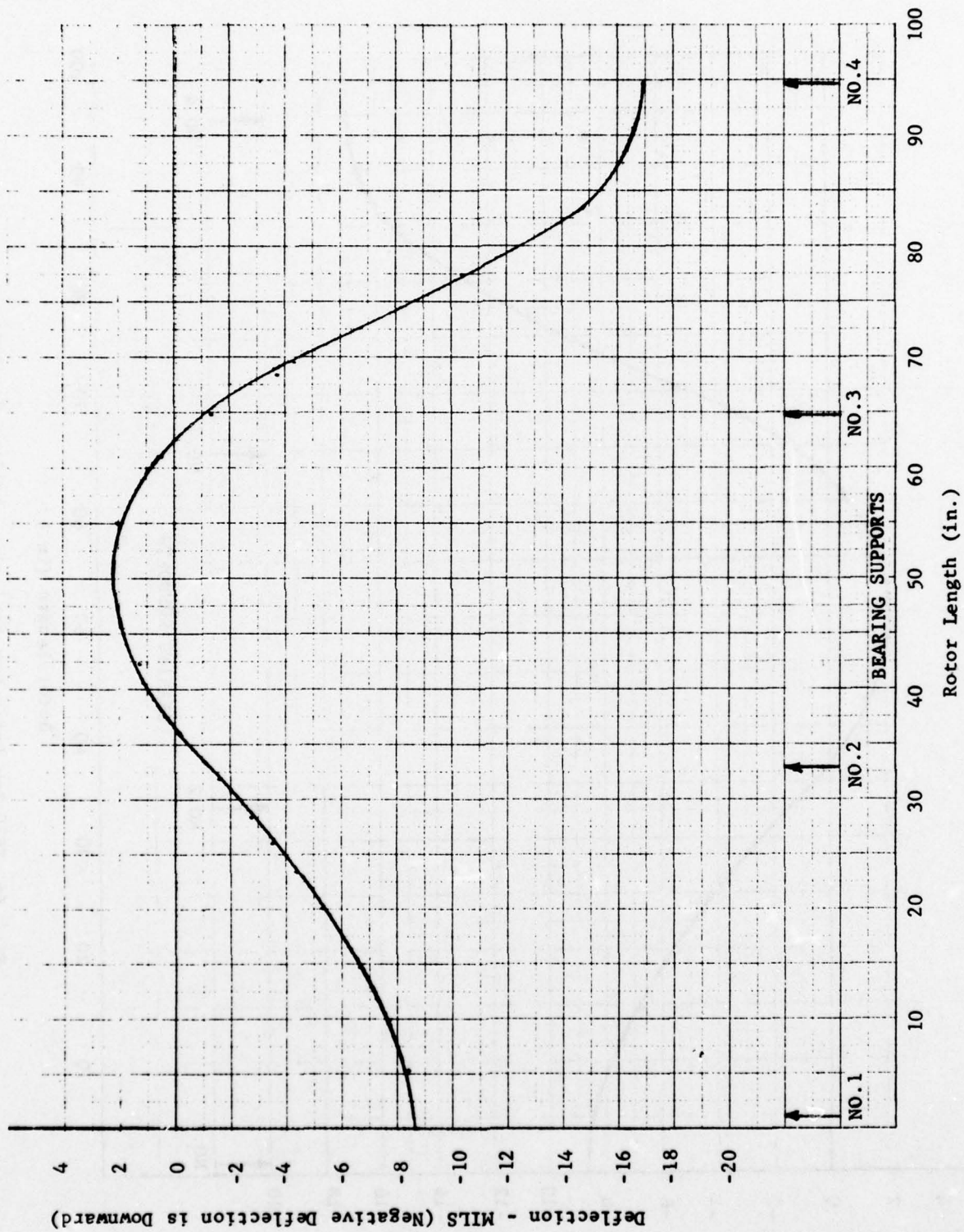


Fig. 67 TF30 Low Rotor Bow Analysis - Flight Condition

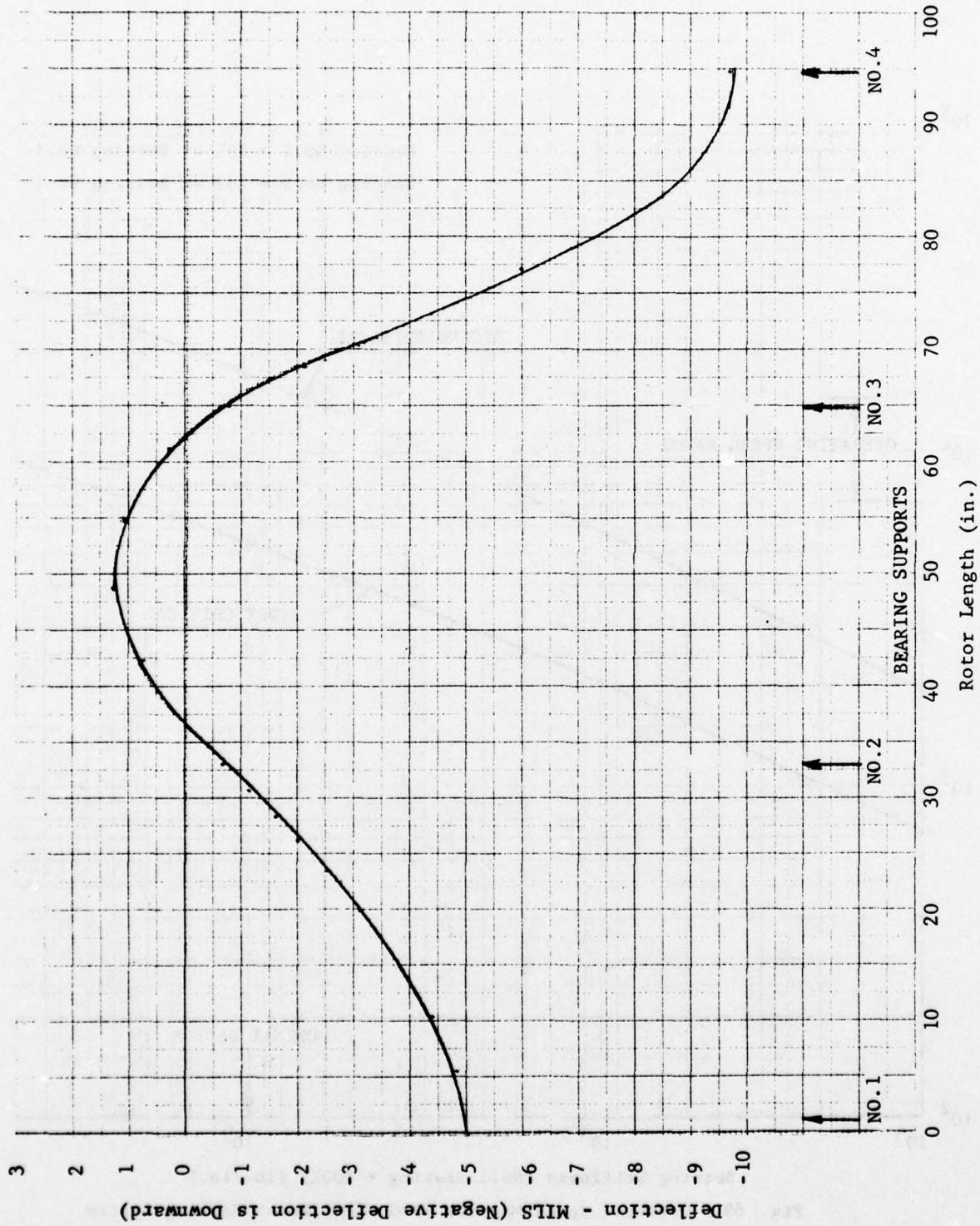


Fig. 68 TF30 Low Rotor Bow Analysis - Catapult Condition

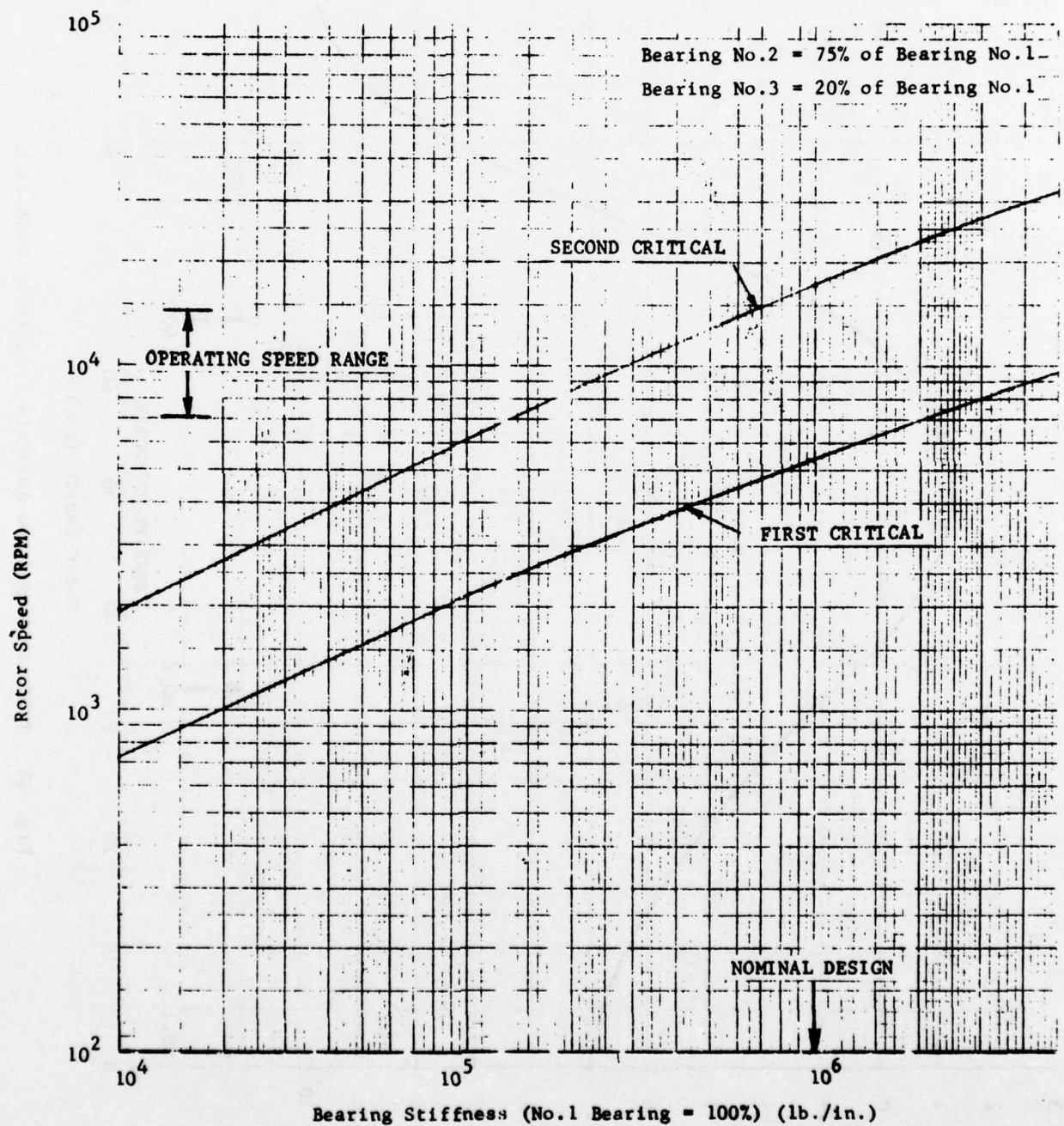


Fig. 69 Critical Speed Map for TF30 High Rotor Bearing System



THIS PAGE IS BEST QUALITY PRACTICABLE  
FROM COPY FURNISHED TO DDC

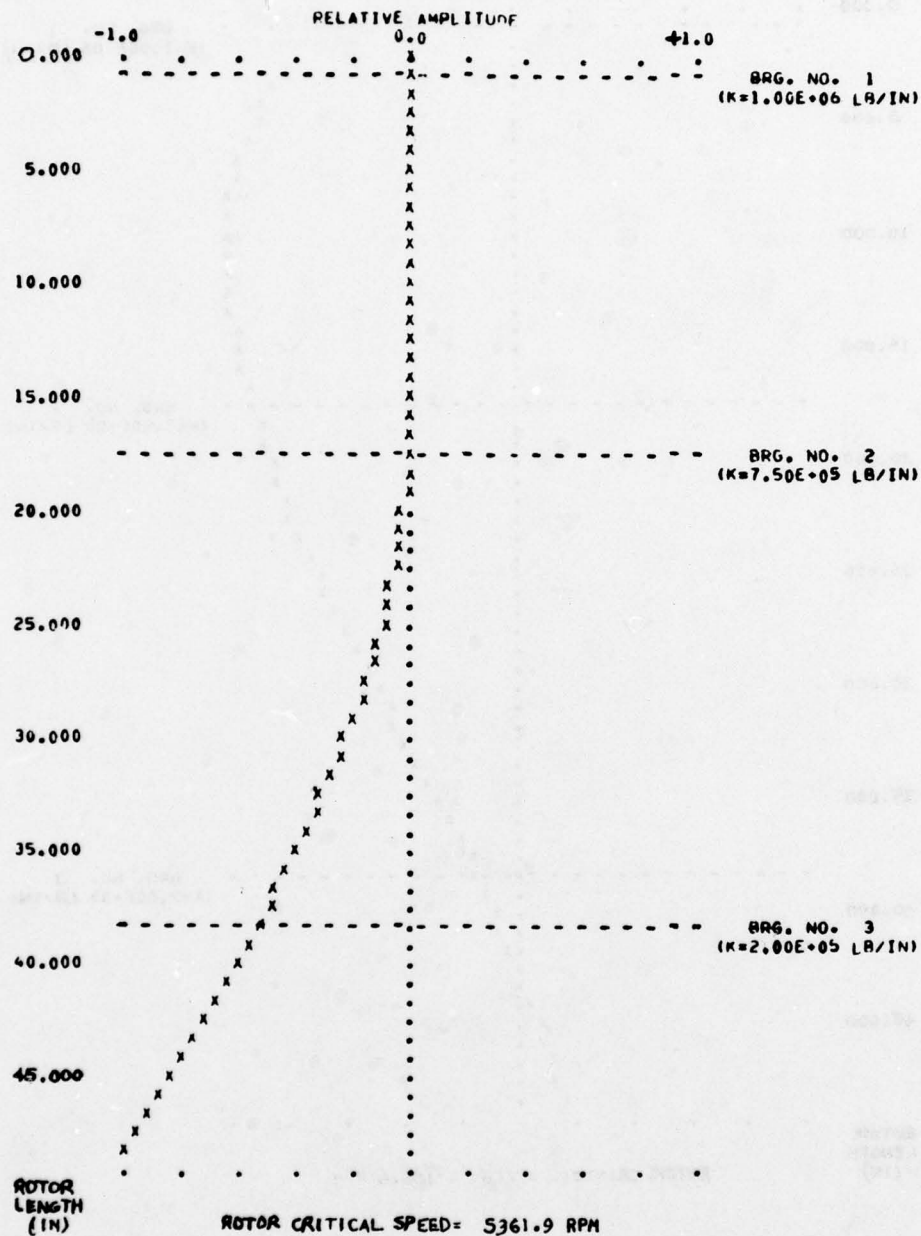


Fig. 70 Undamped Mode Shape at First Critical  
Speed for the TF30 High Rotor System  
(Cantilevered Turbine Mode)

THIS PAGE IS BEST QUALITY PRACTICABLE  
FROM COPY FURNISHED TO DDC

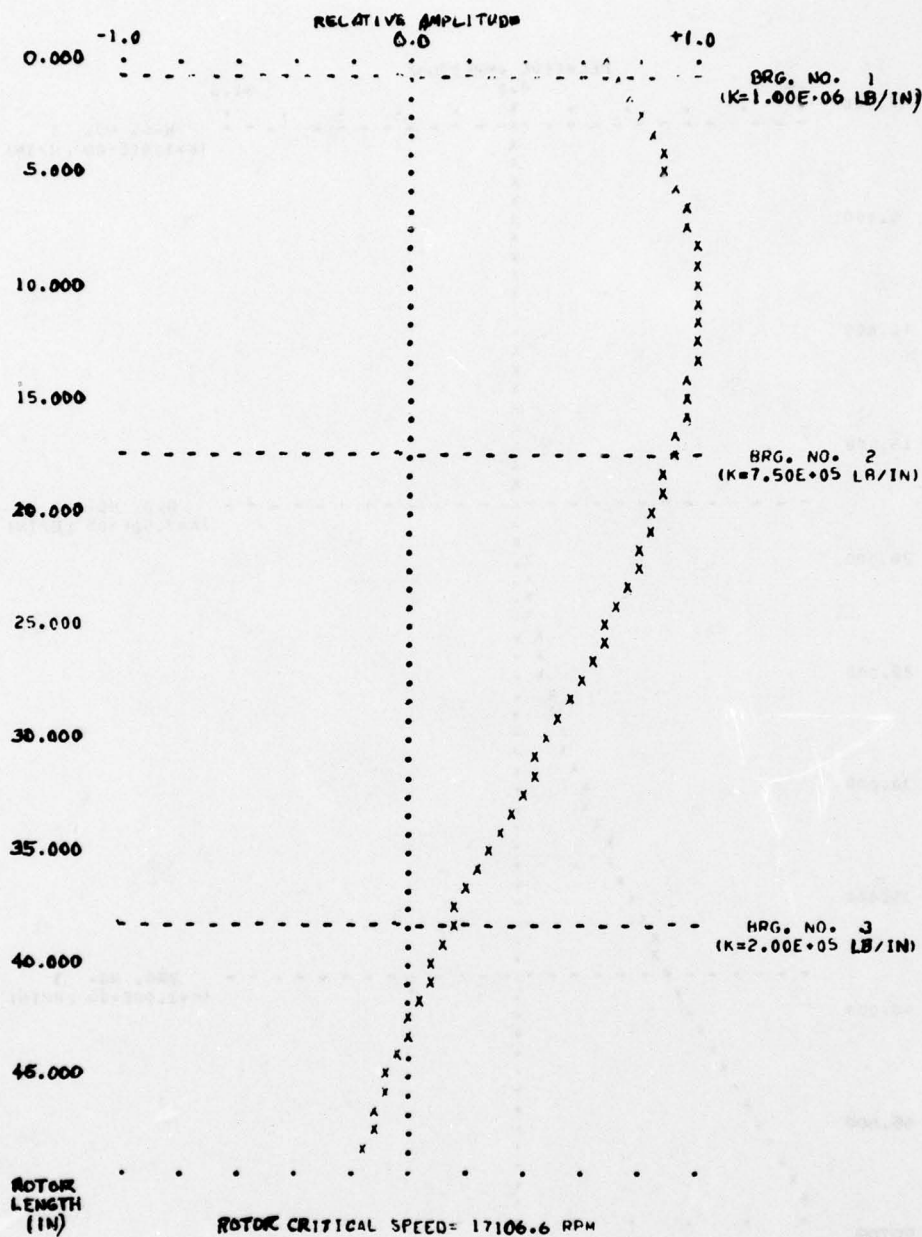


Fig. 71 Undamped Mode Shape at Second Critical Speed for the TF30 High Rotor System (Compressor Bounce Mode)

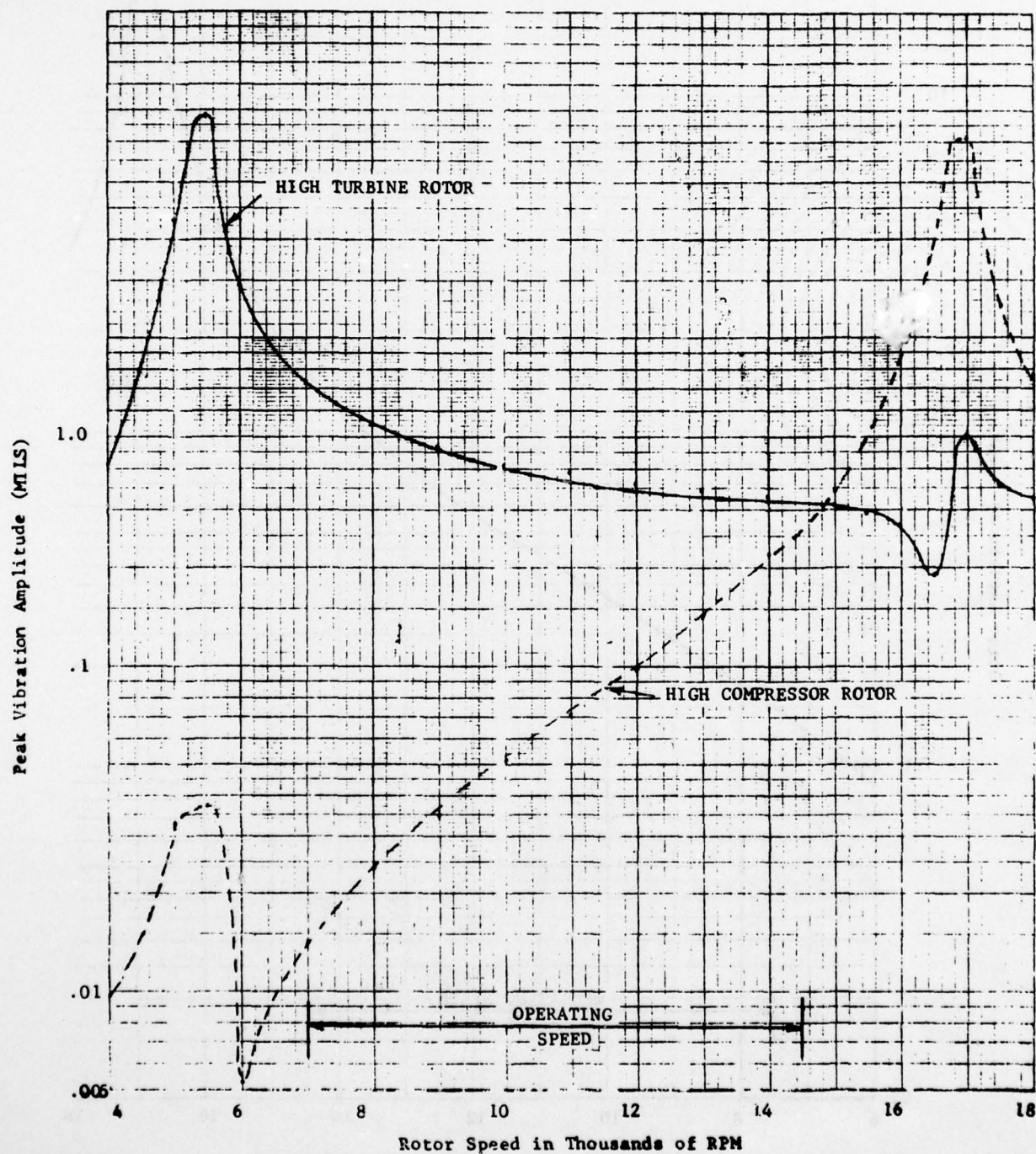


Fig. 72 Calculated Unbalance Response for TF30 High Rotor System with Random Distributed Unbalance



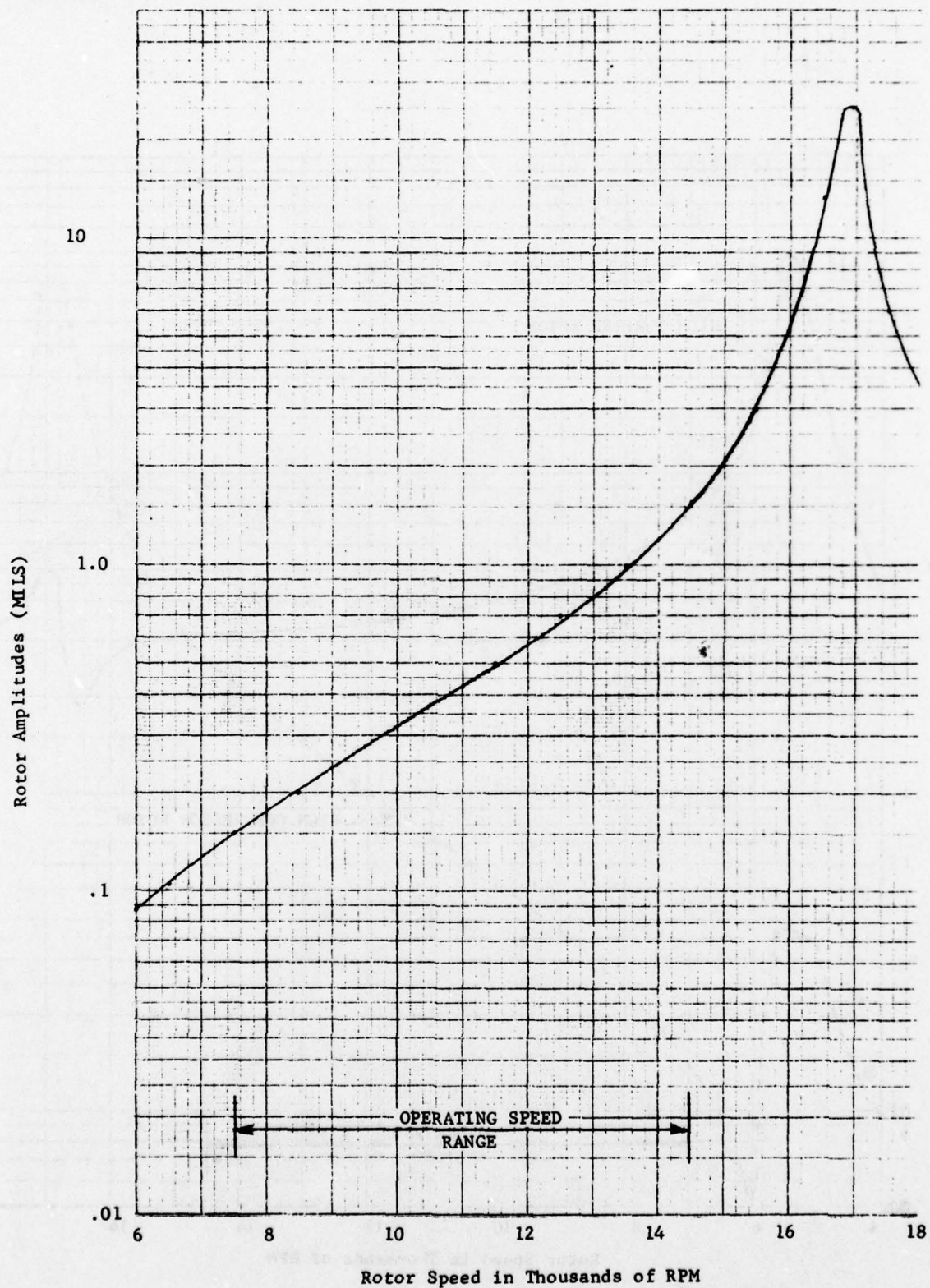


Fig. 73 Compressor Amplitude for the High Rotor System of the TF30 Engine for a First Compressor Stage Blade Loss

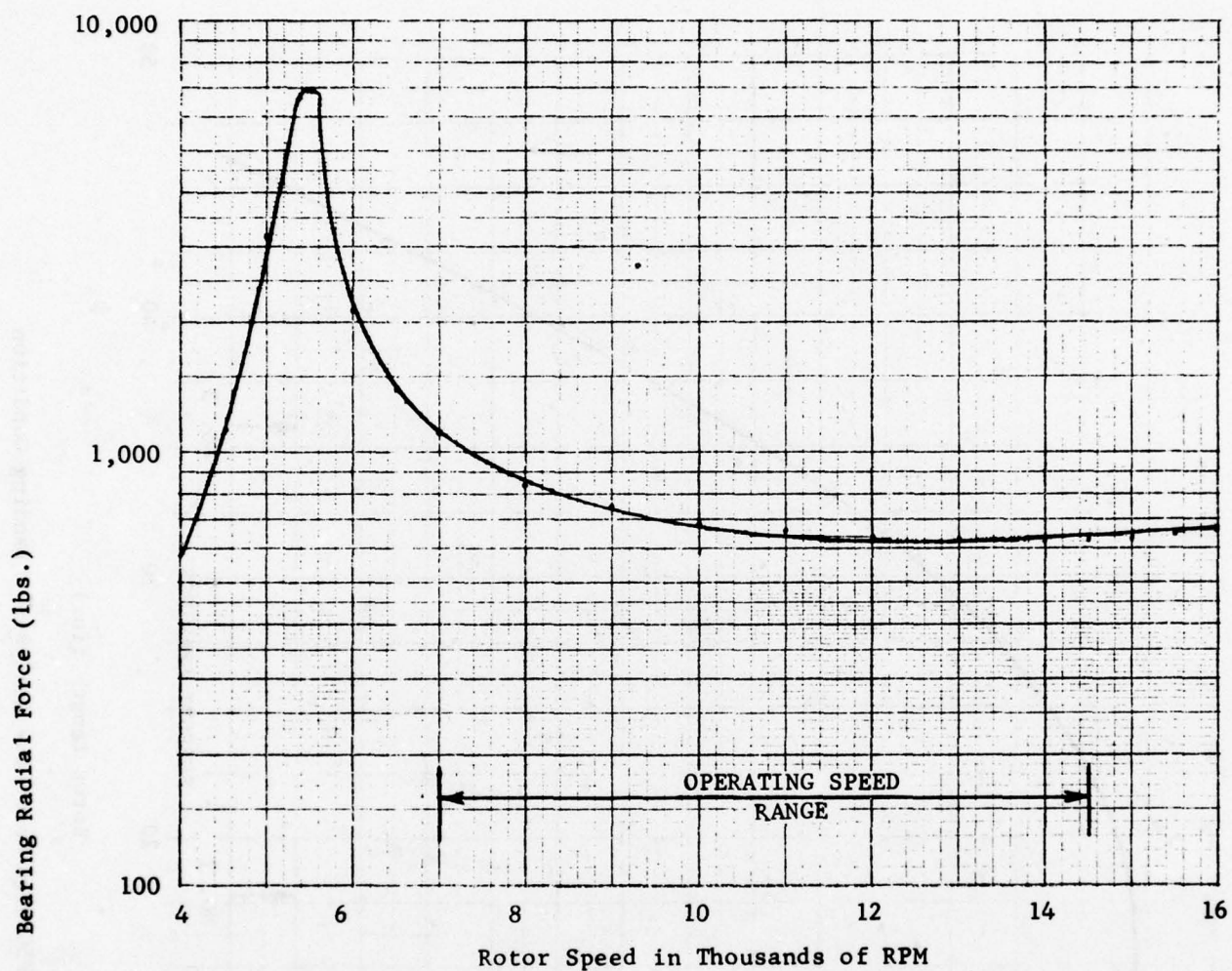


Fig. 76 No.3 Bearing Radial Force for a Turbine Blade Loss of the TF30 High Rotor System

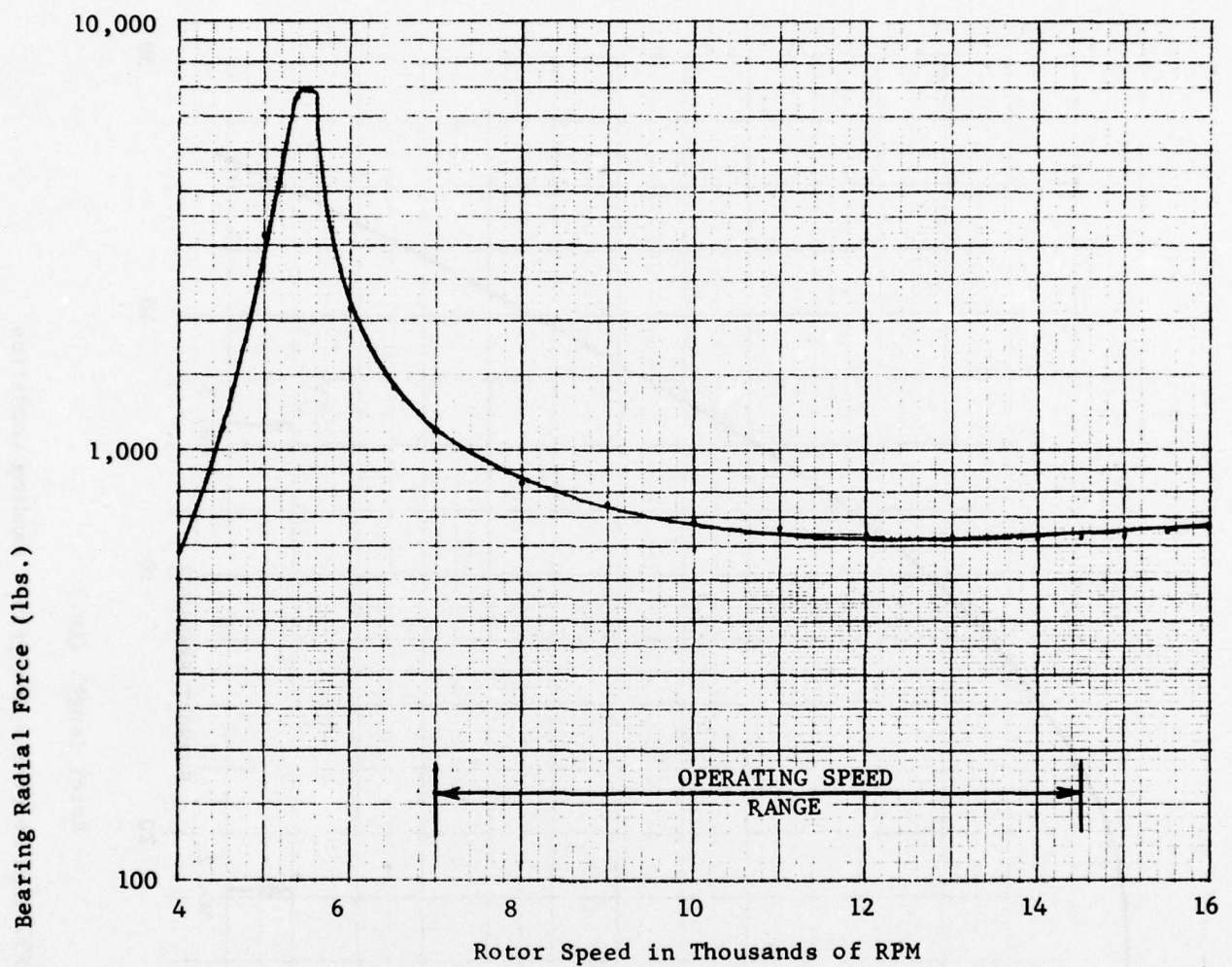


Fig. 76 No.3 Bearing Radial Force for a Turbine Blade Loss of the TF30 High Rotor System



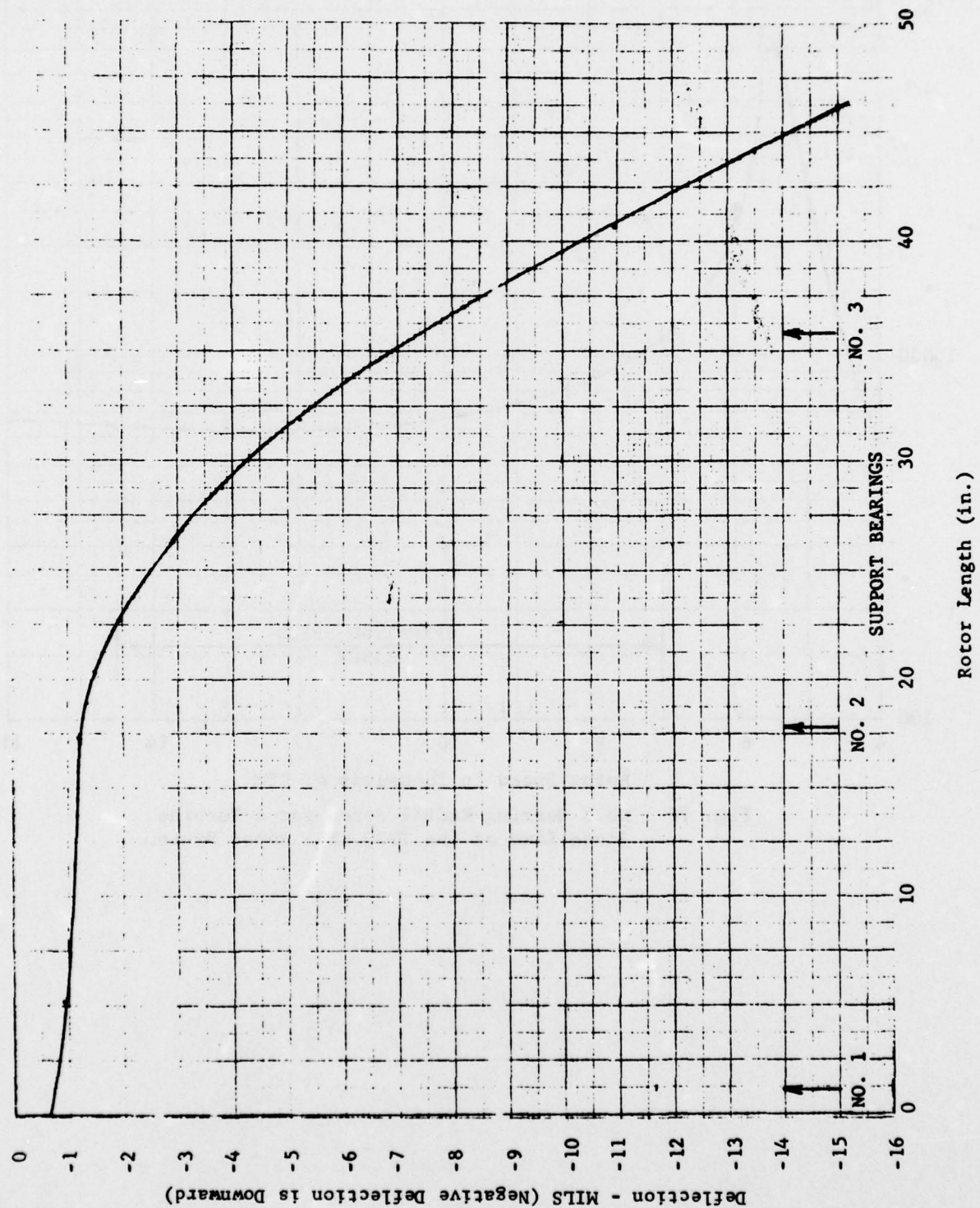


Fig. 77 TF30 High Rotor Bow Analysis - Landing Condition

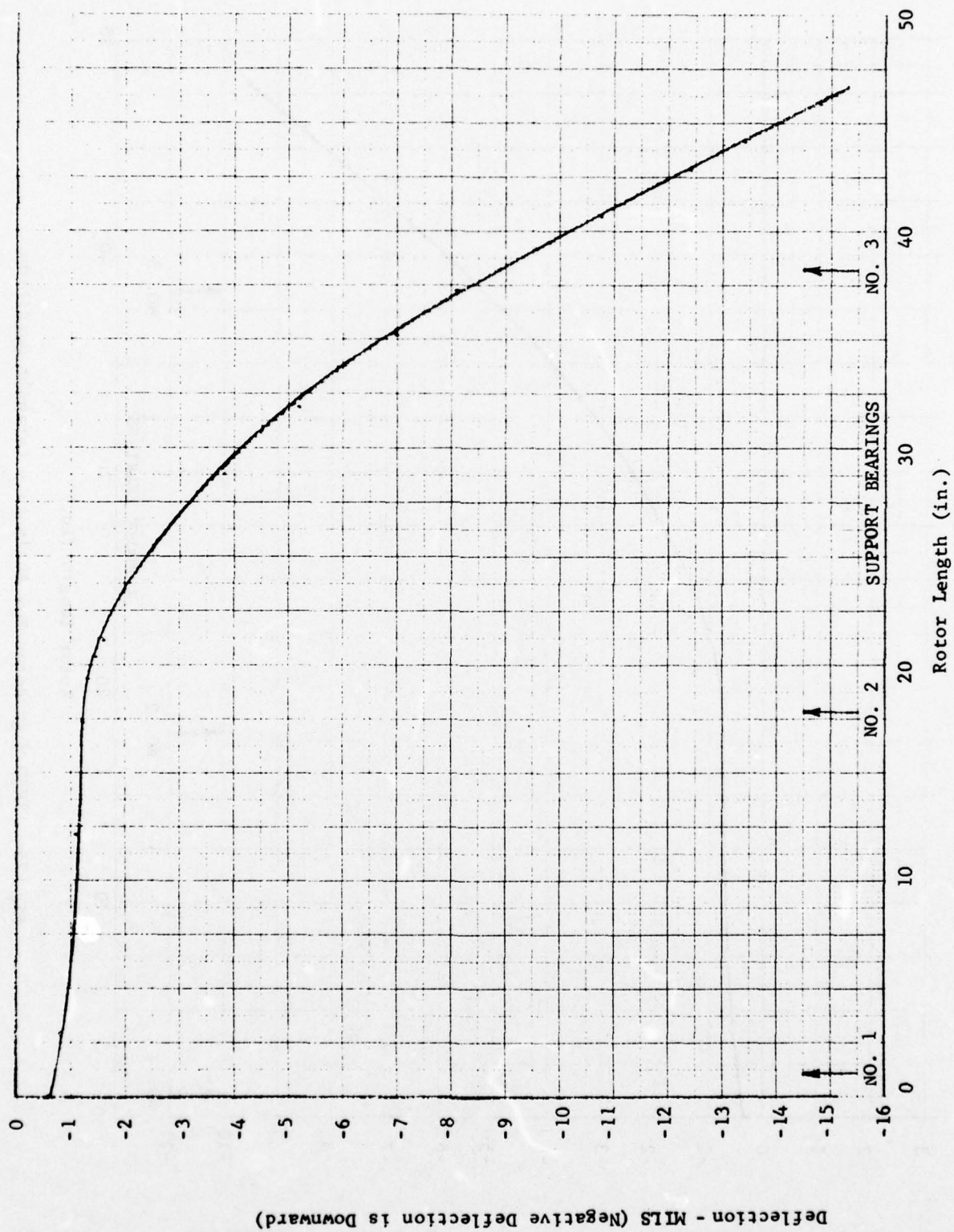


Fig. 78 TF30 High Rotor Bow Analysis - Flight Condition

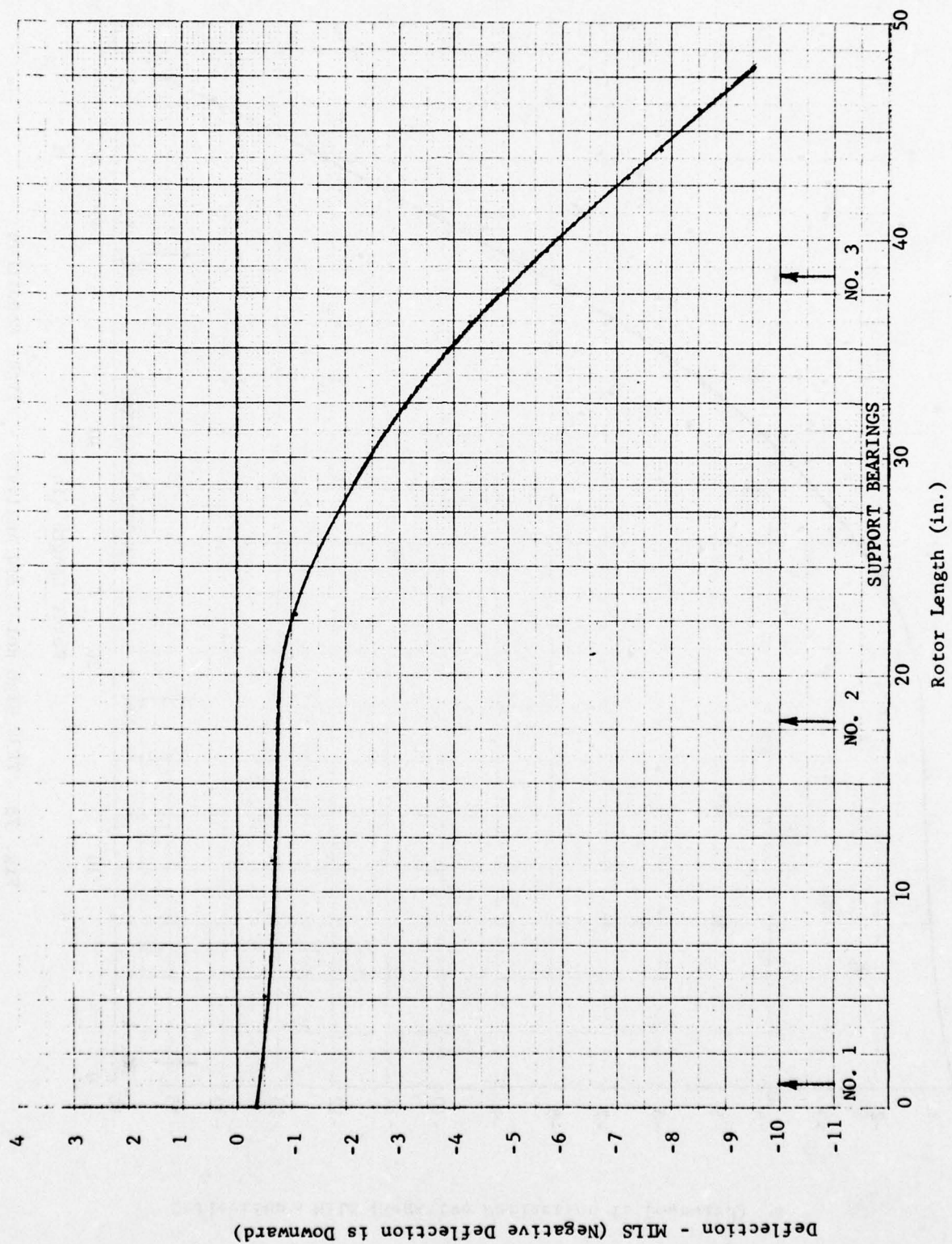


Fig. 79 TF30 High Rotor Bow Analysis - Catapult Condition



Brg. No. 2 = 120% of Brg. No. 1  
 Brg. No. 3 = 100% of Brg. No. 1  
 Brg. No. 4 = 15% of Brg. No. 1

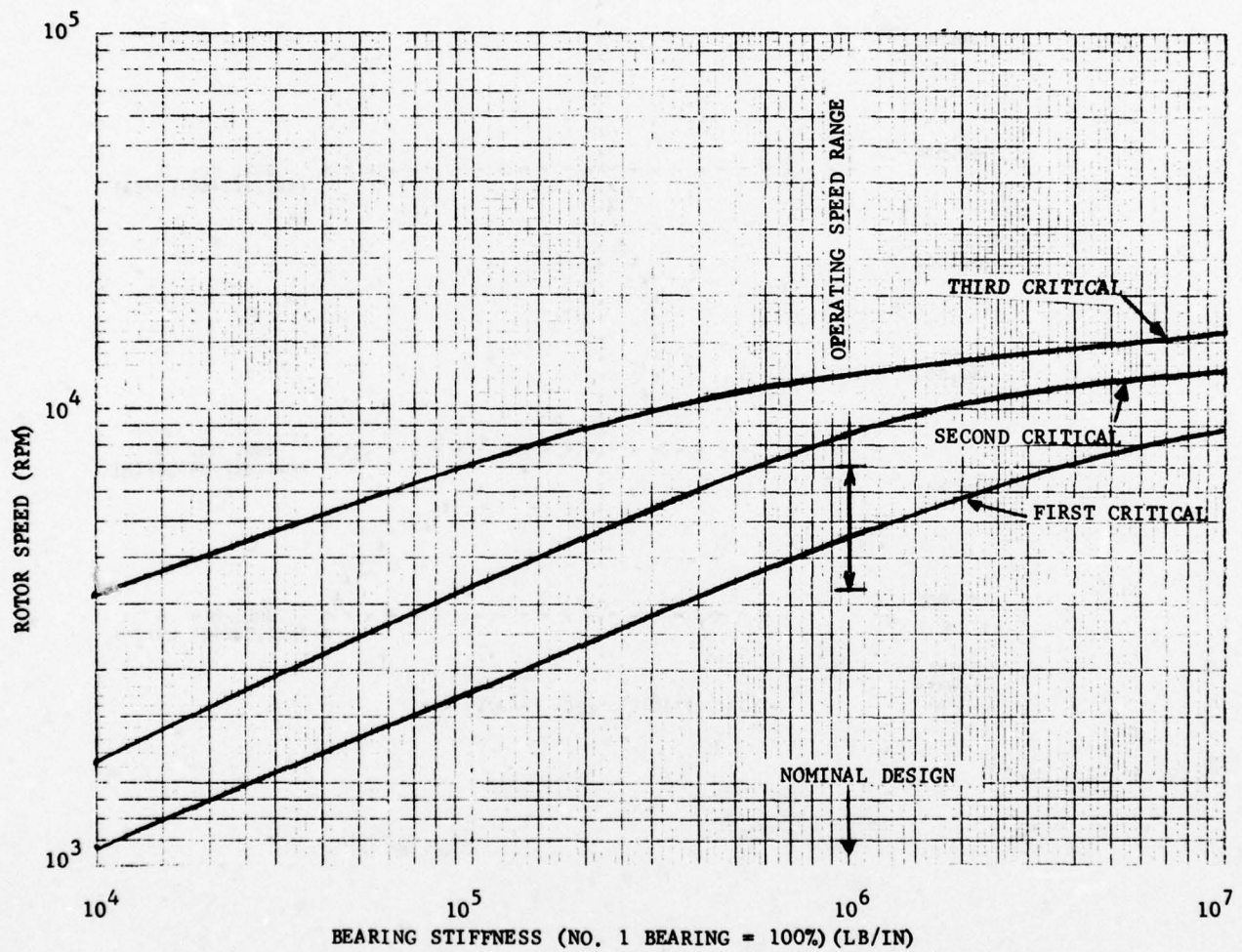


Fig. 80 Critical Speed Map for TF 33 Low Rotor Bearing System

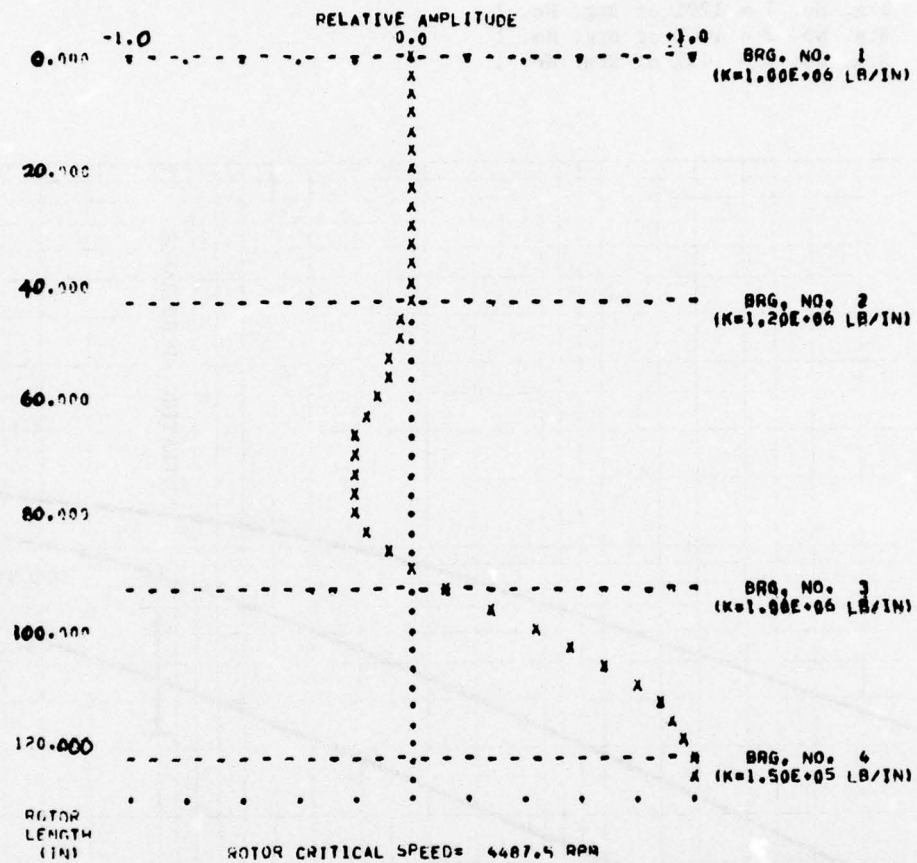


Fig. 81 Undamped Mode Shape at First Critical Speed of TF33 Low Rotor System (Low Turbine Bounce Mode).

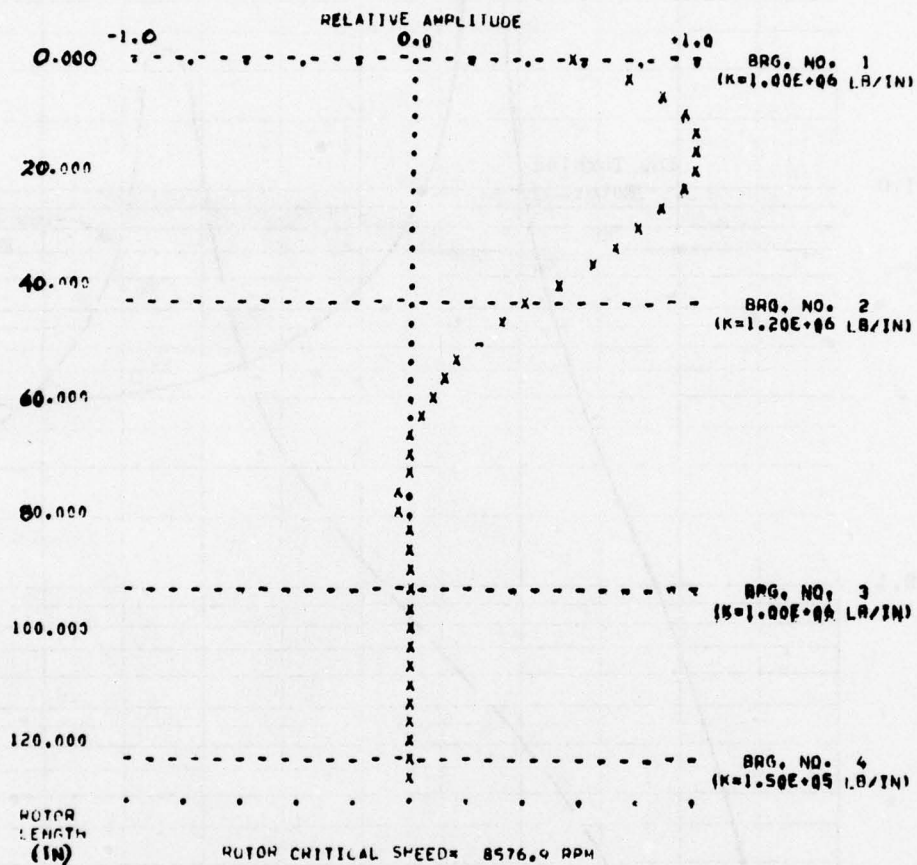


Fig. 82 Undamped Mode Shape at Second Critical Speed of TF33 Low Rotor System (Low Compressor Bounce Mode).



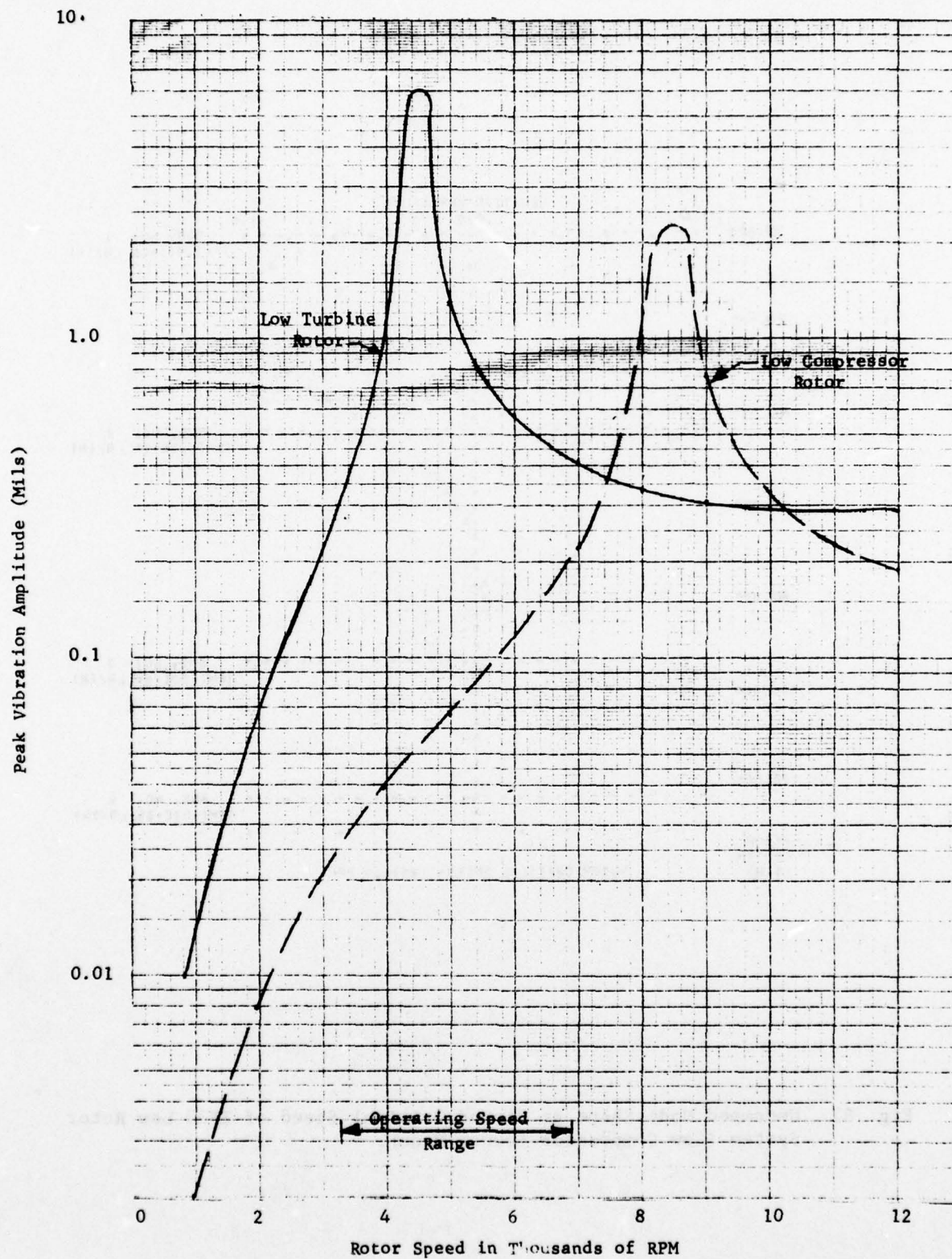


Fig. 83 Calculated Unbalance, Response for TF33 Low Rotor System with Random Distributed Unbalance.

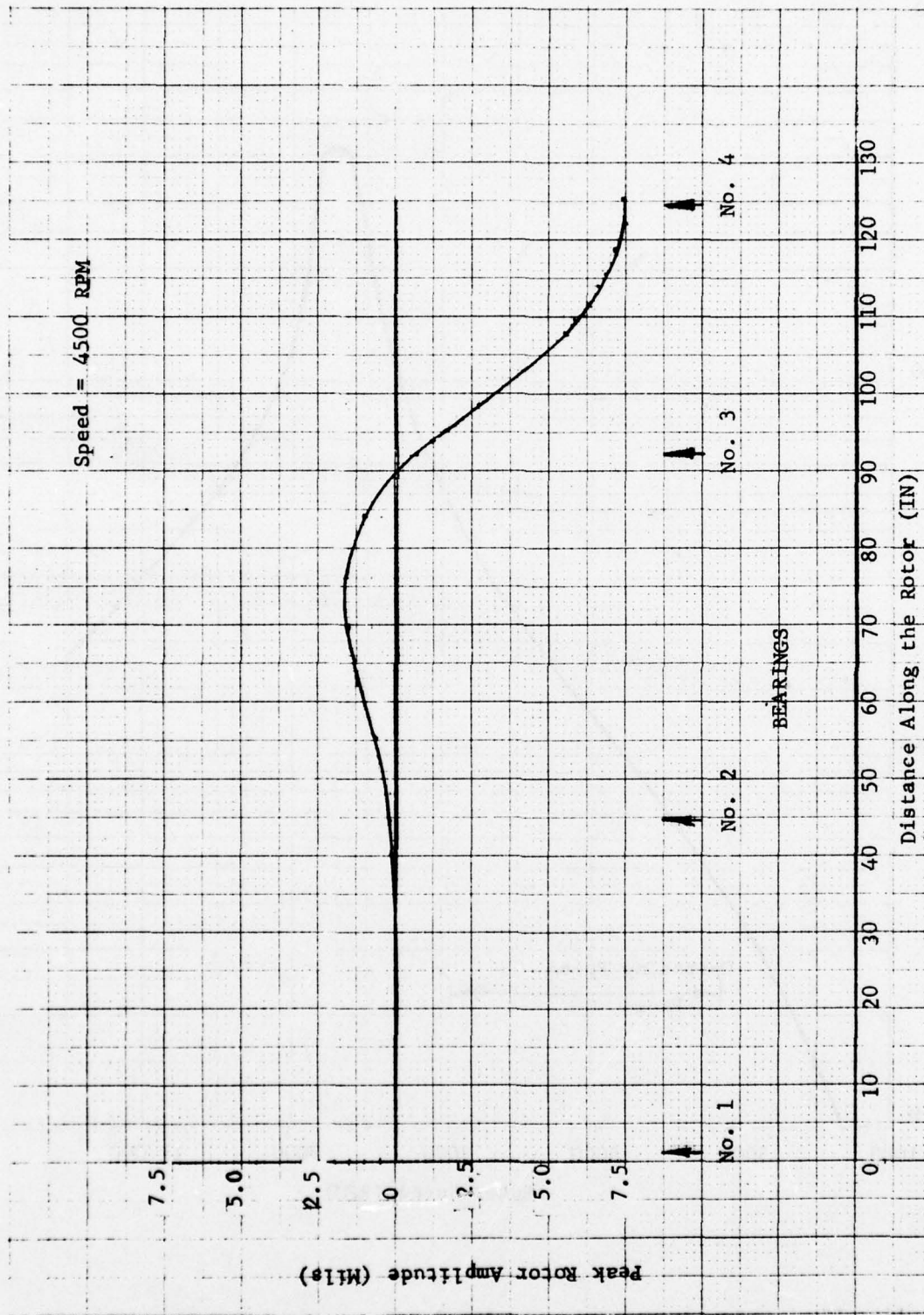


Fig. 84 Unbalance Response Mode Shape at Operating Speed of 4500 RPM  
for the TF33 Low Rotor System.

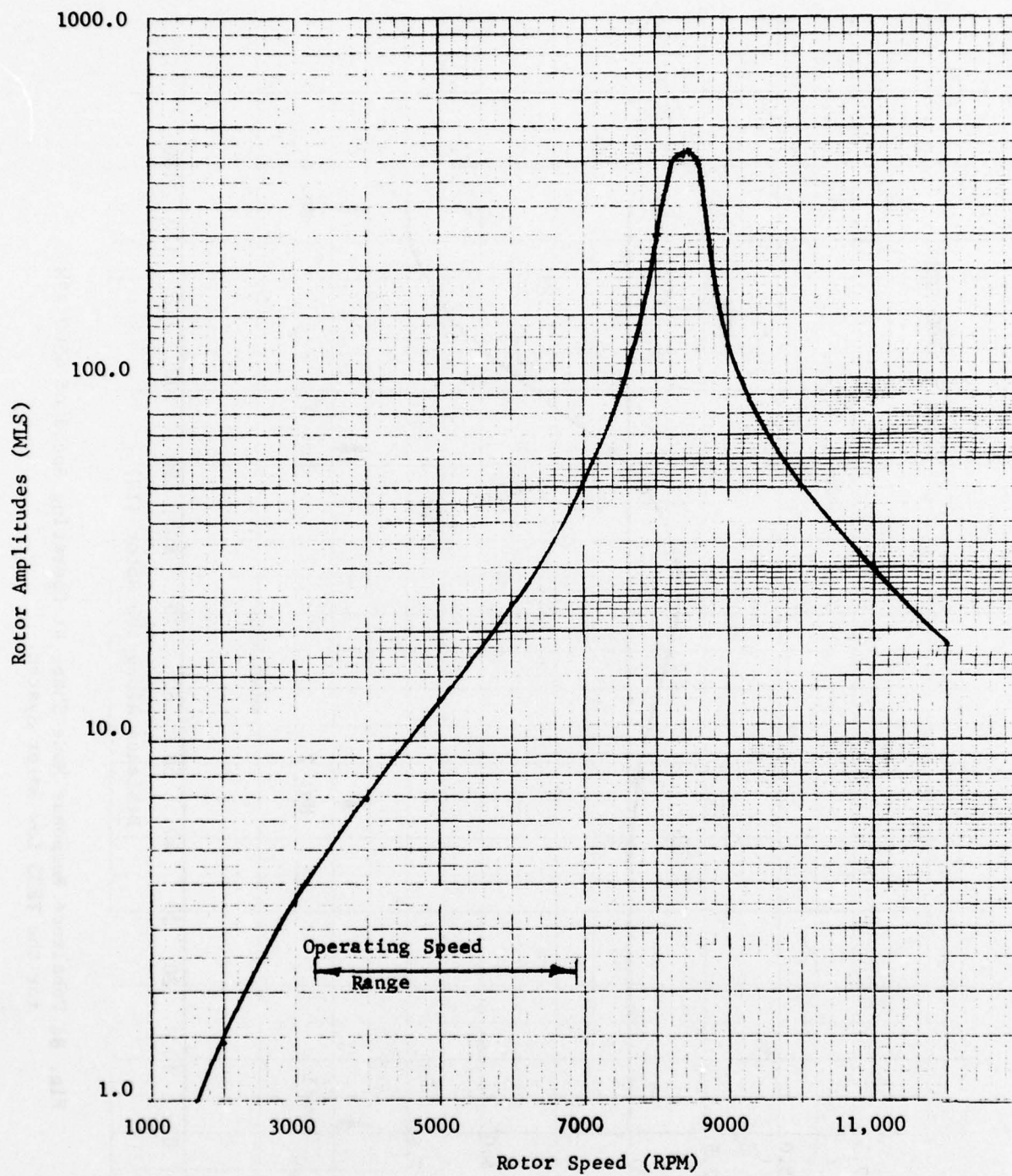


Fig. 85 Low Compressor Rotor Amplitudes for a First Fan Stage Blade Loss of the TF33 Engine.



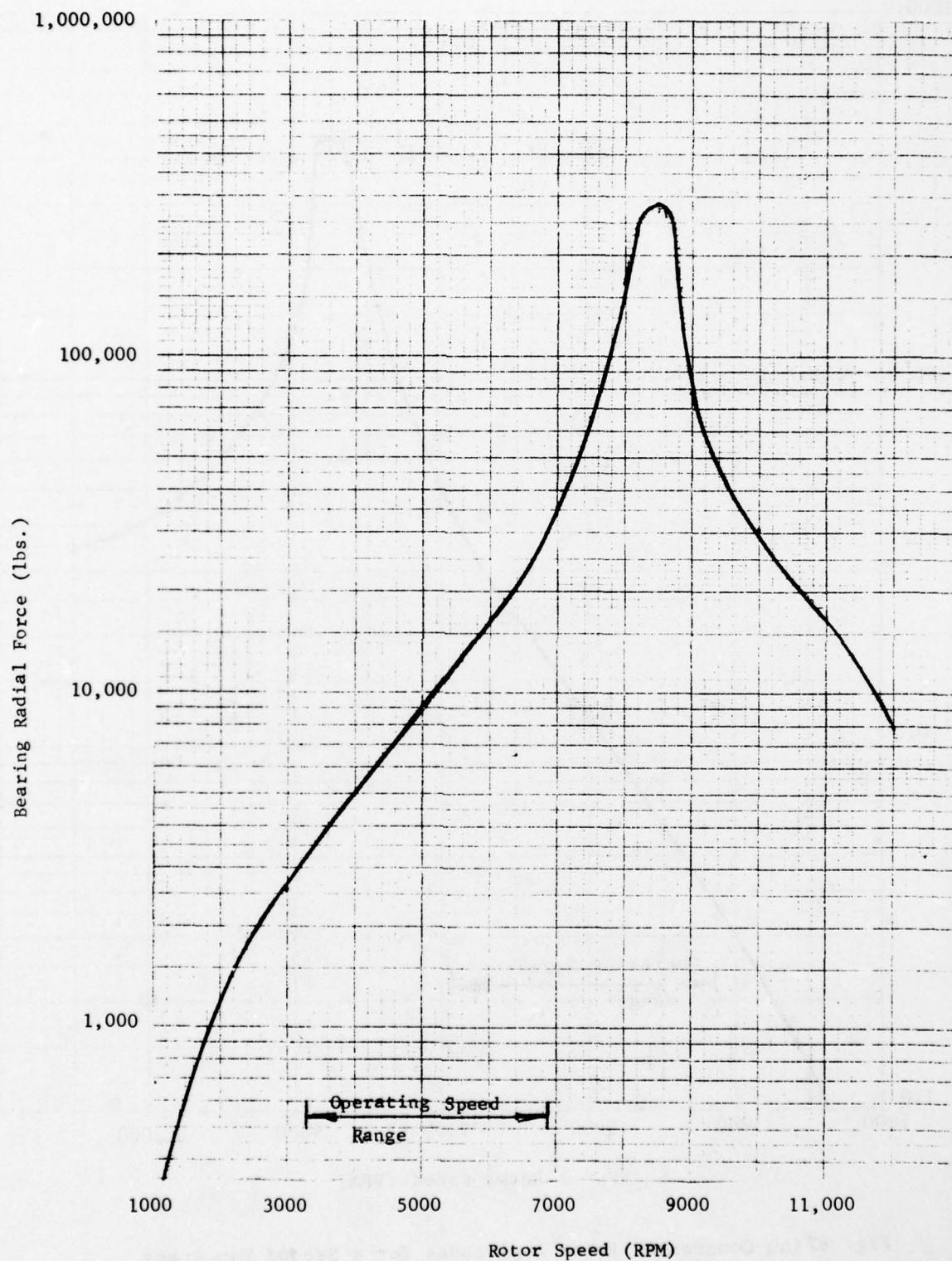


Fig. 86 TF33 Low Rotor No. 1 Bearing Radial Force for the First Fan Stage Blade Loss.

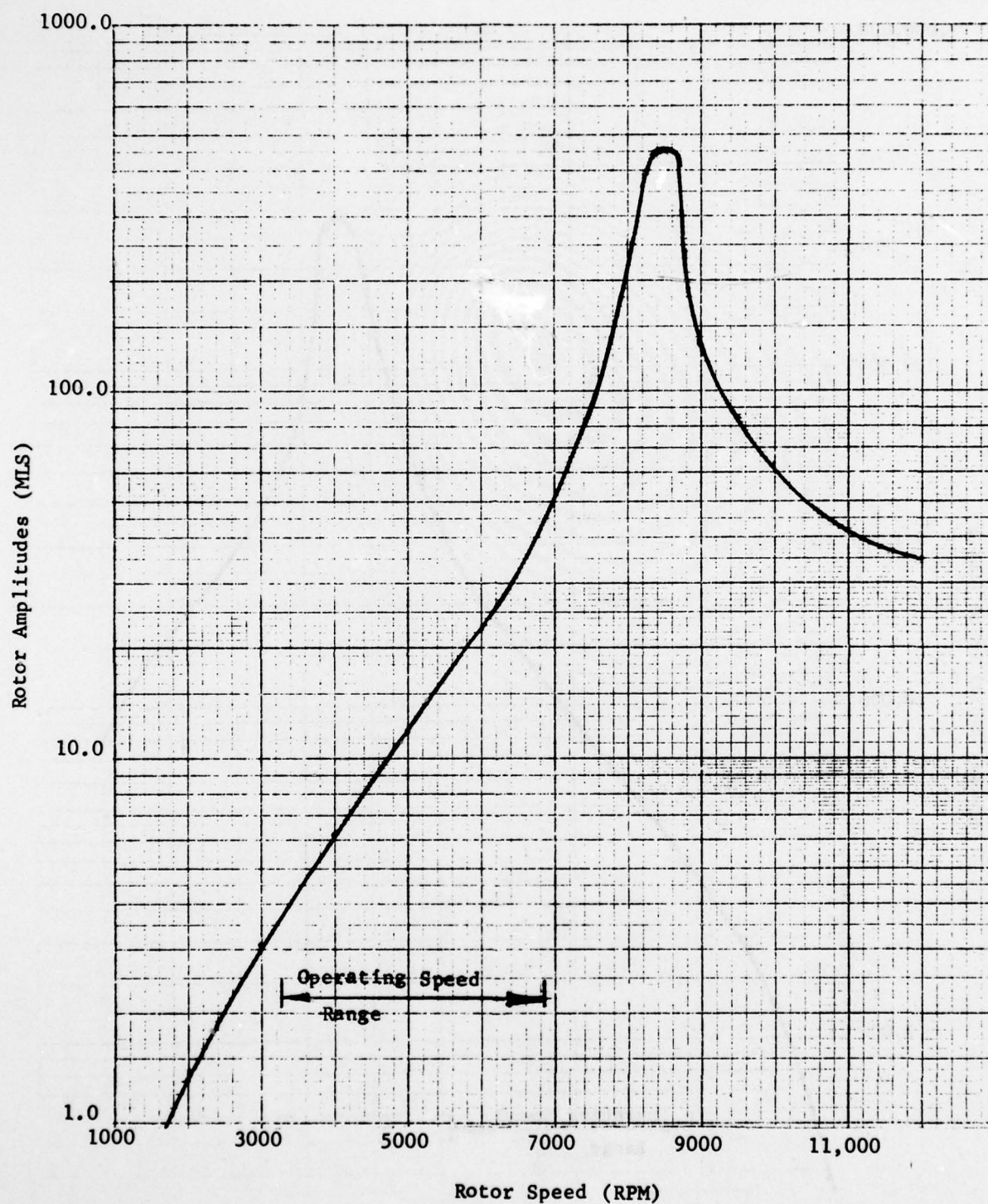


Fig. 87 Low Compressor Rotor Amplitudes for a Second Fan Stage Blade Loss of the TF33 Engine.

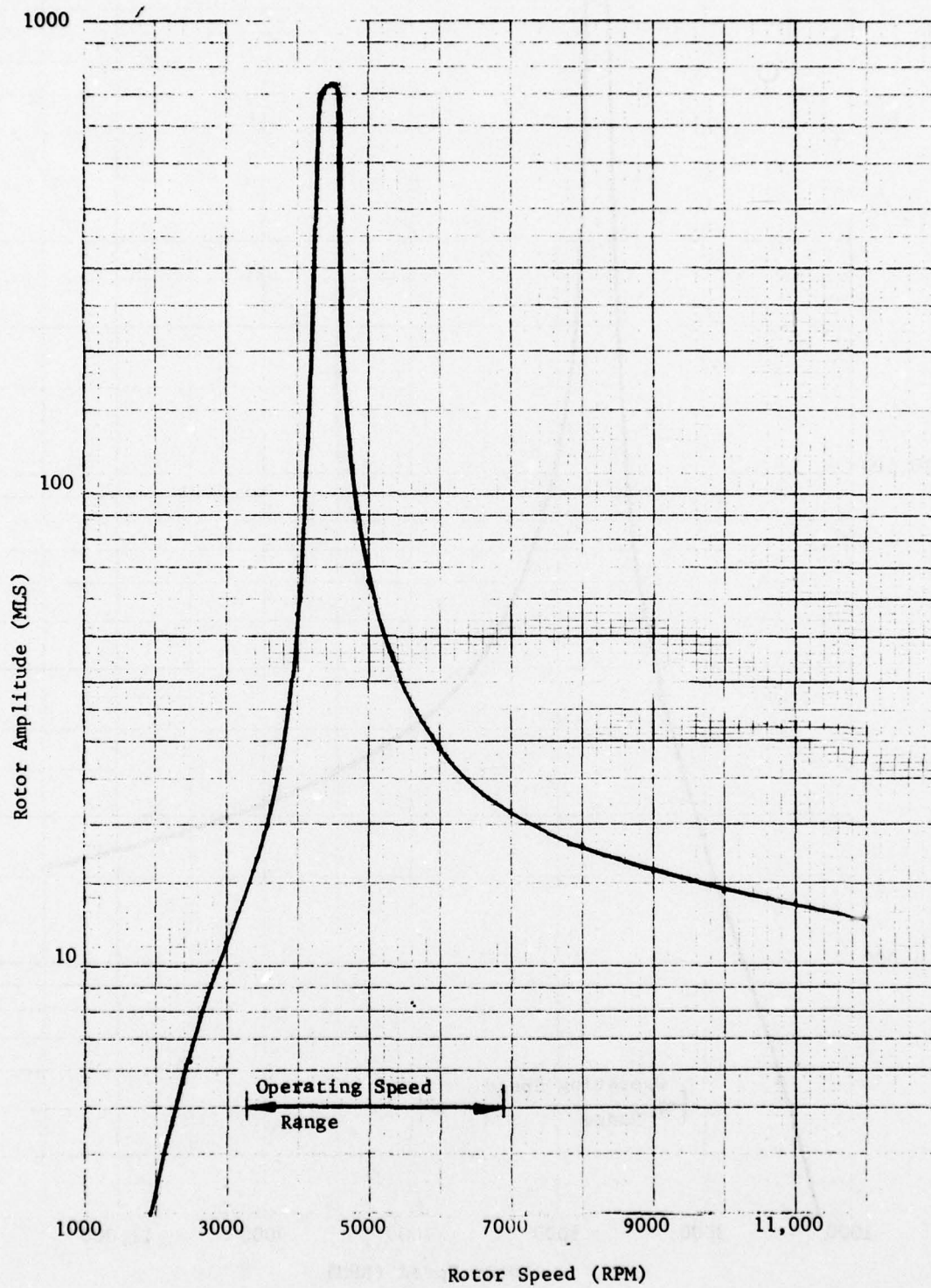


Fig. 88 Low Turbine Rotor Amplitudes for a Third Stage Turbine Blade Loss of the TF33 Engine.



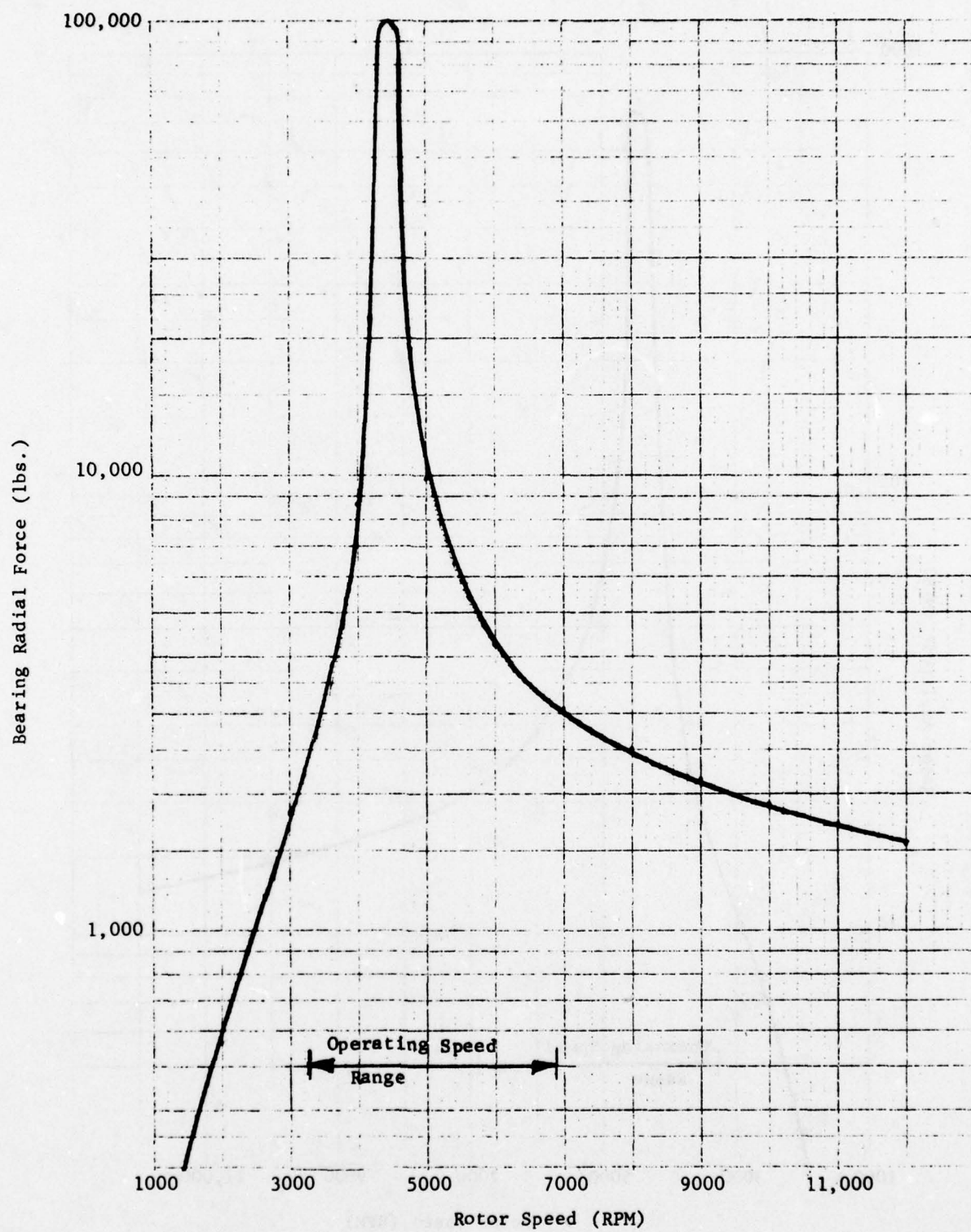


Fig. 89 TF33 No. 4 Bearing Radial Force for the 3rd Stage Low Turbine Blade Loss.

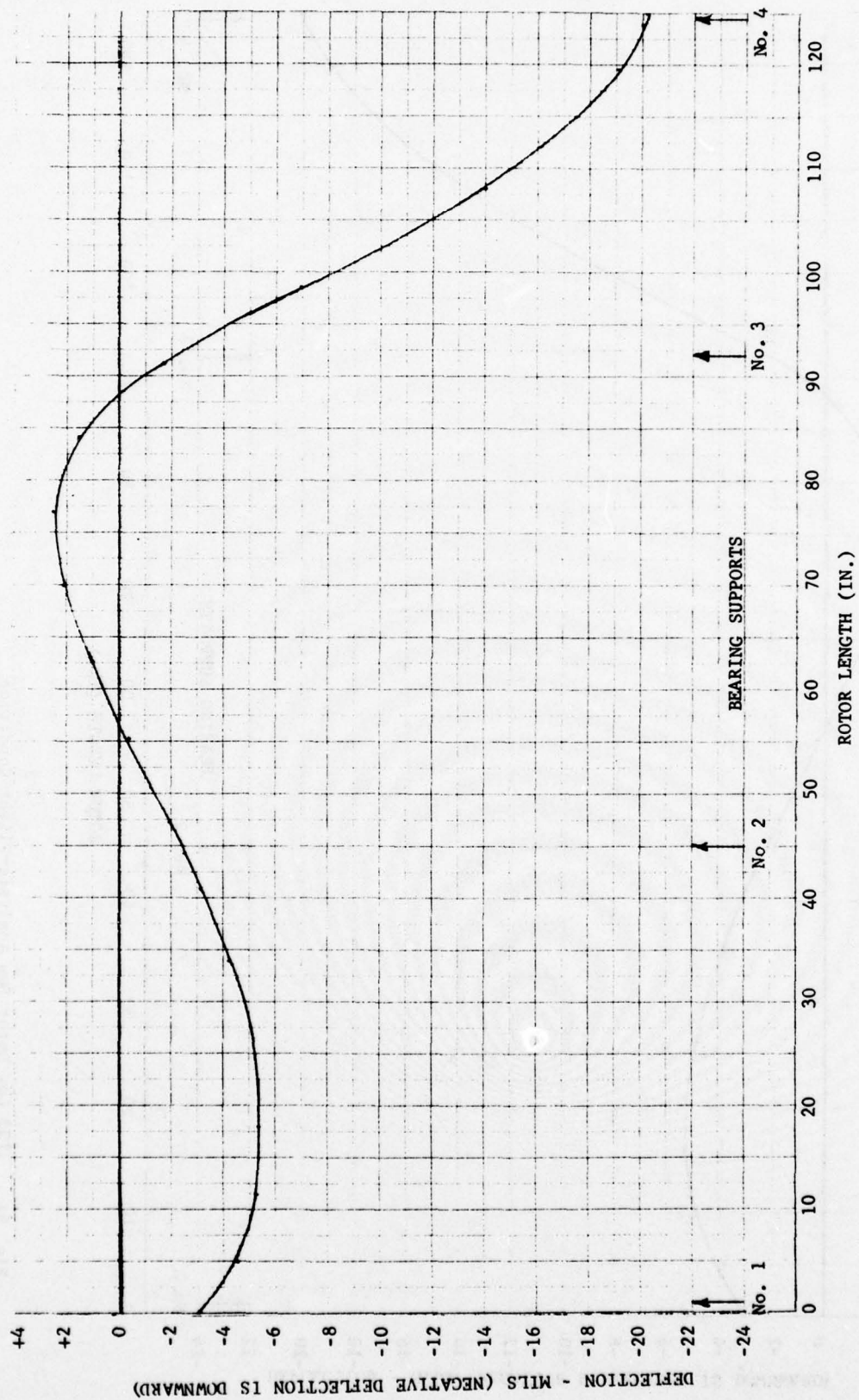


Fig. 90 TF33 Low Rotor Bow Analysis - Landing Condition

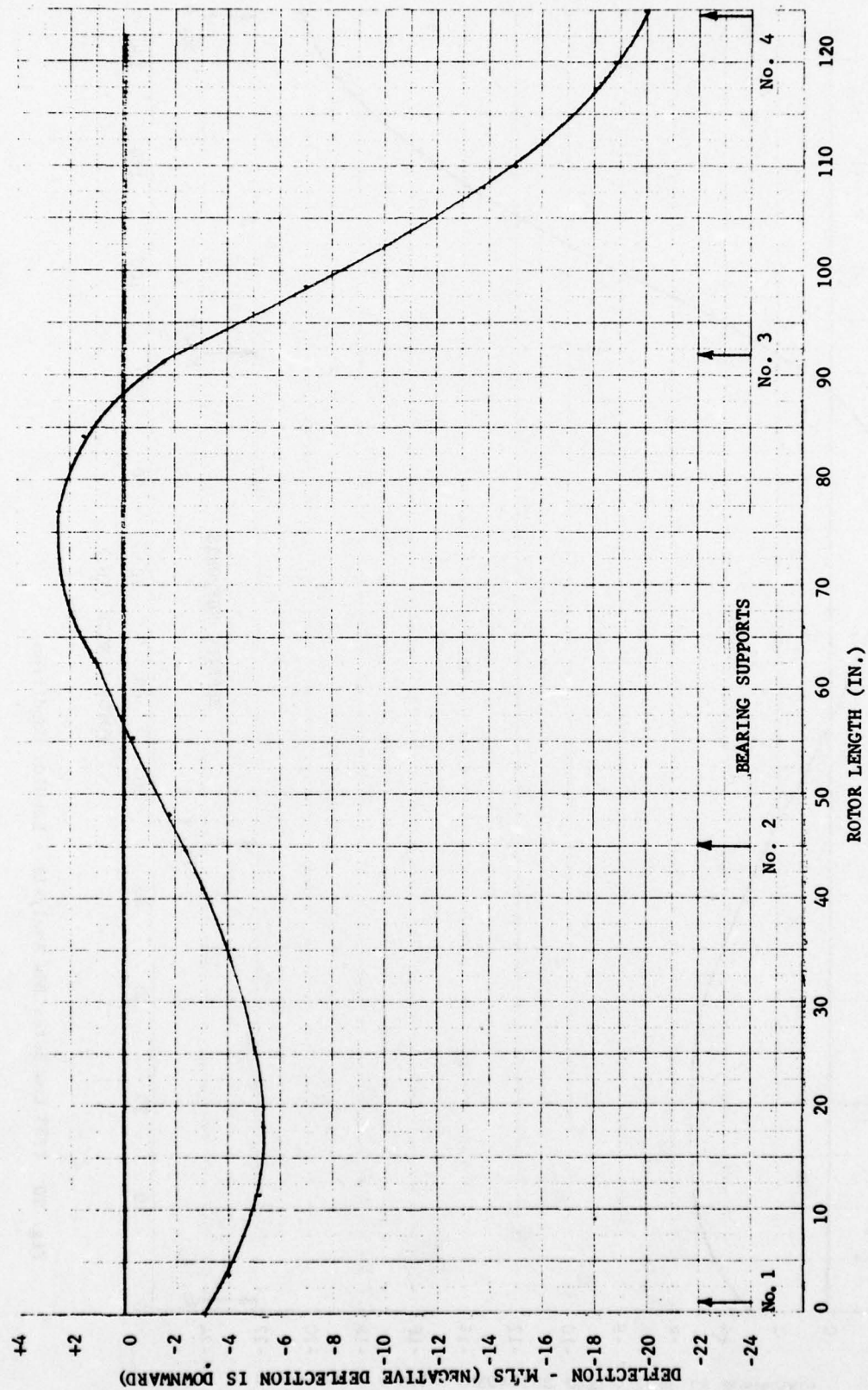


Fig. 91 TF33 Low Rotor Bow Analysis-Flight Condition



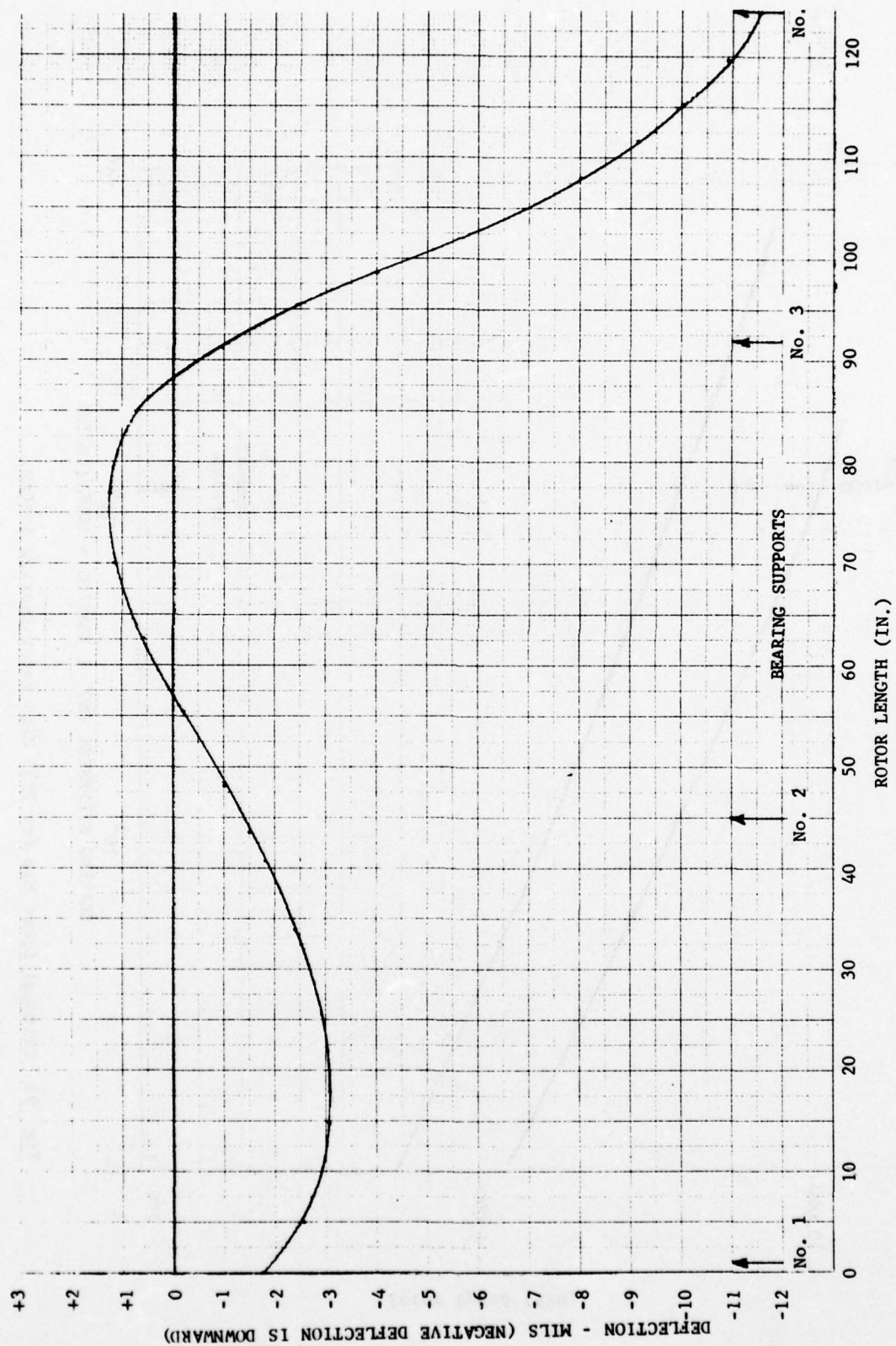


Fig. 92 TF33 Low Rotor Bow Analysis - Catapult Condition

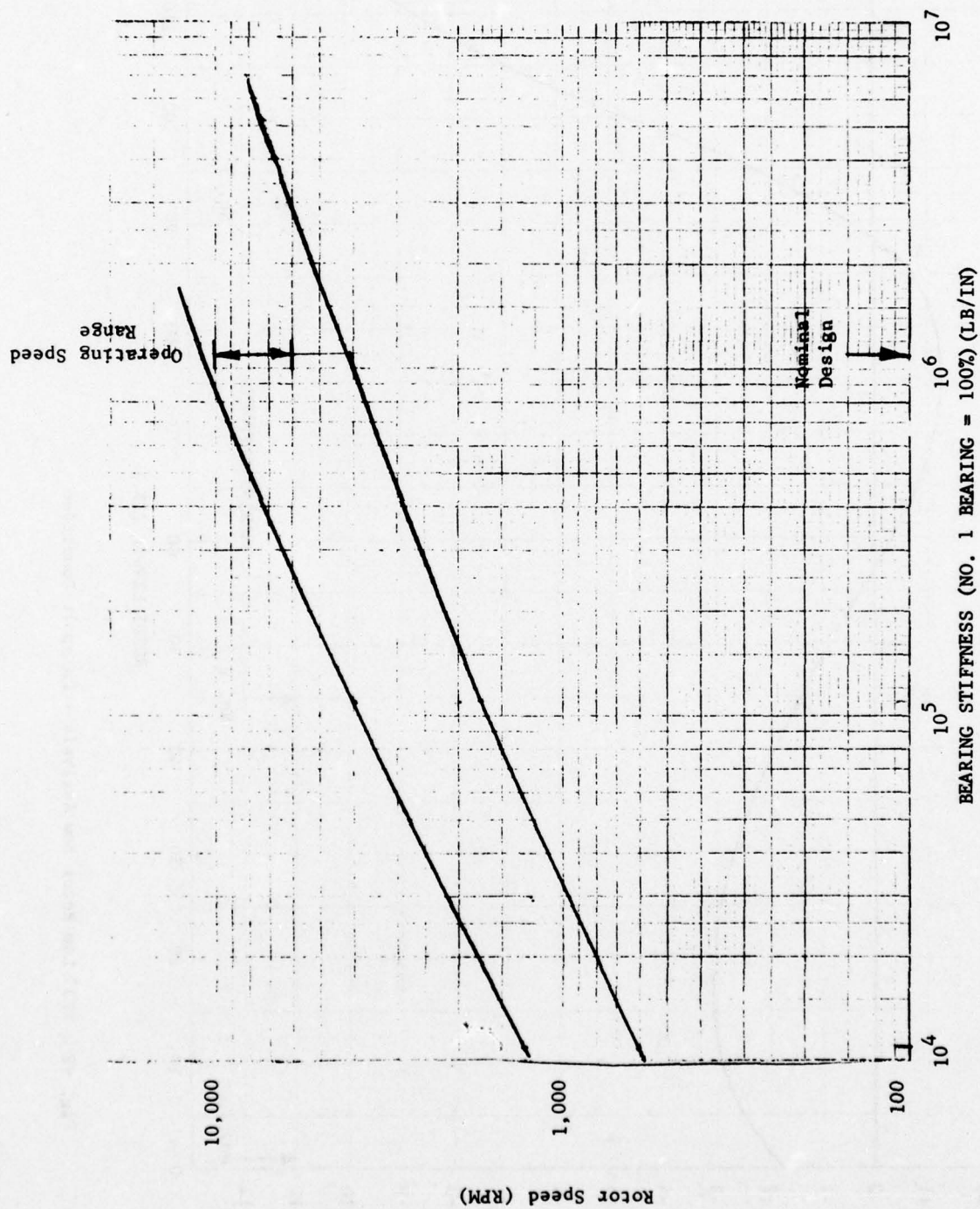


Fig. 93 Critical Speed Map for TF33 High Rotor Bearing System.

Brg. No. 2 = 91% of Brg. No. 1; Brg. No. 3 = 16% of Brg. No. 1

THIS PAGE IS BEST QUALITY PRACTICABLE  
FROM COPY FURNISHED TO BDC

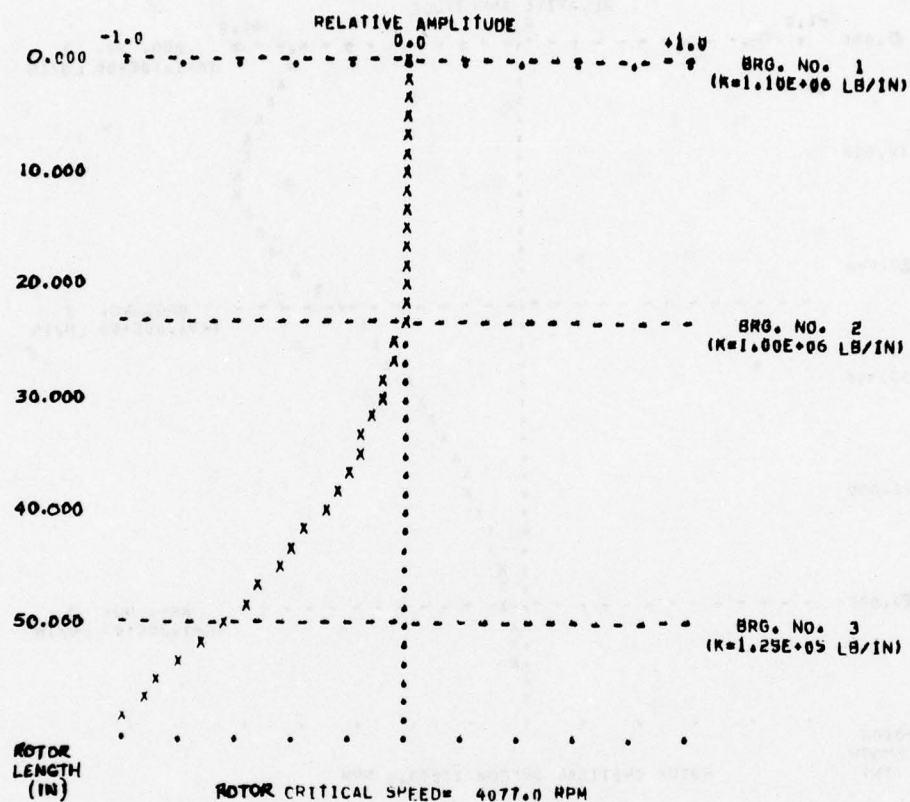


Fig. 94 Undamped Mode Shape at First Critical Speed for the  
TF33 High Rotor System (Cantilevered Turbine Mode).



THIS PAGE IS BEST QUALITY PRACTICABLE  
FROM COPY FURNISHED TO DDG

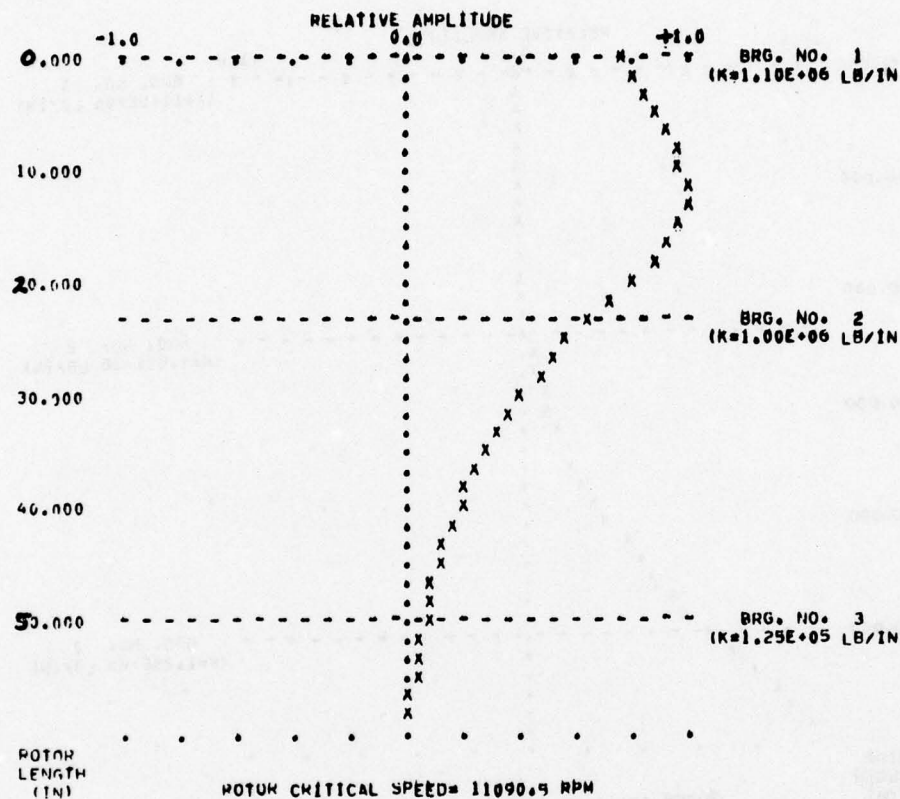


Fig. 95 Undamped Mode Shape at Second Critical Speed for the TF33 High Rotor System (Compressor Bounce Mode).

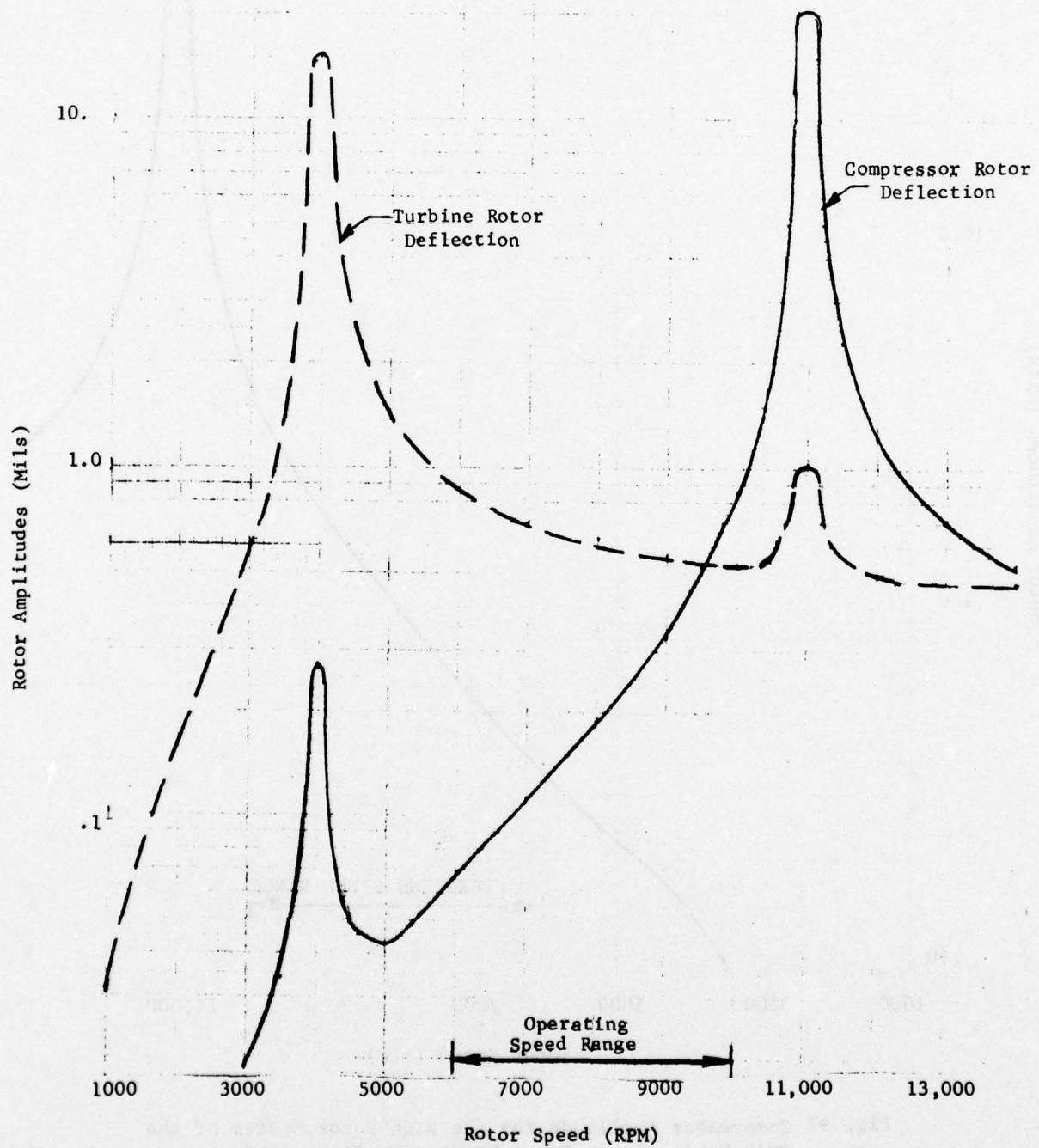
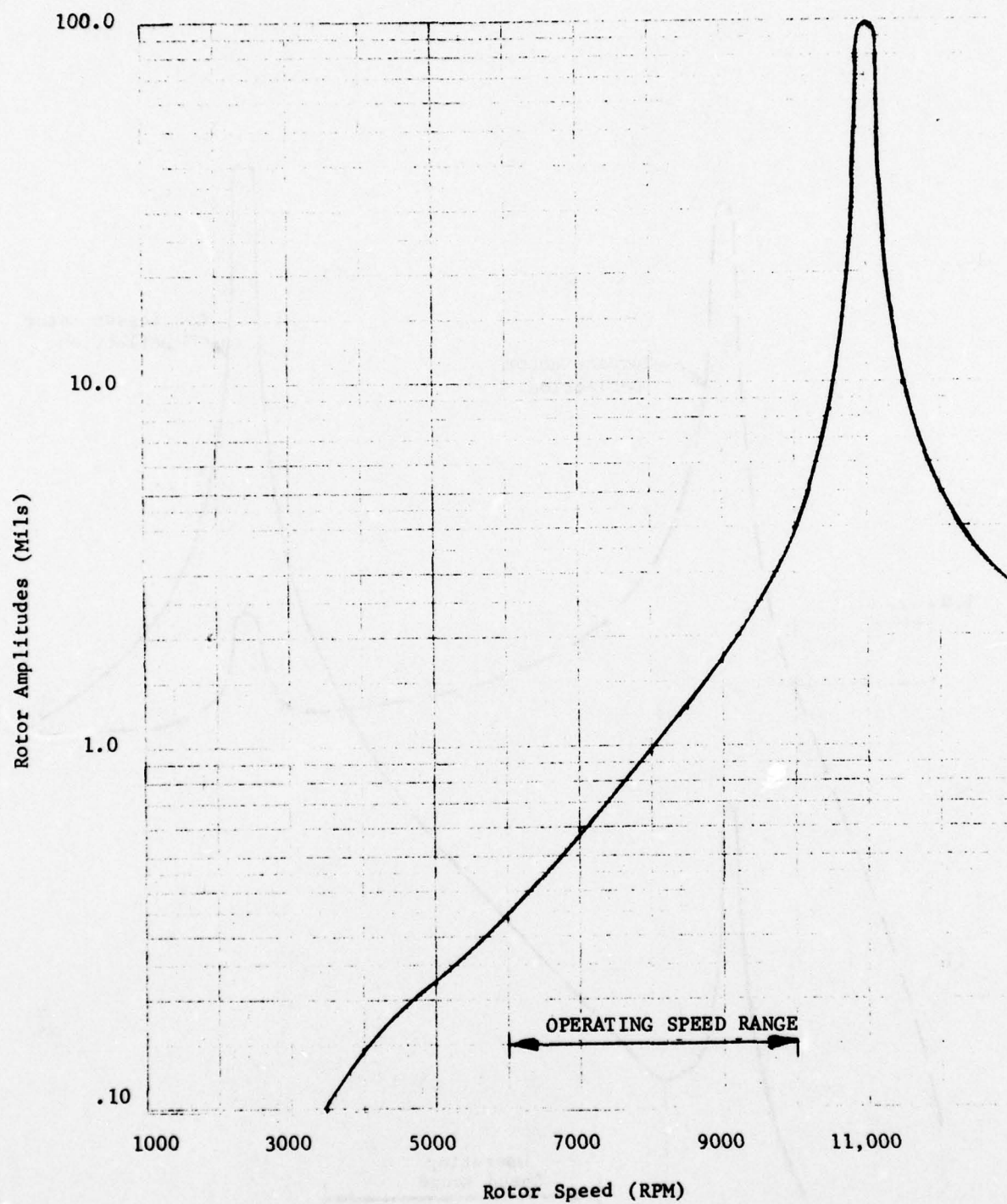


Fig. 96 Calculated Unbalance Response Vibration for the TF33 High Rotor with Distributed Unbalance.



**Fig. 97 Compressor Amplitude for the High Rotor System of the TF33 Engine for a First Compressor Stage Blade Loss.**



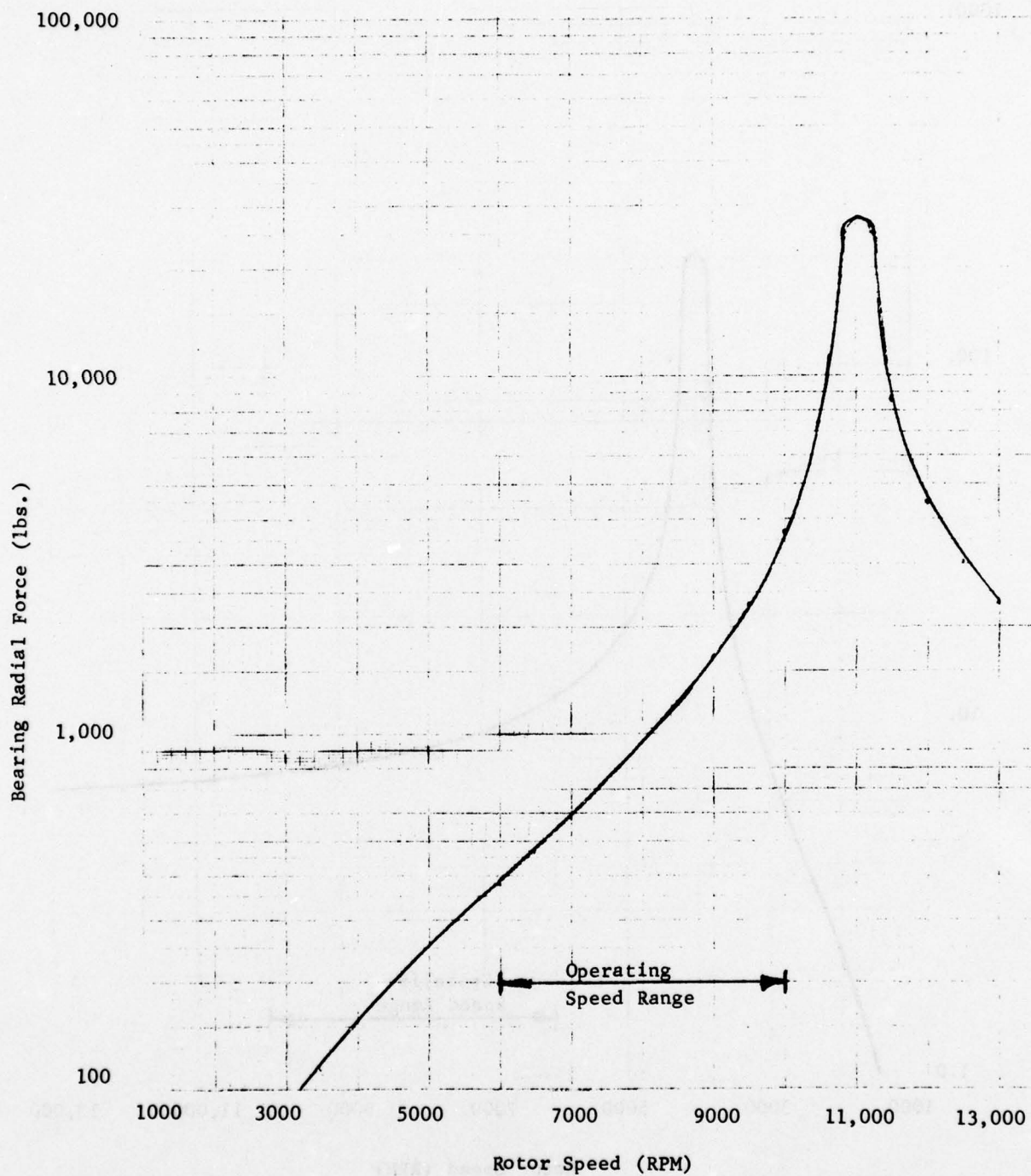
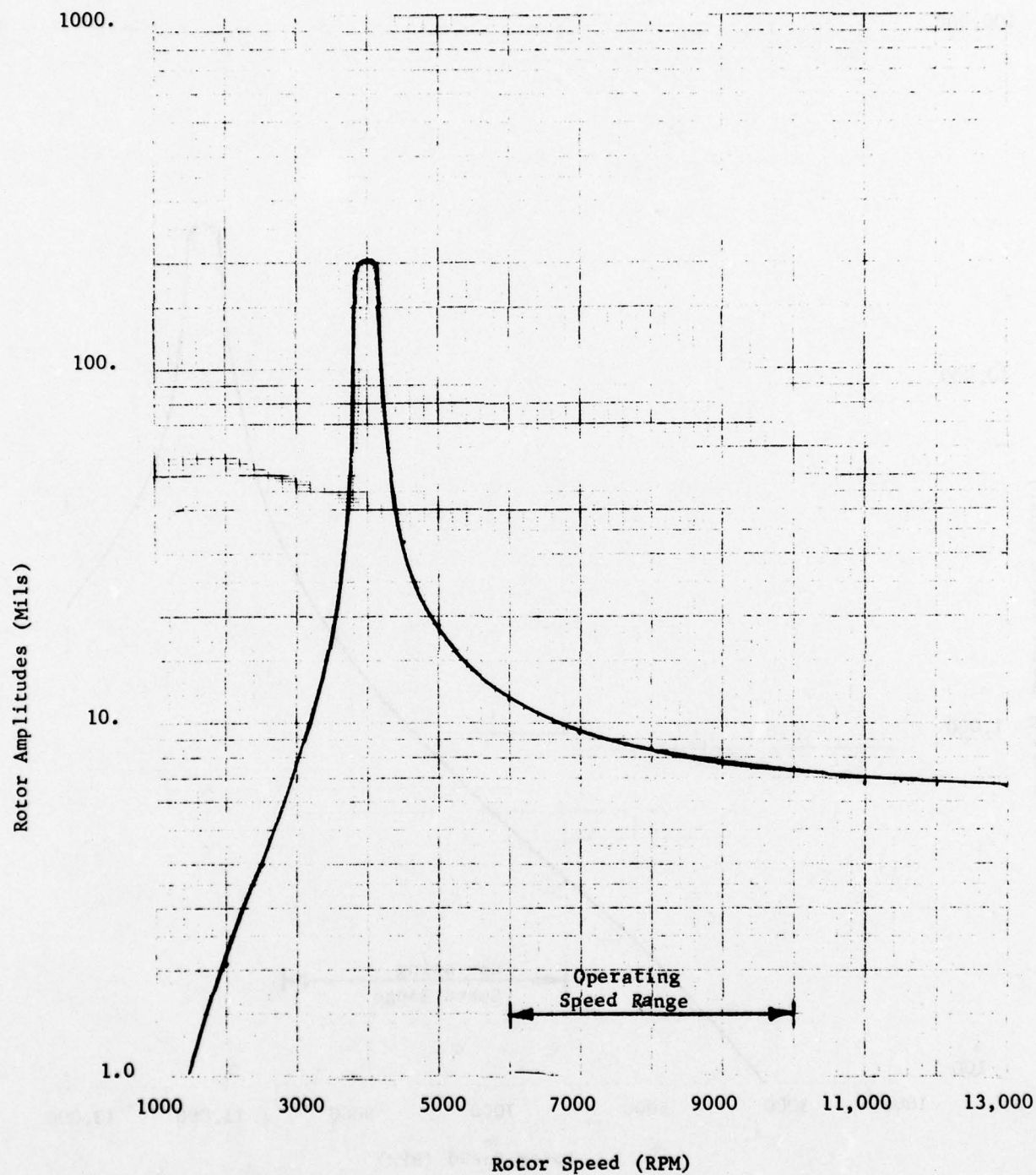


Fig. 98 No. 1 Bearing Radial Load for a First Stage Compressor Blade Loss of the TF33 High Rotor System.



**Fig. 99** Turbine Amplitude for the High Rotor System of the TF33 Engine for a High Turbine Blade Loss.

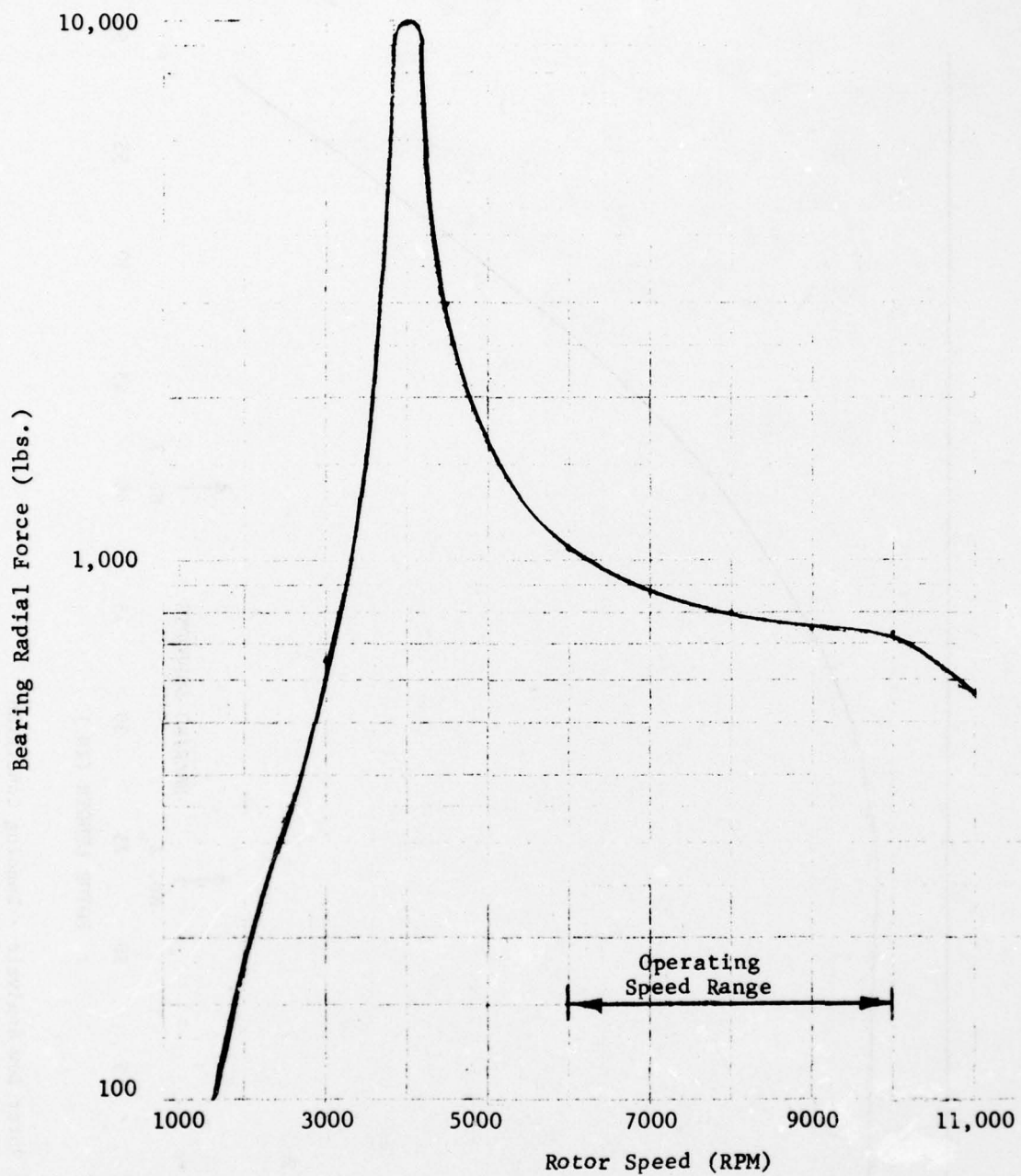


Fig. 100 No. 3 Bearing Radial Force for a Turbine Blade Loss of the TF33 High Rotor System.



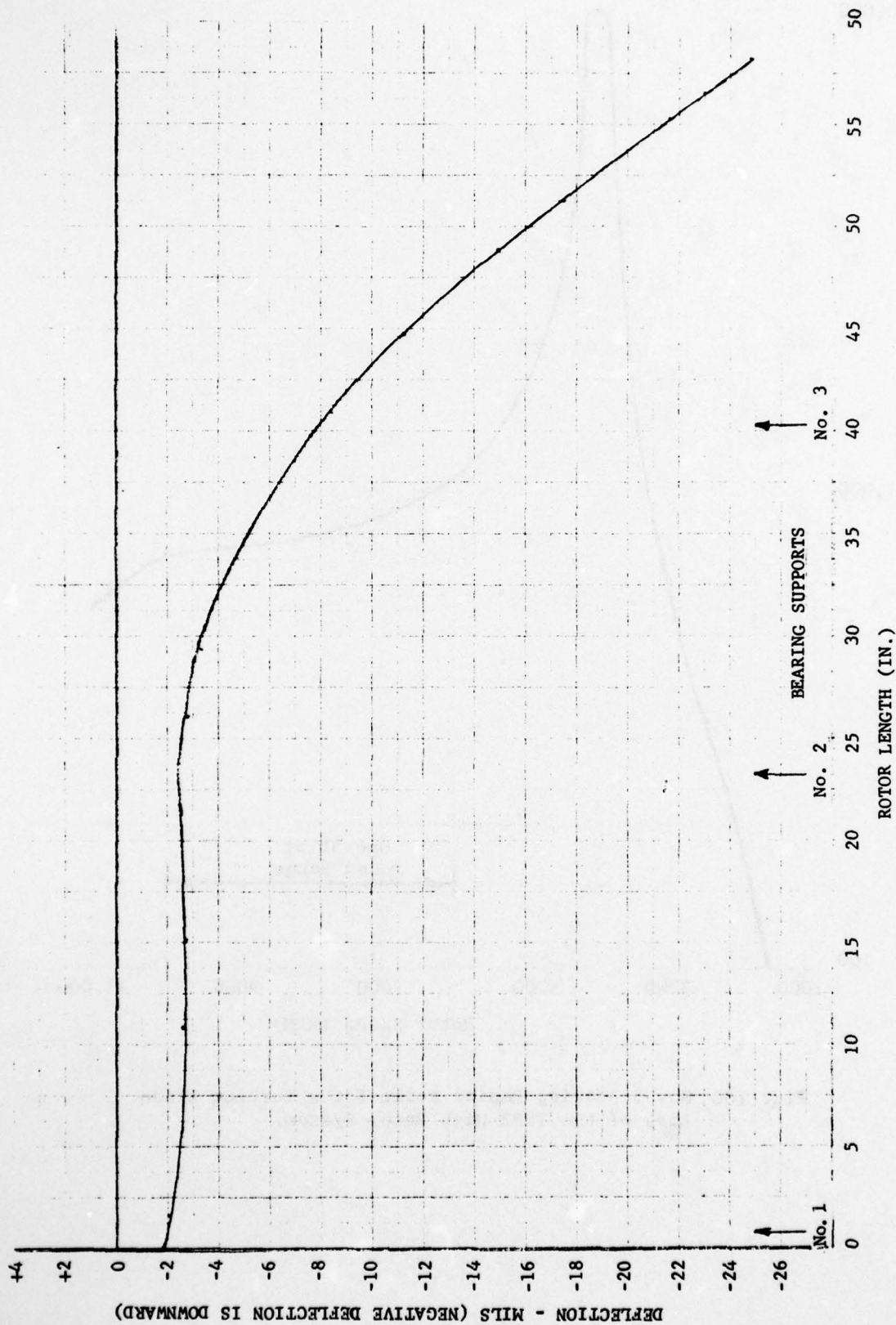


Fig. 101 TF33 High Rotor Bow Analysis - Landing Condition

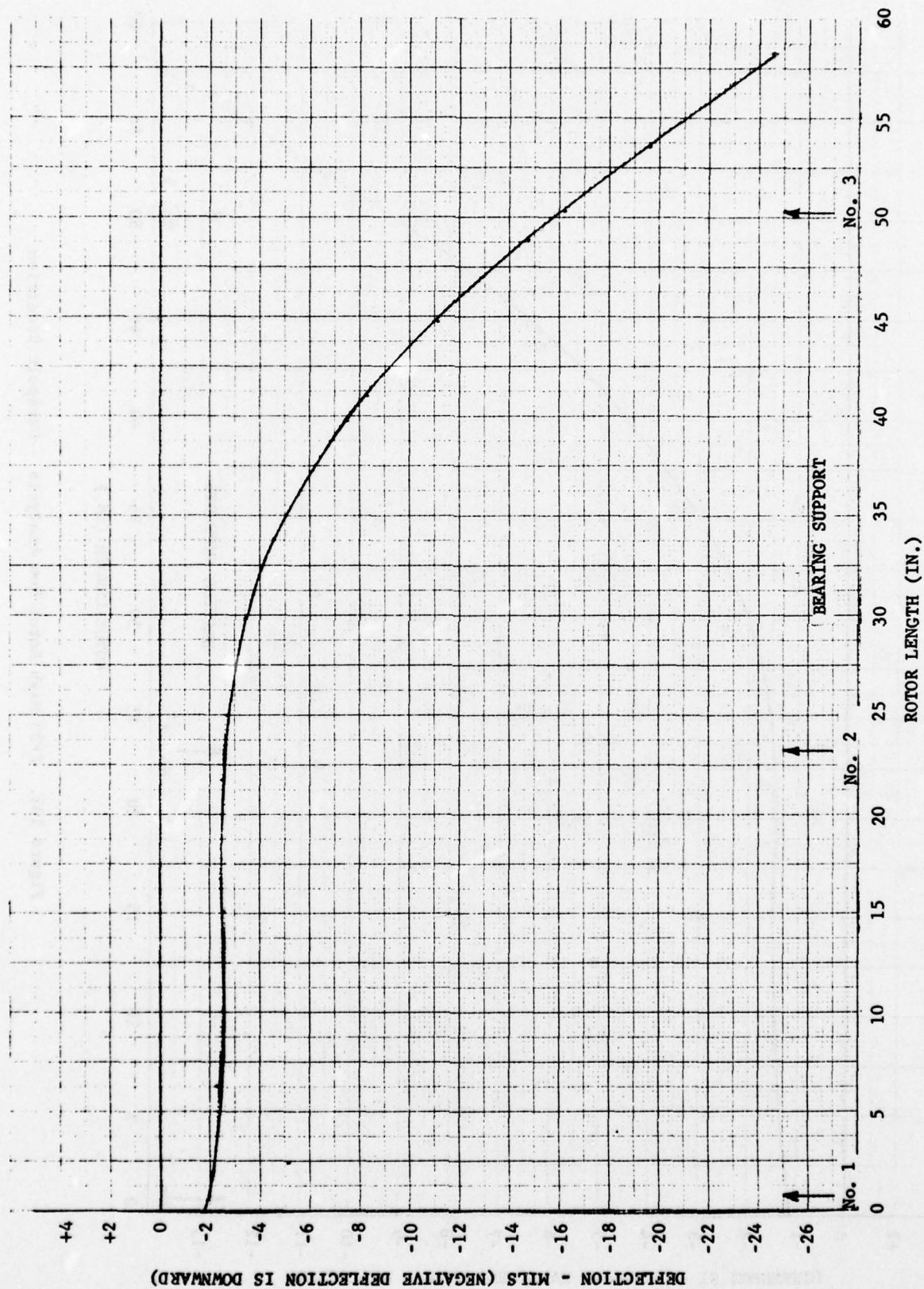


Fig. 102 TF32 High Rotor Bow Analysis - Flight Condition

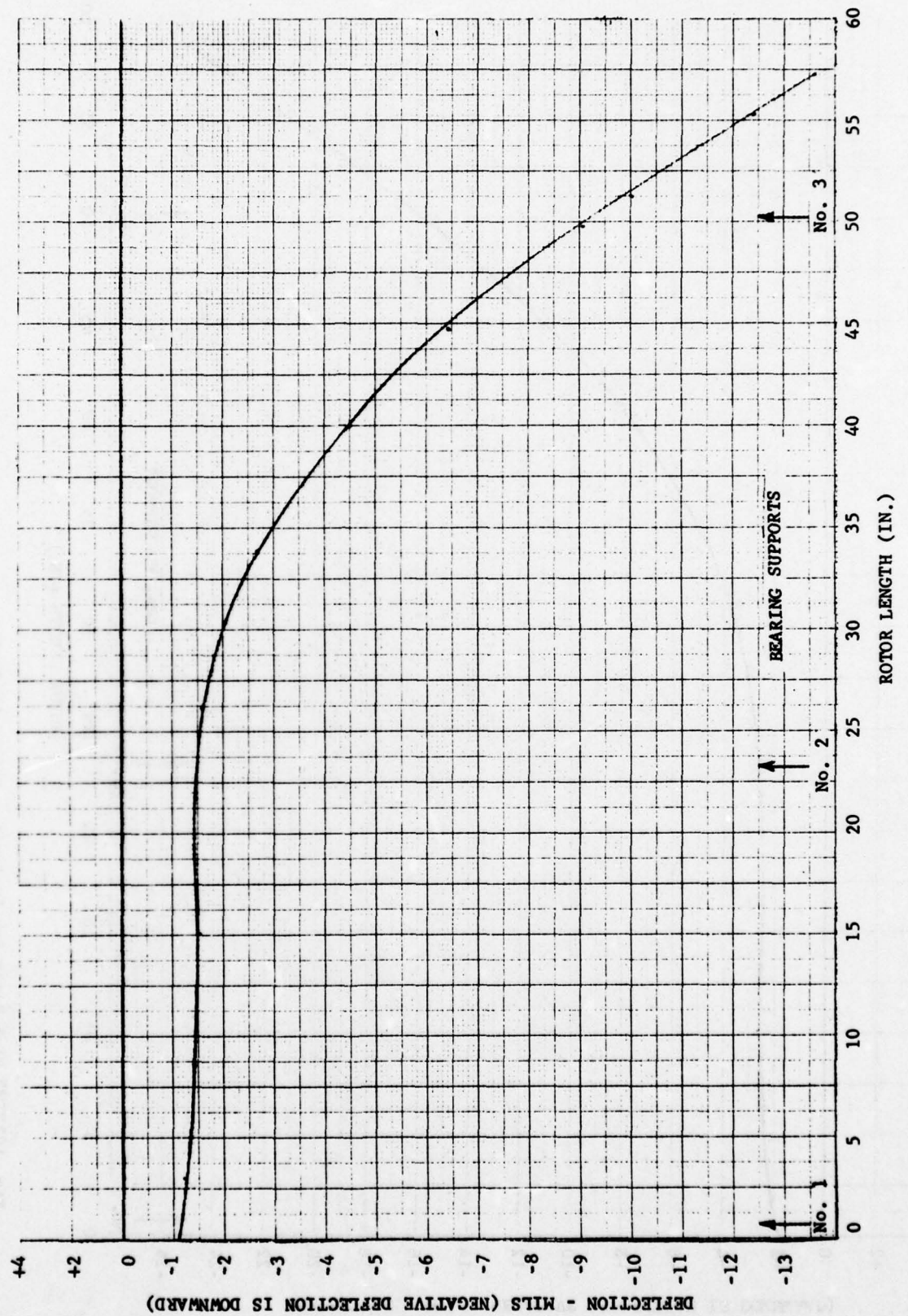


Figure 103. TF33 High Rotor Bow Analysis - Catapult Condition



Pedestal Data:

BRG. NO.	MASS (LB)	STIFFNESS (LB/IN)
1	400.	$6.0 \times 10^6$
2	500.	$5.0 \times 10^6$
3	300.	$4.3 \times 10^6$
4	200.	$5.0 \times 10^6$

BRG. NO. 2 = 176.5% of BRG. NO. 1  
 BRG. NO. 3 = 176.5% of BRG. NO. 1  
 BRG. NO. 4 = 36.8% of BRG. NO. 1

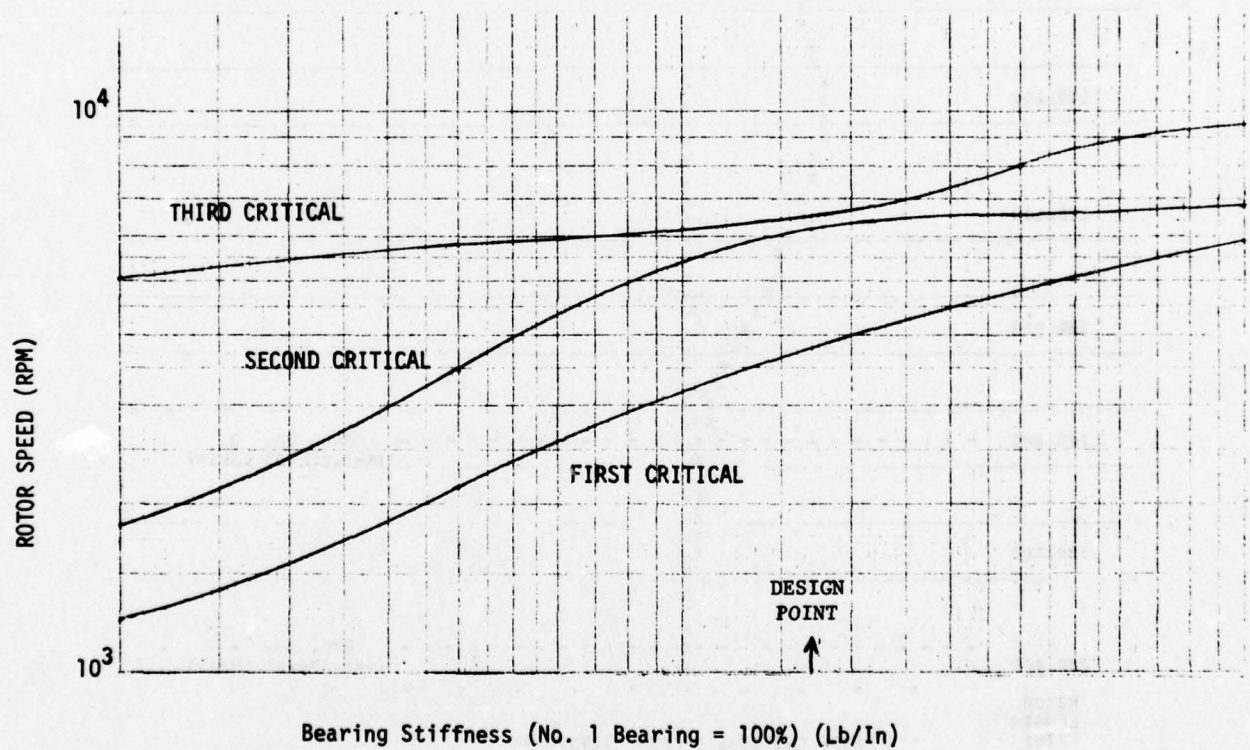


Figure 104 Critical Speed Map for Fan-Shaft Rotor System - TF39

THIS PAGE IS BEST QUALITY PRACTICABLE  
FROM COPY FURNISHED TO DDG

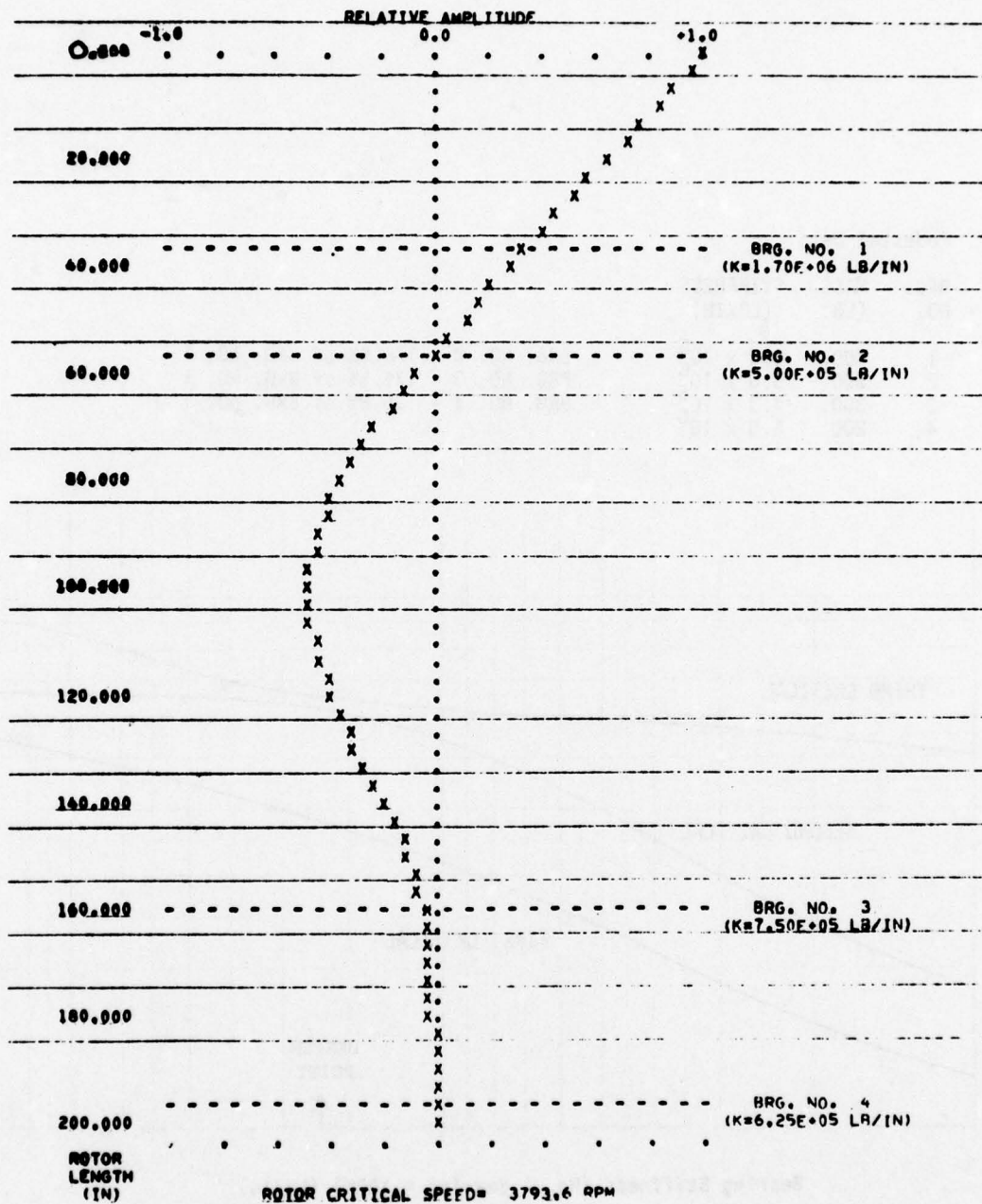


Figure 105 Undamped Mode Shape at First Critical Speed of  
TF39 Fan Spool

THIS PAGE IS BEST QUALITY PRACTICABLE  
FROM COPY FURNISHED TO DDG

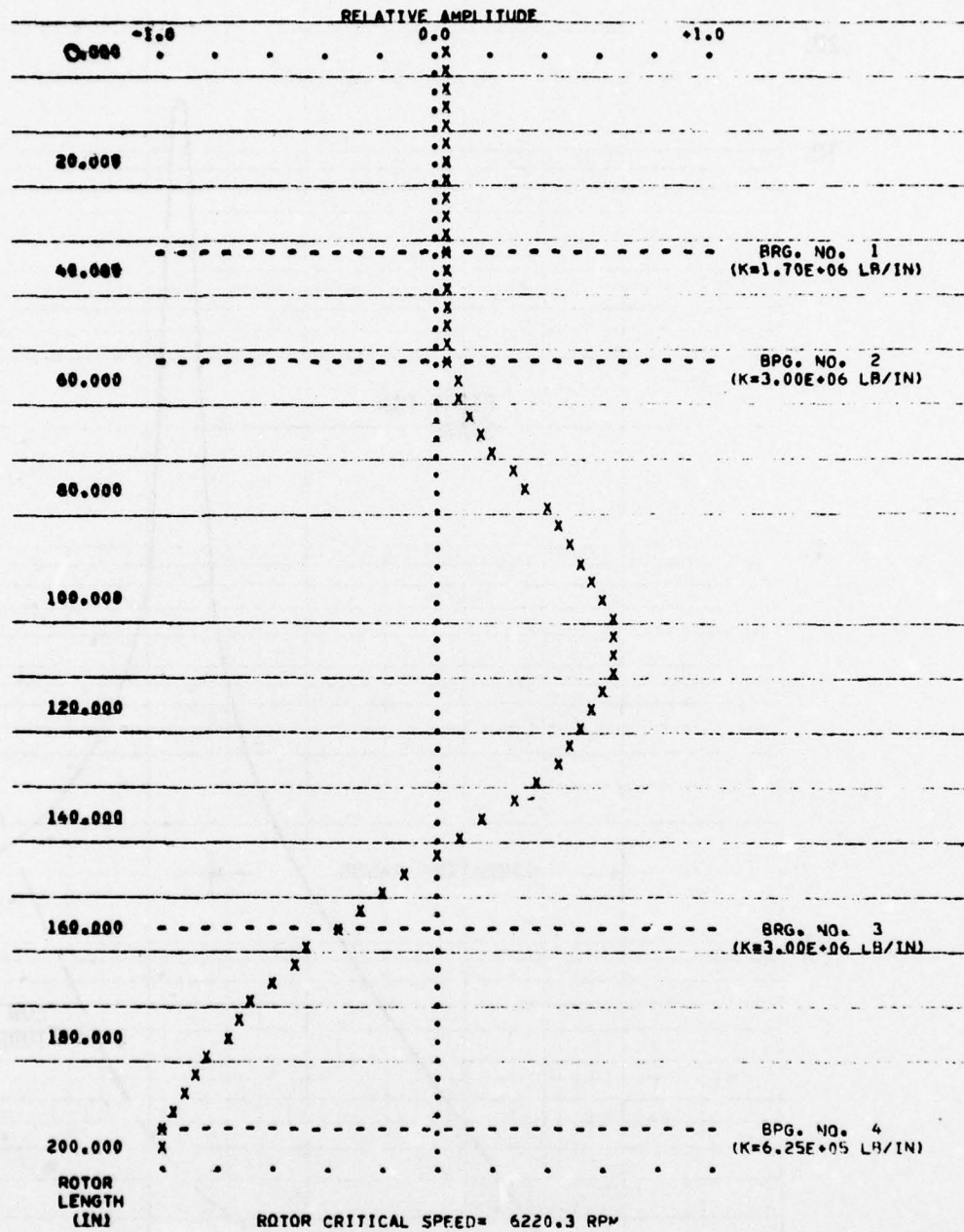


Figure 106 Undamped Mode Shape at Second Critical Speed  
of TF39 Fan Spool



Shaft Peak Amplitude (mils)

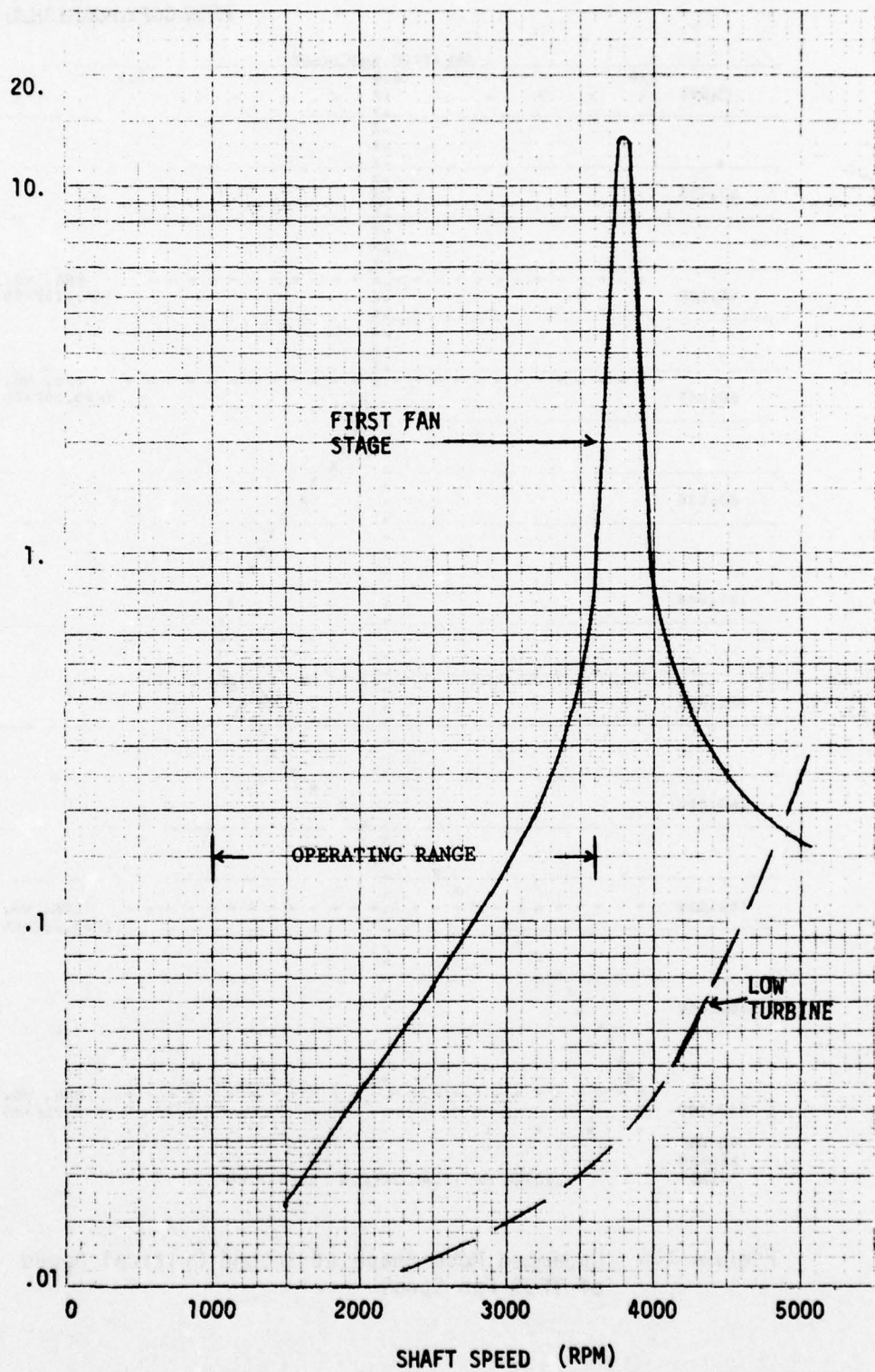


Figure 107 Calculated Peak Unbalance Response  
Vibration For TF 39 Fan Spool

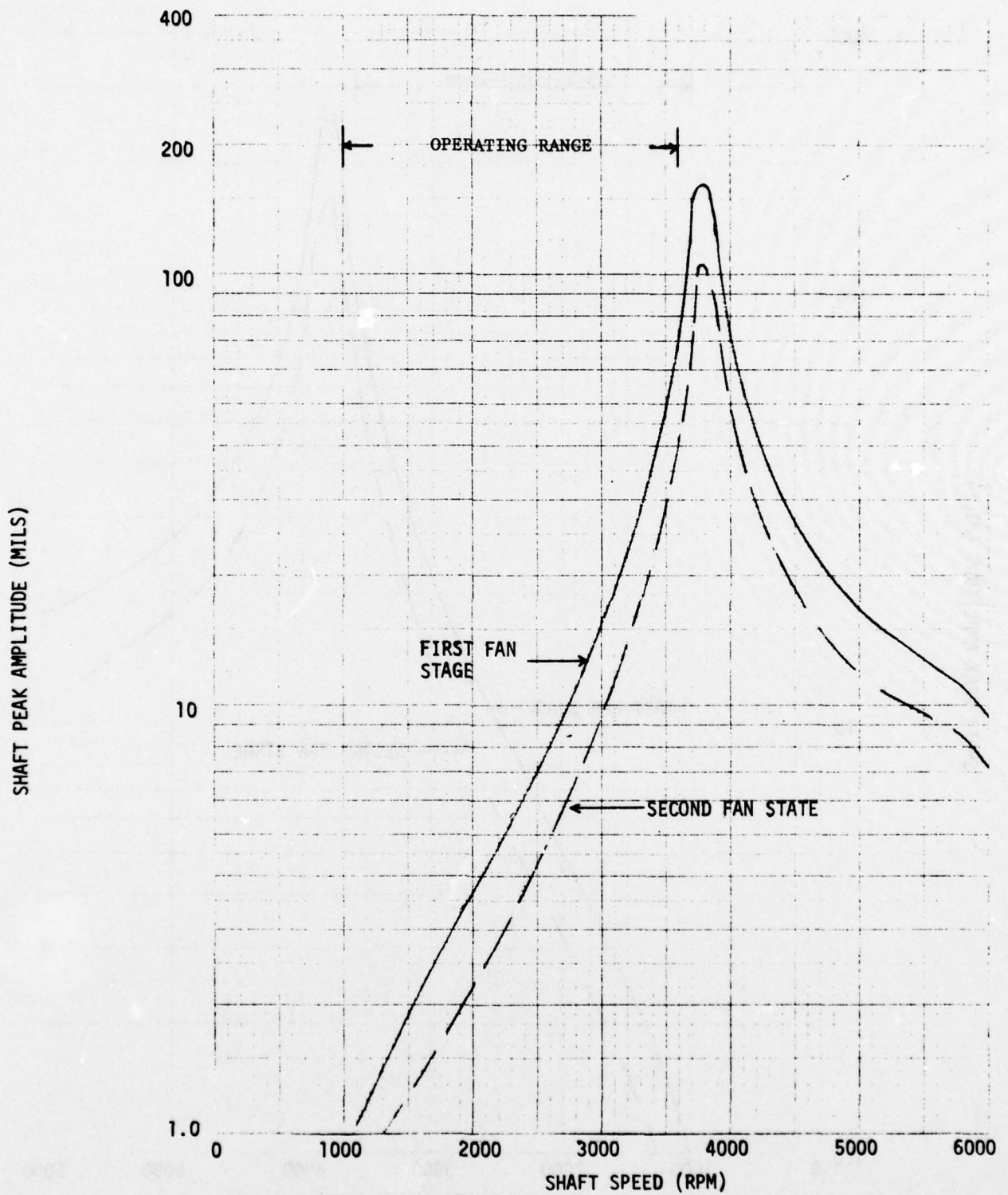


Figure 108 Shaft Amplitudes for Low-Rotor System For First Fan Stage Blade Loss

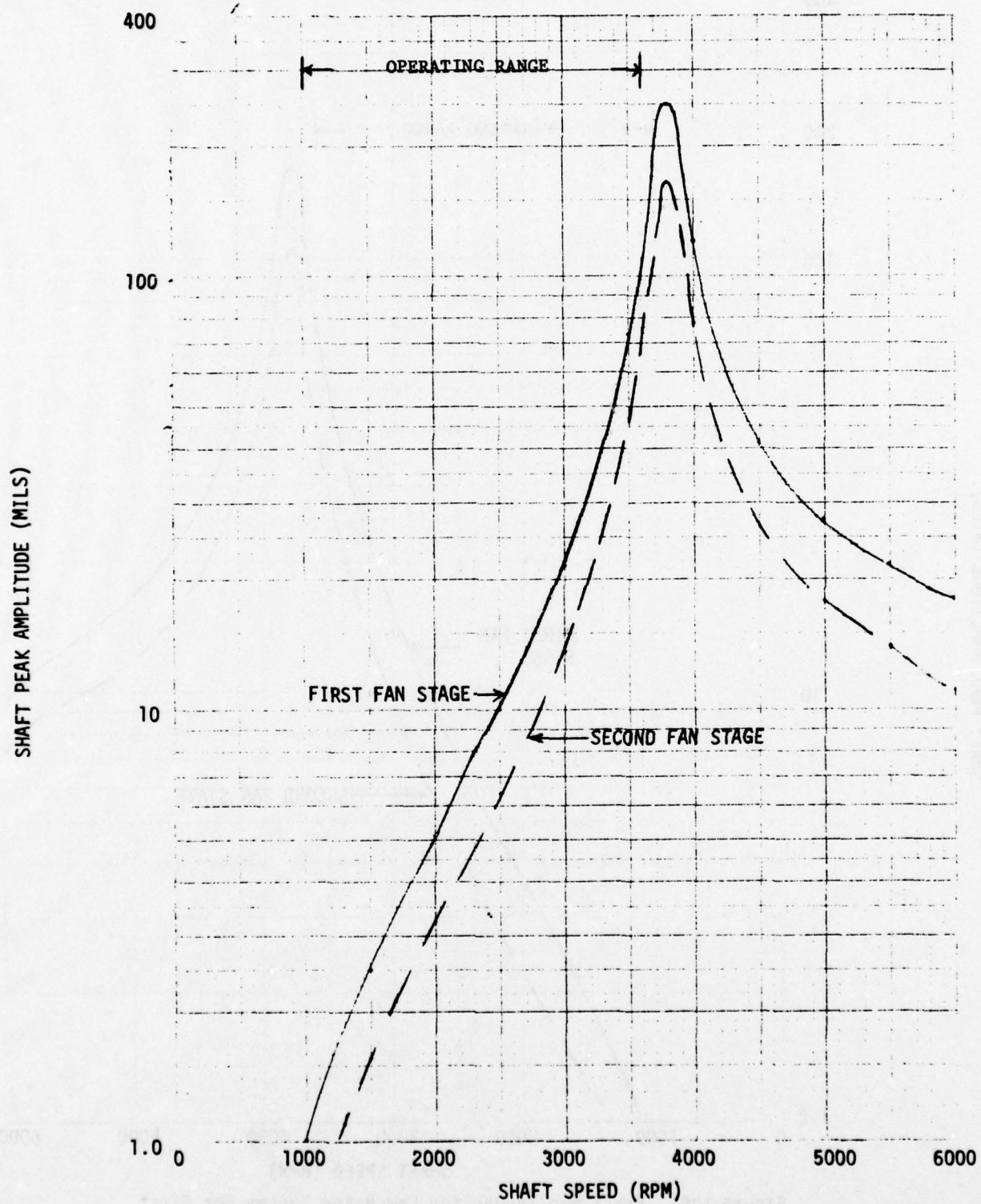


Figure 109 Shaft Amplitude For Low-Rotor System for Second Fan Blade Loss



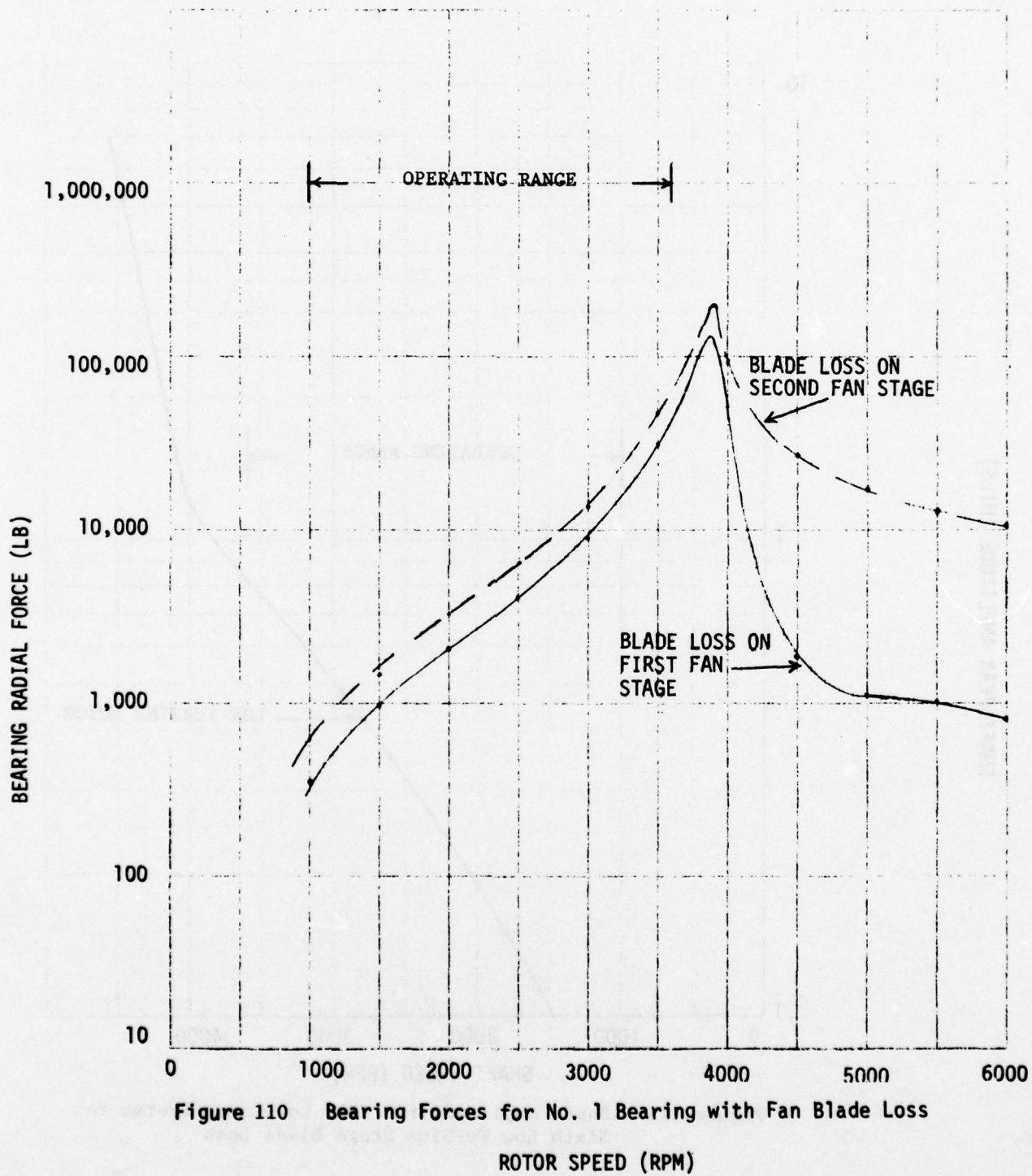


Figure 110 Bearing Forces for No. 1 Bearing with Fan Blade Loss

SHAFT PEAK AMPLITUDE (MILS)

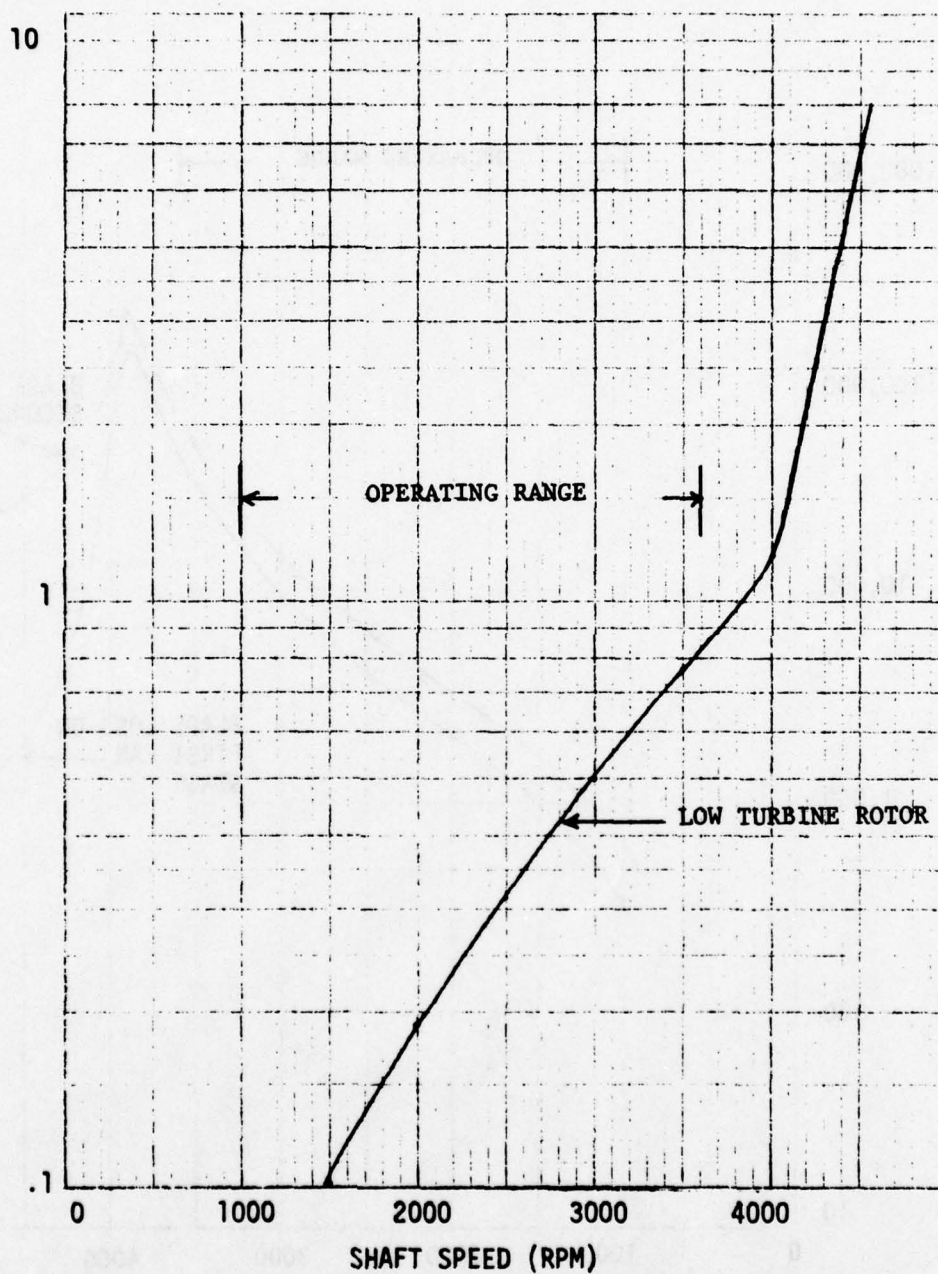


Figure 111 Shaft Amplitude for TF39 Low-Rotor System for Sixth Low Turbine Stage Blade Loss

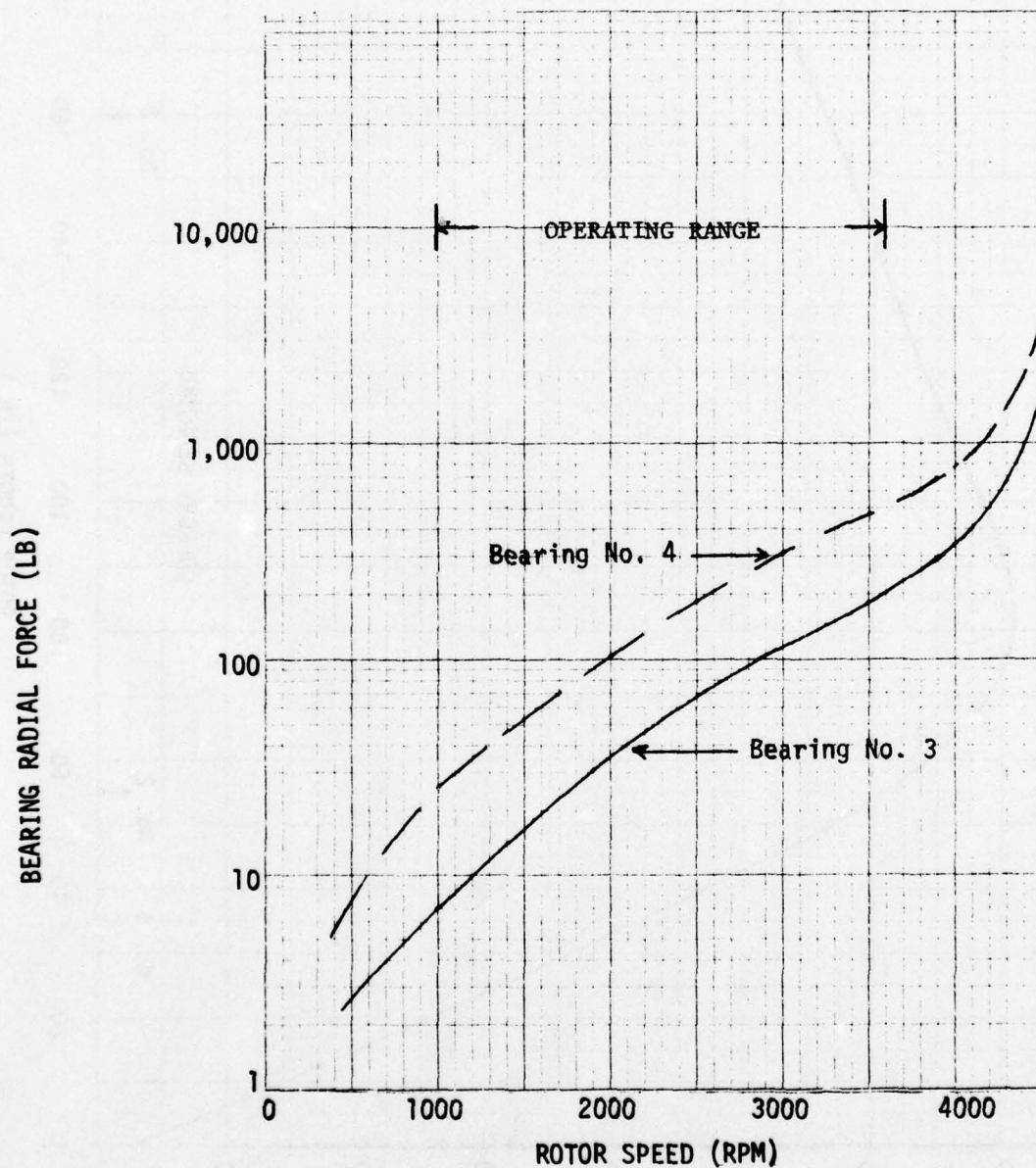


Figure 112 Bearing Forces for TF39 No. 3 and No. 4 Bearings for Low Turbine Blade Loss



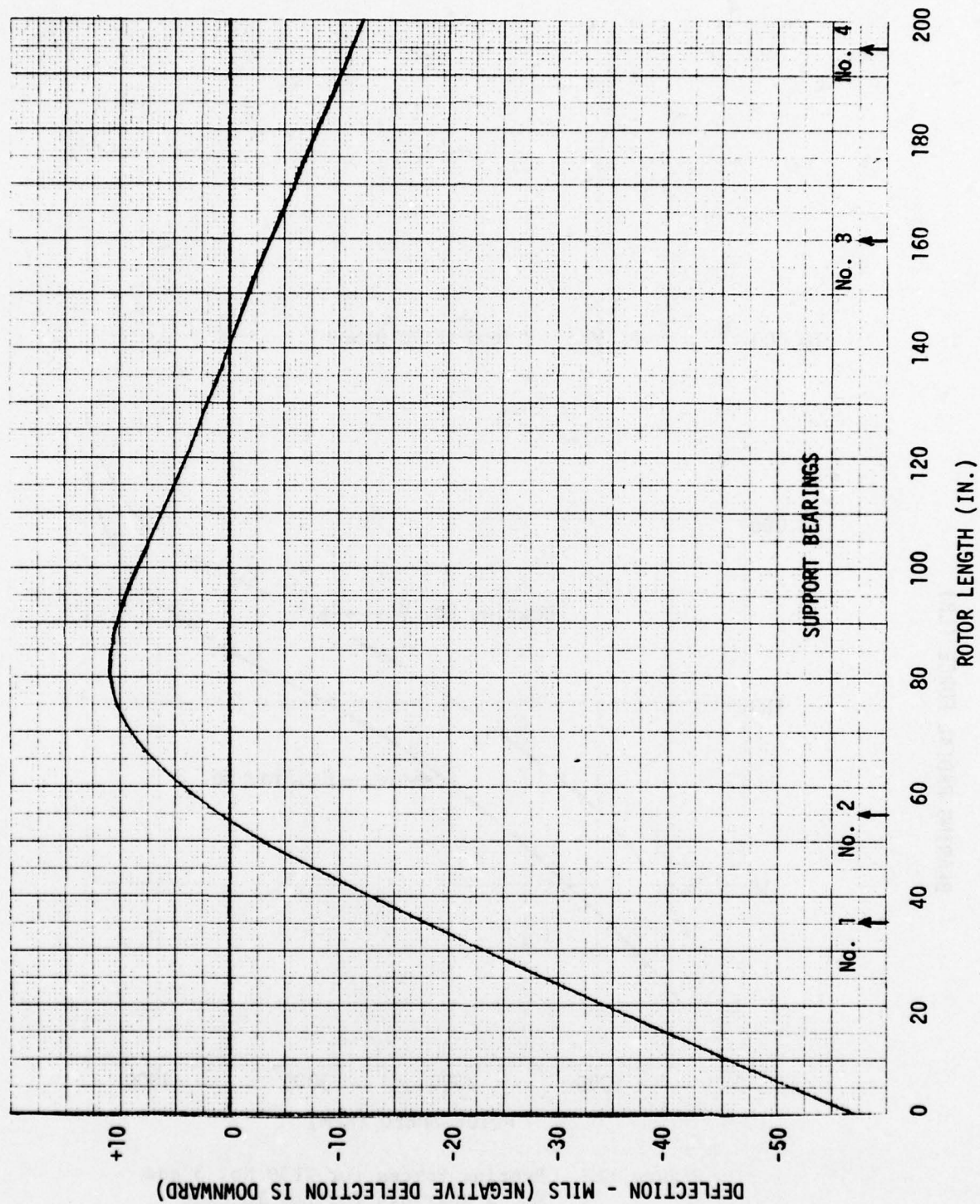


Figure 113 TF39 Low Rotor Bow Analysis - Landing Condition

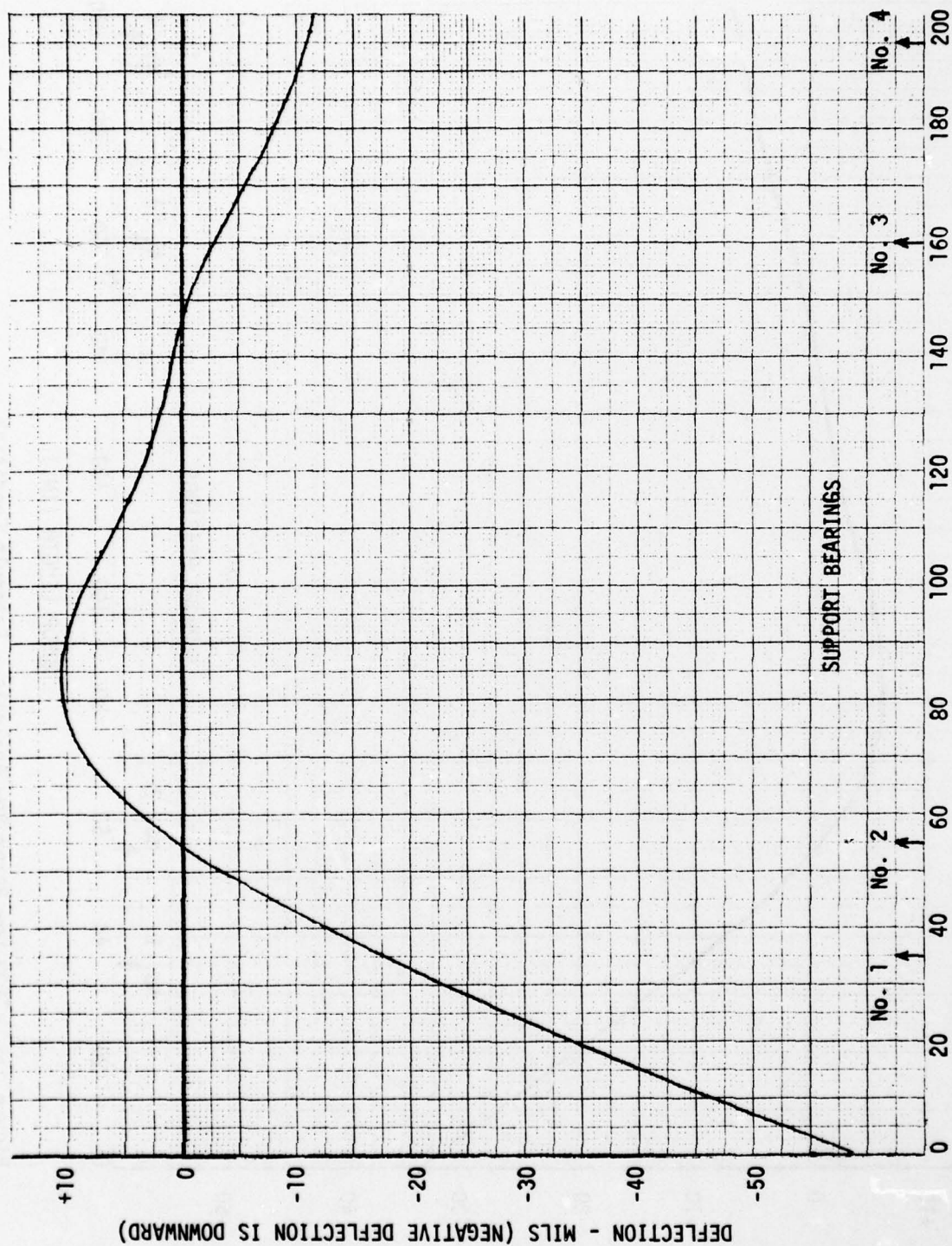


Figure 114 TF39 Low Rotor Bow Analysis - Flight Condition

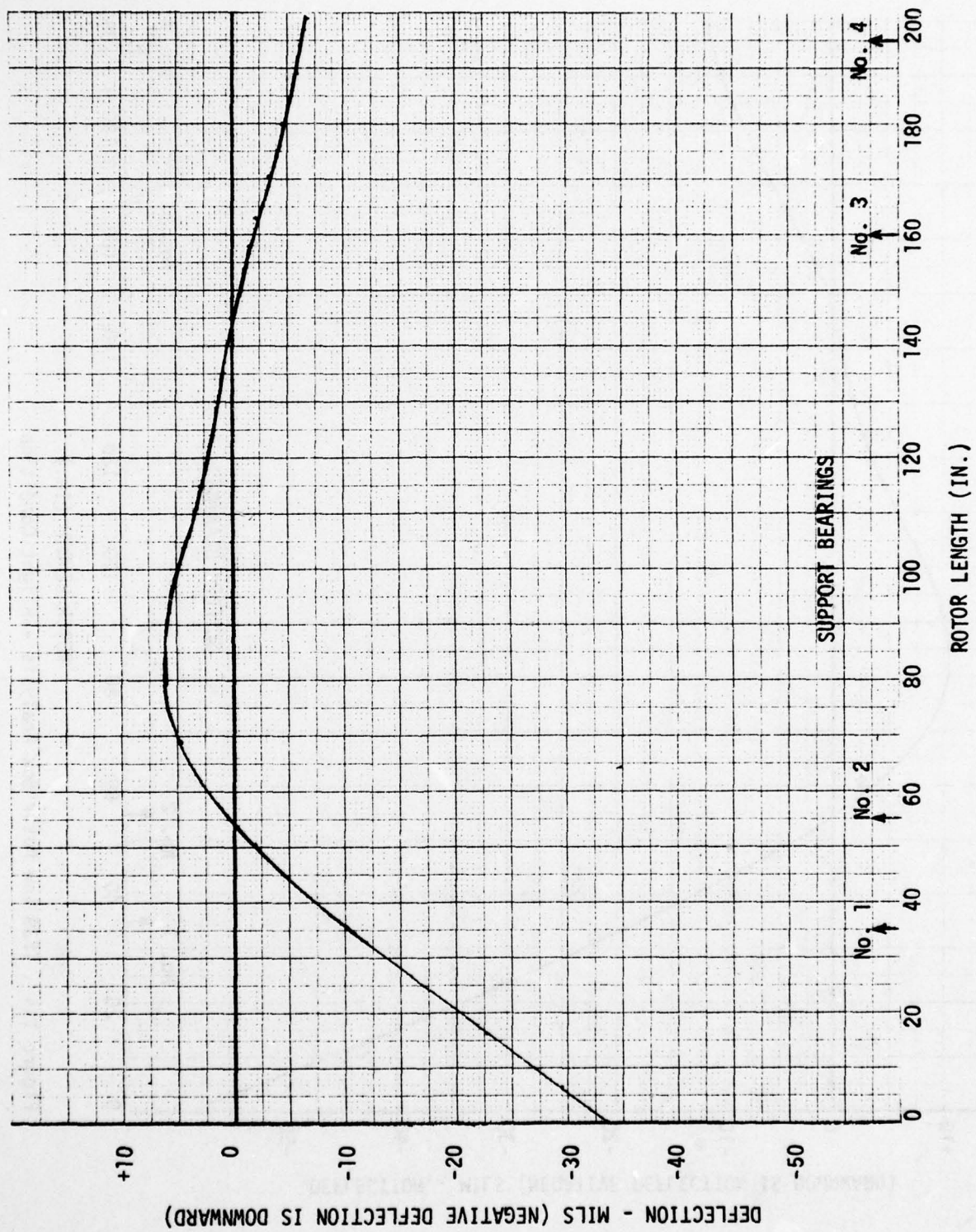


Figure 115 TF39 Low Rotor Bow Analysis - Catapult Condition



Pedestal Data:

BRG NO.	MASS (LB)	STIFFNESS (LB/IN)
1	200	$3.0 \times 10^6$
2	300	$2.5 \times 10^5$
3	300	$2.5 \times 10^5$
4	300	$1.0 \times 10^6$

Brg. No. 2 = 120% of Brg. No. 1  
 Brg. No. 3 = 60% of Brg. No. 1  
 Brg. No. 4 = 100% of Brg. No. 1

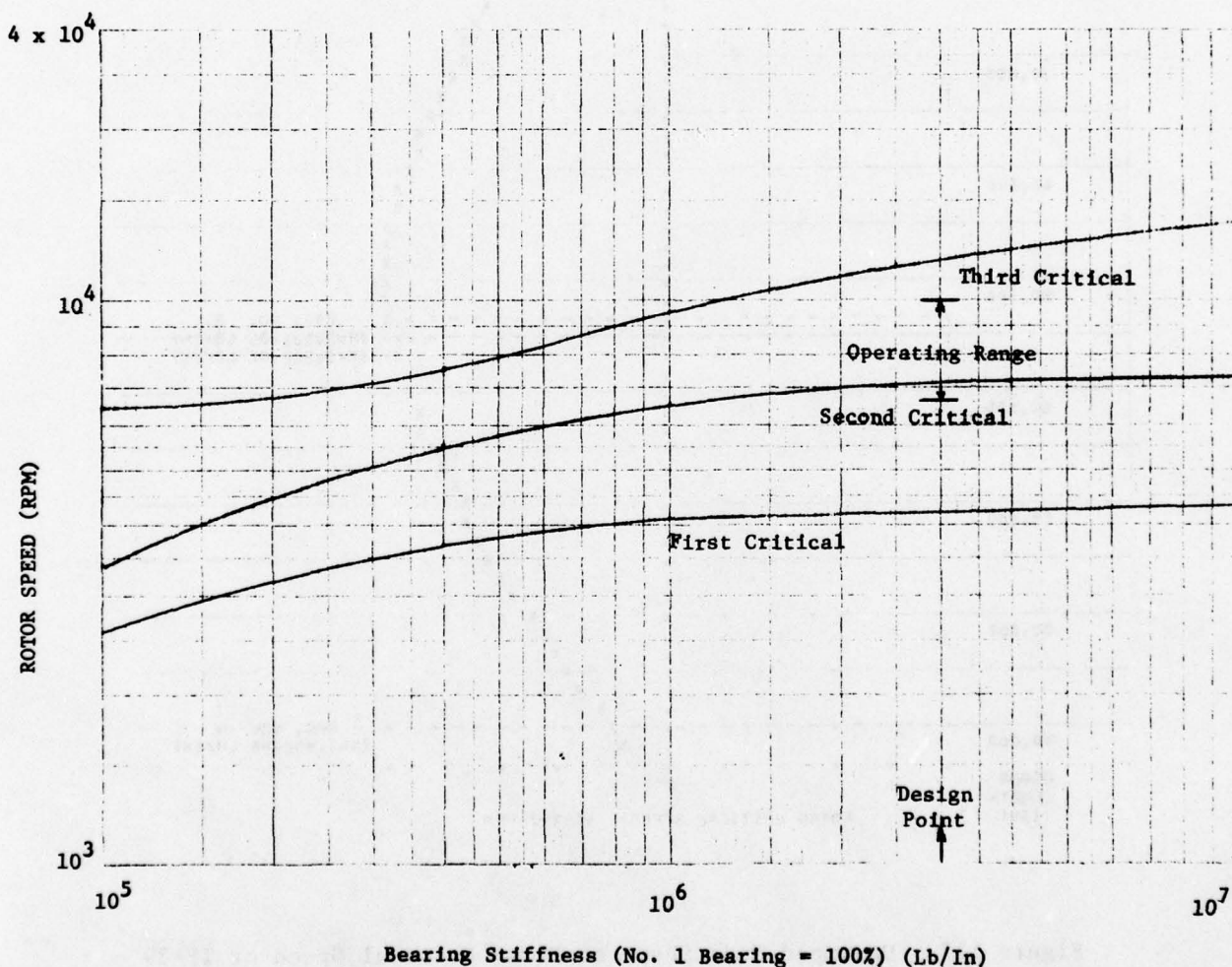


Figure 116 Critical Speed Map For TF-39 Gas Generator Rotor

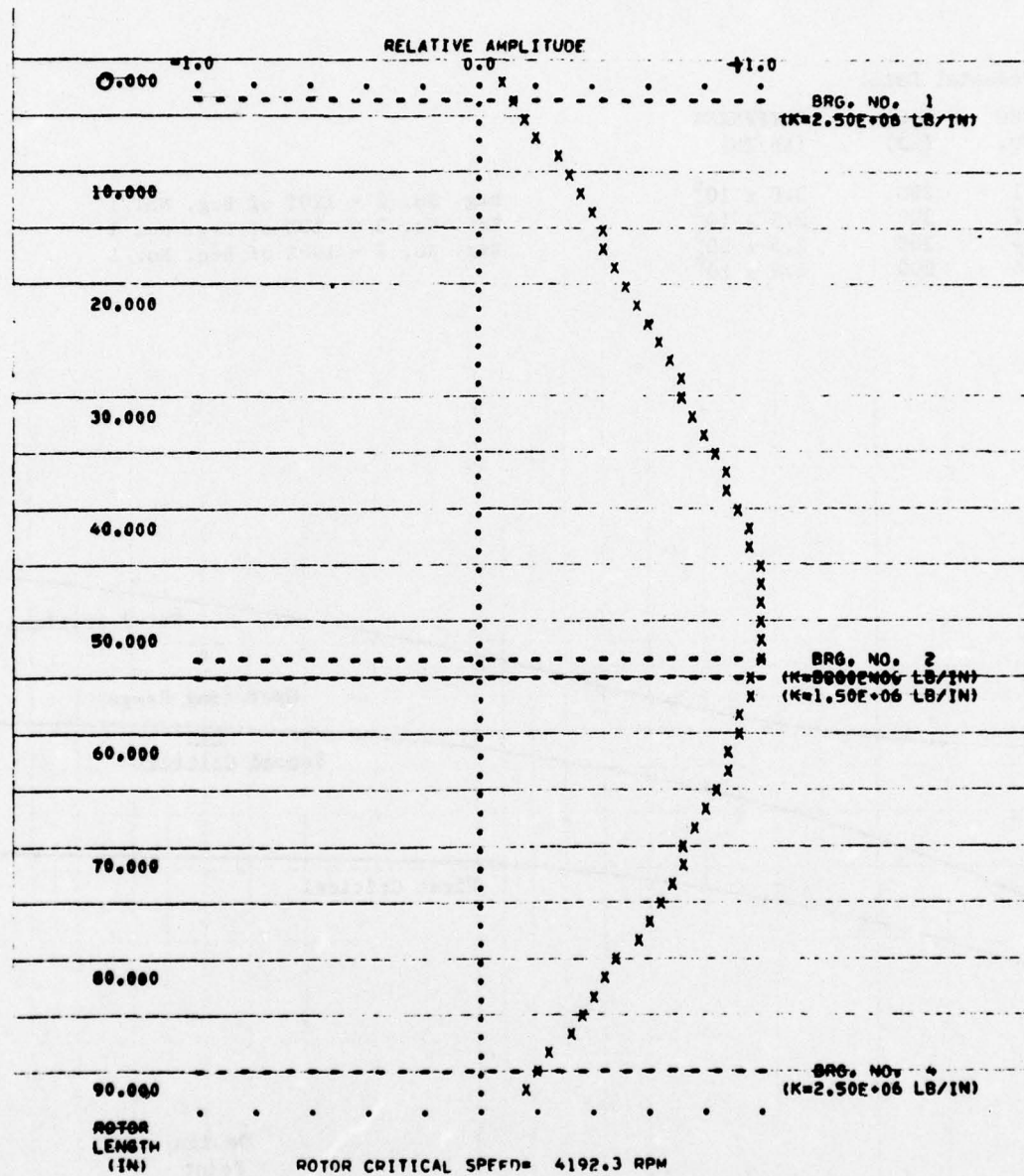


Figure 117 Undamped Mode Shape at First Critical Speed of TF-39 Gas Generator Spool

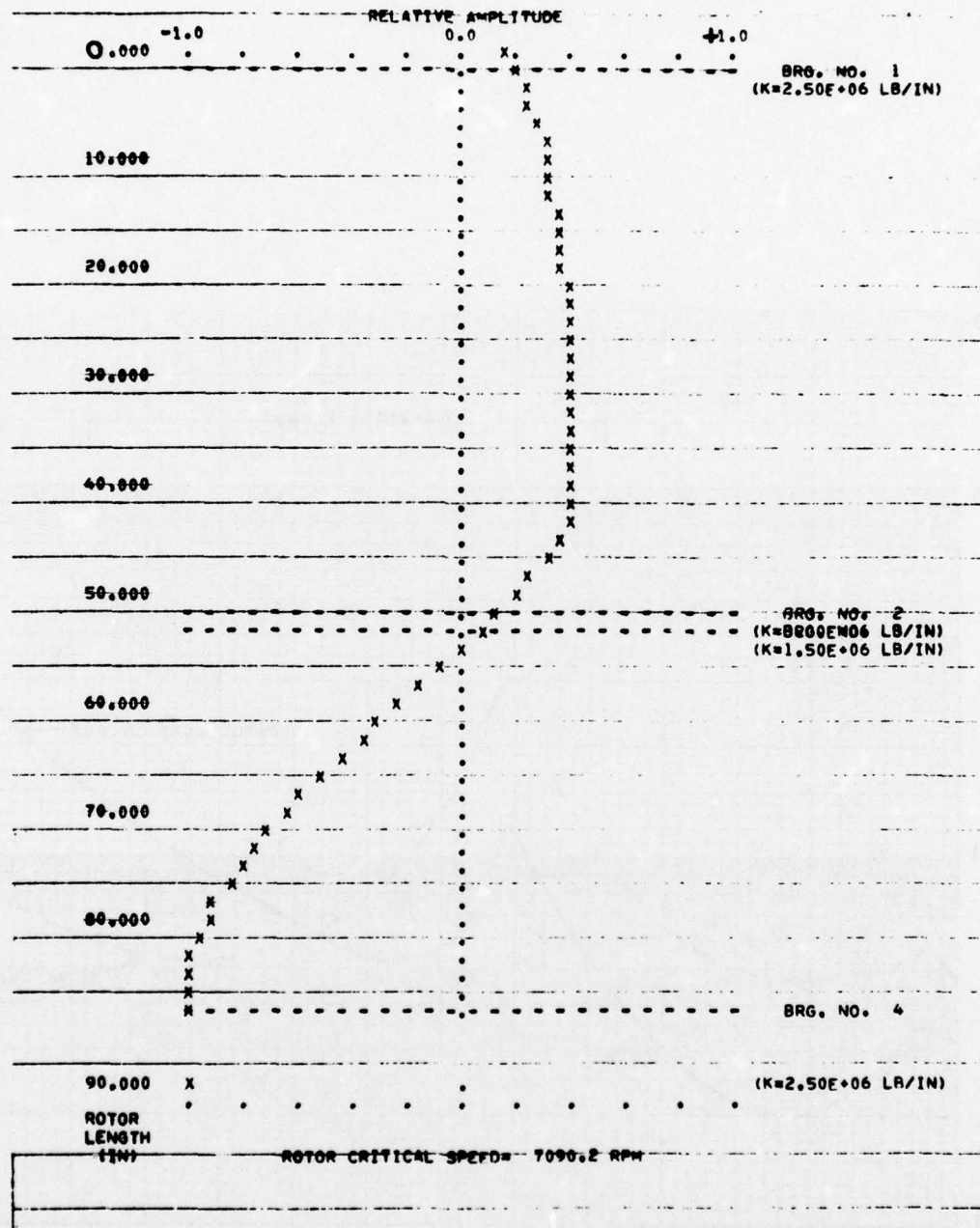


Figure 118 Undamped Mode Shape at Second Critical Speed of TF-39 Gas Generator Spool



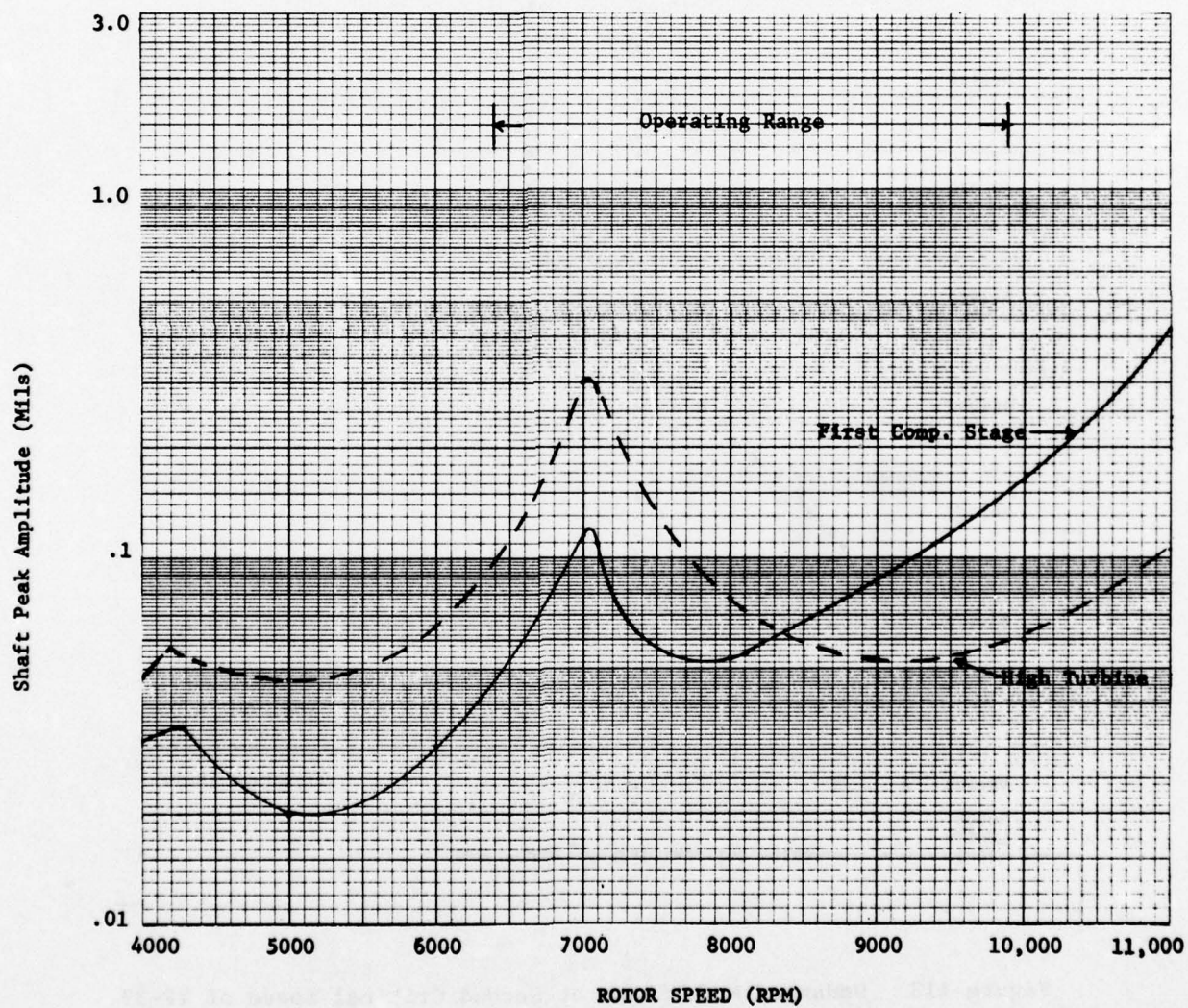


Figure 119 Calculated Peak Damped Unbalance Response Vibration for TF-39 Gas Generator Spool

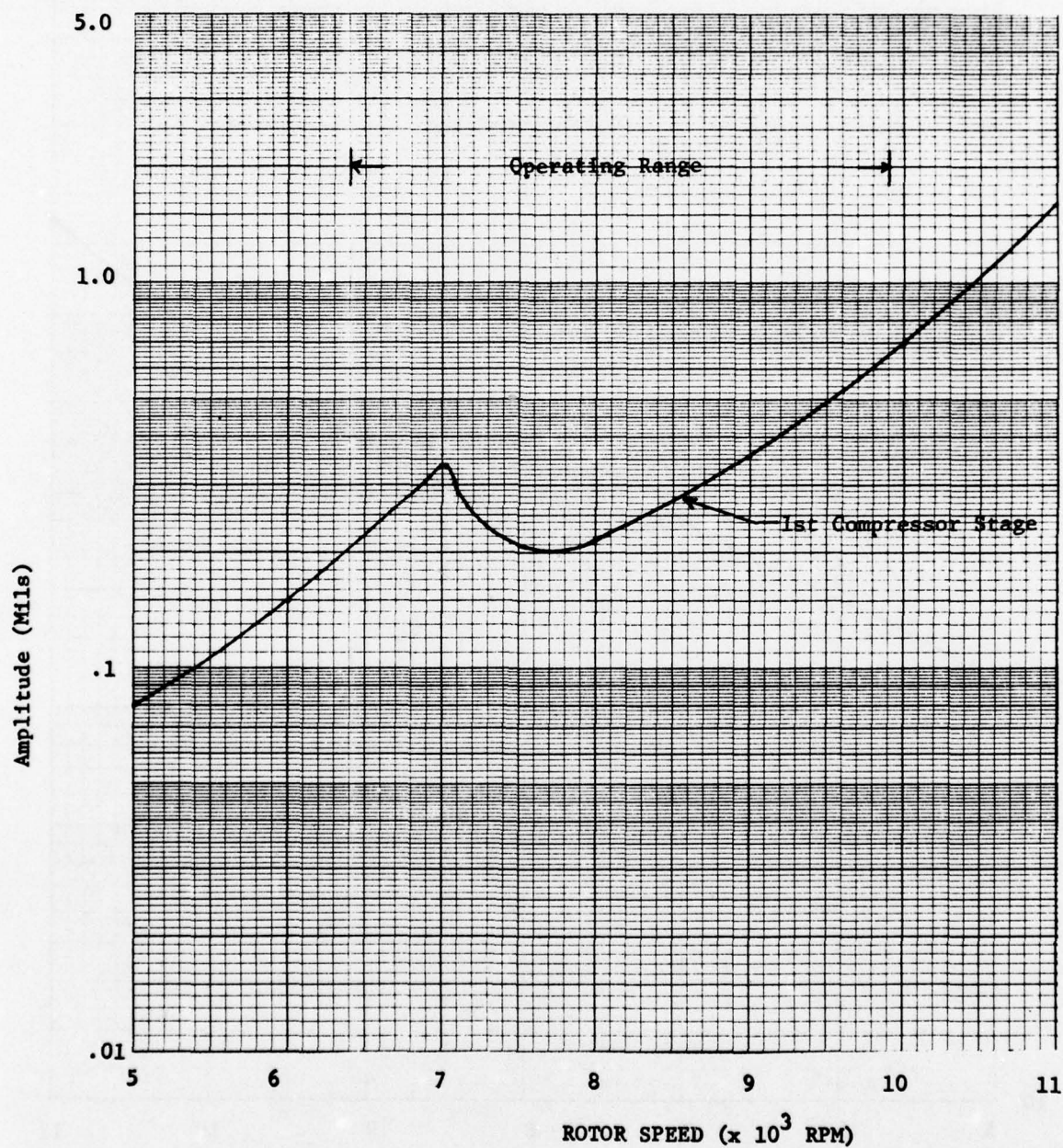


Figure 120 Rotor Amplitudes for a First Compressor Stage Blade Loss for the TF-39 Gas Generator Spool



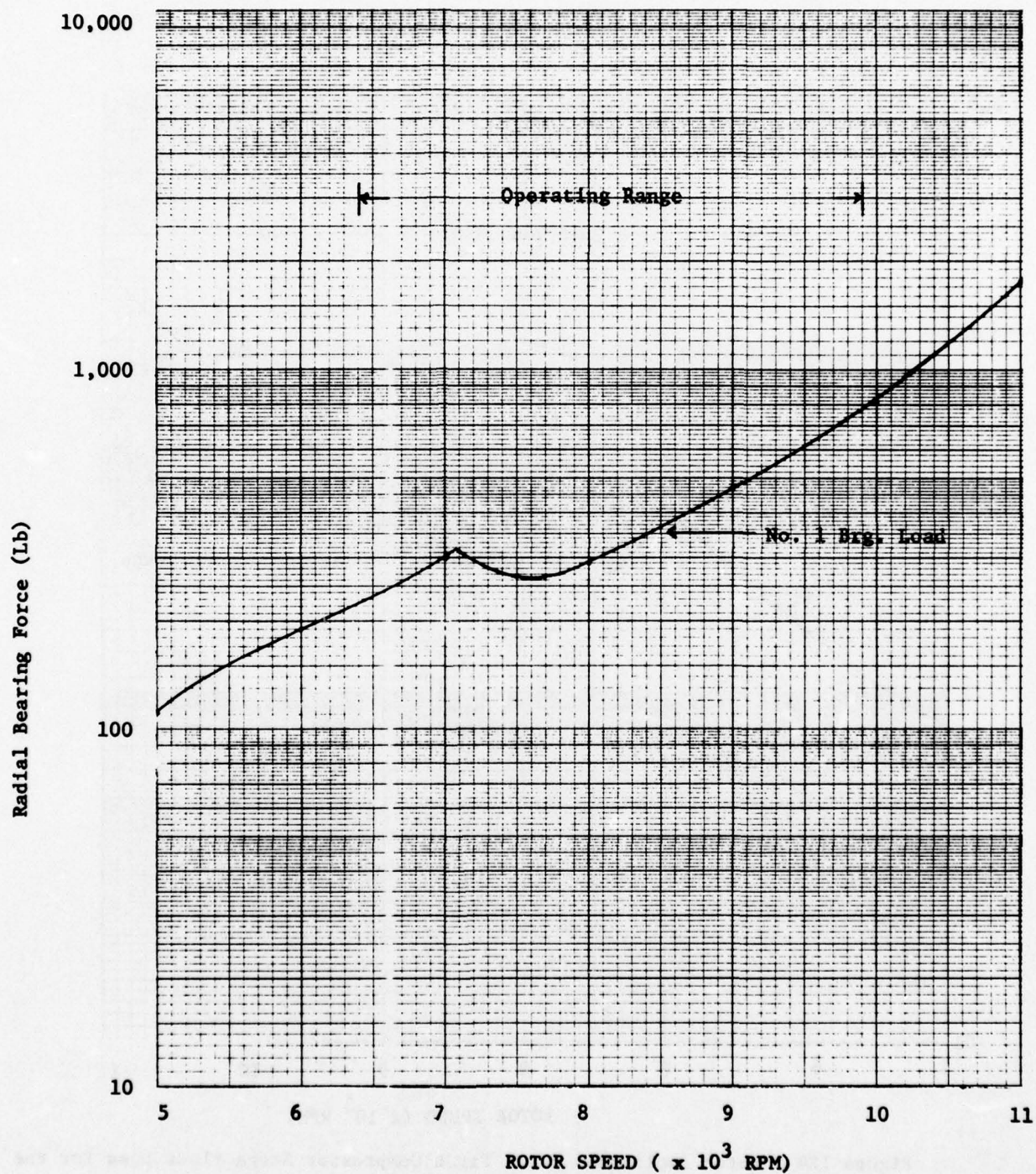


Figure 121 No. 1 Bearing Force for First Compressor Stage Blade Loss for TF-39 Gas Generator Spool



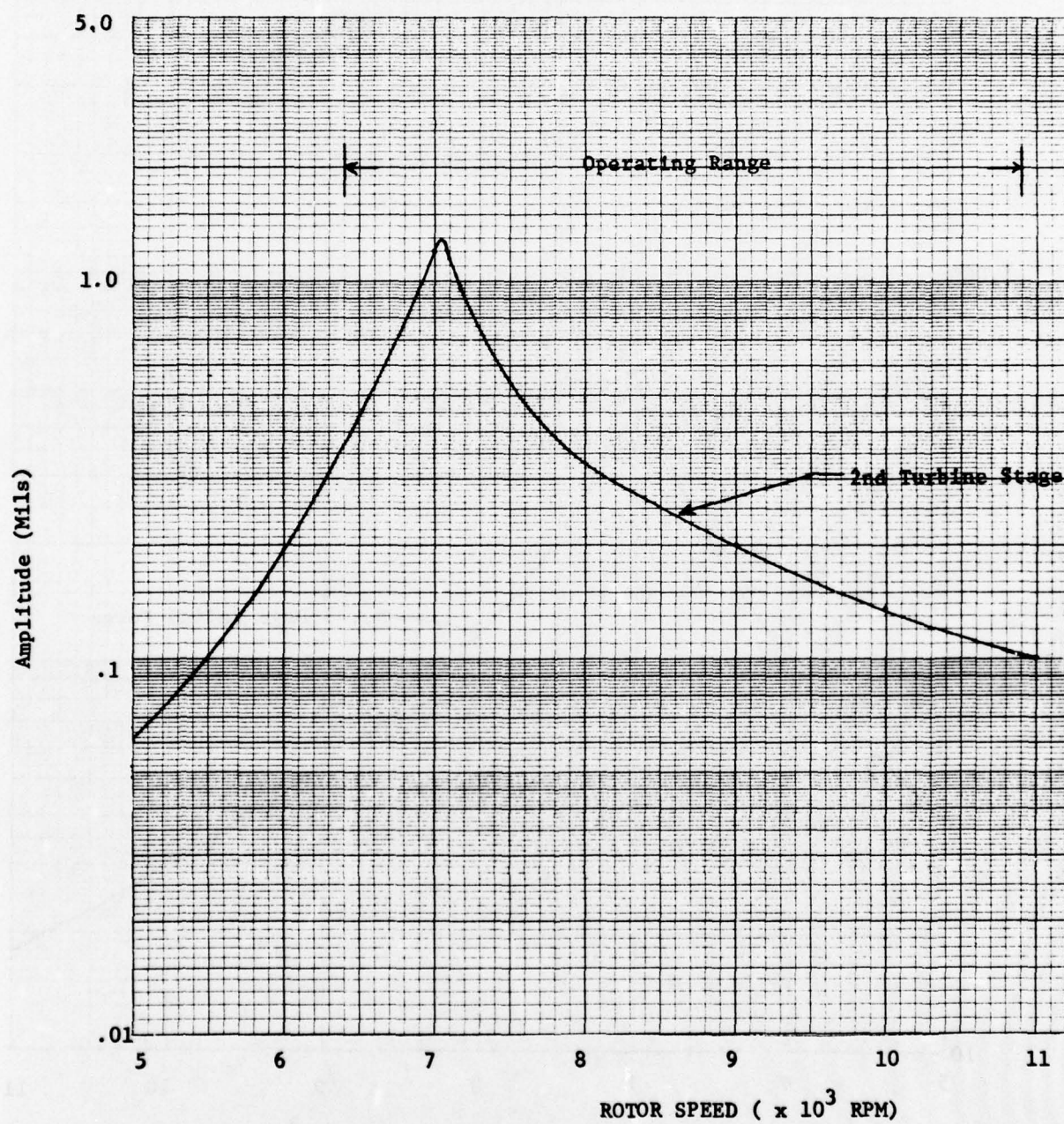


Figure 122 Rotor Amplitudes for a Second Turbine Stage Blade Loss for the TF-39 Gas Generator Spool

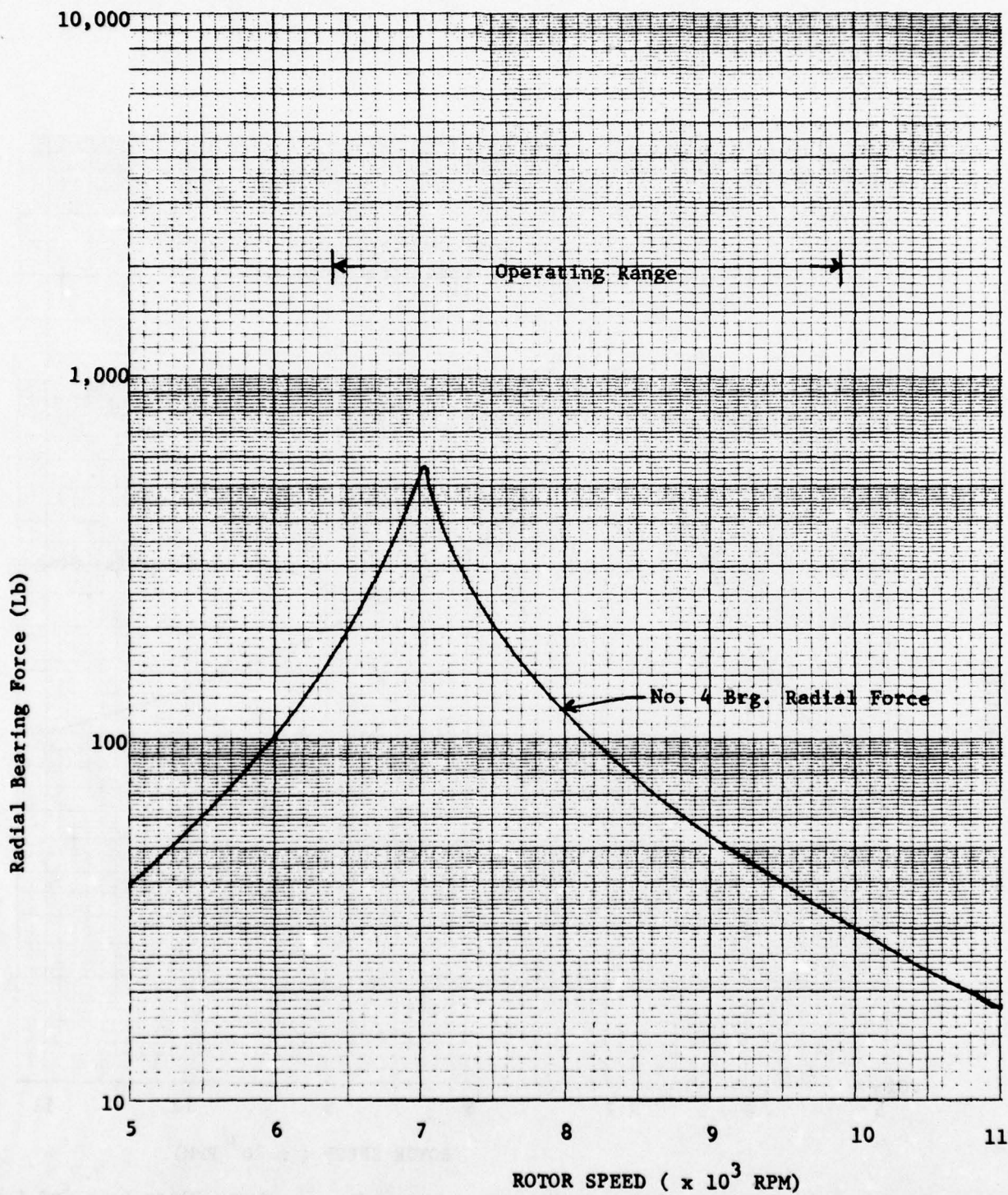


Figure 123 No. 4 Bearing Force for Second Turbine Stage Blade Loss for TF-39 Gas Generator Spool



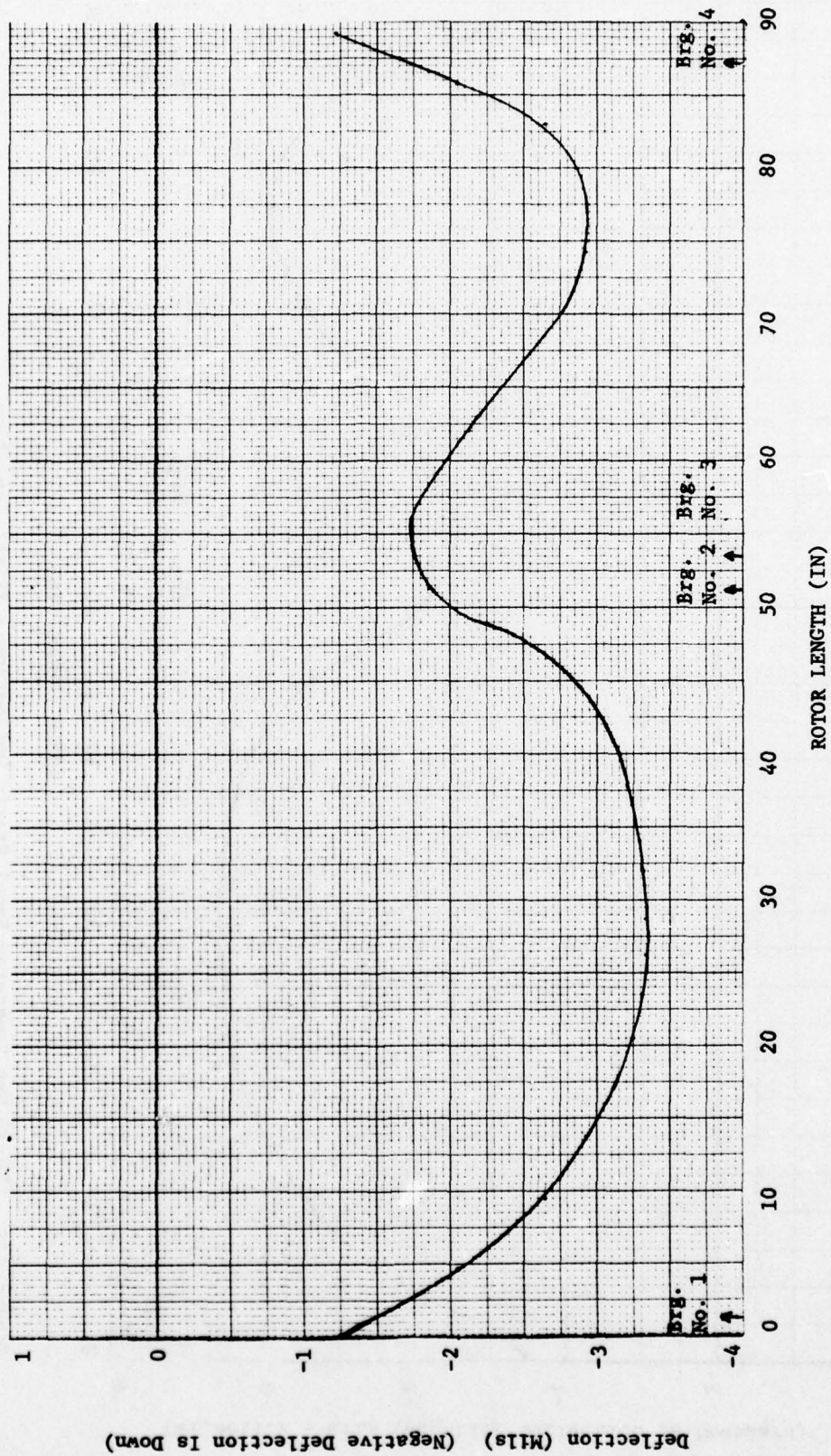


Figure 124 TF-39 Gas Generator Spool Static Deflection - Landing Condition



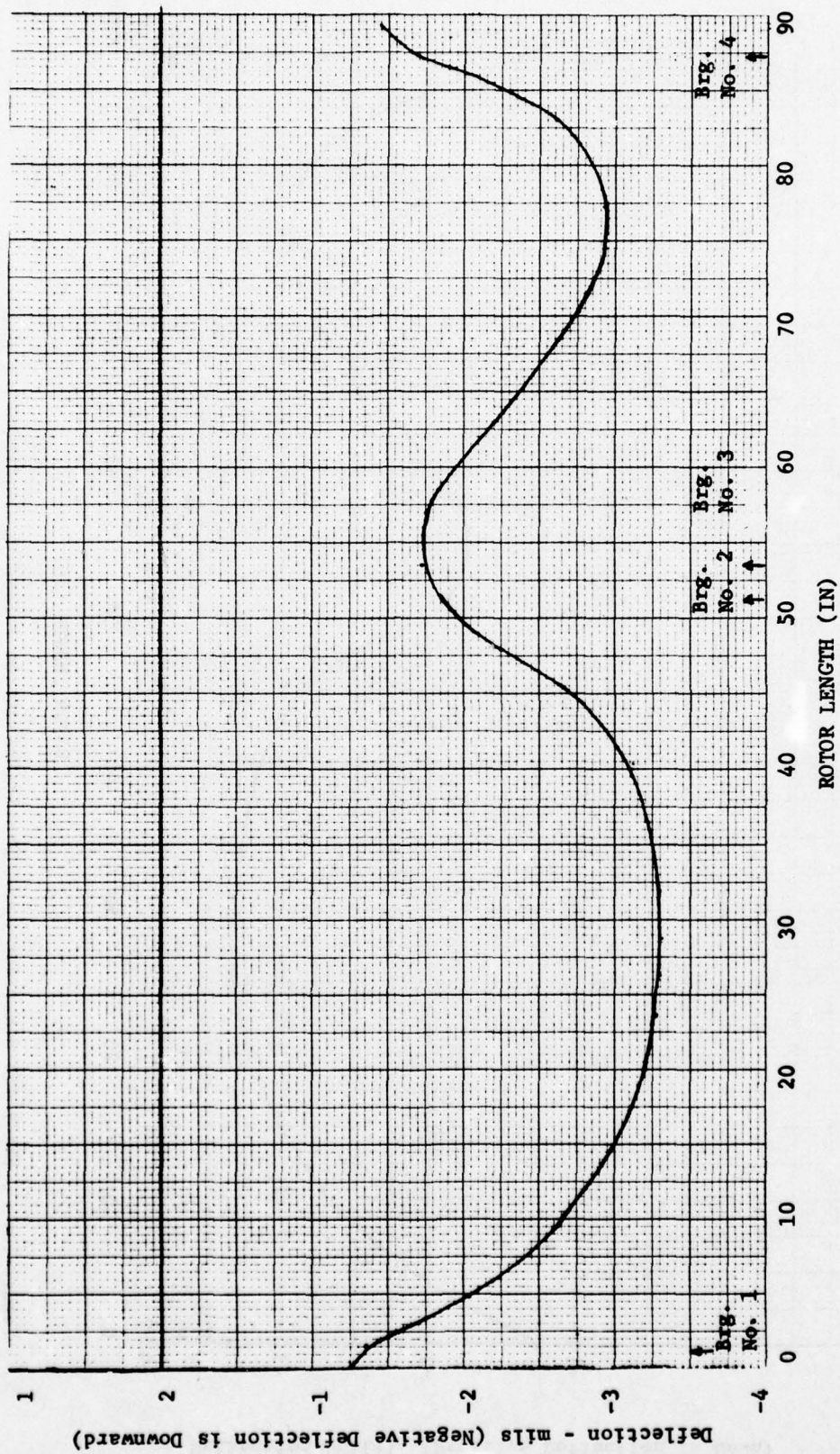


Figure 125 TF-39 Gas Generator Spool Static Deflection - Flight Condition

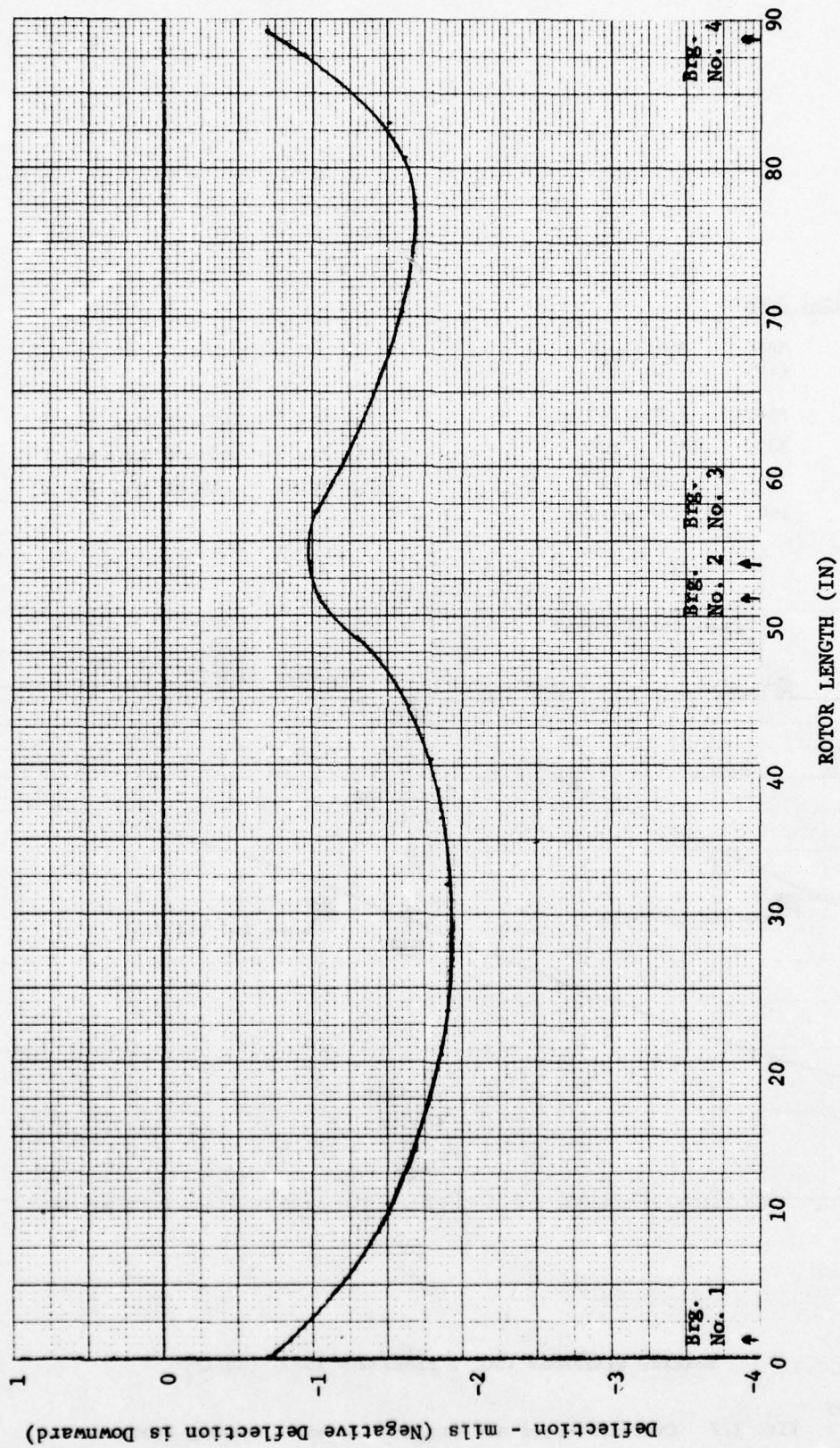


Figure 126 TF-39 Gas Generator Spool Static Deflection - Catapult Condition



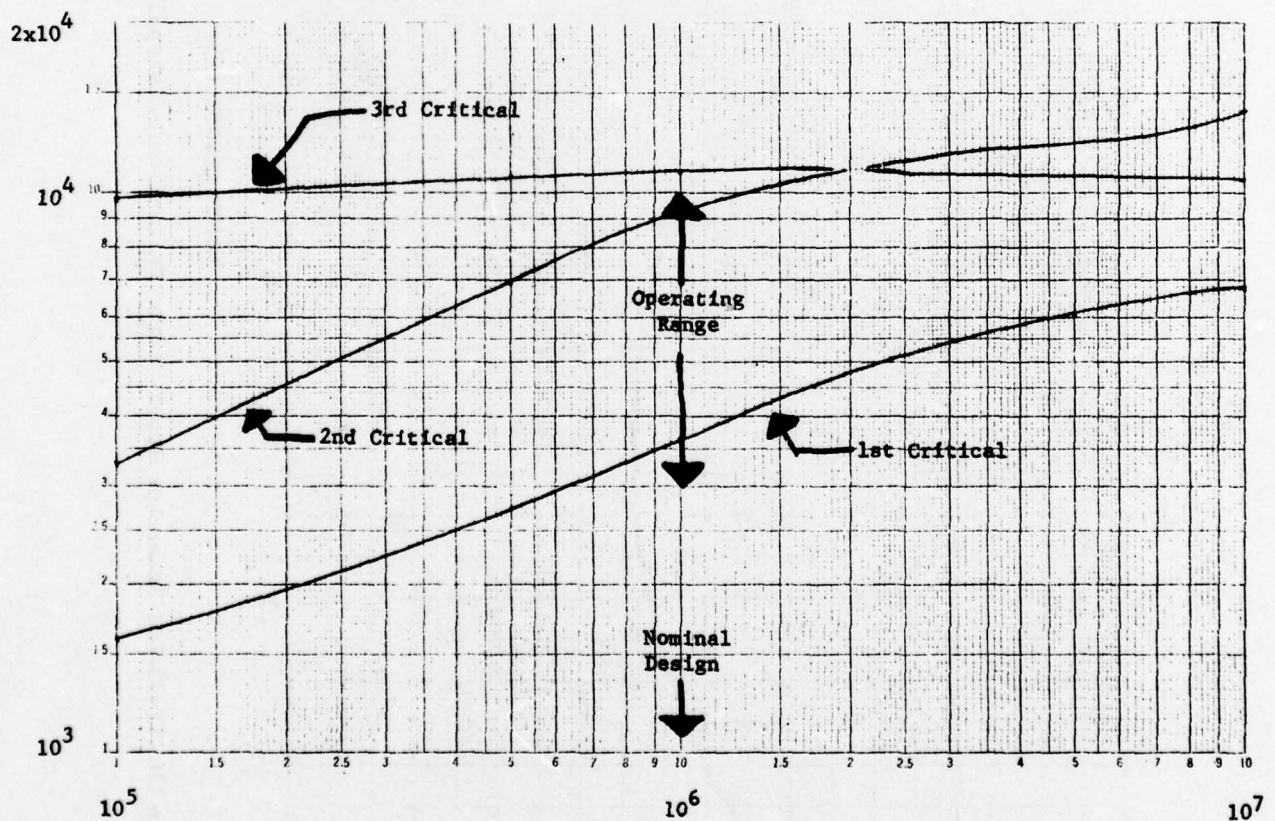
Pedestal Data

Brg. No.	MASS (lb)	Stiffness (lb/in)
1	320.	$8.8 \times 10^6$
2	380.	$10.0 \times 10^6$
3	350.	$1.2 \times 10^6$
4	160.	$.48 \times 10^6$

Brg. No. 2 = 200% of Brg. No. 1

Brg. No. 3 = 160% of Brg. No. 1

Brg. No. 4 = 4% of Brg. No. 1



BEARING STIFFNESS (NO. 1 BEARING = 100%) (LB/IN)

Fig. 127 Critical Speed Map for TF41 LP Rotor Bearing System



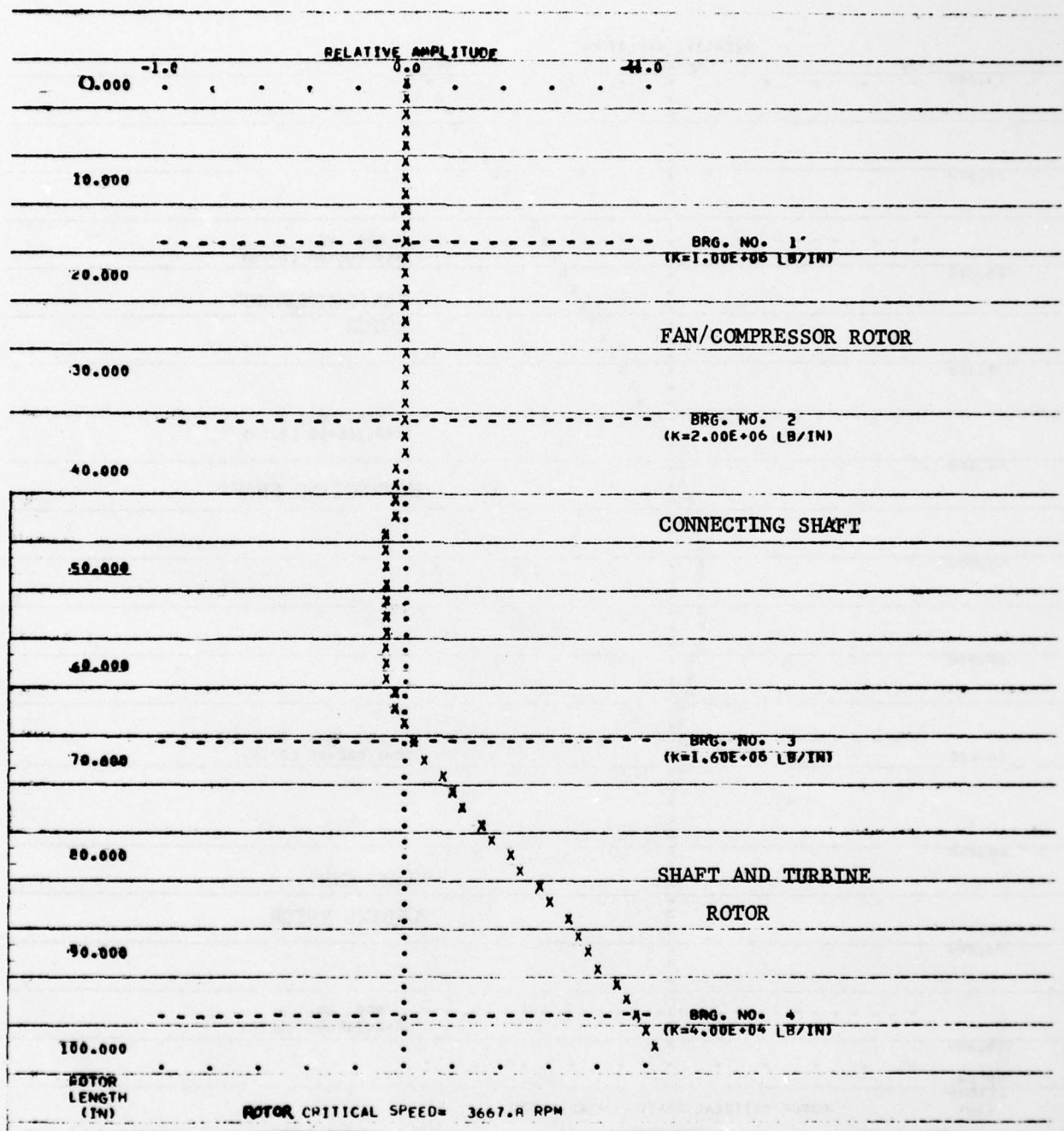
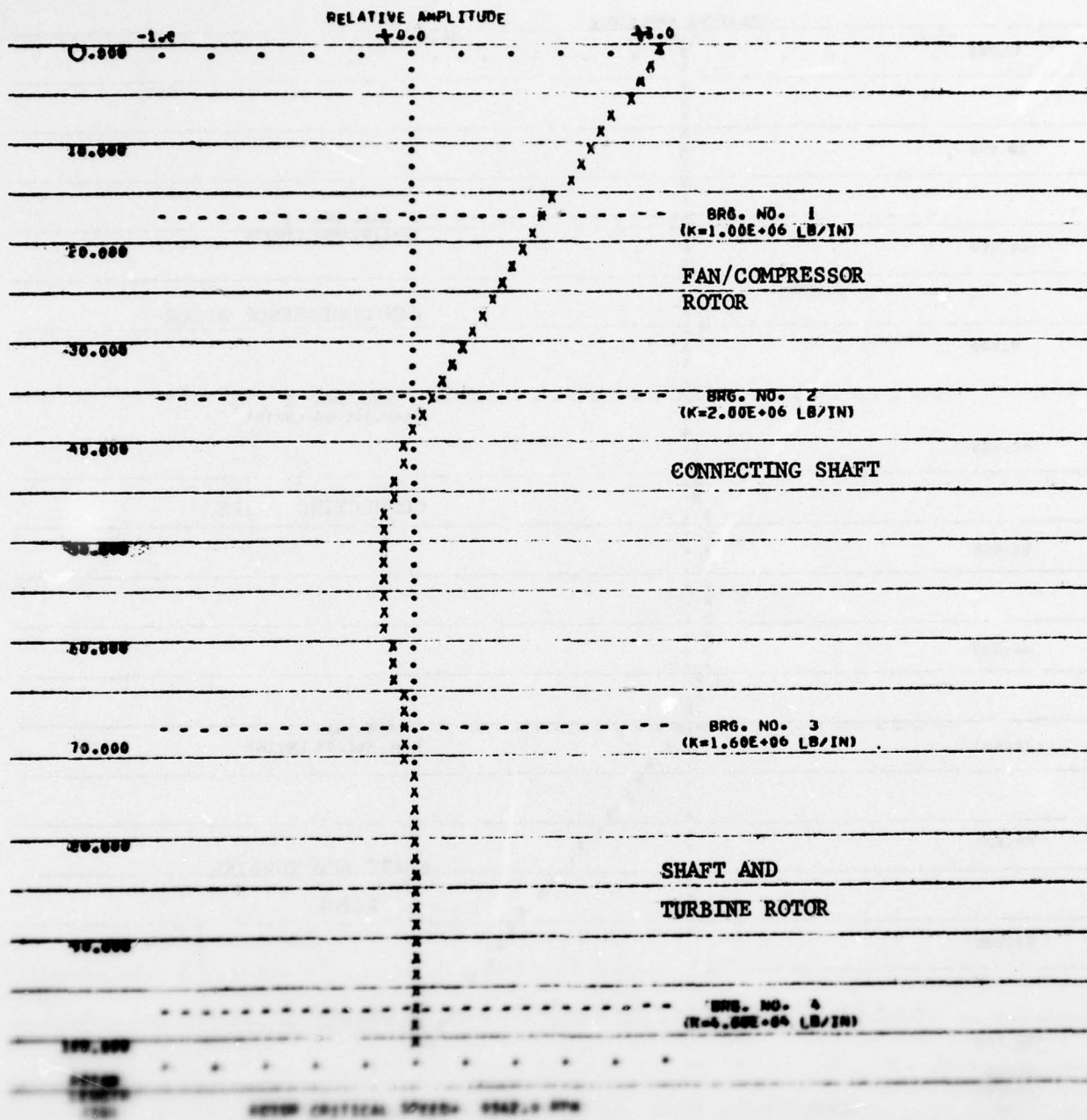


Fig. 128 Undamped Mode Shape at First Critical Speed of TF41 LP Rotor Bearing System.



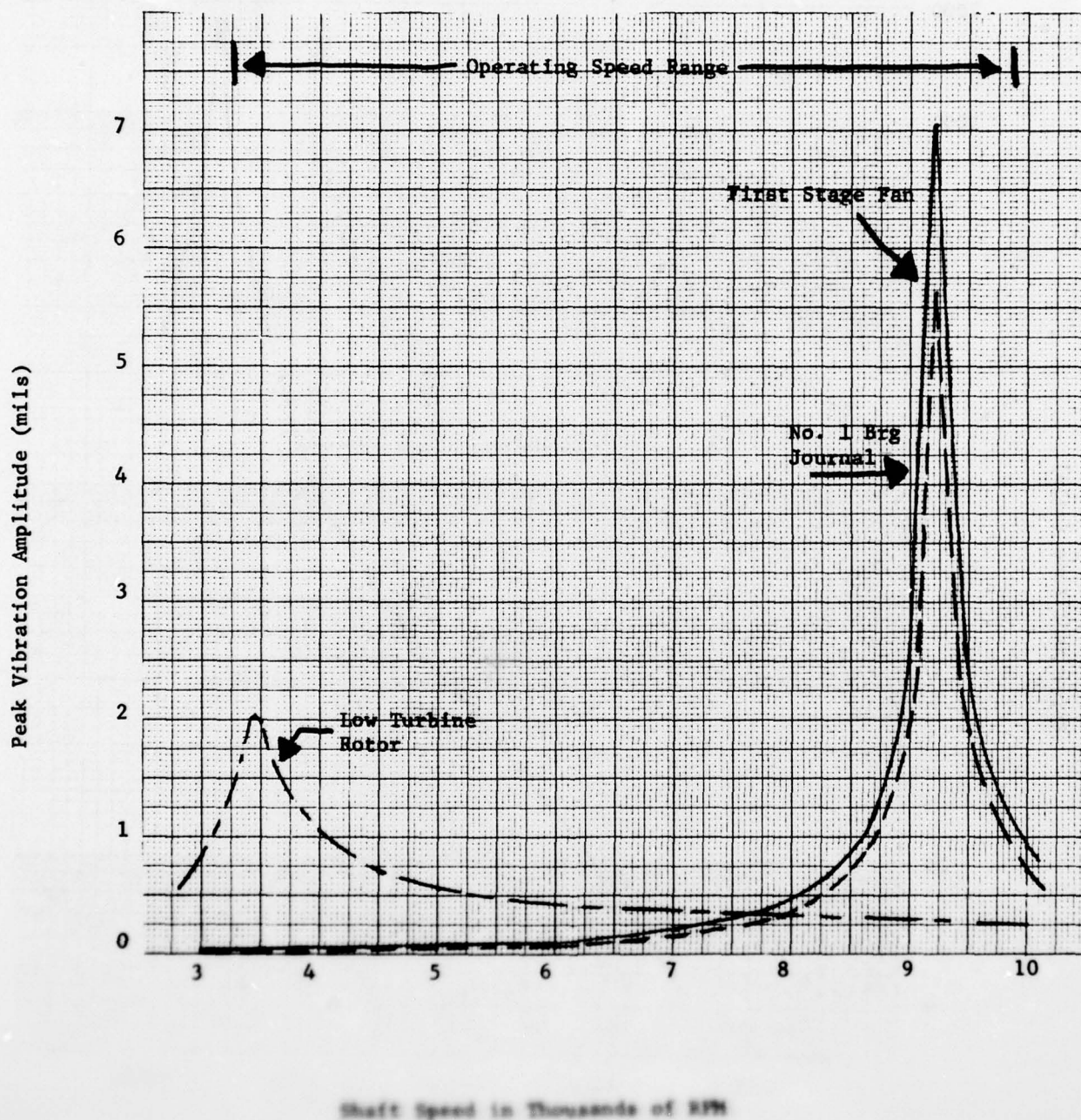


Fig. 120 Calculated Peak Unbalance Response Vibration  
(for 100% of Rotor Bearing System (undamped))



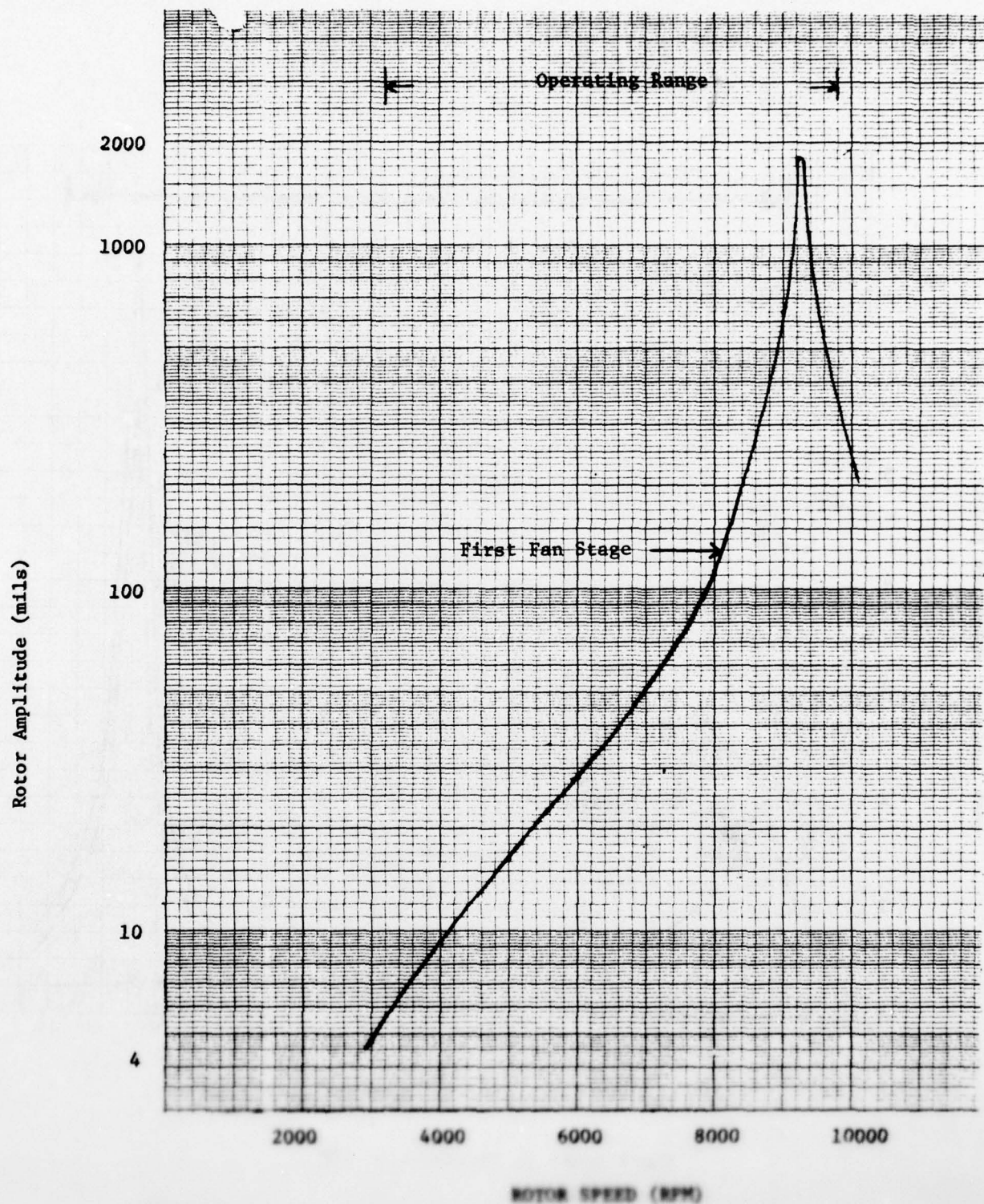


Fig. 131 Low Compressor Rotor Amplitude for a First Fan Stage Blade Loss of the TF41 Engine

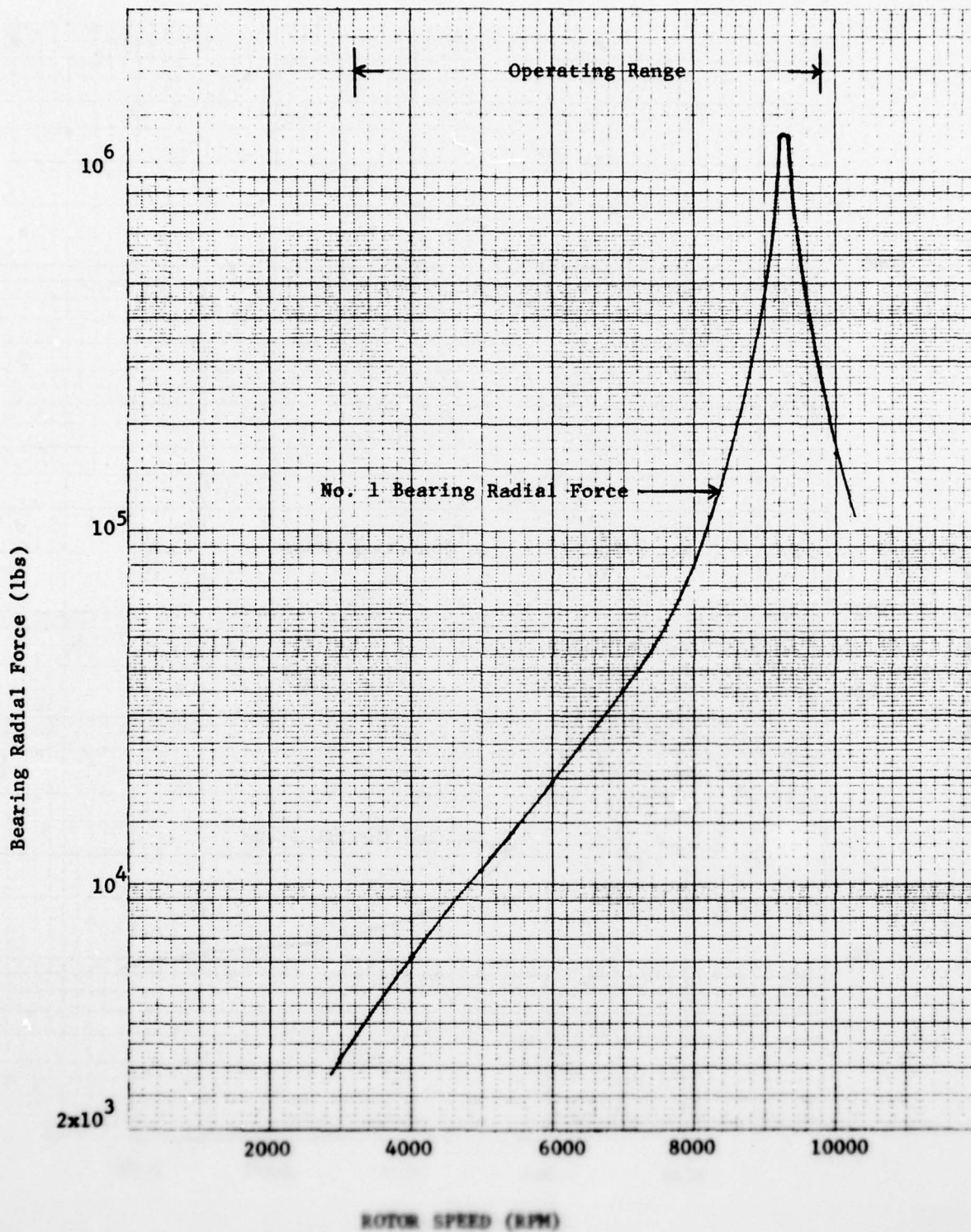


Fig. 132 TF61 Low Rotor System No. 1 Bearing Force  
for the First Fan Stage Blade Loss



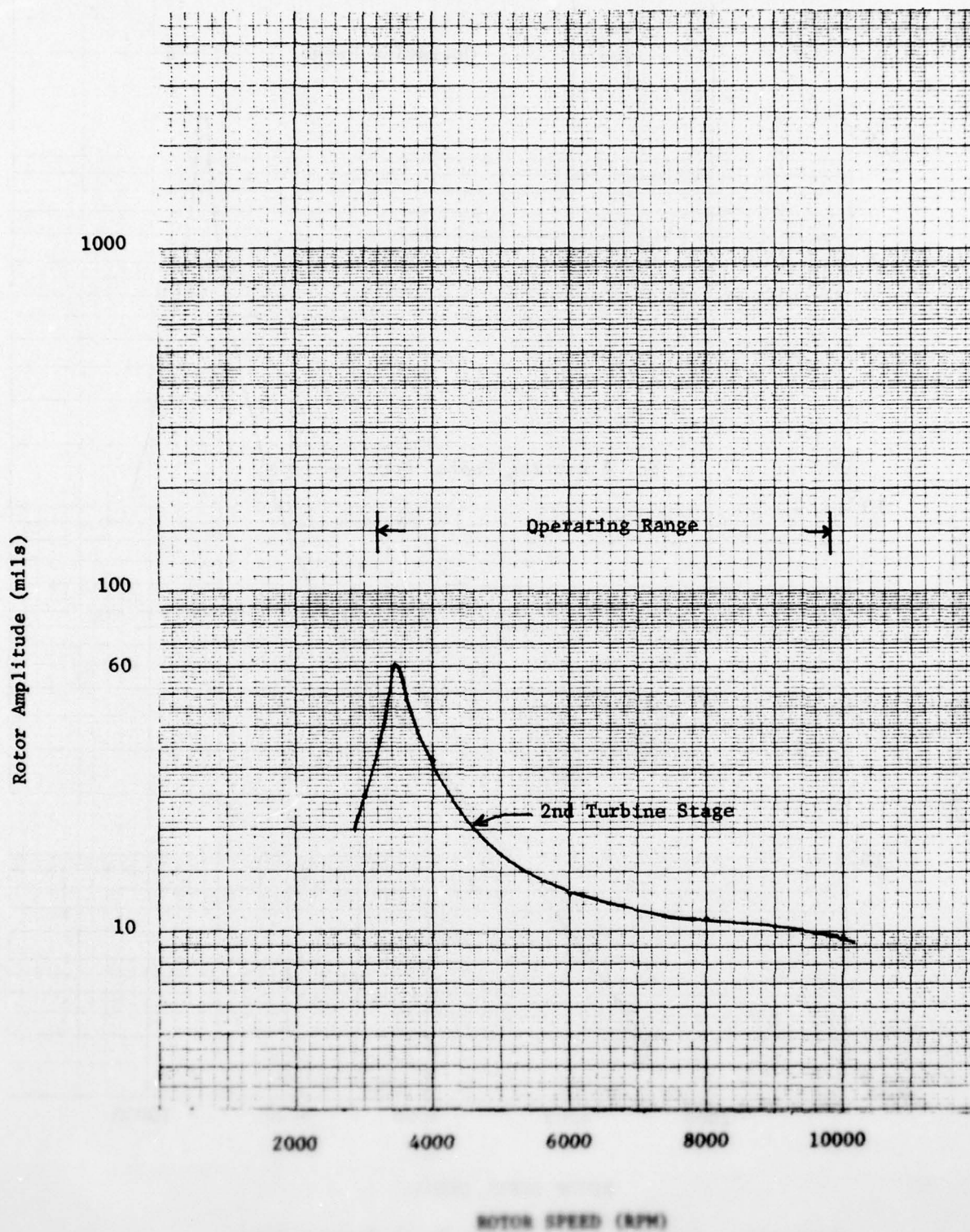


Fig. 111 Low Turbine Rotor Amplitudes for a Second Turbine Stage Loss of the 1951 Reactor



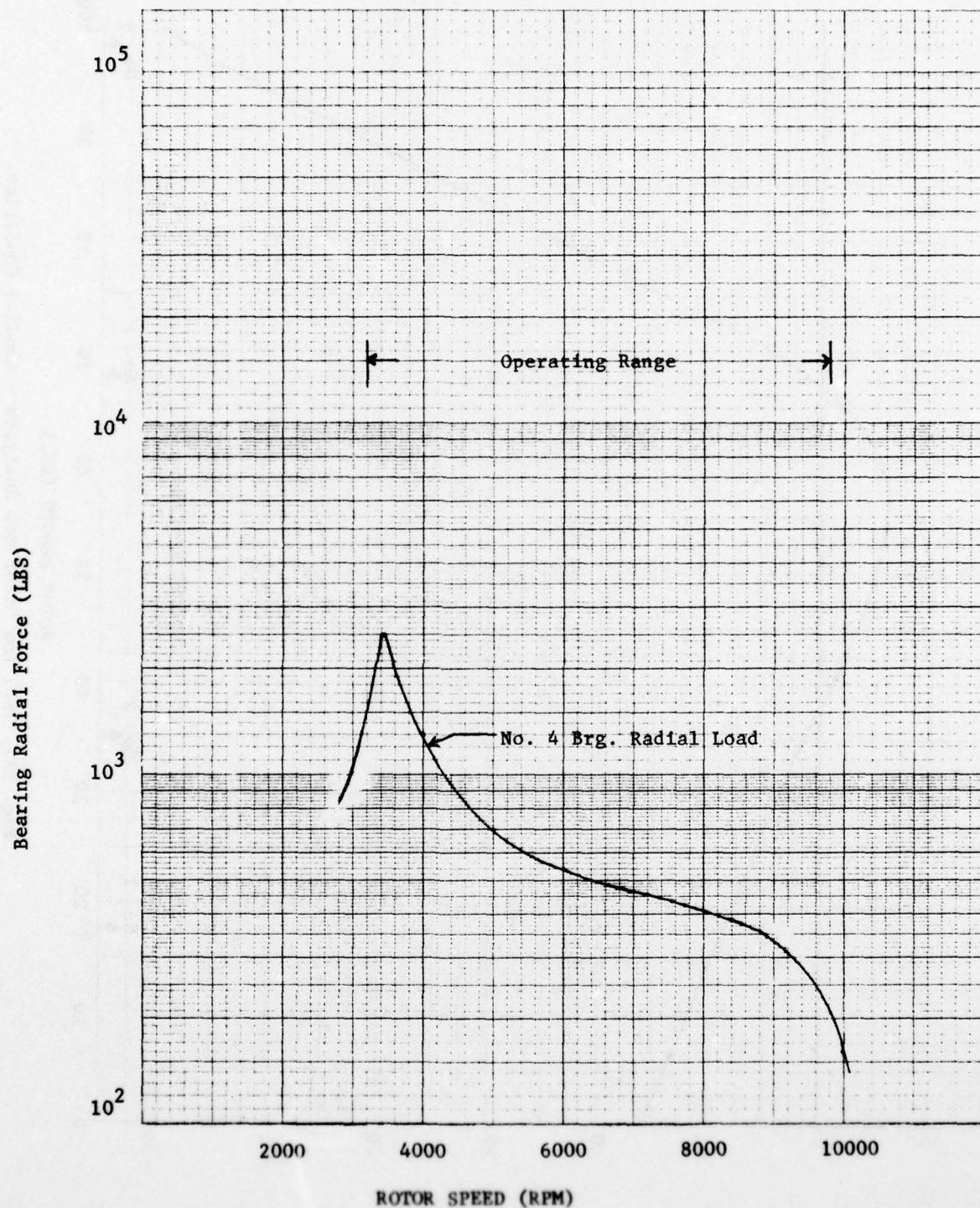


FIG. 134 TF41 Low Rotor System No. 4 Bearing Force  
For The Second Turbine Blade Loss

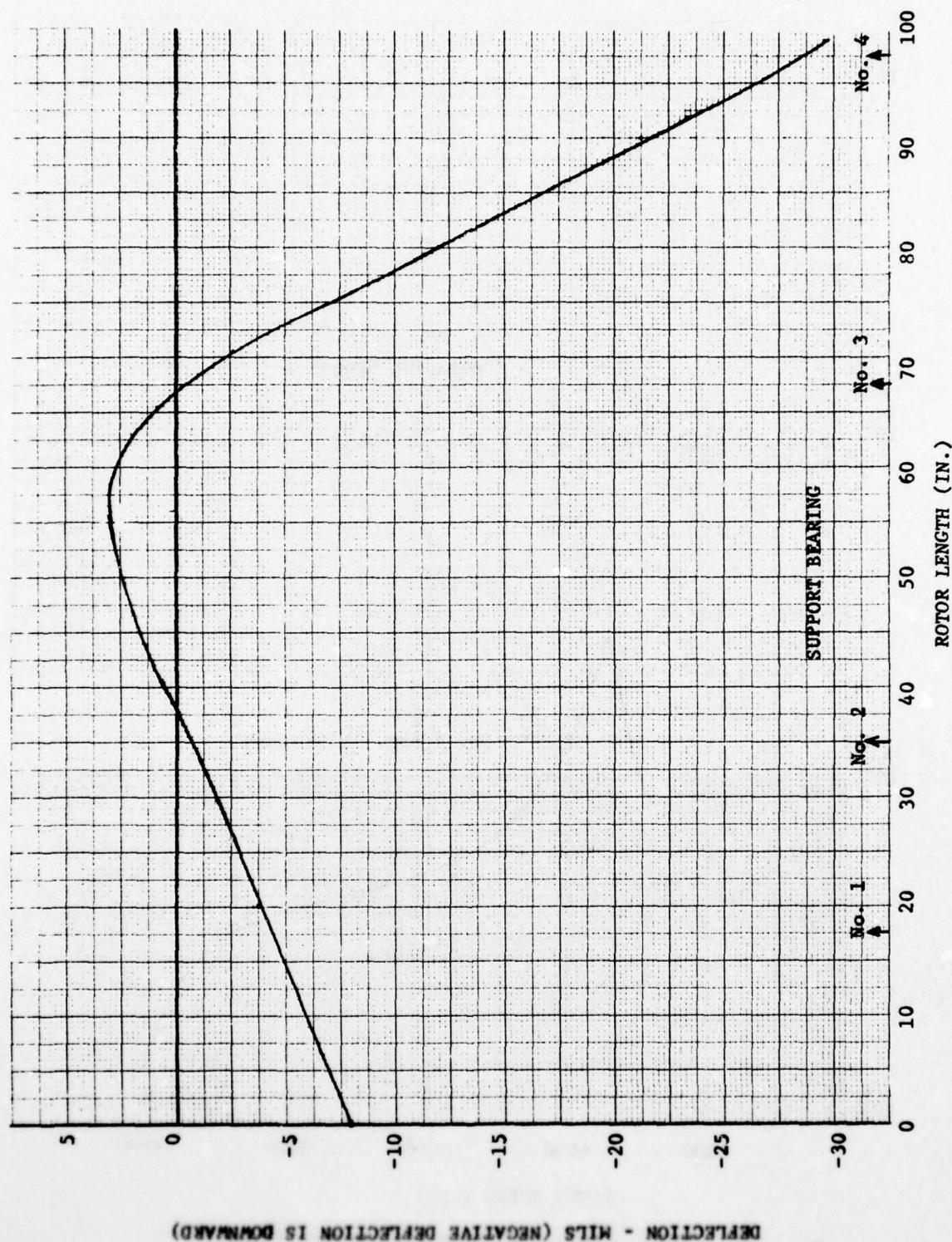


Fig. 135 TF41 Low Rotor Bow Analysis - Landing Condition

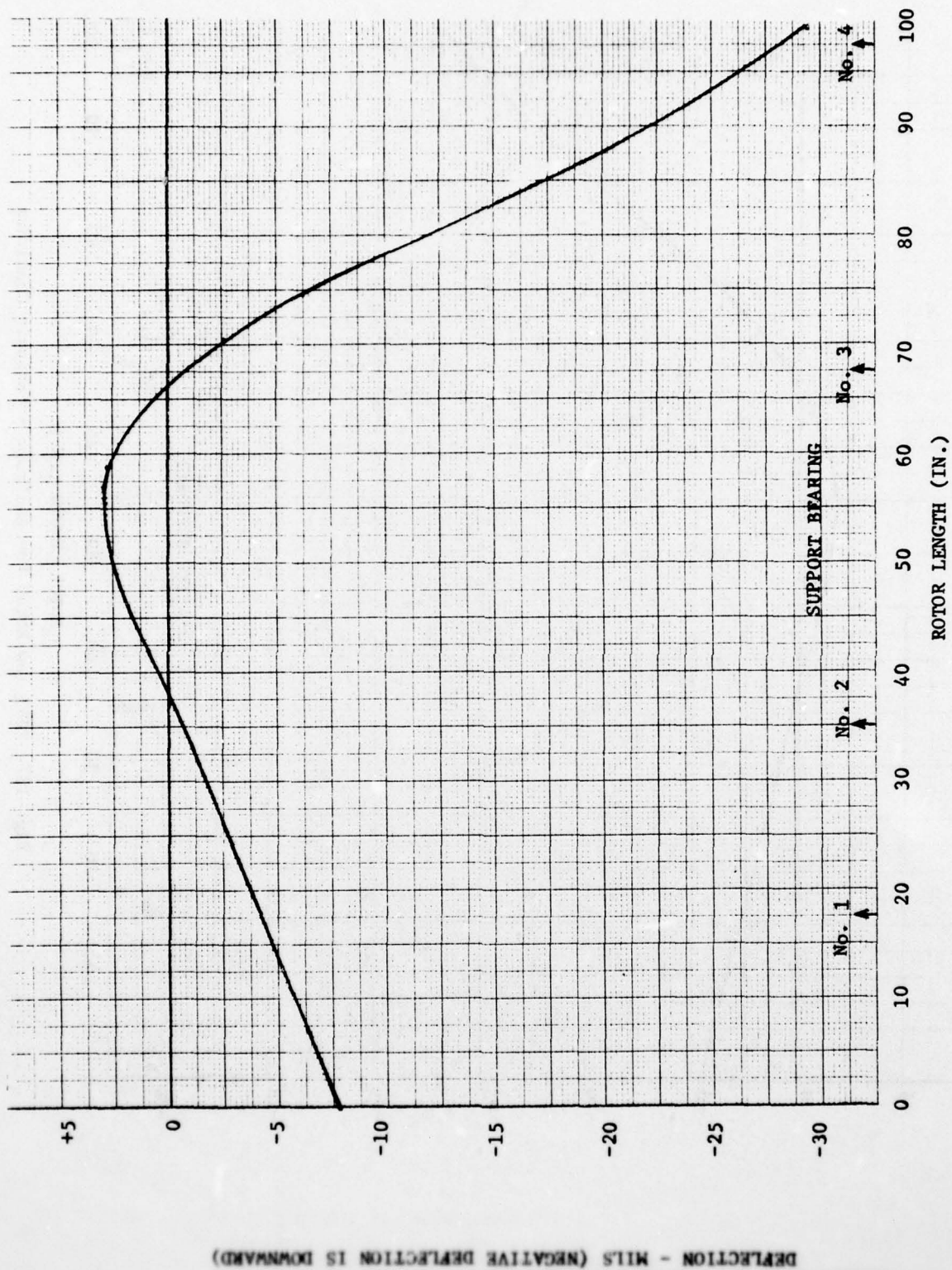


Fig. 136 TFA1 Low Rotor Bow Analysis - Flight Condition



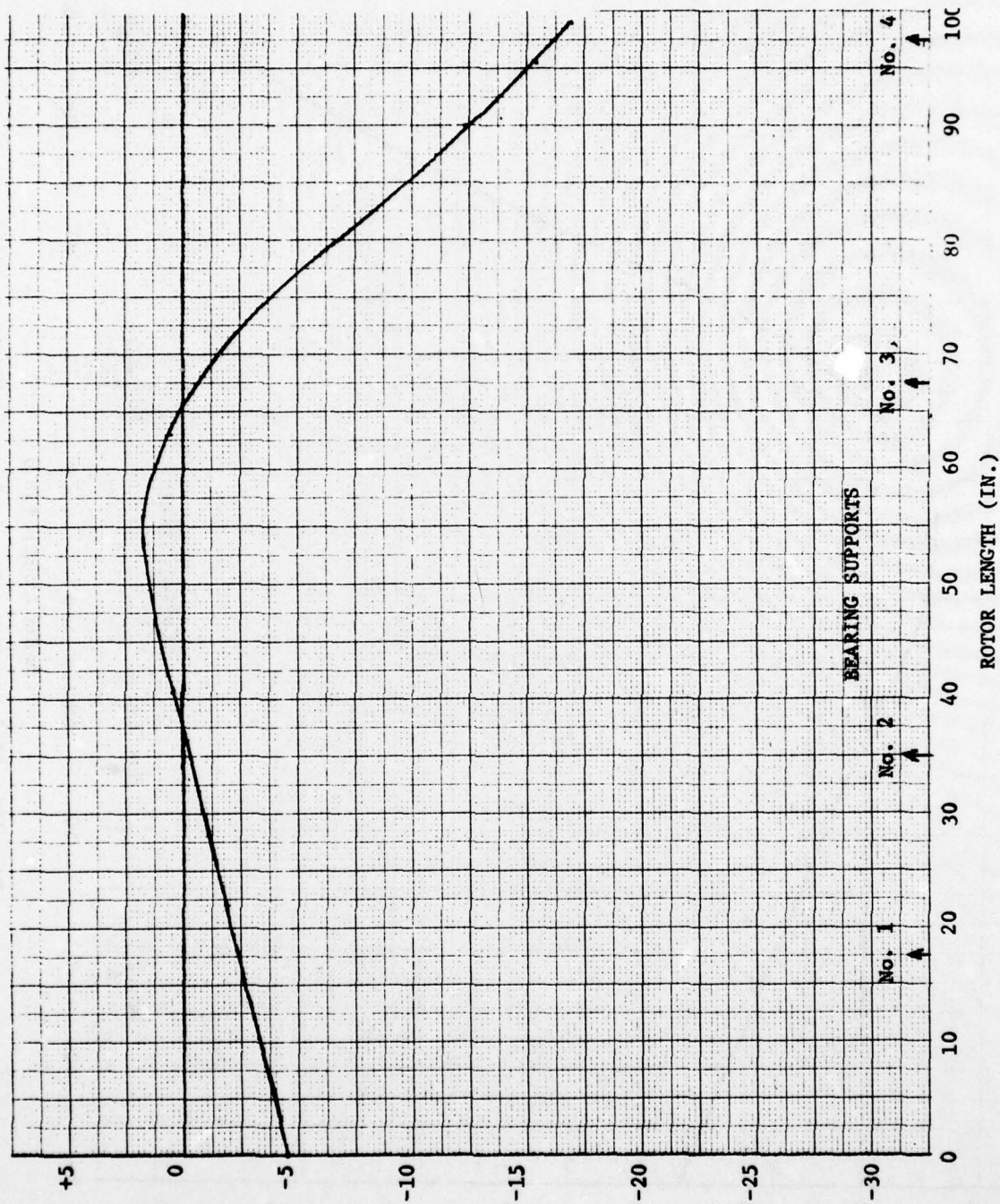


Fig. 137 TF41 Low Rotor Bow Analysis - Catapult Condition

DEFLECTION - MILS (NEGATIVE DEFLECTION IS DOWNWARD)

Pedestal Data:

Brg. No.	Mass (LB)	Stiffness (LB/IN)
1	380.	$12.0 \times 10^6$
2	250.	$3.9 \times 10^6$
3	150.	$1.2 \times 10^6$

Brg. No. 2 = 85% of Brg. No. 1  
Brg. No. 3 = 120% of Brg. No. 1

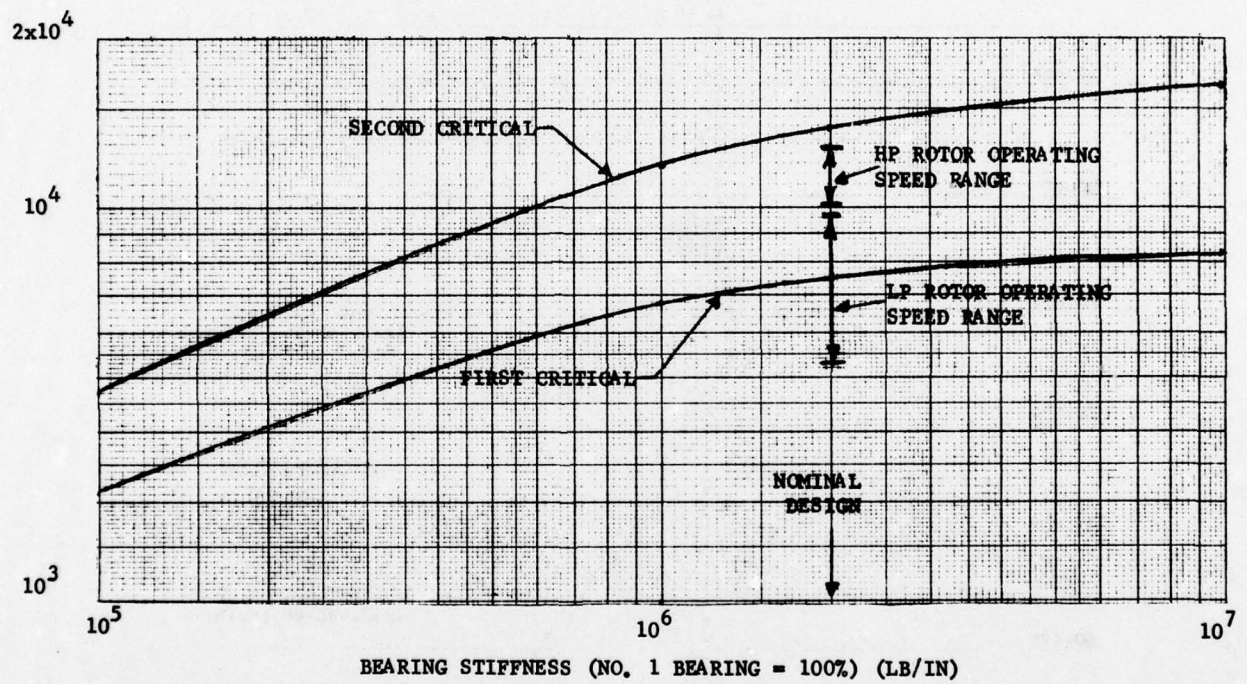


Fig. 138 Critical Speed Map for TF41 HP Rotor Bearing System

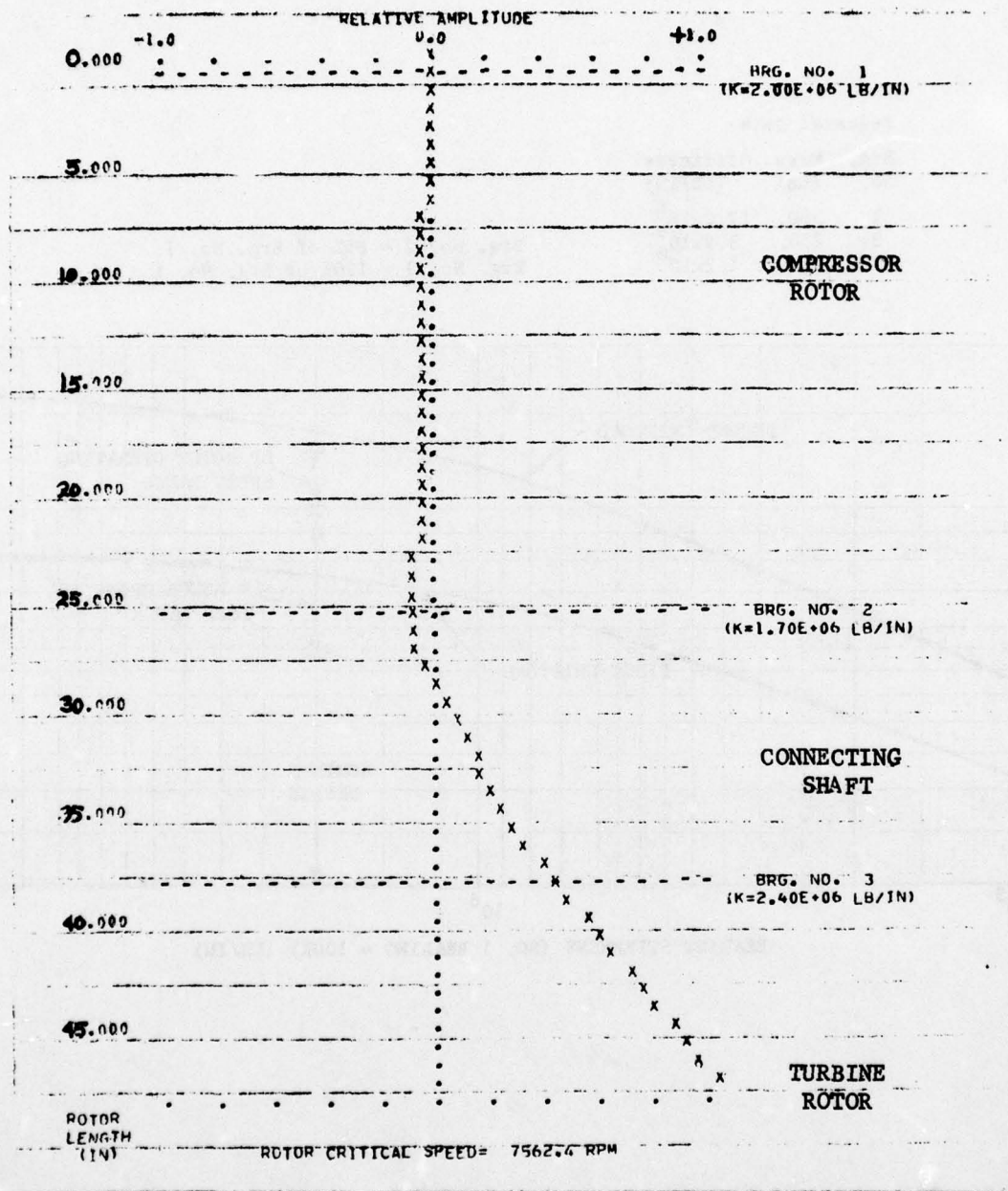


Fig. 139 Undamped Mode Shape at First Critical Speed of TF41 HP Rotor Bearing System.



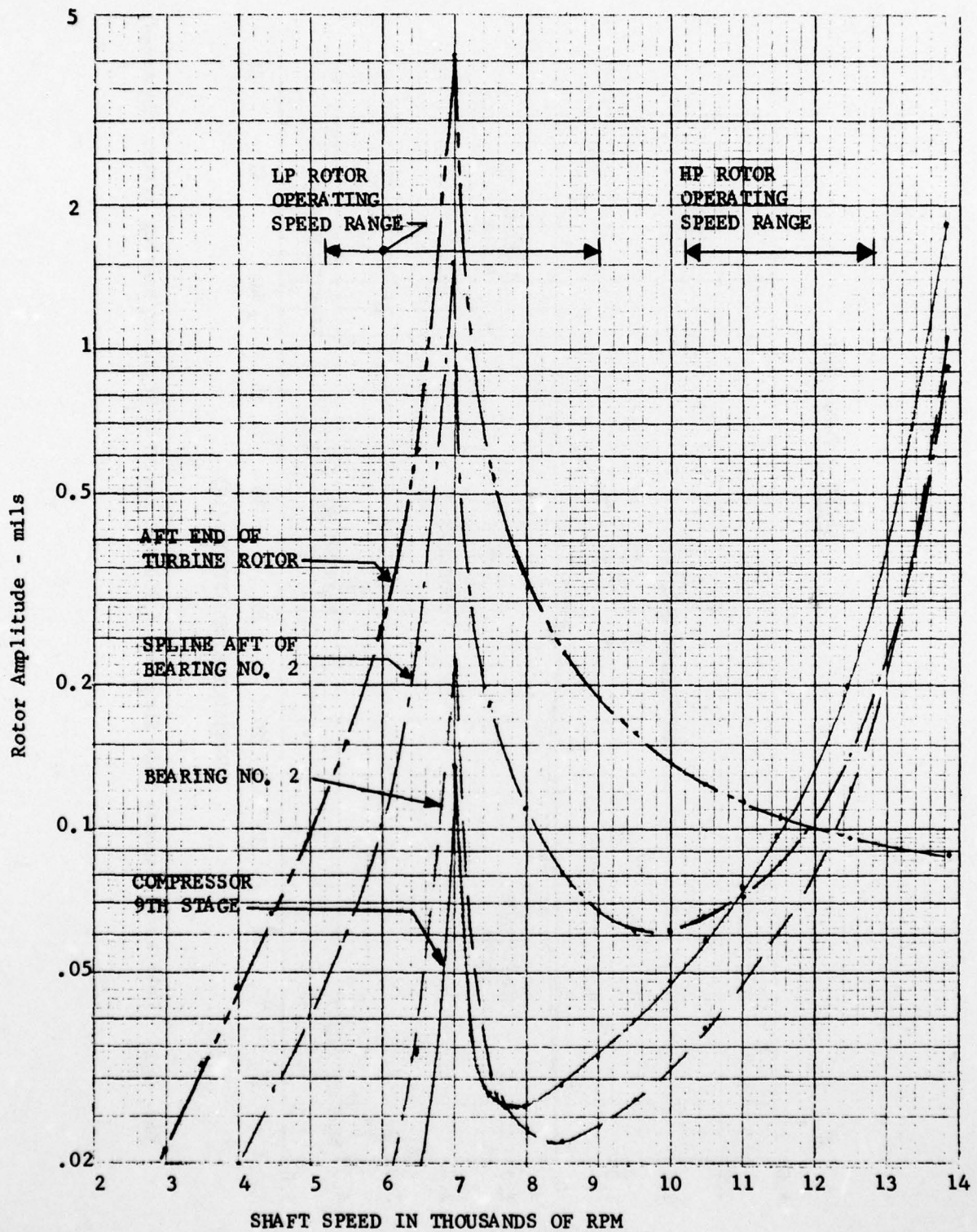


Fig. 140 Calculated Peak Unbalance Response Vibration for TF41 HP Rotor Bearing System (Undamped)

SPEED = 7000. RPM

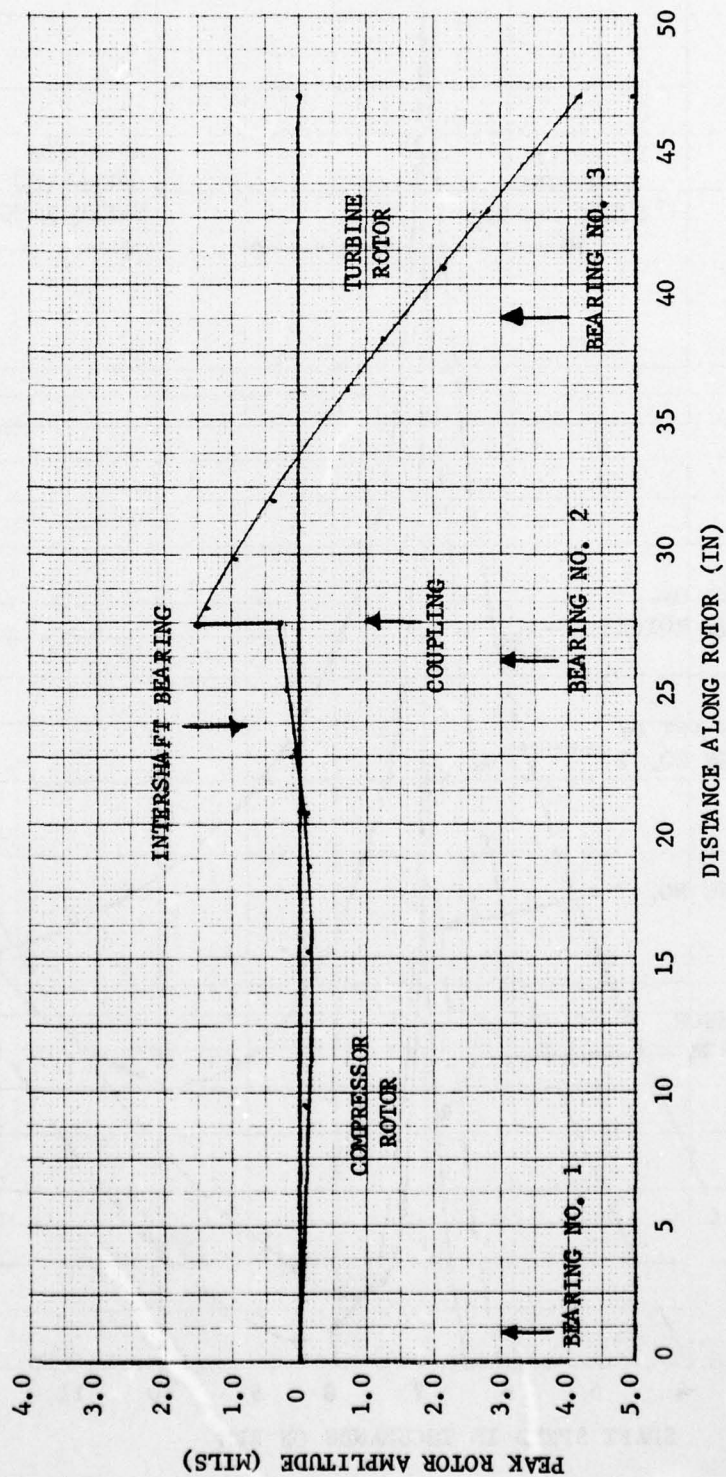


Fig. 141 Unbalance Response Mode Shape at 7,000 RPM for TF41 HP Rotor Bearing System (Undamped)

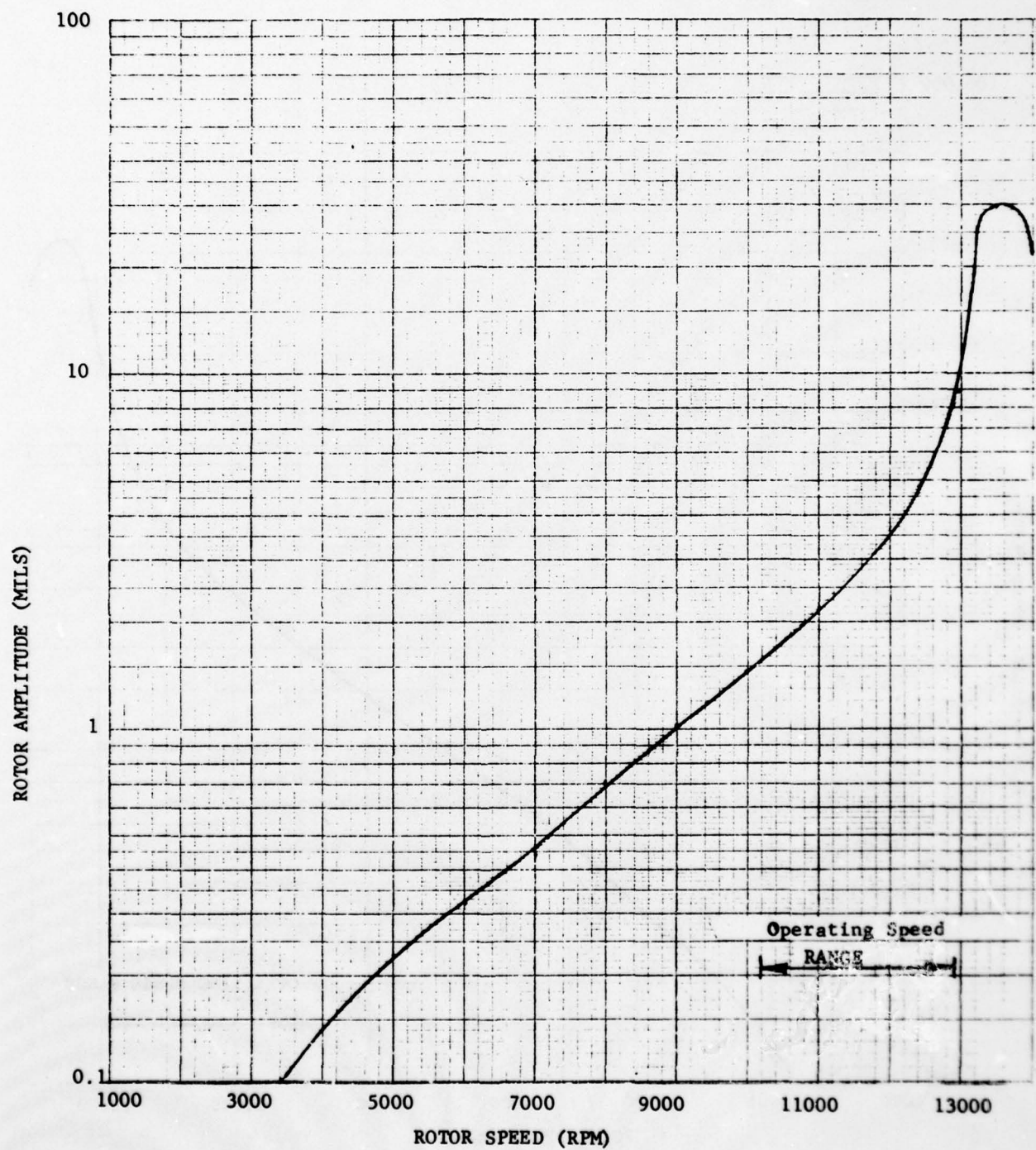


Fig. 142 TF41 High Compressor Rotor Amplitude for a First Stage Compressor Blade Loss.



AD-A055 262

MECHANICAL TECHNOLOGY INC LATHAM N Y  
TURBINE ENGINE ROTORDYNAMIC EVALUATION. VOLUME I. (U)

F/G 21/5

JAN 78 R A RIO  
MTI-76TR41

F33615-75-C-2035

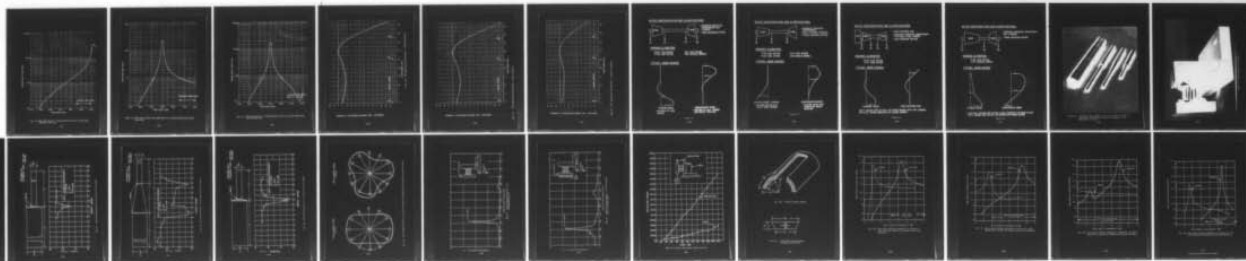
AFAPL-TR-76-81-VOL-1

NL

UNCLASSIFIED

3 OF 3

AD  
A055262



END

DATE  
FILMED

7 -78

DDC

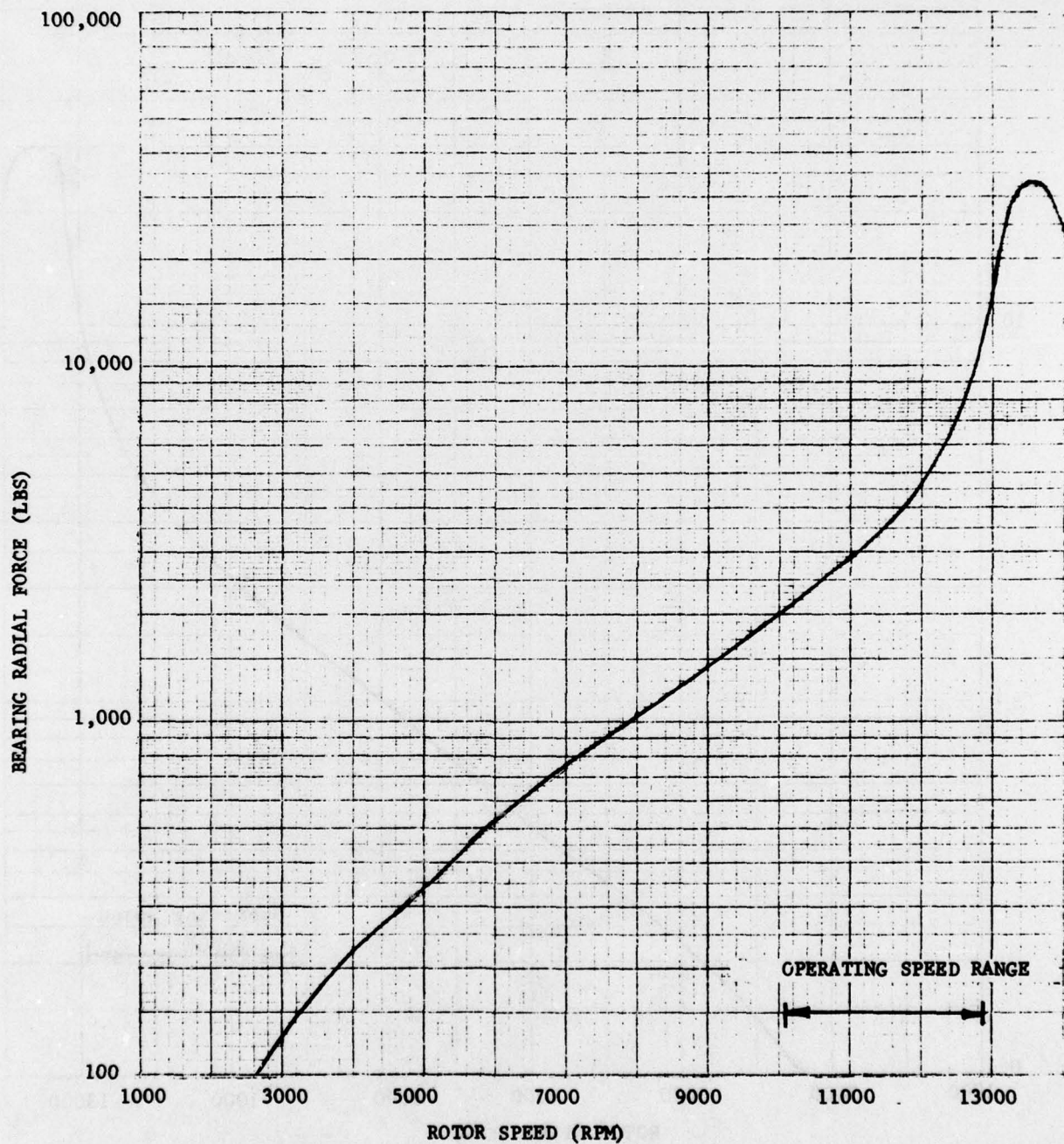


Fig. 143 TF41 High Rotor No. 1 Bearing Radial Load for a First Stage Compressor Blade Loss.

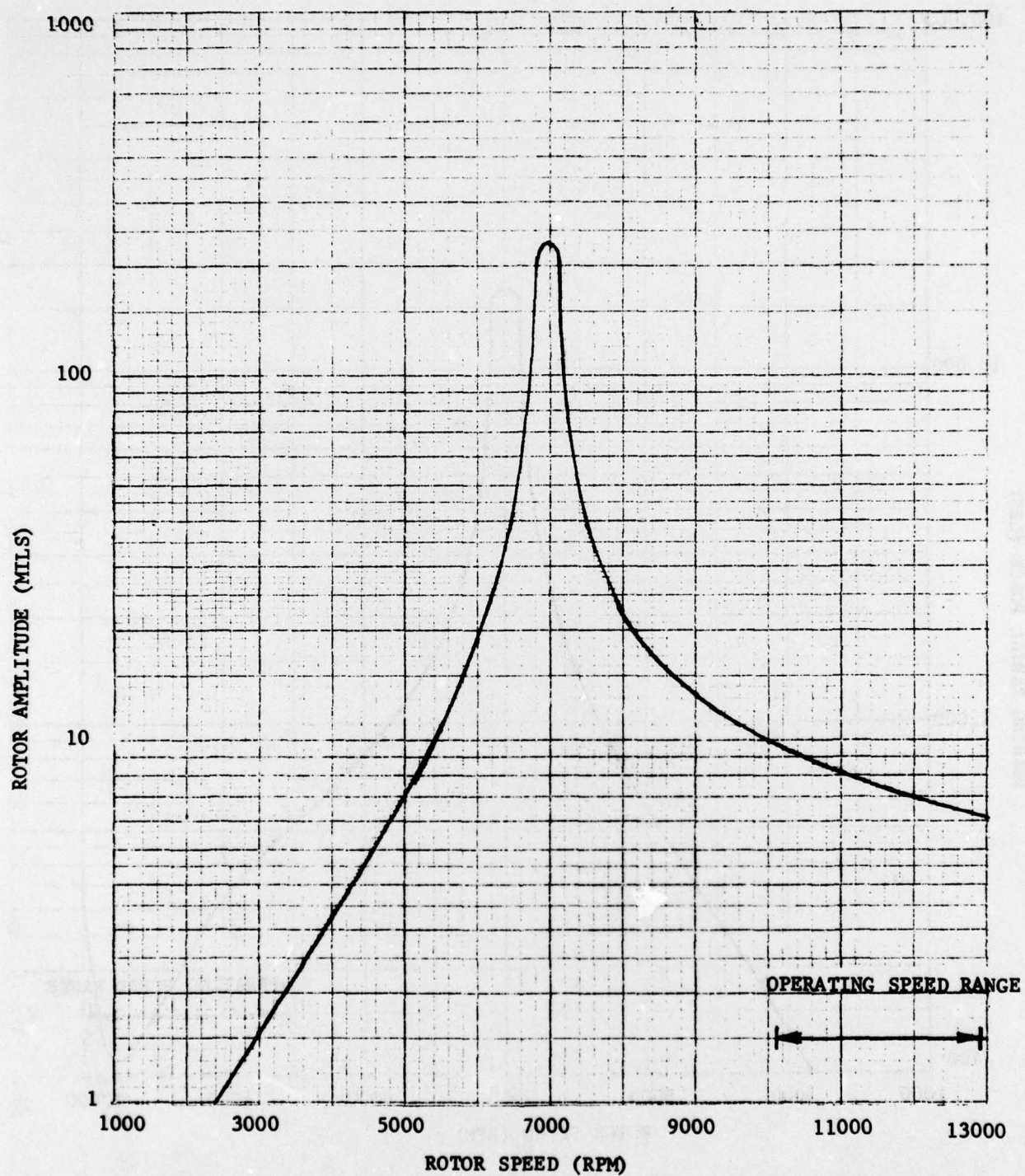


Fig. 144 TF41 High Turbine Rotor Amplitude for a Second Stage High Turbine Blade Loss



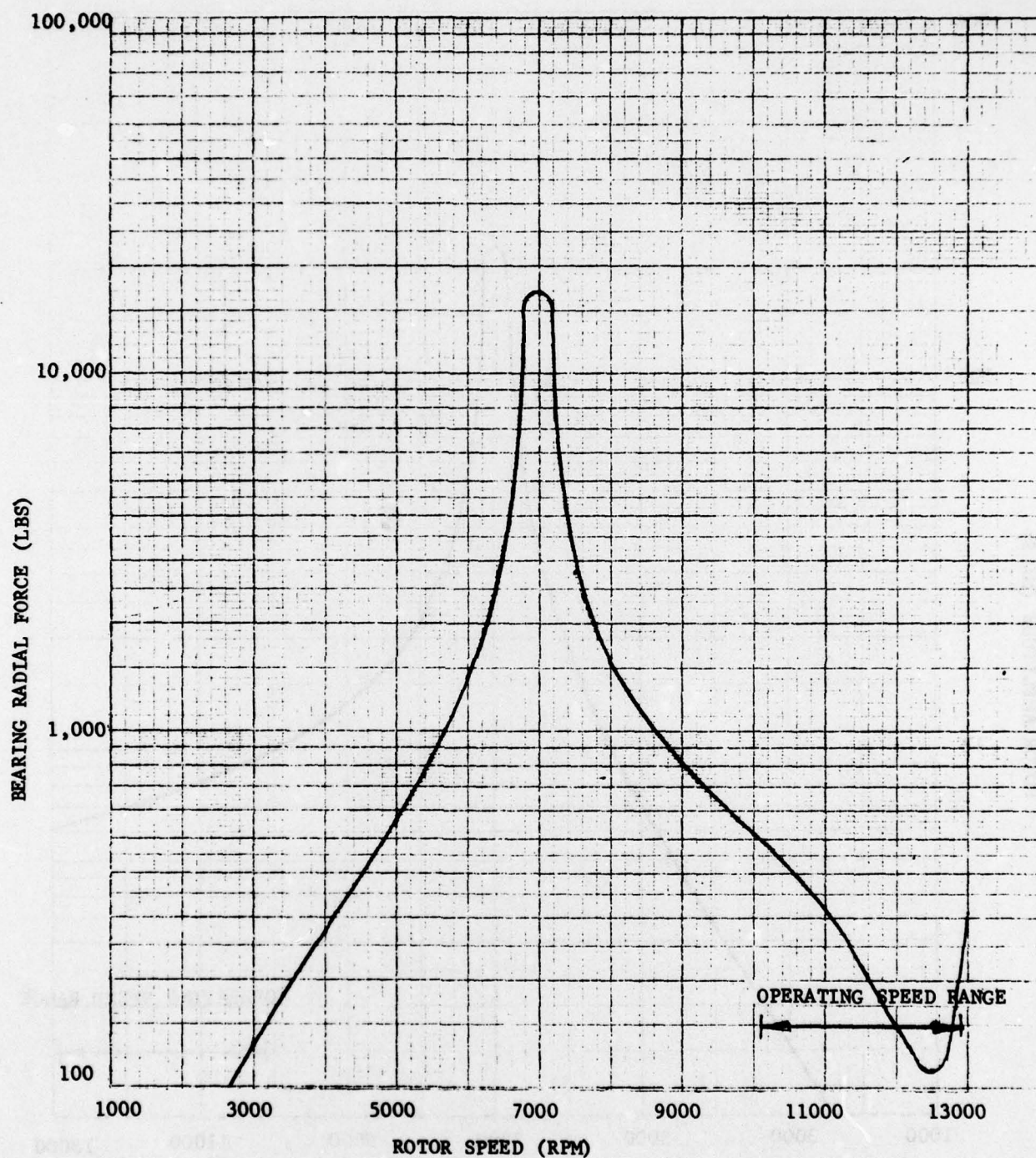


Fig. 145 TF41 High Rotor No. 3 Bearing Radial Load for a Second Stage High Turbine Blade Loss.

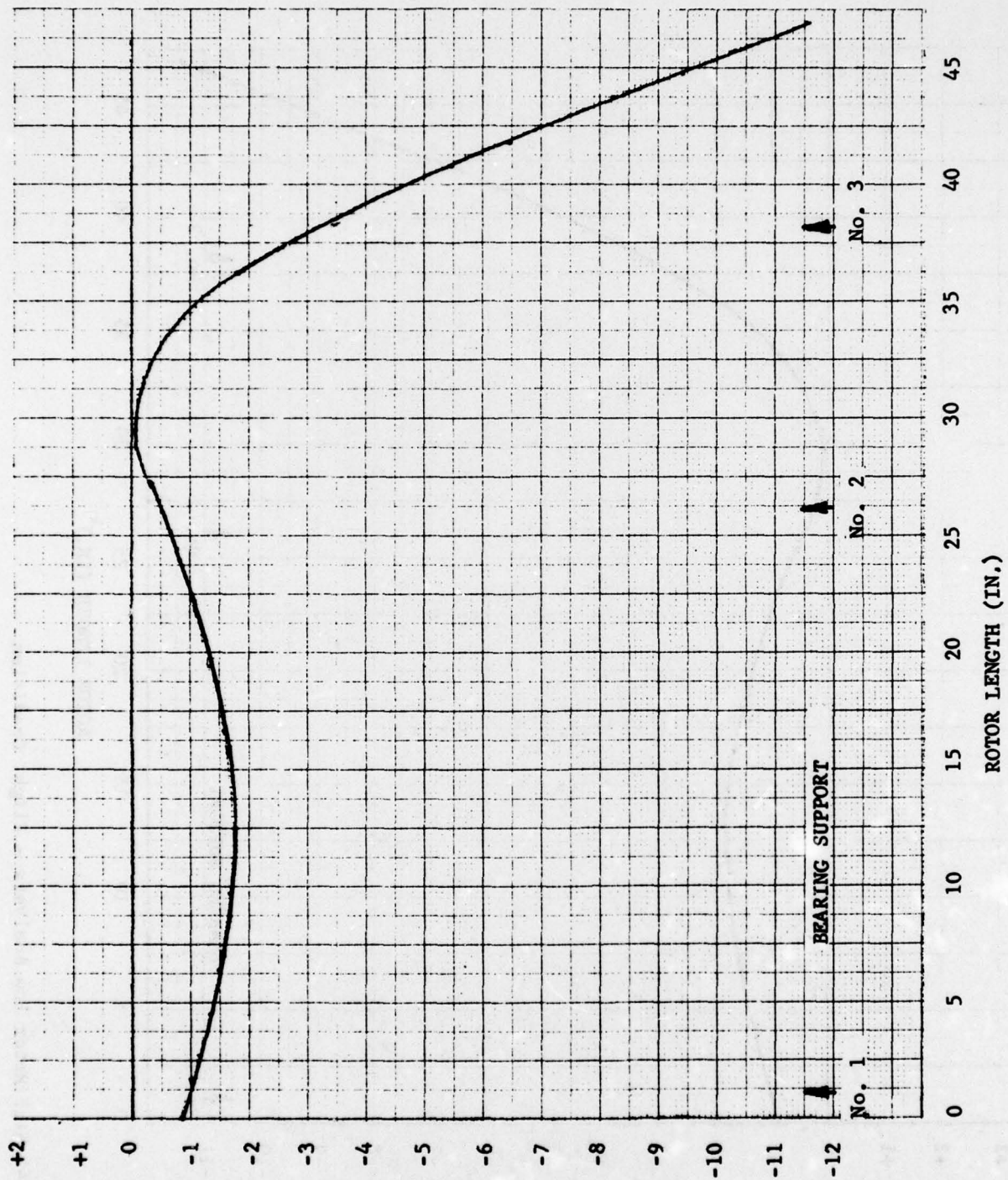
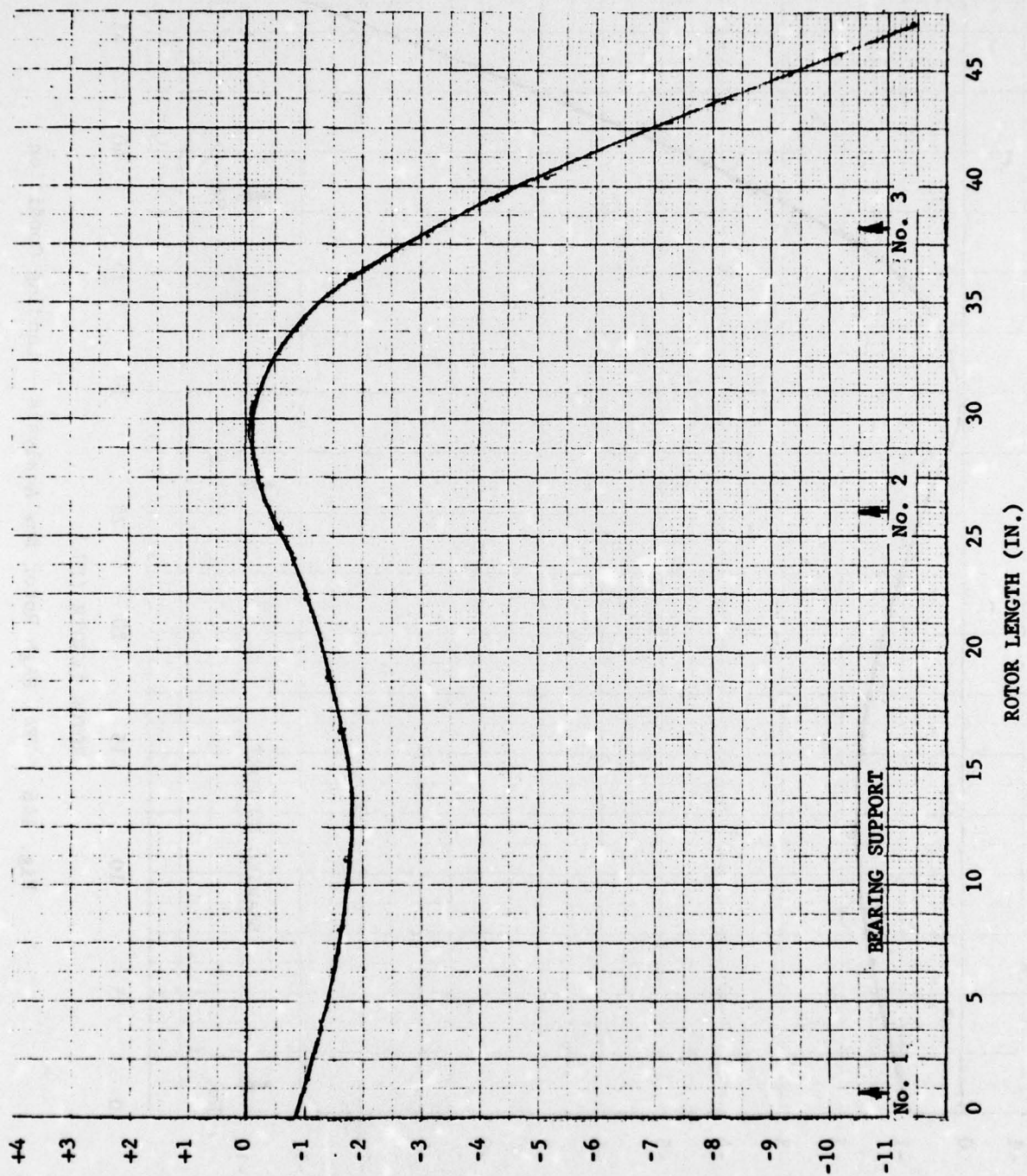


Fig. 146 TF41 High Rotor Bow Analysis - Landing Condition

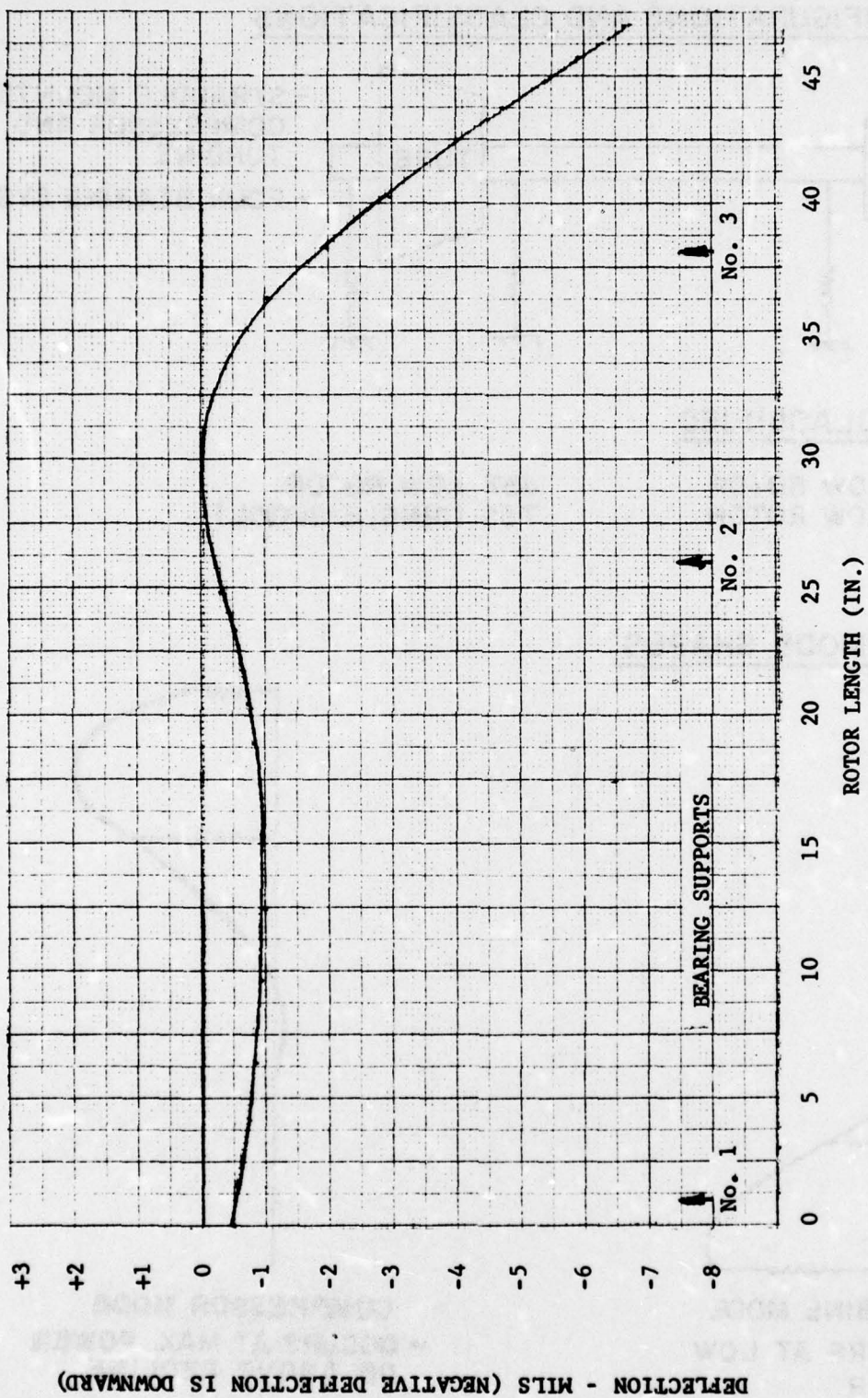




DEFLECTION - MILS (NEGATIVE DEFLECTION IS DOWNWARD)

Fig. 147 TF41 High Rotor Bow Analysis - Flight Condition

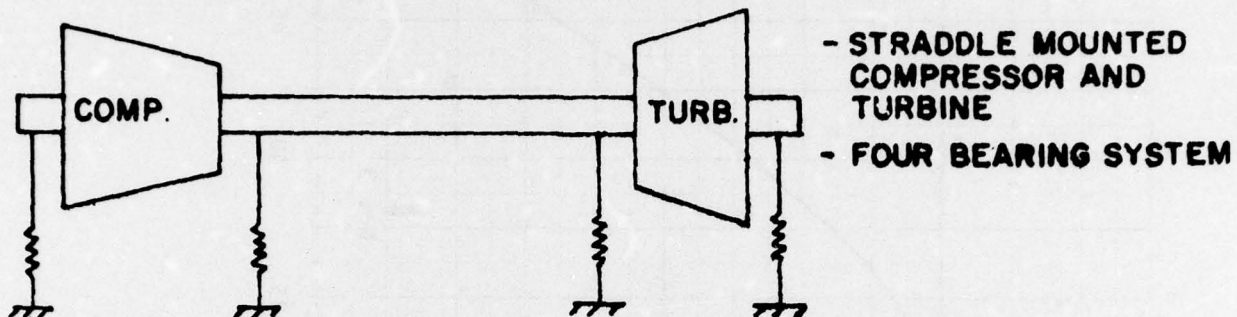




DEFLECTION - MILS (NEGATIVE DEFLECTION IS DOWNWARD)

Fig. 148 TF41 High Rotor Bow Analysis - Catapult Condition

## ROTOR CONFIGURATIONS AND CLASSIFICATIONS



## ENGINES CLASSIFIED

TF30 LOW ROTOR  
TF33 LOW ROTOR

J57 LOW ROTOR  
T56 (SINGLE SPOOL)

## TYPICAL MODE SHAPES

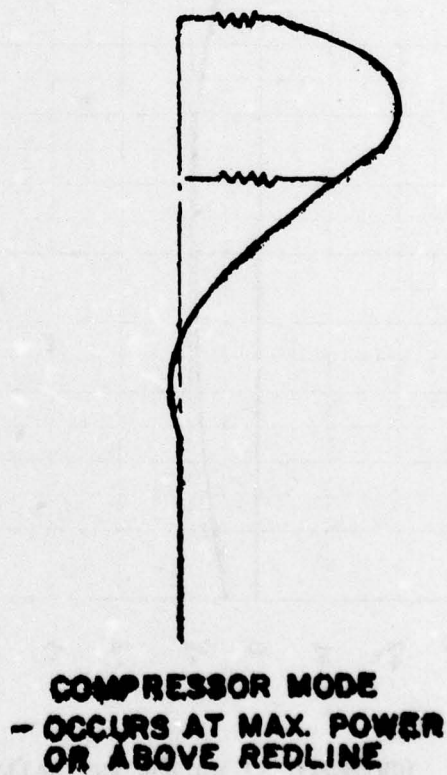
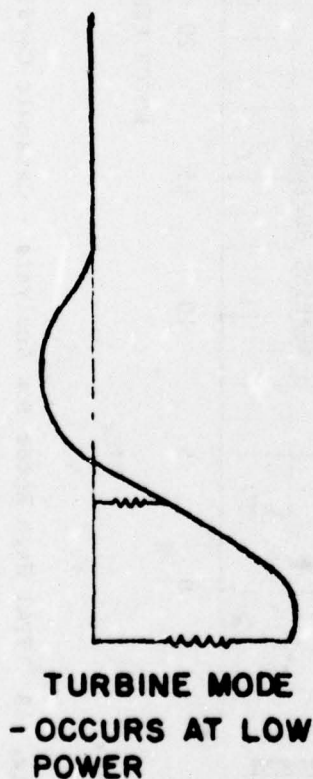
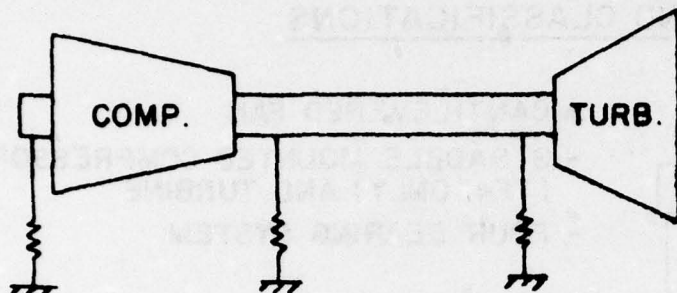


Figure 149

## ROTOR CONFIGURATIONS AND CLASSIFICATIONS



- STRADDLE MOUNTED COMPRESSOR
- CANTILEVERED TURBINE
- THREE BEARING SYSTEM

## ENGINES CLASSIFIED

TF30 HIGH ROTOR

TF33 HIGH ROTOR

TF41 HIGH ROTOR

J85 (SINGLE SPOOL)

## TYPICAL MODE SHAPES



CANTILEVERED TURBINE

- OCCURS BELOW IDLE OR AT PART POWER



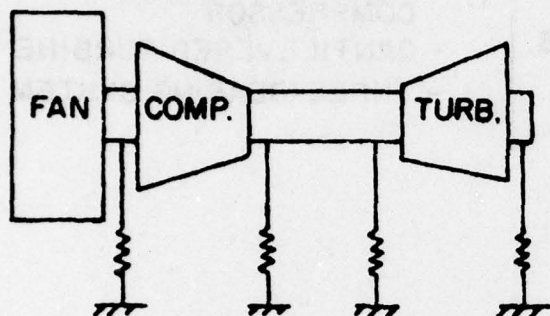
COMPRESSOR BOUNCE

- OCCURS NEAR MAX. POWER OR ABOVE REDLINE

Figure 150



## ROTOR CONFIGURATIONS AND CLASSIFICATIONS



- CANTILEVERED FAN
- STRADDLE MOUNTED COMPRESSOR (TF41 ONLY) AND TURBINE
- FOUR BEARING SYSTEM

## ENGINES CLASSIFIED

TF39 LOW ROTOR  
TF41 LOW ROTOR

## TYPICAL MODE SHAPES



TURBINE - MODE

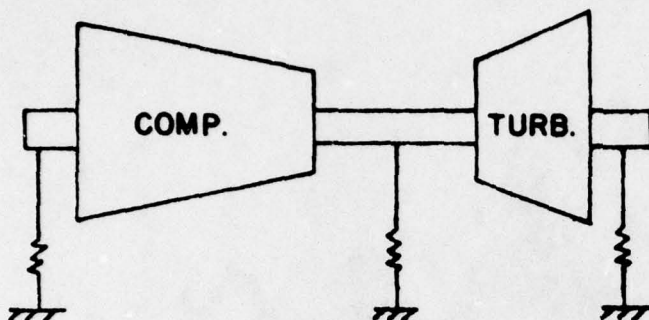


CANTILEVERED FAN

BOTH MODES ARE WITHIN THE SPEED RANGE WITH THE TURBINE CRITICAL SPEED OBSERVED AT LOWER POWER.

Figure 151

## ROTOR CONFIGURATIONS AND CLASSIFICATIONS

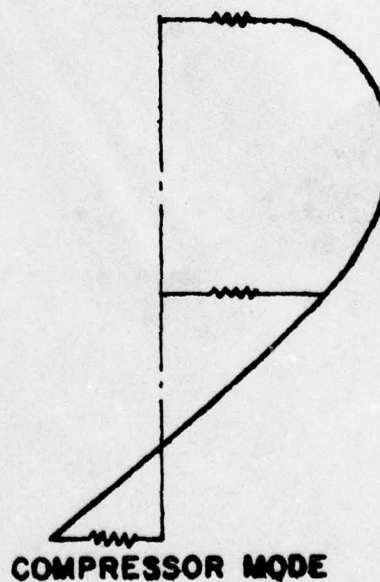
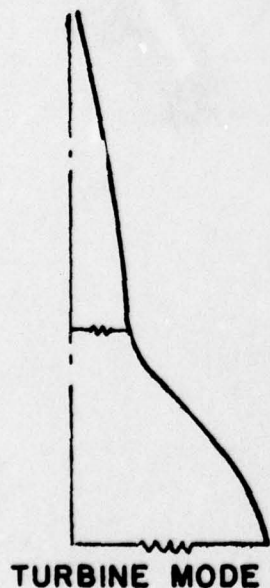


- STRADDLE MOUNTED COMPRESSOR AND TURBINE
- THREE BEARING SYSTEM

## ENGINES CLASSIFIED

TF39 HIGH ROTOR  
J79 (SINGLE SPOOL)

## TYPICAL MODE SHAPES



- CRITICAL SPEEDS ARE WITHIN CLOSE PROXIMITY OF EACH OTHER.
- BOTH MODES ARE WITHIN THE OPERATING SPEED RANGE.

Figure 152

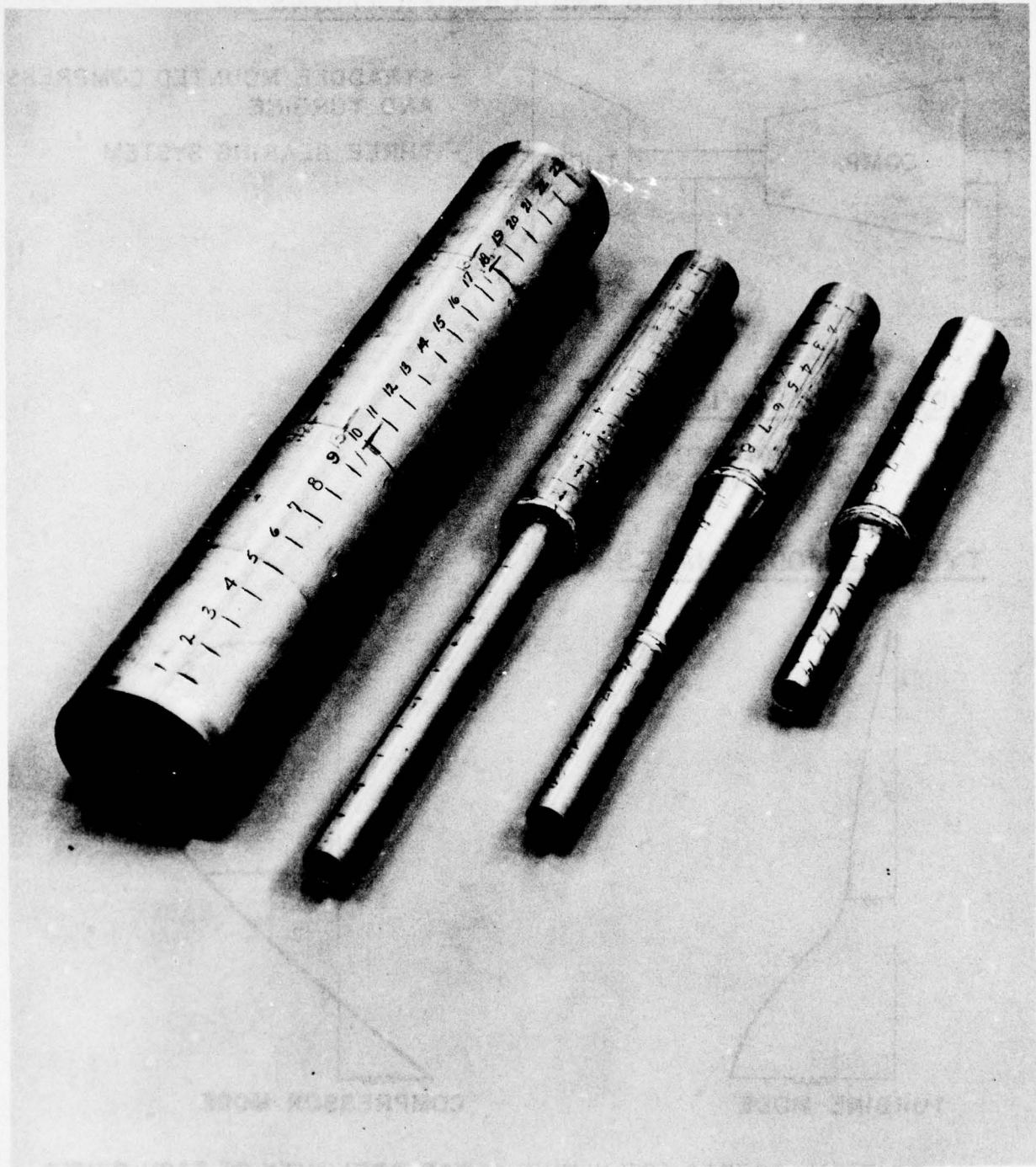


Figure 153 Cylindrical Test Specimens. From Left to Right, Thin Shell, Step Change, Shallow Cone and Steep Cone Elements. Grid Markings are in Inches.



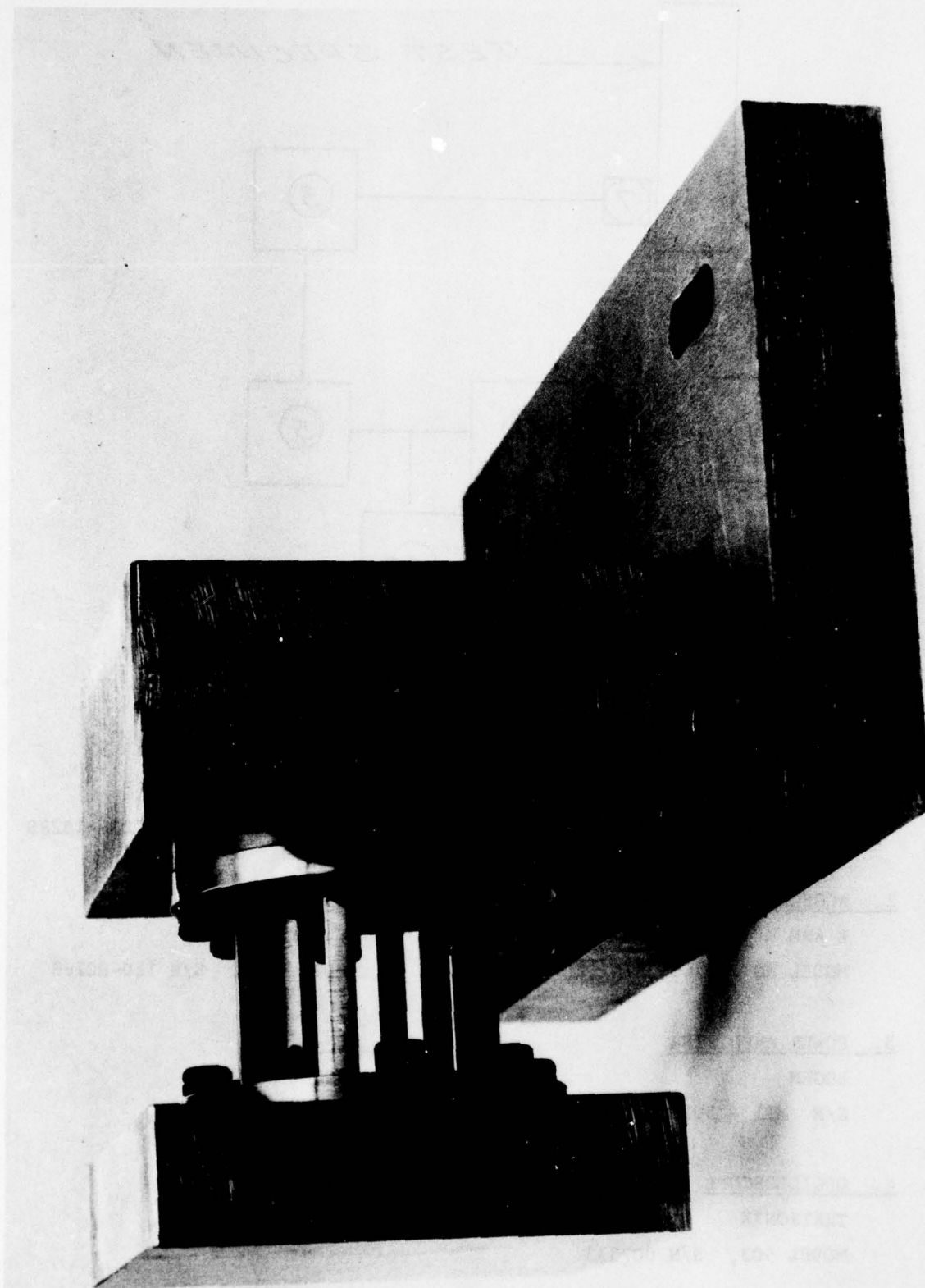
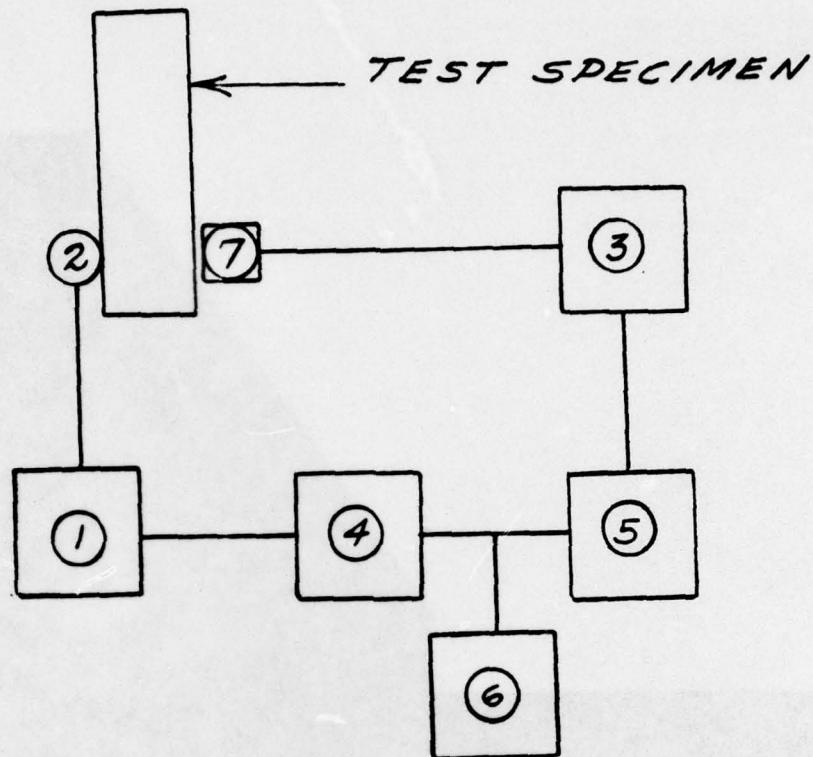


Figure 154 Flexural Support Test Element



THE FOLLOWING INSTRUMENTS WERE USED:

1. CHARGE AMPLIFIER

KISTLER

MODEL NO. 568M108, S/N 314

5. AUDIO OSCILLATOR

HEWLETT-PACKARD

MODEL 200ABR, S/N 234-15280

2. ACCELEROMETER

B AND K

MODEL NO. 4344, S/N 420761

6. ELECTRONIC COUNTER

HEWLETT-PACKARD

MODEL 521G, S/N 120-00268

3. POWER AMPLIFIER

BOGEN

S/N MTI - 301

7. AC - COIL

ENCORE

CUSTOM MADE

4. OSCILLOSCOPE

TEKTRONIX

MODEL 503, S/N 007333

Figure 155 Schematic of the Test Setup with List of Equipment

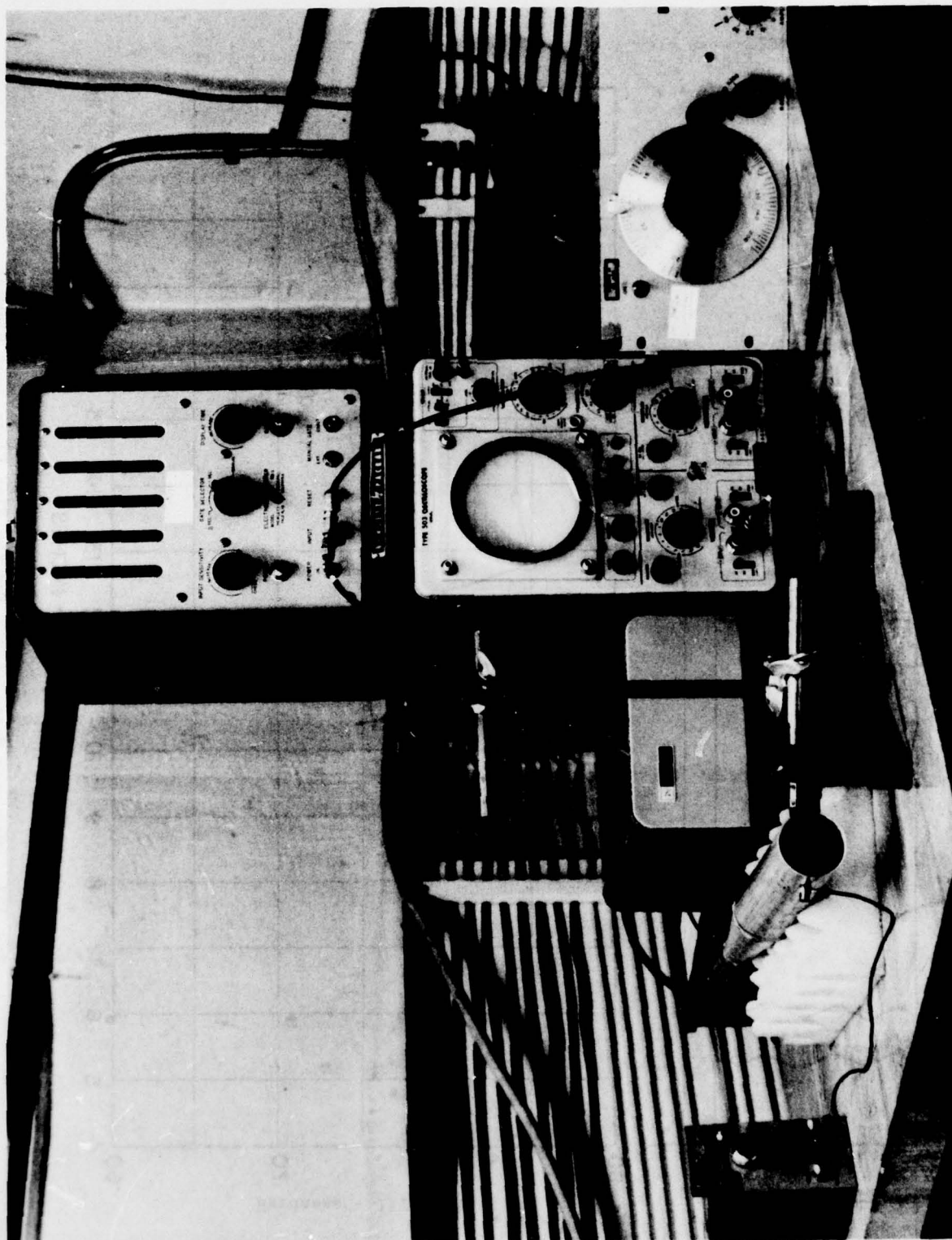


Figure 156 Pictorial View of Test Setup to Obtain Cylindrical Specimen Natural Frequency



SPECIMEN NO. 1  
ALUMINUM TUBING - .065" WALL  
THICKNESS

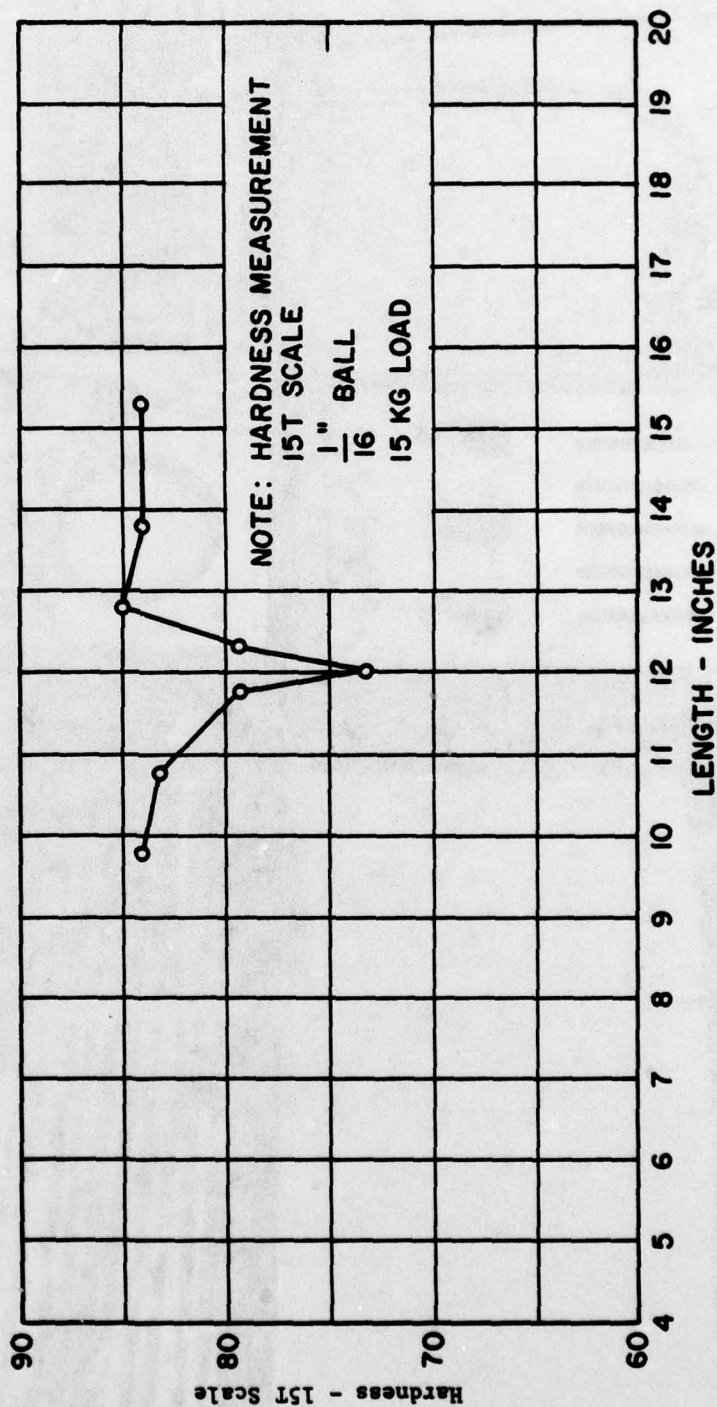
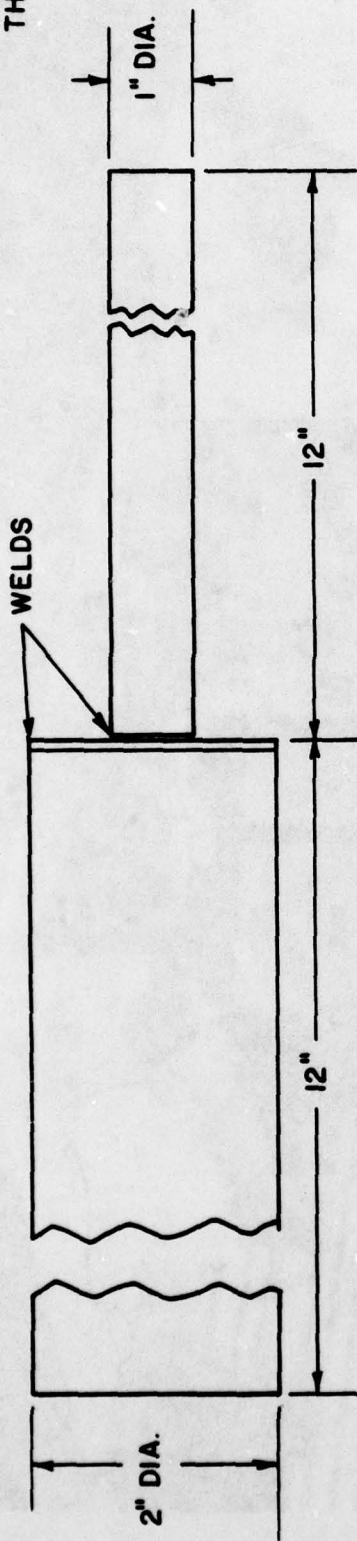


Fig. 157 Hardness Measurements for the Flat Plate Test Element

SPECIMEN NO. 2  
ALUMINUM TUBING - .065" WALL  
THICKNESS

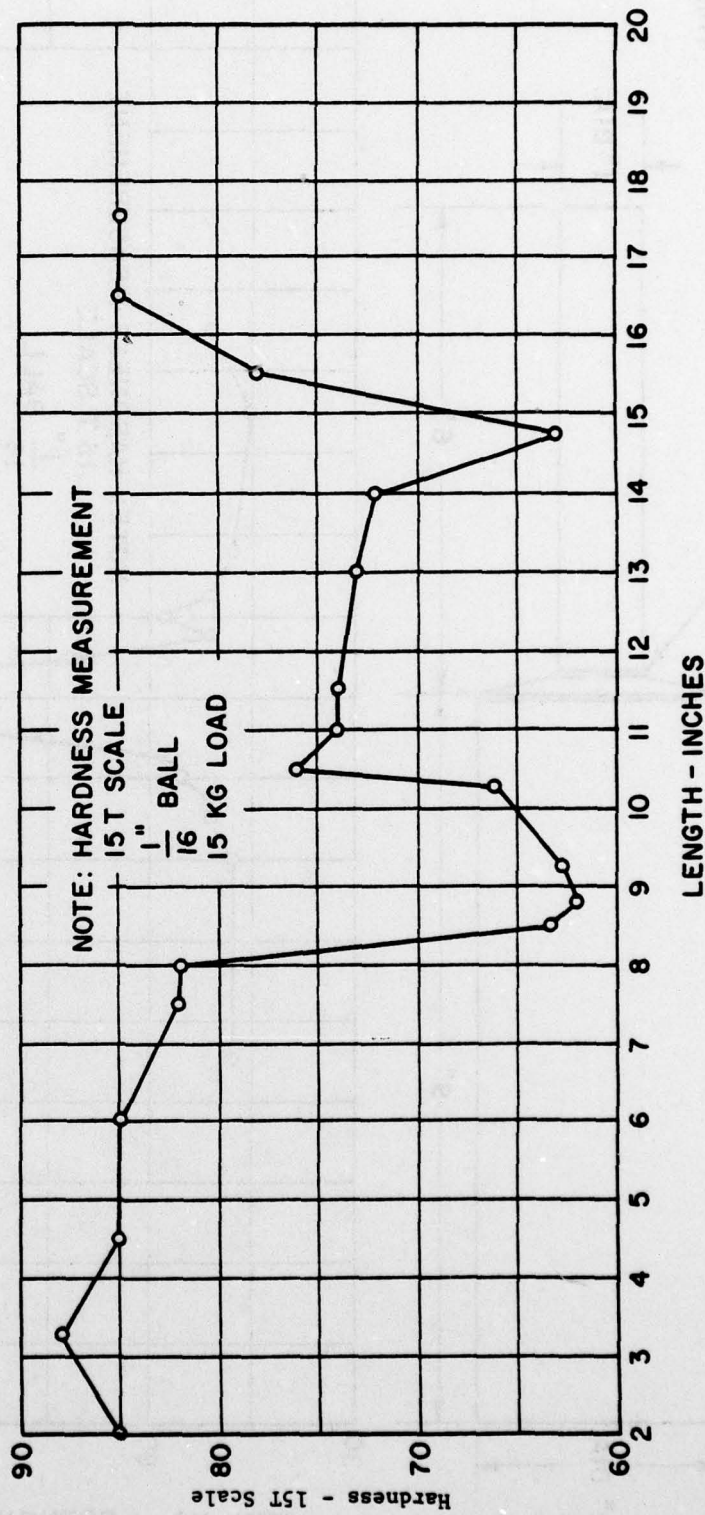
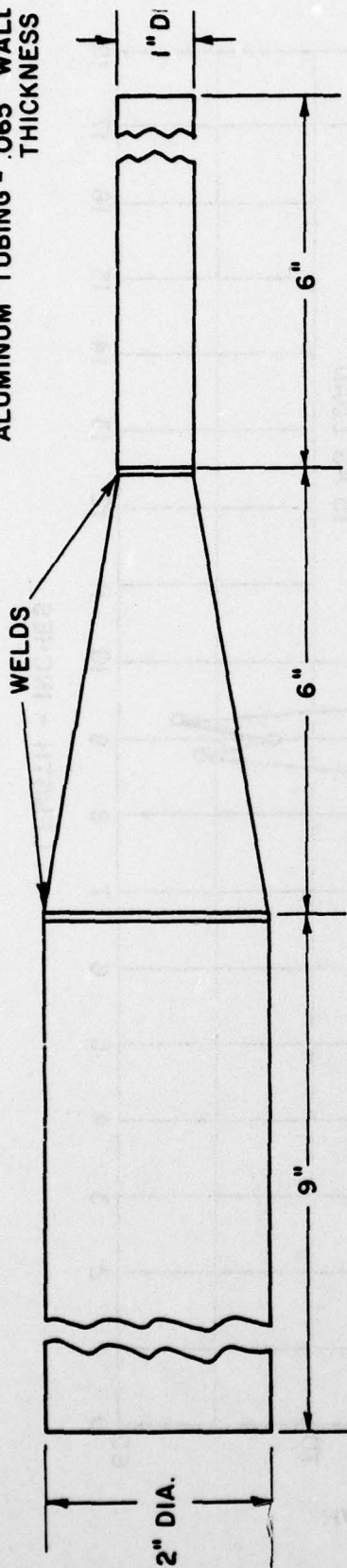


Fig. 158 Hardness Measurements for the Shallow Cone Test Element

SPECIMEN NO. 3  
ALUMINUM TUBING - .065" WALL  
THICKNESS

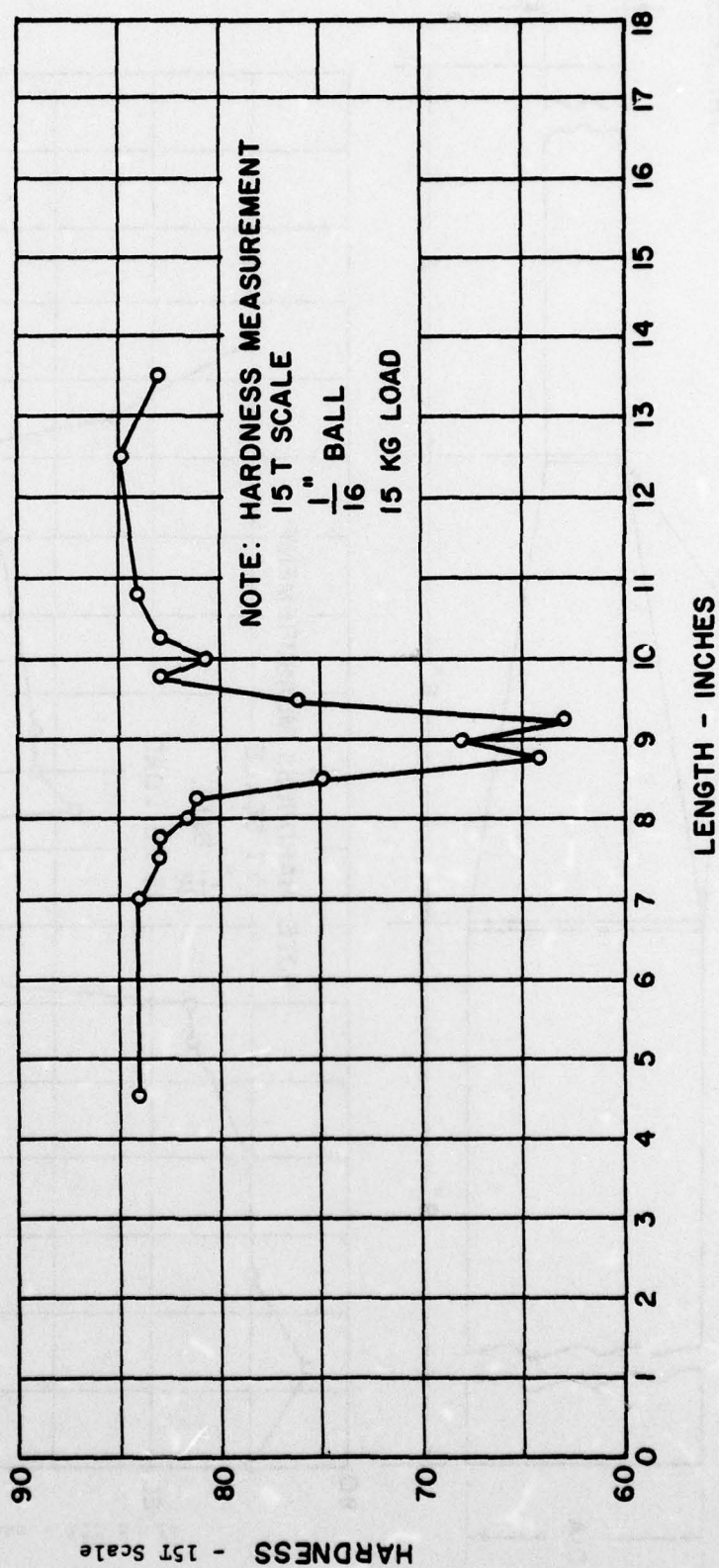
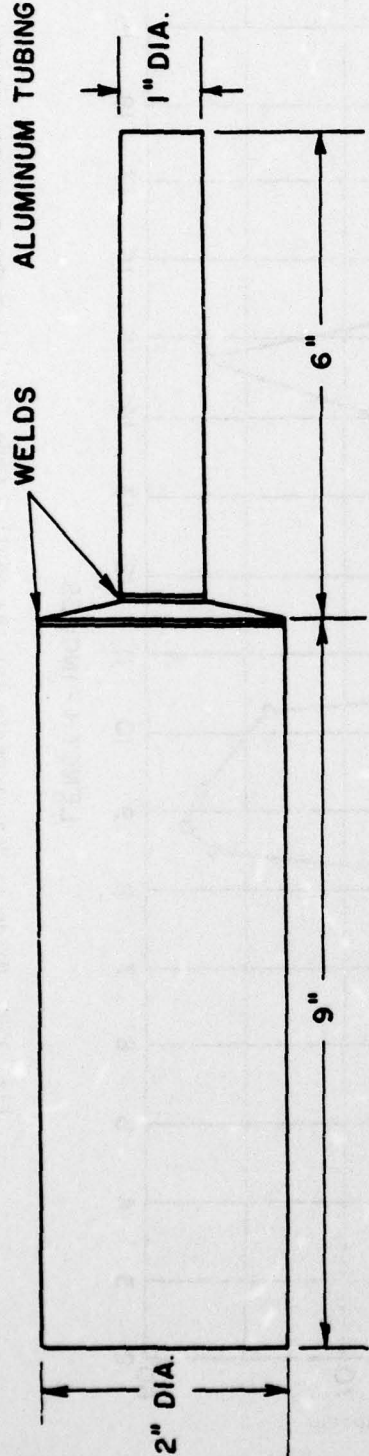
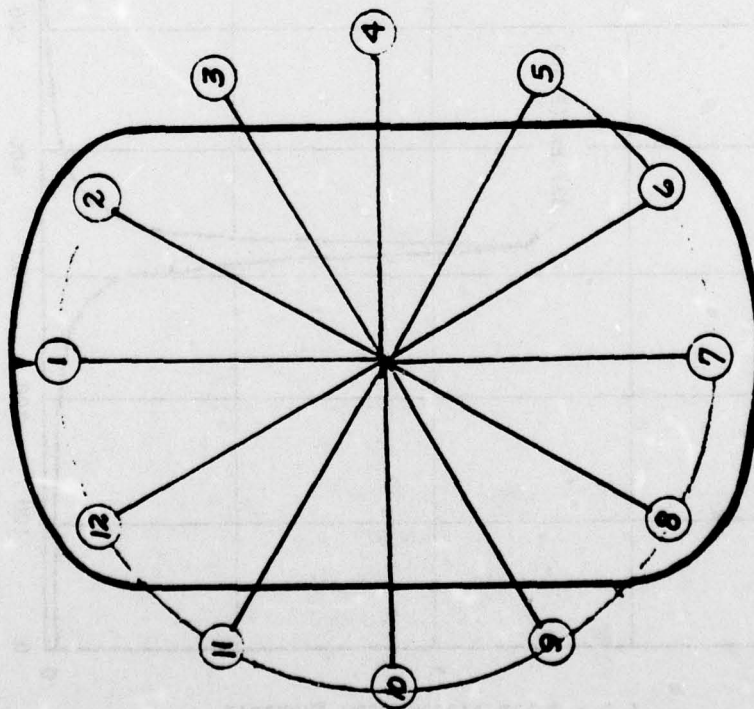


Fig. 159 Hardness Measurements for the Steep Cone Test Element



2 NODAL DIAMETER PATTERN  
(240 Hz)



3 NODAL DIAMETER PATTERN  
(710 Hz)

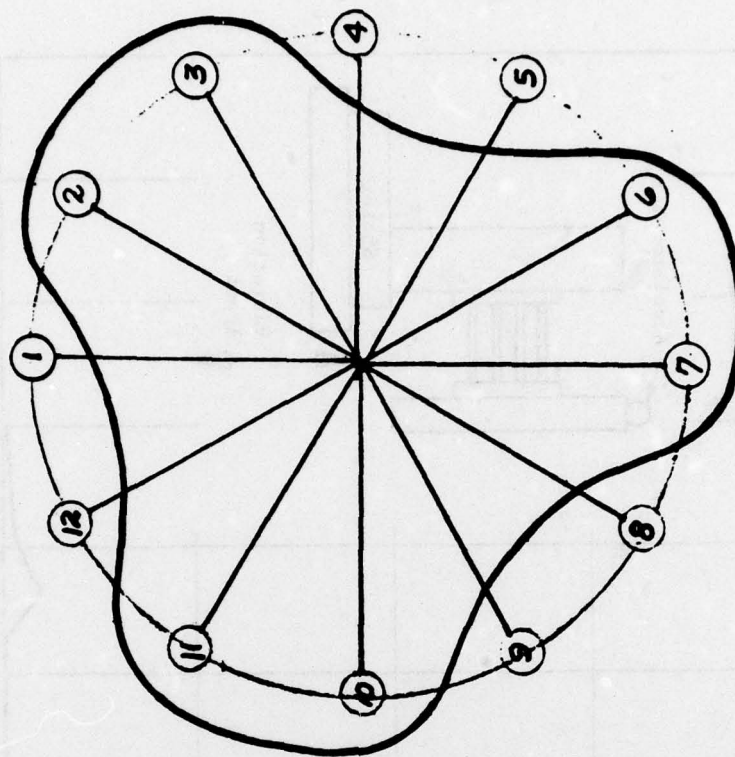
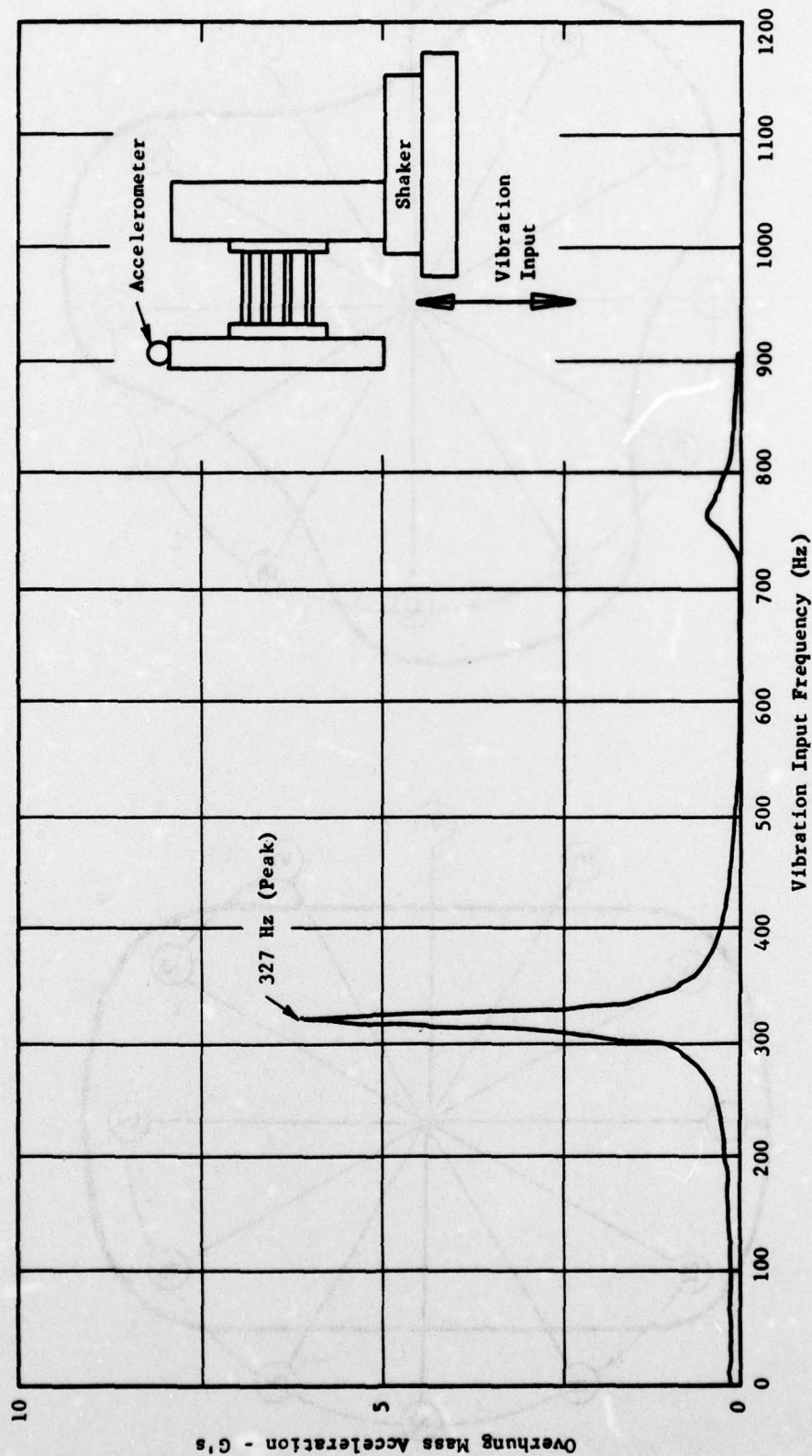
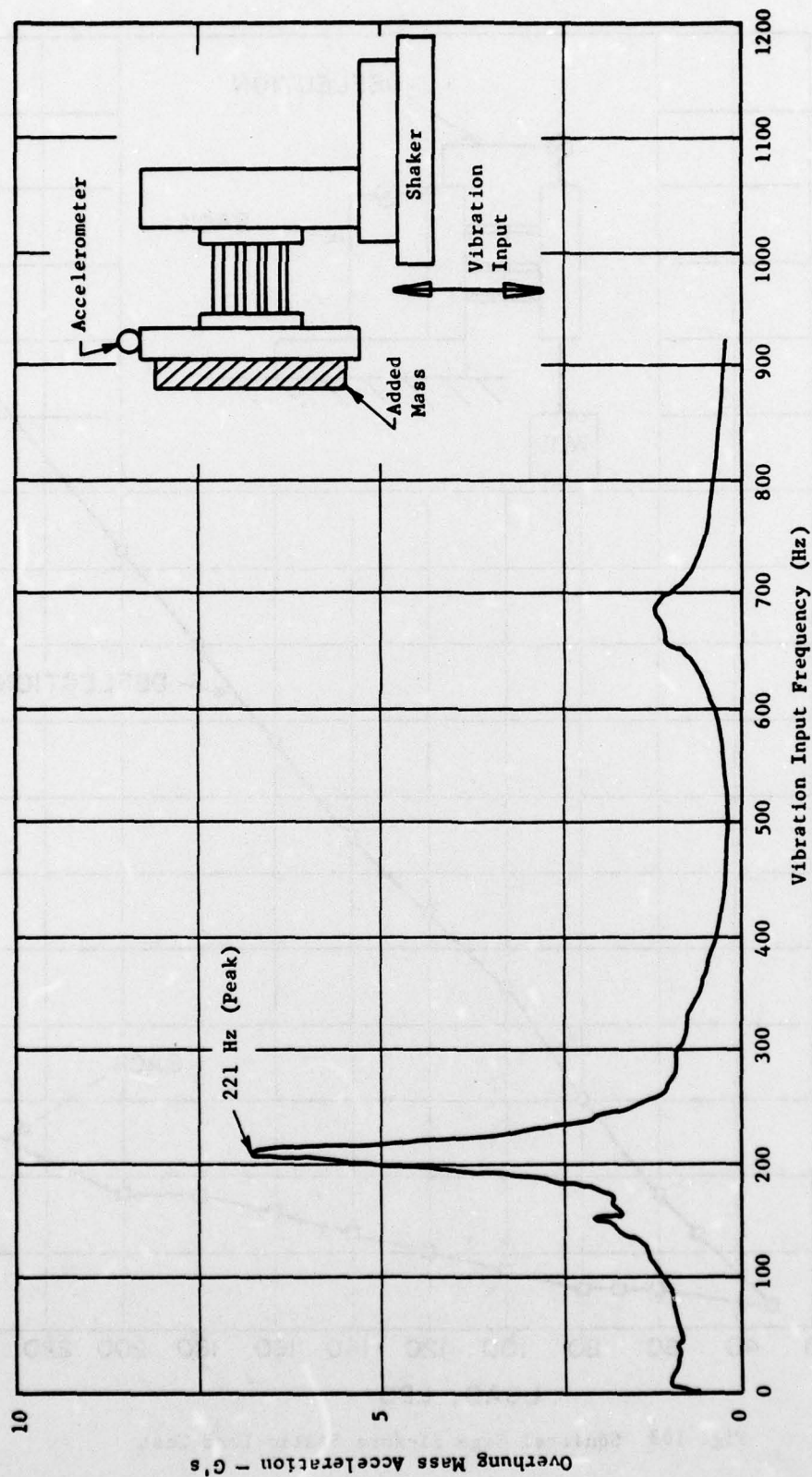


Fig. 160 Shell Modes Observed on the Thin Cylindrical Element During Vibration Excitation Tests



**Fig. 161** Flexible Support Response at the Overhung Mass Section



**Fig. 162** Flexible Support Response at the Overhung Mass with a 5.5 lb Mass Added



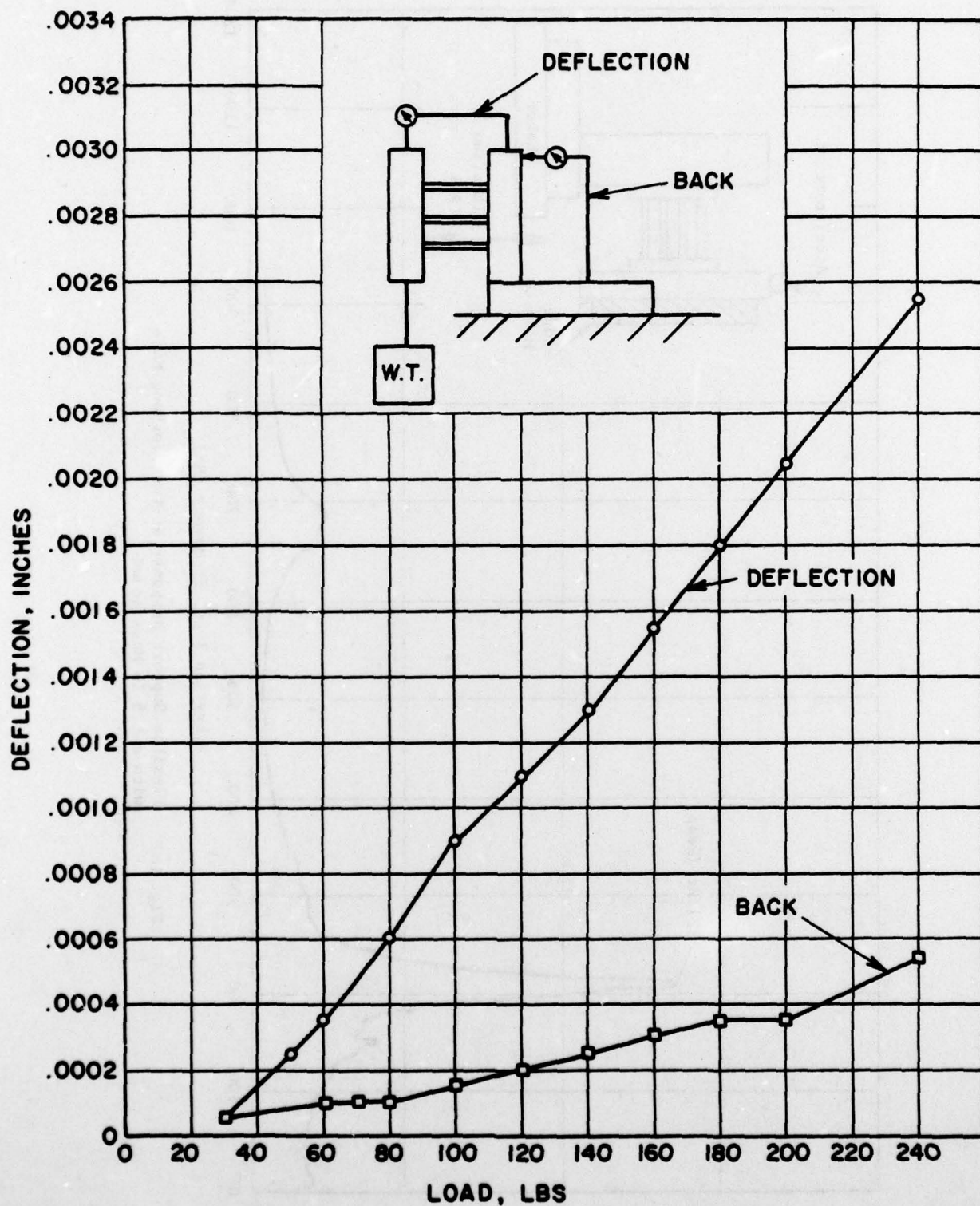


Fig. 163 Squirrel Cage Flexure Static Load Test

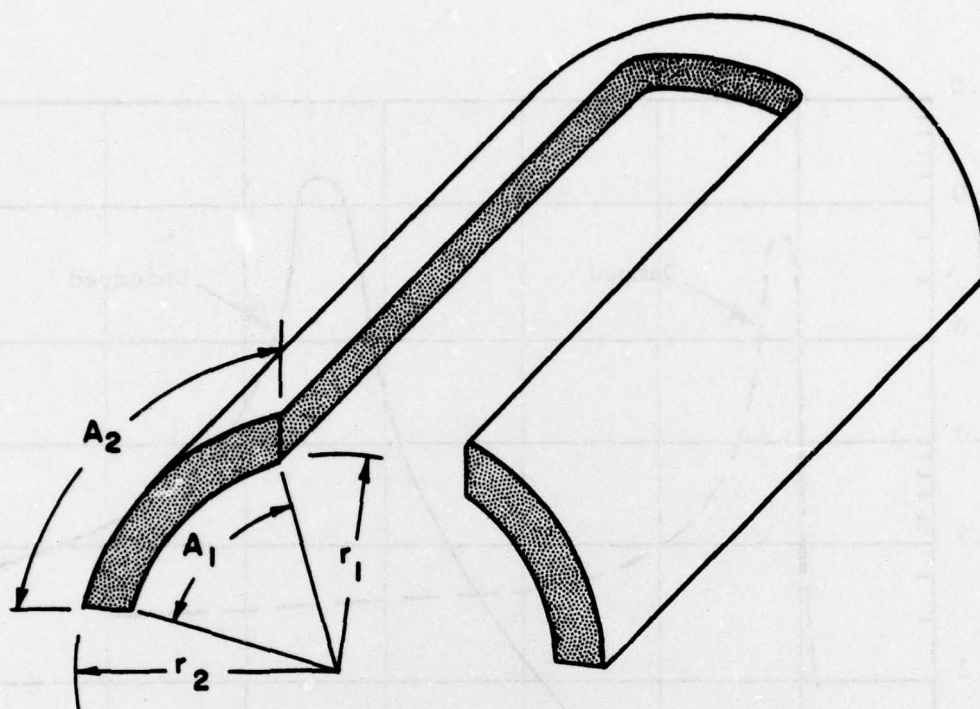


Fig. 164 Flexural Support Spokes

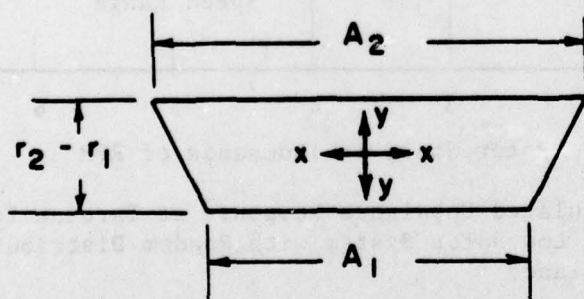


Fig. 165 Trapezoidal Representation of Spoke Cross-Section

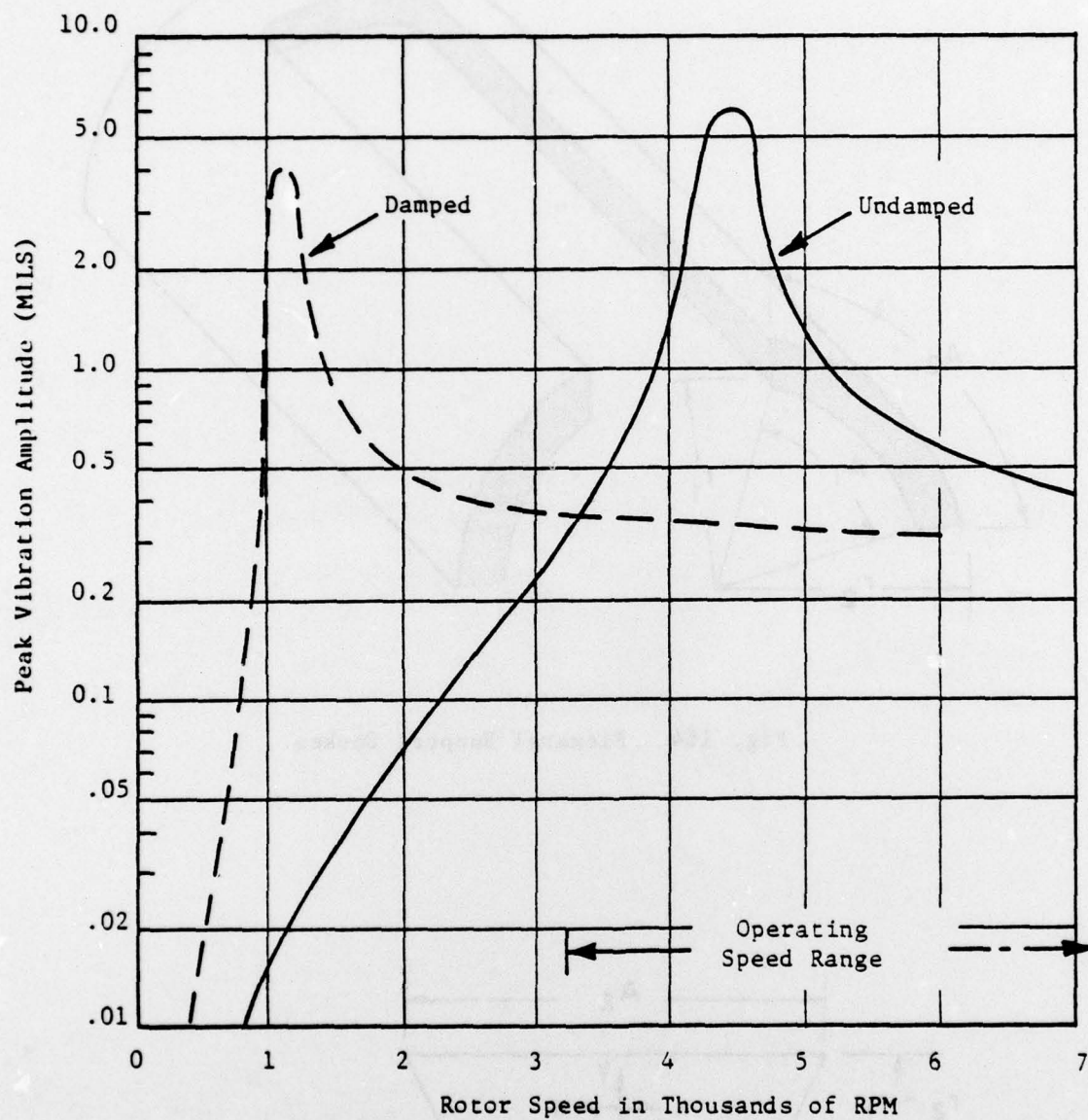


Fig. 166 Calculated Unbalance Response at Turbine for TF33 Low Rotor System with Random Distributed Unbalance



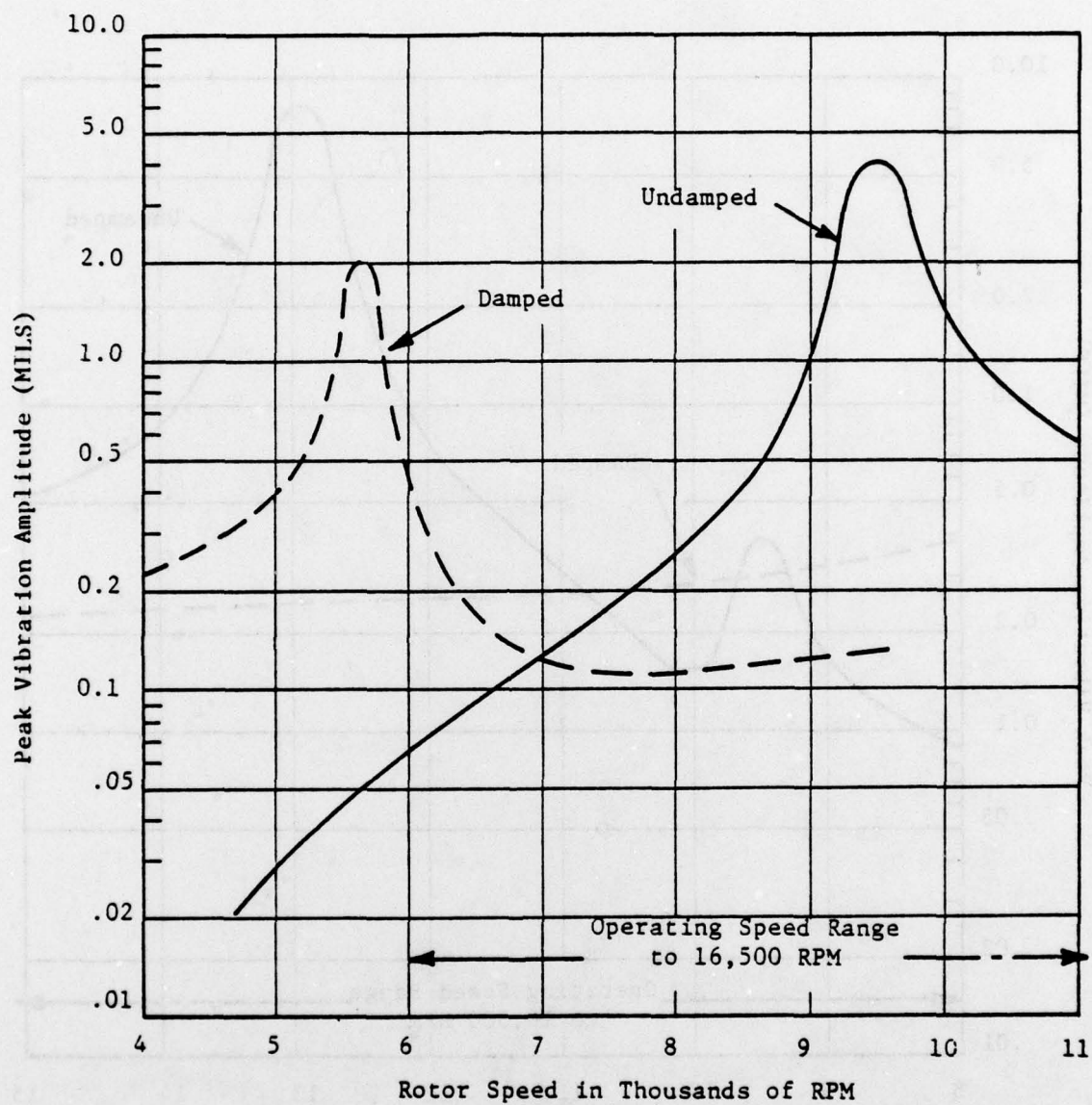


Fig. 167 Calculated Unbalance Response at Turbine for J35-21 Engine Rotor System with Random Distributed Unbalance

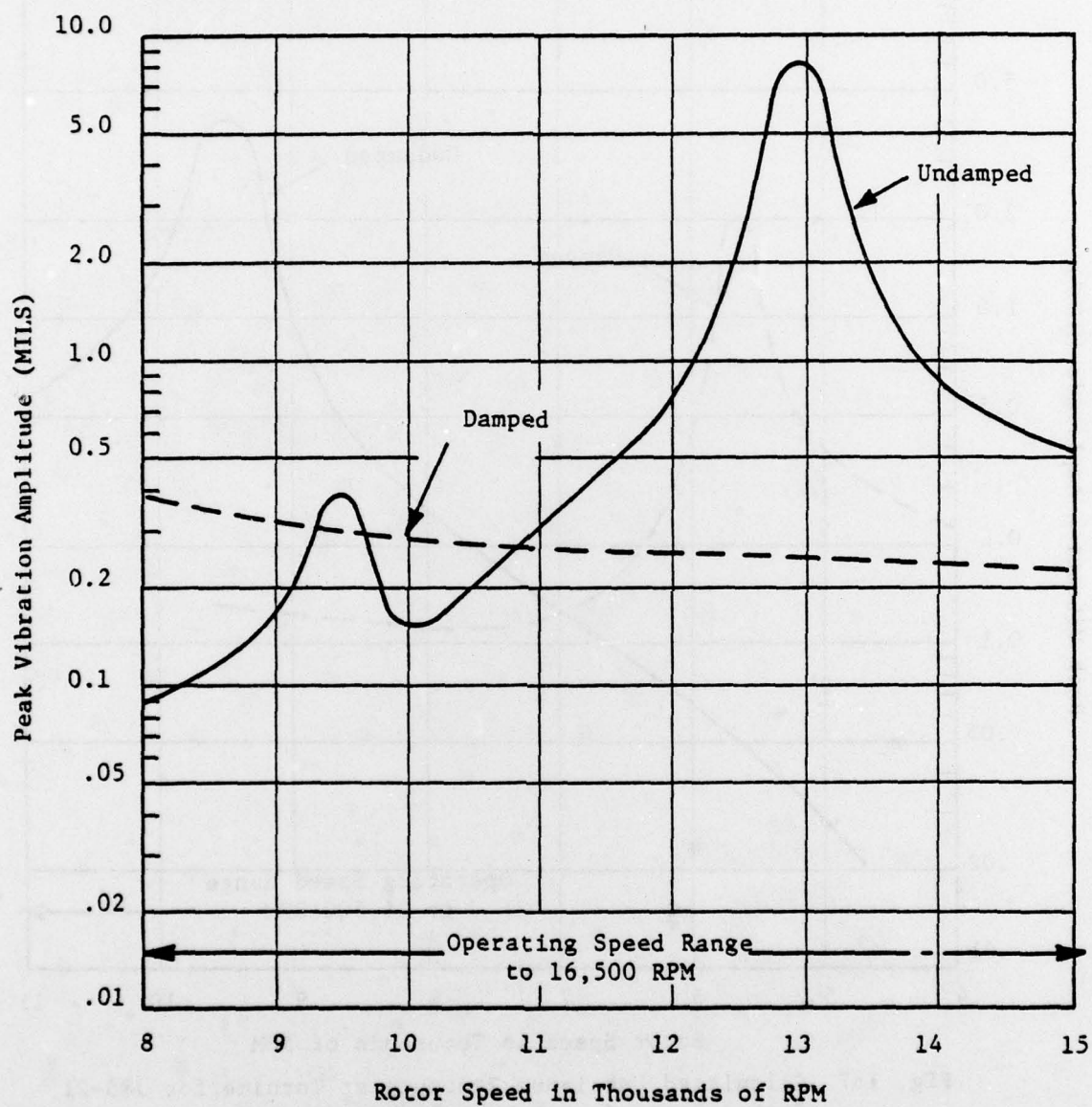


Fig. 168 Calculated Unbalance Response at Compressor for J85-21 Engine Rotor System with Random Distributed Unbalance

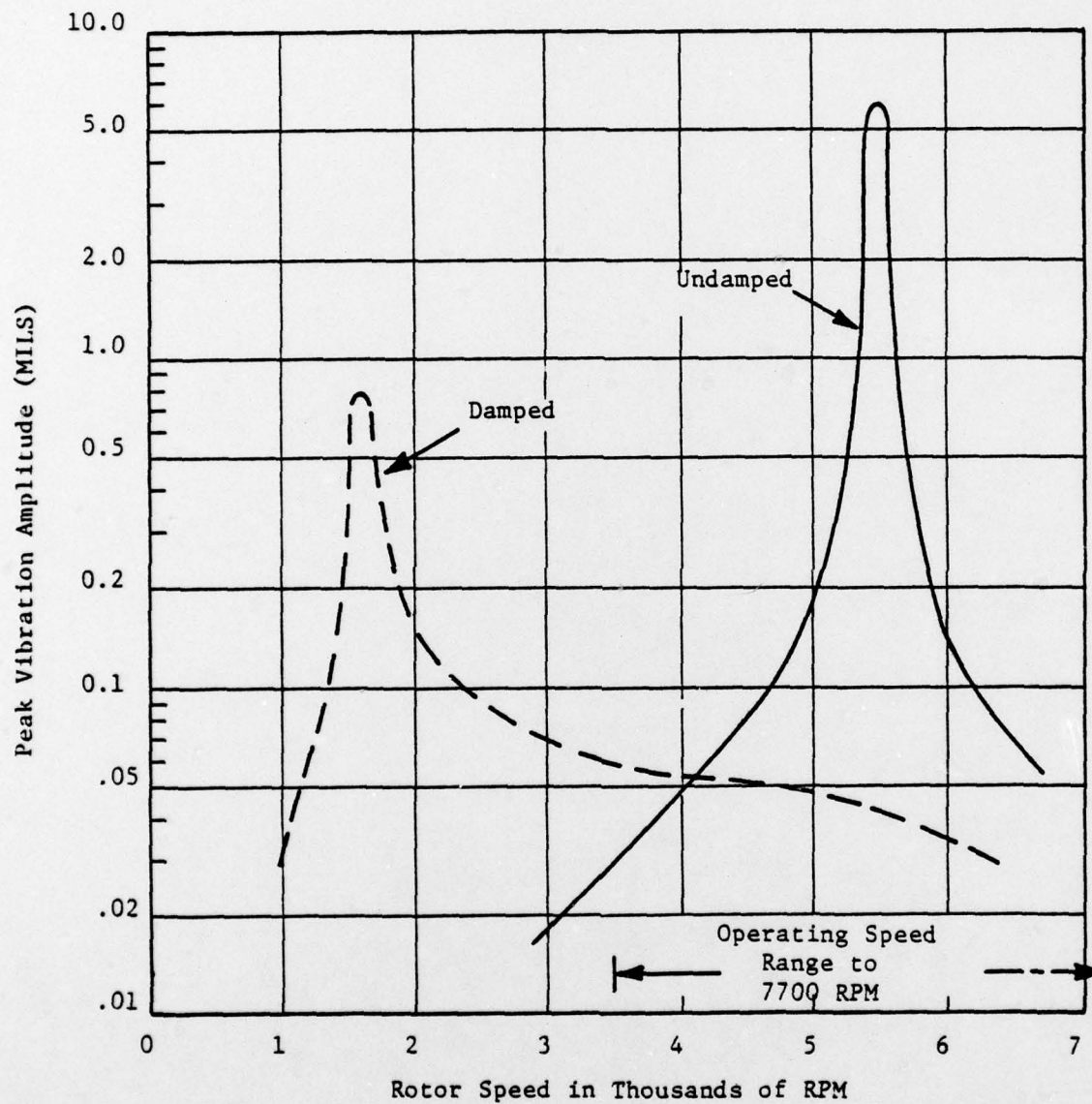


Fig. 169 Calculated Unbalance Response at Turbine for J79 Rotor Systems with Random Distributed Unbalance